UNIVERSITÀ DEGLI STUDI DI MILANO

SCUOLA DI DOTTORATO
TERRA, AMBIENTE E BIODIVERSITÀ

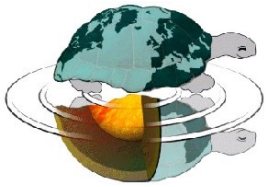

Dottorato di Ricerca in Scienze Naturalistiche e Ambientali
Ciclo XXVII

Coupling Glacio-Hydrological Response to Climate Variability in Mt. Everest Region (Central Himalaya)

Ph.D. Thesis

Sudeep Thakuri
Matricola R09761

Tutor	Academic Year	*Coordinator*
Prof. Claudio Smiraglia	2013–2014	Prof. Nicola Saino

Co- Tutor
Dr. Franco Salerno
Dr. Tobias Bolch

Abstract

Mt. Everest region in the central Himalaya is one of the most heavily glacierized parts of the Himalaya that is characterized by large debris-covered glaciers and many glacial lakes. The glaciers and ice are important sources of fresh water and play vital role in modulating the climate and the hydrological process. Previous studies from different parts of the Himalaya and around the world have revealed climate change at regional and global-scale and in general, shrinking of glaciers and ice caps. Climate change is thus, expected to impact in many ways to Cryosphere, hydrological process, and human livelihood. Temperature is often suggested to be increasing and considered as the main driver of change, however, in the higher elevations where the glaciers exist, climatic data are rarely available and limiting the climate related interpretation. This study is therefore conducted with the aim of linking variation of glaciers, glacial lakes, and river flow to local climatic trends in the higher elevations of Mt. Everest region. The study uses a comprehensive multi-temporal data from different sources: satellite observations, ground hydro-meteorological stations, and regular gridded and reanalysis climate data from the regional and global products (1960s to 2013).

First, using the weather data from ground stations, gridded, and reanalysis products, the climatic trends and climate variability are evaluated. From 1979 to 2013, temperature has increased by 0.052 °C a^{-1}, while the precipitation has shown an increasing tendency in 1960s to early 1990s and significantly decreasing afterward. During 1994–2013 period, at an elevation of ~ 5000 m, minimum temperature (0.072 ± 0.011 °C a^{-1}) has increased more than maximum temperature (0.009 ± 0.012 °C a^{-1}), with an average temperature increase of 0.044 ± 0.008 °C a^{-1} in the last two decades. The increases in the temperature are observed during the pre- and post-monsoon months, favouring melting ice close to the glacier terminus. At the same elevation, precipitation has significantly decreased (-9.3 ± 1.8 mm a^{-1}) for all months, corresponding to a loss of 47 % during the monsoon.

Second, the glacier changes are studied within the Sagarmatha (Mt. Everest) National Park (SNP; glacier area: ~ 400 km^2) between 1962 and 2011, using multi-temporal optical satellite imagery, assisted by topographic maps. During the period, glaciers have experienced a surface area loss of 13.0 ± 3.1 %, an average terminus retreat of 403 ± 9 m, a Snow-Line Altitude (*SLA*) upward shifting of 182 ± 22 m, and an increasing of debris-covered area by 17.6 ± 3.1 %. An accelerated rate of glacier shrinkage is observed after the 1990s, which is caused not only due to increased temperature, but also as a result of a significant decreasing precipitation over the last decades. Moreover, selected glaciers have indicated a significant decreasing glacier flow velocities from the 1990s to recent year and a significant loss of glacier thickness (0.73 ± 0.63 m a^{-1}) in the last decade.

Third, a complete mapping and characterization of a total of 624 glacial lakes with surface area of 7.43 km^2 (±18 %) are conducted in the SNP, with particular focus on conditions related to the formation of lakes using 2008 satellite imagery. Further, evolutions of glacial lakes are examined using the satellite imagery and topographic maps between 1963 and 2013. Three types of glacial lakes (*supra*, *pro*, and *unconnected*) present in the SNP have their distinctive potential to explain the glaciological and climatic conditions. Results show that the slope of the glacier where lakes are located influence the supraglacial lake formation. Furthermore, the slope to glacier upstream favours the formation of the supraglacial lakes, as a boundary condition. The formation of proglacial lakes is related to the growing and coalescing of the supraglacial lakes. The unconnected lakes are evaluated as a useful indicator of precipitation trend. During the study period (1960s–2011), both number and surface area of supraglacial lakes has continuously increased (number +109.7 %; area +13.3 %) with an accelerated rate in the last decade due to increase in the glacier melting. Proglacial lakes are more or less constant in both numbers and size, except Imja Lake that have exceptionally increased, while the surface area of unconnected lakes has increased from 1960s–1990s (+4.3 %) and decreased from early 1990s afterward (-10.9 %). The thesis has shown that the accelerated rate of glacier shrinkage and the decreasing of the unconnected lakes in the last decades are associated to decreasing precipitation. Supraglacial lakes behaviour confirms the acceleration of the negative mass balance of glaciers due to the reduced ice velocities caused by decreased precipitation.

Finally, the hydrological dynamics of the Dudh Koshi river examined by stochastic frequency analysis, physically-based hydrological models, and multilinear regression using river discharge data and climate data. The analysis suggests that the Dudh Koshi river discharge is mainly dependent on precipitation from 1960s to 2000s, however a non-stationarity in the river discharge is observed since the early 2000s, indicating increased discharge, not justifiable by the observed weakening monsoon. The study concludes by underlining that an accelerated glacier melting as observed through the glacier change analysis affects an increasing of the discharge.

Acknowledgements

This study would not be possible without contributions from several persons and institutions. The Ph.D. was funded by the Intergovernmental Panel for Climate Change (IPCC) and the Prince Albert II of Monaco Foundation under the framework of the IPCC Scholarship Programme, and the Italian National Research Council–Water Research Institute (IRSA-CNR). Further, this work was supported by the MIUR through Ev-K2-CNR/SHARE and CNR-DTA/NEXTDATA projects within the framework of collaboration between the Ev-K2-CNR Association and the Nepal Academy of Science and Technology (NAST). NASA Land Processes Distributed Active Archive Center (LP DAAC) provided access to Terra ASTER scenes and USGS Earth Resources Observation & Science Center (EROS) provided access to the Landsat and Corona scenes freely. The Department of Hydrology and Meteorology (DHM) of Nepal and the Ev-K2-CNR Association, Italy provided the ground station data.

I would like to thank to Prof. Claudio Smiraglia for accepting to be my Ph.D. tutor and supporting for successfully completion of the study. I am indebted to Franco Salerno (IRSA-CNR) for his continuous support, encouragement, and guidance to my research, not only during the Ph.D., but also from the beginning of my research career. Without his support, I would not be in my current position. Further, my special thank goes to Tobias Bolch (University of Zurich) for providing valuable inputs on Glaciological techniques and suggestions on my work; Nicolas Guyennon (IRSA-CNR) provided significant input in climate and hydrological analysis; Gaetano Viviano (IRSA-CNR) continuously supported me in addressing practical issues related to research as well as administration; he and his parents (Caterina and Franco) treated me as a family member and supported in every occasion during my stay in Italy. Further, I would like to thank to Carlo D'Agata, Department of Earth Sciences, University of Milan and Amy L. Smith from the IPCC Secretariat, for their contributions for successful completion of the study.

Gianni Tartari (IRSA-CNR) has taken guardianship hosting me in his institute and providing full research and technical supports. My sincere thanks also goes to Agostino Da Polenza and Chiara Belloti for providing support from Ev-K2-CNR. Bivek Raj Thakuri, Anil Thakuri, and Samjana Malla provided logistic support from Nepal for collecting data and encouraging me to study. Moreover, I must acknowledge the contributions and support of all my co-authors and colleagues during the Ph.D. research.

Finally, I am forever indebted to my beloved wife, Usha Rana, for her patience during the study period and to my parents (Sushila and Raj Kumar) for their loving support.

Contents

List of Figures

List of Tables

Articles

This thesis is based on four articles and other unpublished works. Out of four articles presented herewith, three articles are already published and one is in peer-review process. The full articles are included in this thesis and have been briefly summarized them in the related chapter. In additional to these articles, other works that are not yet published are presented and discussed in detail under the related chapter. These works are also in the process of developing into a full article form. I have presented my thesis work in this way for preventing repetition of the contents of the work as they are already structured. I assume that it will be easier to follow, when presented in a compact way, accompanied by a summary of the article in the main body of the thesis. I have tried to avoid the possible repetition, however, there might exist in some places for logical connection of the work.

Article I

Salerno, F., N. Guyennon, S. Thakuri, G. Viviano, E. Romano, E. Vuillermoz, P. Cristofanelli, P. Stocchi, G. Agrillo, Y. Ma, and G. Tartari (2014) Weak precipitation, warm winters and springs impact glaciers of south slopes of Mt. Everest (central Himalaya) in the last two decades (1994-2013). *The Cryosphere Discuss.,* 8, 5911-5959, doi: 10.5194/tcd-8-5911–2014.

Article II

Thakuri, S., F. Salerno, C. Smiraglia, T. Bolch, C. D'Agata, G. Viviano, and G. Tartari (2014) Tracing glacier changes since the 1960s on the south slope of Mt. Everest (central Southern Himalaya) using optical satellite imagery. *The Cryosphere,* 8, 1297–1315, doi: 10.5194/tc-8-1297–2014.

Article III

Thakuri, S., F. Salerno, T. Bolch, N. Guyennon, and G. Tartari (2015) Increased Imja Lake expansion as response to reduced Imja Glacier flow velocity (Mt. Everest region, Nepal). *Submitted.*

Article IV

Salerno, F., S. Thakuri, C. D'Agata, C. Smiraglia, E. C. Manfredi, G. Viviano, and G. Tartari (2012) Glacial lake distribution in the Mount Everest region: Uncertainty of measurement and conditions of formation. *Global Planet. Change*, 92-93, 30–39, doi: 10.1016/j.gloplacha.2012.04

1

General Introduction

1.1 Motivation

The Himalayan glaciers and ice, also referred the Asian water tower, are receiving increased attention due to their role in the hydrological process and climate system (Immerzeel et al., 2010; Kaser et al., 2010). They contribute to 10 major river system in central and southern Asian and are important sources of water resources for about 1.4 billion (20 %) of the world population (Immerzeel et. al., 2010). It provides water to downstream population for agriculture, hydropower, and household consumption (Viviroli et al., 2011). The controversies concerning the possibly faster glacial shrinkage in the Himalaya than in any other parts of the world (Cogley et al., 2010; Bagla, 2009) have focused global attention on the necessity for a more comprehensive study in this region. The uncertainties are mainly attributable to a lack of measurements, both of glaciers and of climate forcing agents (Bolch et al., 2012).

Rivers originating in the high mountains of the Himalaya are among the most meltwater-dependent river systems on the earth (Yao et al., 2012; Schaner et al., 2012), however across the Himalayan river basins, there are a large variation in the contribution of glaciers and snowmelt to the total runoff (Gardelle et al., 2013), which is poorly quantified. The lack of understanding of the hydrological regimes of High Asia's rivers is one of the main sources of uncertainty in assessing the regional hydrological impacts of climate change (Lutz et al., 2014).

The climate in this part of the Himalayas is characterized by the south Asian monsoon system, causing a bulk of precipitation to occur during June–September (Tartari et al., 2002). Climates, in particular, temperature and precipitation are both drivers of the glacier and snow melting, but the actual behaviour of these variables in the high elevations is not existing (Beniston, 2003 Rangwala and Miller, 2012). The changes in the temperature and precipitation have been foreseen to change the hydrological regime. Agreements can be seen on a projected future temperature rise in global as well as regional-scale, e.g. the Himalaya (IPCC, 2013), while the trend of the summer monsoon precipitation change is still unclear. Some studies showed an increasing of the river runoff due to increased precipitation and glacier melt despite the continuing decreasing of the glaciers in the

twenty-first century in glacierized basins (Immerzeel et al., 2012; Immerzeel et al., 2013; Lutz et al., 2014), however the global climate models fail to capture the monsoon in this region (Kang et al., 2002) and the regional models do not agree each others about the precipitation change in the Himalaya (Ashfaq et al., 2009; Kumar et al., 2006). Ashfaq et al. (2009) show a monsoon onset delaying and strong reduction in the monsoon precipitation in the 21st century. Some other studies suggest the reduction in the summer monsoon precipitation due to impacts of aerosols on precipitation (Bollasina et al., 2011; Ramanathan et al., 2005). Few studies based on ground station data (with the datasets mainly from lower elevations) indicate that the temperature is increasing since early 1970s in the Nepal Himalaya (Shrestha et al., 1999; Kattel and Yao, 2013) and precipitation are decreasing due to weakening of south Asian monsoon (Sharma et al., 2000; Yao et al., 2012; Palazzi et al., 2013).

Moreover, there are still many challenges related to find the fine-scale variability in climate and glacier variations, and potential impacts to river flow due to high uncertainty associated with the complex topographic settings, spatially heterogeneous climatic behaviour, and the rarely available dataset (Bookhagen and Burbank, 2010). The shrinkage of the glacier and snow cover is expected to have detrimental impacts on the water availability in river systems in the glacierized basin in the mountains. However, due to limited studies, the reliable and sufficient data are still missing in the Himalaya.

The needs for a fine-scale investigation are particularly evident on the south slope of Mt. Everest, which encompasses the highest elevation range and is one of the most heavily glacierized parts of the Himalaya. The glaciers here are characterized by abundant debris coverage (Fujii and Higuchi, 1977; Scherler et al., 2011), an effect that has often been neglected in predictions of future water availability. Furthermore, this region is characterized by a large number of glacial lakes (Gardelle et al., 2011). Some of moraine-dammed glacial lakes are rapidly expanding by accumulating large quantities of water. Such lakes are susceptible to catastrophic outburst floods, called Glacial Lake Outburst Floods (GLOFs; e.g., Richardson and Reynolds, 2000; Bajracharya and Mool, 2009; Benn et al., 2012) with potential consequent loss of human lives and properties in the downstream valley. There were already some devastating GLOFs events in Mt. Everest region in past, for example, Nare (1977), Dig Tsho (1985), Tam Pokhari (1998) (Fushimi et al., 1985; Yamada and Sharma, 1993; Bajracharya et al., 2007).

We realized that an integrated knowledge on climatic, glaciologic, and hydrologic components (Fig. 1 & 3) at fine-scale are inevitable for understanding their complete behaviour and future water availability in this region. For this reason, this thesis takes advantage of available data from ground stations, gridded, and reanalysis climate products, and satellite observations for exploring the nexus between evolving state of the climate, glaciers, lakes, and river flow in a medium-scale glacierized basin. A general outline of this study, with methods and datasets for analysis of different components, is presented in Figure 1.

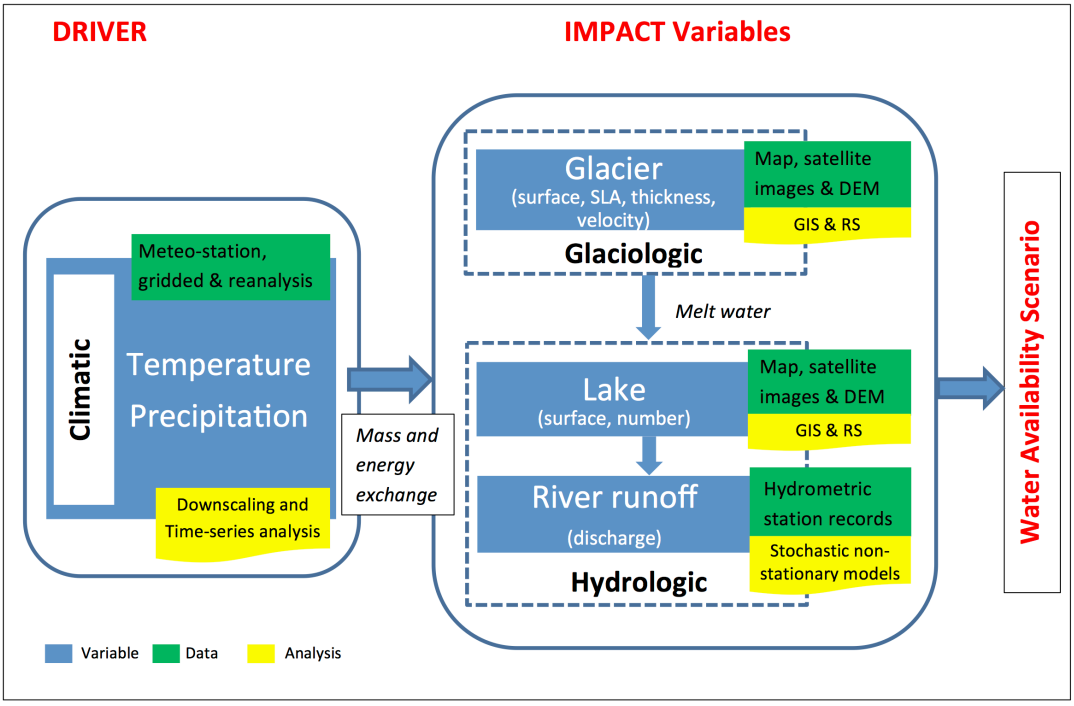

Figure 1. Schematic diagram indicating all research components: Climatic, glaciologic, and hydrologic in a unidirectional conceptual framework.

1.2 Aim and Objectives

This study is focused on linking the glacio-hydrological response to climate variability in the monsoon-dominated glacierized basin in the south slope of Mt. Everest region, with the aim understanding the behaviour of the hydrological process and future water availability.

The main objective of the study is achieved by addressing these specific two objectives:

a) *Driver*: To evaluate the climatic trends (temperature and precipitation) and their variability;
b) *Impact*: To enumerate how the climate variations streamlining the state of glaciers, evolution of the glacier lakes, and river discharge system (hydrological process).

To address these objectives, this research identifies several key questions, in specific, represented in the following questions:

1) How do the climate variables (temperature and precipitation) behave at local scale?
2) What are the status, trend and morphometric behaviour of glaciers since 1960s to recent time?
3) How do the glacier lakes evolving since the 1960s to recent time?

4) Which climate variable play vital role in glacier and lake variation and the severity of impacts on them?
5) How do the changes in glacier melt runoff influences the river discharge?

1.3 Study Area

1.3.1 Geographical Settings

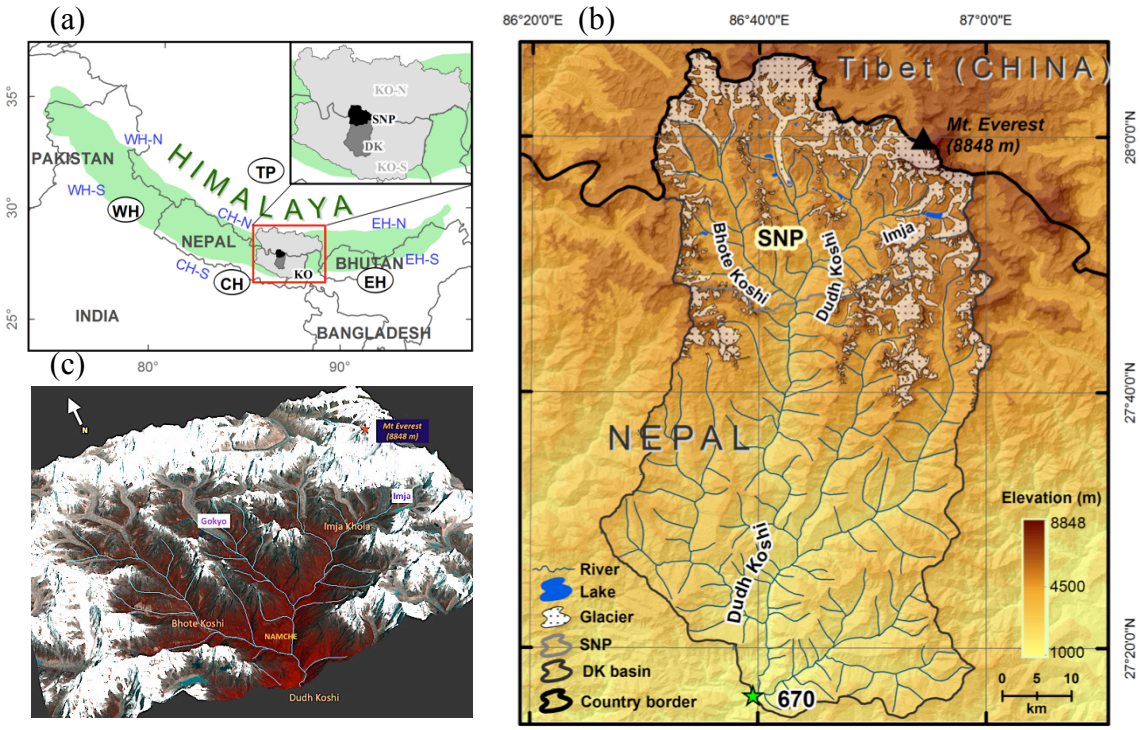

Figure 2. Location of the reference study site: Mt. Everest region in Nepal Himalaya. **(a)** The study site in a map of the Himalaya range. The abbreviations EH, CH, WH, and TP represent the eastern Himalaya, central Himalaya, western Himalaya, and Tibetan Plateau, respectively (suffixes –N and –S indicate the northern and southern slopes); Inset is a plot for the Koshi basin (KO) indicating the Sagarmatha (Mt. Everest) National Park (SNP) and the Dudh Koshi (DK) river basin; **(b)** The focused map of the DK basin (in reference to 670 discharge station, the outlet), locating the SNP, glaciers and lakes in 2011; **(c)** 3D perspective view of the SNP as seen from the Landsat 8 OLI image of 10 October 2013.

This study is focused on Mt. Everet region, in particular, in the Sagarmatha (Mt. Everest) National Park (SNP; 27.75° to 28.11° N; 85.98° to 86.51° E; Fig. 2). Covering an area of 1148 km^2, the SNP is the highest protected mountain area in the world. Nestled in the upper Dudh Koshi river basin (area: 3717 km^2), the SNP is situated in the Northeast of Nepal, corresponding to the southern slope of central Himalaya. Placing the SNP in central interest, this study also takes different geographic domains as reference sites – the Dudh Koshi river basin, the Koshi river basin (covering both north and south of the Mt. Everest), and whole central Himalaya – for different research components (Fig. 2 & 3) and referred them frequently in this thesis. Further, references are taken from some other

parts of the Himalaya for comparison. The glaciers and lakes variation were studied, in particular, within the SNP; the climatic analysis performed for the SNP, the Koshi basin, and the central Himalaya; and the hydrological analysis was conducted at the Dudh Koshi and other basins within the Koshi basin.

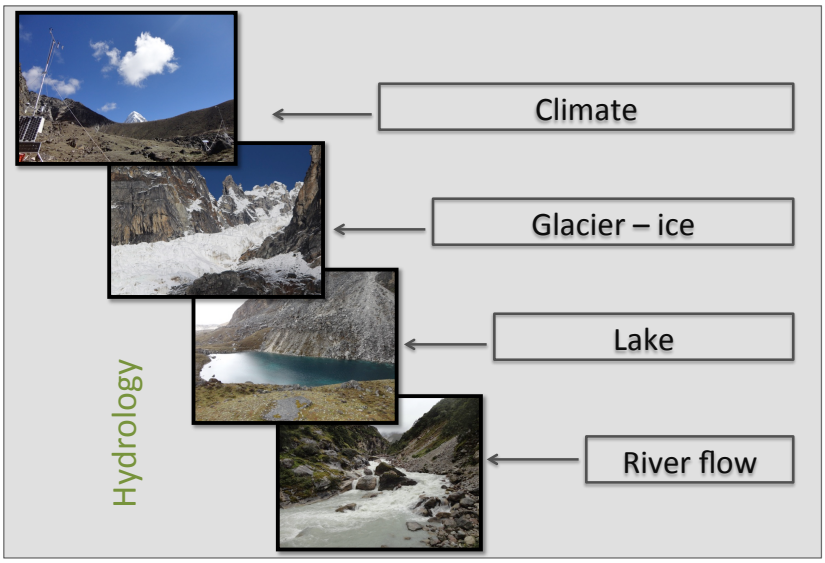

Figure 3. Different components covered in this study. All photographs are taken from the Sagarmatha National Park (SNP) in the central Himalaya.

1.3.2 Glacio-Hydrology

The Dudh Koshi river originating through melting of snow and glacier ice in the high mountains in the SNP and flowing towards the south, is one of the main tributaries of the Koshi river that contributes to Ganges river. This region is one of the heavily glacierized parts of the Himalaya. Bajracharya and Mool (2009) indicated that there are 278 glaciers in the Dudh Koshi basin, with 40 glaciers accounting for most of the glacierized area (70 %) and all of these being valley-type. Land cover classification shows that almost one-third of the territory characterized by glaciers and ice cover (Salerno et al., 2008; Tartari et al., 2008), while less than 10 % of the park area is forested (Bajracharya et al., 2010). Most of the large glaciers are debris-covered type (i.e., d-type), with their ablation zone almost entirely covered by surface debris (Fujii and Higuchi, 1977; Scherler et al., 2011). Several debris-covered glaciers have stagnant ice at their terminus that is potential to develop widespread melting ponds and build up moraine-dammed lakes (Bolch et al., 2008; Quincey et al., 2009).

The southern side of the Mt. Everest is the region that is most characterized by glacial lakes (Gardelle et al., 2011). They are very vulnerable to climate change and some of them, like Nare, Dig Tsho, Tam Pokhari have already experienced GLOFs in 1977, 1985, and 1998 respectively (Fushimi et al., 1985; Yamada and Sharma, 1993; Bajracharya et al., 2007). All glacial lakes plotted by Tartari et al. (2008) on the 1992 topographic map for

the northeastern sector of Everest region indicates the distribution of the glacial lakes between 4460 m and 5560 m in altitude, with the maximum frequency of altitude distribution falling between 5100 m and 5300 m.

1.3.3 Climatic Characteristics

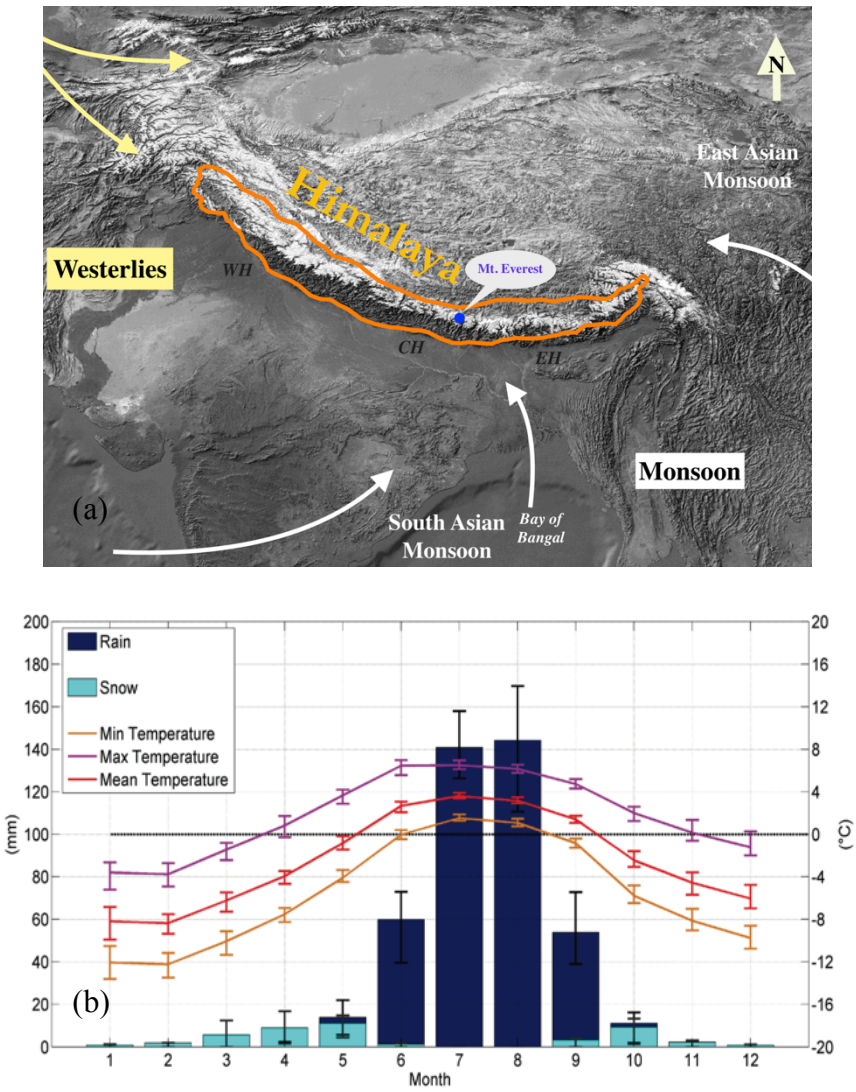

Figure 4. Climatic characteristics of Mt. Everest region. **(a)** Directions of the wind during monsoons and the mid-latitude westerlies; EH, CH, and WH represent the eastern, central, and western Himalaya, respectively; the map prepared based on concept from Ichiyanagi et al. (2007). **(b)** Mean monthly cumulative precipitation subdivided into snowfall and rainfall and minimum, maximum, and mean temperature at 5050 m asl. (reference period 1994–2013); The bars represent the 1σ (standard deviation); Figure from *Article I*.

The South Asian monsoon and the mid-latitude westerlies control the climate of Mt. Everest region. Furthermore, a significant interannual climatic variability associated with El Nino Southern Oscillation can be observed in the region (Owen and Benn, 2005; Ichiyanagi et al., 2007). The relative importance of the South Asian monsoon and the mid-latitude westerlies varies along the Himalaya (Benn and Owen, 1998). The prevailing

direction of the monsoon is South-North and Southwest-Northeast (e.g., Rao, 1976; Ichiyanagi et al., 2007; Fig. 4a). The monsoon is strong on the eastern and southern slopes of the Himalaya resulting maximum precipitation during summer, while the mid-latitude westerlies deliver heavy snowfalls during winter in western and northern Himalaya (Benn and Owen, 1998).

The data records from the Automatic Weather Stations (AWSs) at the Pyramid Observatory Laboratory (27.96 N, 86.81 E; elevation 5050 m asl.) in the SNP from 1994 to 2013 (Fig. 4b, from Article I) show an annual mean temperature of -2.4 ± 0.5°C and a total annual precipitation of 449 ± 75 mm a^{-1}, with about 90 % of the annual precipitation amount recorded during the summer months (June–September) during the monsoon and very minimal during winter by mid-latitude westerly wind. Thus, the glaciers in this region are identified as summer–accumulation type, fed mainly by the monsoon precipitation (Ageta and Fujita, 1996; Tartari et al., 2002; Fig. 4b). The temperature decreases with altitude (5.9 °C km^{-1}) and the precipitation increases (1160 mm km^{-1}) until ~ 2600 m and decreases afterwards, along the Dudh Koshi valley.

2

Climatic Trend and Climate Variability

2.1 Introduction

Uncertainties related to glaciers shrinkage in the Himalaya are mainly attributable to the lack of measurements on both the glaciers and the climatic forcing agents (e.g., Bolch et al., 2012). This is associated with the remote location of glaciers, the rugged terrain, and a complex political situation; all of these make physical access to the glaciers difficult (Bolch et al., 2012). Long-term measurements of climatic parameters at high elevation area are challenging due to their remoteness and difficulty in accessing them, combined with the complications of operating AWSs at these altitudes, (Vuille, 2011). Nearly all, global and regional climate models report increased sensitivity to warming at high elevations (e.g., Rangwala and Miller, 2012), while observations are less clear (Pepin and Lundqist, 2008). Moreover, changes in the timing or amount of precipitation are much more ambiguous and difficult to detect, and there is no clear evidence of significant changes in total precipitation patterns in most mountain regions (Vuille, 2011).

Existing few studies in the central Himalaya, mainly studying at lower elevation, have shown spatially non-uniform, but in general increasing temperature trend since 1970s (Shrestha et al., 1999; Kattel and Yao, 2013) and decreasing precipitation trend due to weakening of the South Asian monsoon (Sharma et al., 2000; Yao et al., 2012; Palazzi et al., 2013). In the higher elevations where the glaciers are located, the meteorological measurements rarely exist. For this reason, to interpret the glacier behaviour in term of climate has a considerable knowledge gap and thus, possible climatic impacts on the glaciers and ice melting have very high uncertainty. The longest time series from central Himalaya at above 5000 m (Mt. Everest region) is only around 20 years (after 1994 to until now) and only rarely stations available above 3000 m. In this regard, before interpreting any climatic impacts on the glaciers and hydrological process, it is essential to have a better understanding of the situation on a fine-scale.

The need of a detailed investigation is utmost importance in the southern slope of Mt. Everest due to concentration of large number of glaciers, presence of the widest altitudinal range on the earth, and lack of climatic data in the higher elevations. Moreover, various glacier studies (e.g., Salerno et al., 2008; Bolch et al., 2008a & 2011; Nuimura et

al., 2012; Nie et al., 2010), including our recent study (*Article II*), shows that the glaciers in this region are shrinking considerably in past decades. To date, there is no continuous meteorological time series able to clarify the causes of this shrinkage in the region.

This chapter, therefore, provides a complete assessment of climatic trends in term of temperature and precipitation in Mt. Everest region for understanding their roles in modulating glaciers, lakes, and river runoff, using the most recently available dataset from ground stations, gridded, and reanalysis products.

2.2 Data and Methods

2.2.1 Ground Stations Data

Temperature and precipitation data from 8 AWSs from a network of Pyramid Observatory Laboratory were used. These stations are in operation from an elevation of 2660 m (Lukla) to 7986 m (South Col) in the Dudh Koshi valley. Further, temperature and precipitation data of all stations in the Koshi basin (South) are used acquiring from the Department of Hydrology and Meteorology (DHM), Nepal. All those stations are located at around 100 m to 2650 m elevation. Among these data, we used 10 stations data for temperature and 19 stations data for precipitation considering the length of the series and the percentage of missing daily data. The stations having > 10 % missing data were discarded from the analysis. In addition, data from two more stations – Dingri (4302 m) and Nylam (3811 m) from the Koshi basin (North) – are used, obtaining from the Chinese Academy of Science (CAS). Details on these data are provided in *Article I*.

2.2.2 Gridded and Reanalysis Data

This thesis attempts to explore the climate trends and variability in the time extent as possible as early 1960s from recent years. A long-term climate data from ground stations at high elevations are unavailable in this part of the Himalaya. Due to lack of long data series, recently available gridded and reanalysis data are used for extrapolating climate. The "gridded data" refer to those data that are simply produced from an interpolation of data from the dense networks of ground-based stations to regular grids that could be at regional or global-level (e.g., Fan and van den Dool, 2008; Yatagai et al., 2012; Harris et al., 2014). The "reanalysis data" are those data that are produced through assimilation of observation data from multiple sources with an unvarying assimilation system (Rood and Bosilovich, 2010; Dee et al., 2014). During reanalysis, observation data are ingested at regular interval (6-12 hours) to the unvarying data assimilation system. Such reanalysis datasets are produced for a variety of applications (e.g., climate variability, process studies; Rood and Bosilovich, 2010).

Table 1. Gridded and reanalysis data with their specifications.

Product	Version	Temporal resolution	Spatial resolution	Period	Coverage	Data source	produced by	Web	Reference
(a) Atmospheric Temperature									
CRU	TS 3.20	monthly	0.5°	1901 - 2011	Global	land stations data	Climatic Research Unit (CRU) at the University of East Anglia	http://badc.nerc.ac.uk/view/badc.nerc.ac.uk__ATOM__ACTIVITY_3ec0d1c6-4616-11e2-89a3-00163e251233	Harris et al. (2014)
APHRODITE	V1204	daily	0.25°	1951-2007	60°E-150°E, 15°S-55°N	land stations data	APHRODITE (Asian Precipitation Highly Resolved Observational Data Integration Towards Evaluation of Water Resources) project in collaboration with the Research Institute for Humanity and Nature and the Meteorological Research Institute of the Japan Meteorological Agency	http://www.chikyu.ac.jp/precip/products/index.html	Yasutomi et al. (2011)
GHCN_CAMS		monthly	0.5°	1948- present	Global land (89.75S - 89.75N, 0.25E - 359.75E)	land stations data	Global Historical Climatology Network (GHCN) and Climate Anomaly Monitoring System (CAMS) data set at the Climate Prediction Center (CPC) of the National Centers for Environmental Prediction (NCEP).	http://www.esrl.noaa.gov/psd/data/gridded/data.ghcncams.html	Fan, van den Dool (2008)
NCEP CFSR	CFSv2	hourly	0.5°	1979- present	Global		developed by NOAA's National Centers for Environmental Prediction (NCEP). The data for this study are from NOAA's National Operational Model Archive and Distribution System (NOMADS) which is maintained at NOAA's National Climatic Data Center (NCDC)	http://cfs.ncep.noaa.gov/cfsr/	Saha et al., 2010
ERA Interim		6-hourly	0.75°	1979-present	Global		ERA-Interim is the latest reanalysis of ECMWF (European Centre for Medium-Range Weather Forecasts)	http://apps.ecmwf.int/datasets/data/interim_full_daily/	Dee et al., 2014
(b) Total precipitation									
CRU	TS 3.20	monthly	0.5°	1901-2011	Global	land stations data	CRU (Climate Research Unit) at the University of East Anglia	http://badc.nerc.ac.uk/view/badc.nerc.ac.uk__ATOM__ACTIVITY_3ec0d1c6-4616-11e2-89a3-00163e251233	Harris et al. (2014)
APHRODITE	V1101	daily	0.25°	1951-2007	60°E-150°E, 15°S-55°N	land stations data	APHRODITE (Asian Precipitation Highly Resolved Observational Data Integration Towards Evaluation of Water Resources) project in collaboration with the Research Institute for Humanity and Nature and the Meteorological Research Institute of the Japan Meteorological Agency	http://www.chikyu.ac.jp/precip/products/index.html	Yatagai et al. (2012)
GPCC	V6	monthly	0.5°	1901-2010	Global	land stations data	GPCC (Global Precipitation Climatology Centre) is operated by Deutscher Wetterdienst (National Meteorological Service of Germany) in the framework of the World Climate Research Program	http://www.esrl.noaa.gov/psd/	Schneider et al. (2013)
NCEP CFSR	CFSv2	hourly	0.5°	1979- present	Global		developed by NOAA's National Centers for Environmental Prediction (NCEP). The data for this study are from NOAA's National Operational Model Archive and Distribution System (NOMADS) which is maintained at NOAA's National Climatic Data Center (NCDC)	http://cfs.ncep.noaa.gov/cfsr/	Saha et al., 2010
ERA Interim		6-hourly	0.75°	1979-present	Global	Reanalysis	ERA-Interim is the latest reanalysis of ECMWF (European Centre for Medium-Range Weather Forecasts)	http://apps.ecmwf.int/datasets/data/interim_full_daily/	Dee et al., 2014

In this thesis, the processed station series of monthly mean surface air temperature and total precipitation are compared with the corresponding series derived from the global and regional gridded and reanalysis datasets. We used the CRU TS (Climate Research Unit - Time Series), APHRODITE (Asian Precipitation–Highly Resolved Observational Data Integration Towards Evaluation of Water Resources), GHCN–CAM (the Global Historical Climatology Centre, the Climate Anomaly Monitoring System), GPCC (Global Precipitation Climatology Centre), NCEP–CFS (National Centers for Environmental Prediction- Climate Forecast System), and ERA-Interim reanalysis of the European Centre for Medium- Range Weather Forecasts (ECMWF). In this way, four gridded (CRU, GPCC, GHCN–CAM, APHRODITE) and two reanalysis (ERA-Interim, NCEP–CFS) data products for temperature and precipitation were used. The datasets used in the current study are briefly described in Table 1.

2.2.3 Trend and Associated Significance Analysis

Using data from 8 AWSs in a network of Pyramid Observatory stations, we reconstructed daily temperature (minimum, maximum, and mean) and precipitation series (*Article I*) for the last twenty years (1994–2013) at 5050 m asl., hereafter referred as "reconstructed Pyramid series". The trends of climate variables, temperature and precipitation, for both reconstructed Pyramid series and other climatic series, were performed using the Sen's slope estimator (SS, Sen, 1968) and the associated significance computed by non-parametric Mann Kendall coefficient (Kendall, 1975). These statistics are considered a robust to detect trends in a series. The annual and monthly trends of temperature and precipitation were analysed for the reconstructed series for 1994–2013.

2.2.4 Downscaling of the Cimate Data

The spatial resolutions of the gridded and reanalysis data are coarse (more than 0.25° resolution) compared to our selected region of interest. Various downscaling techniques are available to convert global and regional climate outputs into local level, making them useful for hydrological impact studies (e.g., Hewitson and Crane, 1996; Fowler et al., 2007). The two approaches exist for downscaling of data, dynamical downscaling and statistical downscaling, exist for downscaling (Guyennon et al., 2013). The statistical downscaling is the most common method that uses statistical links between the larger and observed local scale weather (Frìas et al., 2006). In this study, we used a monthly quantile mapping for statistical downscaling of the gridded and reanalysis data at local scale (Guyennnon et al., 2013).

In order to evaluate the downscaling performance, we made the monthly quantile comparison. The downscaled climate series was used to extrapolate and evaluate climatic trends in the past, when the station data from the station. Further, these downscaled series was used for hydrological analysis in Chapter 5.

2.3 Summary of Article I

Weak precipitation, warm winters and springs impact glaciers of south slopes of Mt. Everest (central Himalaya) in the last two decades (1994–2013)

Given the paucity of observations, a great deal of uncertainty remains concerning climate changes at very high altitudes. In this respect, studies on recent climate trends from the Himalayan range are limited, and even completely absent at high elevation. In this study, we explored the small-scale climate variability of the south slopes of Mt. Everest by analysing the minimum, maximum, and mean air temperature and precipitation time series available from ground weather station data. Here we did not apply any gridded and reanalysis data. The study concentrated to the longest possible period (1994–2013) from the ground station data for high elevation (~5000 m). The ultimate goal of the study is to link the observed climate change patterns at high elevation with the glacier responses over the last twenty years, during which a more rapid glacier shrinkage was observed (*Article II*) in this region.

We reconstructed the minimum, maximum, and mean temperature and precipitation time series from seven AWSs located at elevations from 2660 to 5600 m a.s.l. over the last 20 years (1994–2013). A simple regression analysis based on quantile mapping (e.g., Déqué, 2007; Themeßl et al., 2012) and a multiple imputation technique (Schneider, 2001) were applied for reconstruction of the series for the location of Pyramid station. Then, we analysed these reconstructed series to explore the temperature and precipitation trend by Mann-Kendall test (Kendall, 1975) and Sen's slope (Sen, 1968). We compared this analysis with all existing weather stations located on both sides of the Himalaya range in Koshi basin.

Overall, at an elevation of ~ 5000 m, we observe that the main and most significant increase of temperature is concentrated outside of the monsoon period. The increasing trends were observed in both minimum and maximum annual air temperatures at higher elevations. The minimum temperature (0.072 ± 0.011 °C a^{-1}, $p < 0.001$) has increased far more than the maximum temperature (0.009 ± 0.012 °C a^{-1}, $p > 0.1$). The mean temperature increased by 0.044 ± 0.008 °C a^{-1}, $p < 0.05$. Temperature trends from the stations in the south and north of the Koshi basin confirms these trends. The minimum temperature is quite stationary and maximum temperature has significantly increased in the south, while in north both the temperatures have increased. In contrary, the maximum temperature trend at higher elevation are quite stationary. The 0 °C isotherm line of the maximum temperature has shifted significantly during the months- April, November, and December while no significant increase in the minimum temperature (that can influence glacier melt) is observed (Fig. 20).

The previous studies from the Himalaya have asserted likelihood of the South Asian monsoon weakening (e.g., Yao et al., 2012; Palazzi et al., 2013; Wagnon et al., 2013). We have confirmed the decreasing precipitation in this part of the Himalaya since early 1990s through the ground station data. We found a substantial precipitation decreasing (9.3 ± 1.8 mm a^{-1}, $p < 0.01$ during the monsoon). The annual rate of decrease at higher elevations is similar to that at lower altitudes on the southern side of the Koshi Basin, but the drier conditions of this remote environment make the fractional loss here much more consistent (47 % during the monsoon period).

This study contributes to a change perspective related to the climatic driver (temperature vs precipitation) led the glacier responses in the last 20 years. The main implications are the following: 1) the observed negative mass balances of glaciers in this region can be ascribed more to less accumulation due to weaker precipitation than to an increase of melting processes; 2) The melting processes have been favoured just during the winter and spring months and just close to the glaciers terminus; 3) A decreasing of the probability of snowfall is interesting significantly just the glaciers ablation zones (10 %, $p < 0.05$), but the phenomenon has a magnitude decidedly lower than the observed decrease of precipitation; 4) The less accumulation could be the cause of the observed lower glacier flow velocity and the current stagnation condition of tongues which in turn could have triggered melting processes under the debris glacier coverage leading to the formation of numerous supraglacial and proglacial lakes that have characterized the region in the last decades. Without demonstrating the causes that could have led to the climate change pattern observed at high elevation, we conclude by listing the recent literature on hypotheses that accord with our observations.

2.4 Gridded and Reanalysis Data

2.4.1 Comparison with Ground Station Data

In order to evaluate the gridded and reanalysis climatic data, first we compared reconstructed Pyramid data with them (Table 2 & 3). Figure 5 presents main gridded and reanalysis products and some selected ground observations of temperature and precipitation in the Dudh Koshi (670) and Tamor river (690) basins (Fig. 23). Two periods (before 1994 and after 1994) have been identified to make homogeneous comparison of precipitation (Table 2), while the lack of local long-term temperature observation does only allow comparison for recent decades (Table 3). Priority has been given to the Pyramid reconstruction in setting recent period (1994-2010) as it is both the only dataset available at high altitude and the only data set not involve in the overall gridded and reanalysis production.

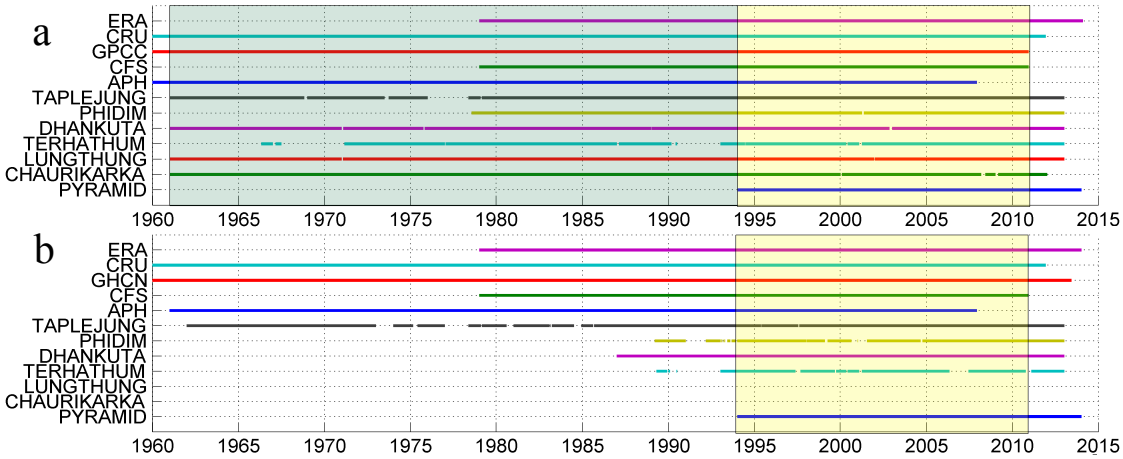

Figure 5. Comparison of main gridded and reanalysis products and some selected ground observations on available length of data for **(a)** precipitation and **(b)** temperature.

In Table 2, the gridded and reanalysis data are compared with the station time series, the reconstructed Pyramid and Chaurikharka, for the 1994-2010 and the 1961-1993 periods for precipitation. The comparisons indicate the highest values of R^2 for GPCC both for the location of the Pyramid and Chaurikharka station (R^2 = 0.52 and 0.97, respectively), suggesting that the GPCC represents the precipitation trend better than other series. It further indicates that the precipitation has increased from 1961 to 1993 by 6.1 mm a^{-1}, while from 1994 to 2010, the precipitation decreased by the same rate (6.1 mm a^{-1}). Table 3 presents a comparison between the different gridded and reanalysis series with the reconstructed Pyramid series for minimum, maximum, and mean temperature. The trends from temperature series of all products strongly suggest an increasing of the temperature in 1994-2013, further indicating that ERA-Interim represent temperature trend relatively better than other series (R^2 = 0.91).

Table 2. Mean bias, coefficient of determination (R^2), and trends in term of Sen's slope (SS) computed for precipitation from the gridded and reanalysis data, compared with the observed station data (OBS) at Pyramid (5050 m) and at Chaurikhark (2660 m) for two periods: 1994–2010 and 1961–1993.

Precipitation			OBS	ERA	CFS	GPCC	CRU	APH
670 (1994–2010)	Pyramid	Mean bias		+1428	+1949	+1182	+1149	+258
		Annual R^2		0.33	0.04	0.52	0.34	0.43
		SS	-16.0	-18.7	+24.8	-6.1	+2.3	+1.2
	Chaurikhark	Mean bias		+100	-1699	-469	-501	-685
		Annual R^2		0.18	0.37	0.97	0.43	0.68
		SS	-7.9	-10.7	+0.4	-6.1	+2.3	+0.7
670 (1961–1993)	Chaurikhark	Mean bias		-155	-1826	-511	-539	-657
		Annual R^2		0.04	0.59	0.78	0.46	0.16
		SS	+1.0	+15.6	+4.0	+6.1	-4.9	+3.9

Table 3. Mean bias, coefficient of determination (R^2), and trends in term of Sen's slope (SS) computed for minimum, maximum, and mean termperature from the gridded and reanalysis data compared with the observed station data (OBS) at Pyramid (5050 m) in 1994–2010 period.

(a)	Min temperature			Max temperature		
	OBS	ERA	CFS	OBS	ERA	CFS
Mean bias		+6.6	-5.0		+3.7	-1.4
Annual R^2		0.87	0.72		0.83	0.70
SS	+0.084	+0.067	+0.150	+0.050	+0.040	+0.087

(b)	Mean temperature					
	OBS	ERA	CFS	GHCN	CRU	APH
Mean bias		+7.7	-2.5	+10.0	+12.4	-0.2
Annual R^2		0.91	0.81	0.85	0.89	0.84
SS	+0.065	+0.063	+0.122	+0.075	+0.055	+0.051

Figure 6 compares the different gridded and reanalysis series with the reconstructed Pyramid temperature and precipitation series (1994–2013) in terms of standardized anomalies. Gridded and reanalysis series were normalized (by their mean and standard deviation) over the 1960–1990 period and reported on the left axis, while Pyramid reconstruction has been normalized over the whole available period and is reported on the right axis. Plotting anomalies instead of absolute values, we are able to compare large-scale products (ranging from 0.25° to 0.75° resolution) and local data despite high elevation variability. In fact, the gridded and reanalysis cannot be representative of the local topography, in particular, for high relief areas such as the SNP, avoiding comparison of 2 m meteorological variables in term of both mean and variance.

Considering the past two decades, most of the products reproduce the observed abrupt precipitation reduction occurring in the mid-2000 as well as the temperature increase acceleration in the early 2000. Since the 1960s, all products, except CFS and Aphrodite, agree on a significant continuous increase temperature accelerating during the past decade. We can also note that the two products starting before 1960 present, decreasing temperature until the mid 1960, even if, no ground observation can support these data in the region. Concerning precipitation since 1960s all products (except, CFS and ERA-Interim starting in the late 1970s) shows a global stationarity (characterized by the numerous changing point indicated by the crossing progressive and retrograde sequential Kendall's tau coefficients) and a recent reduction.

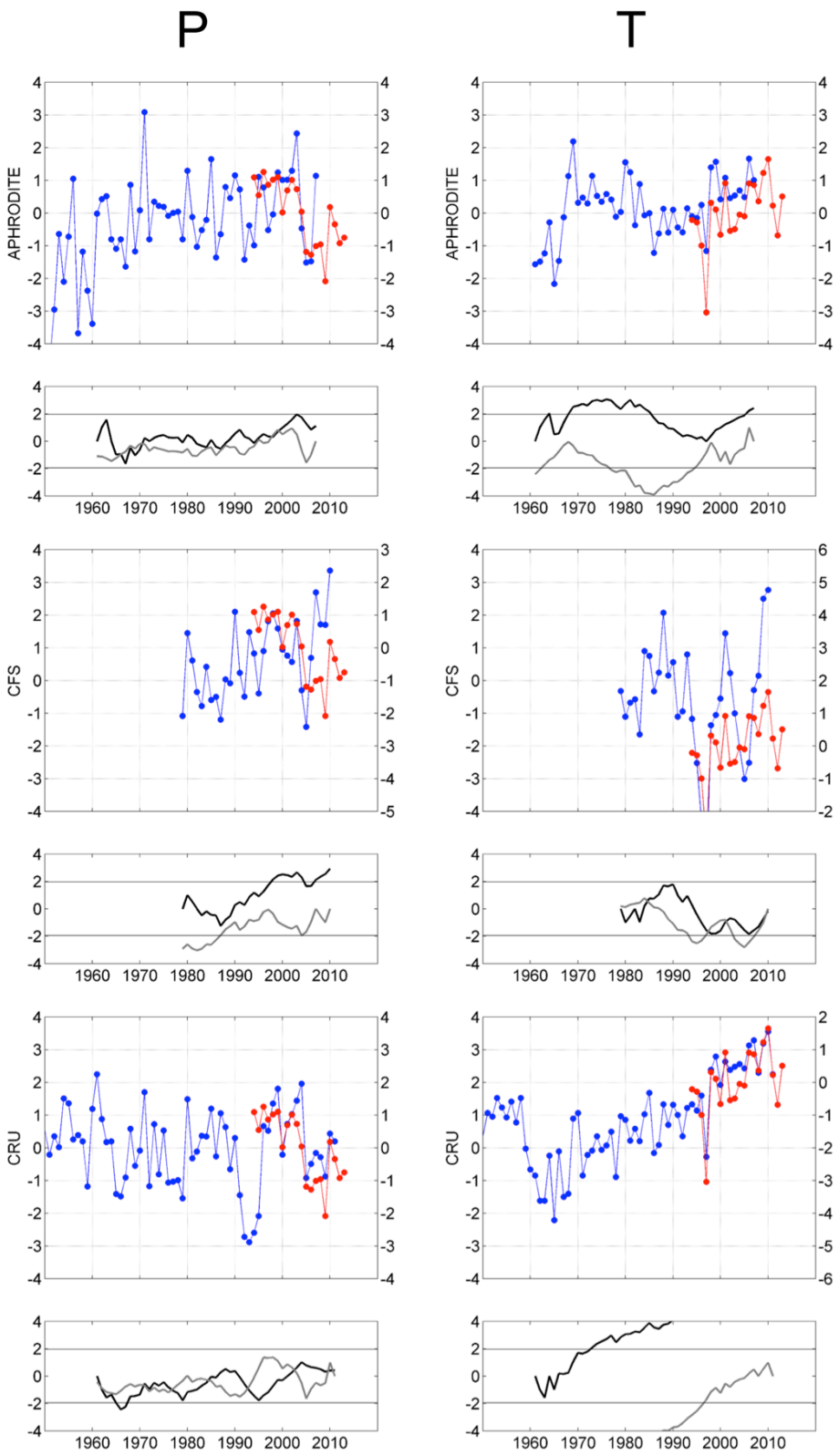

Figure 6. To be continued in next page.

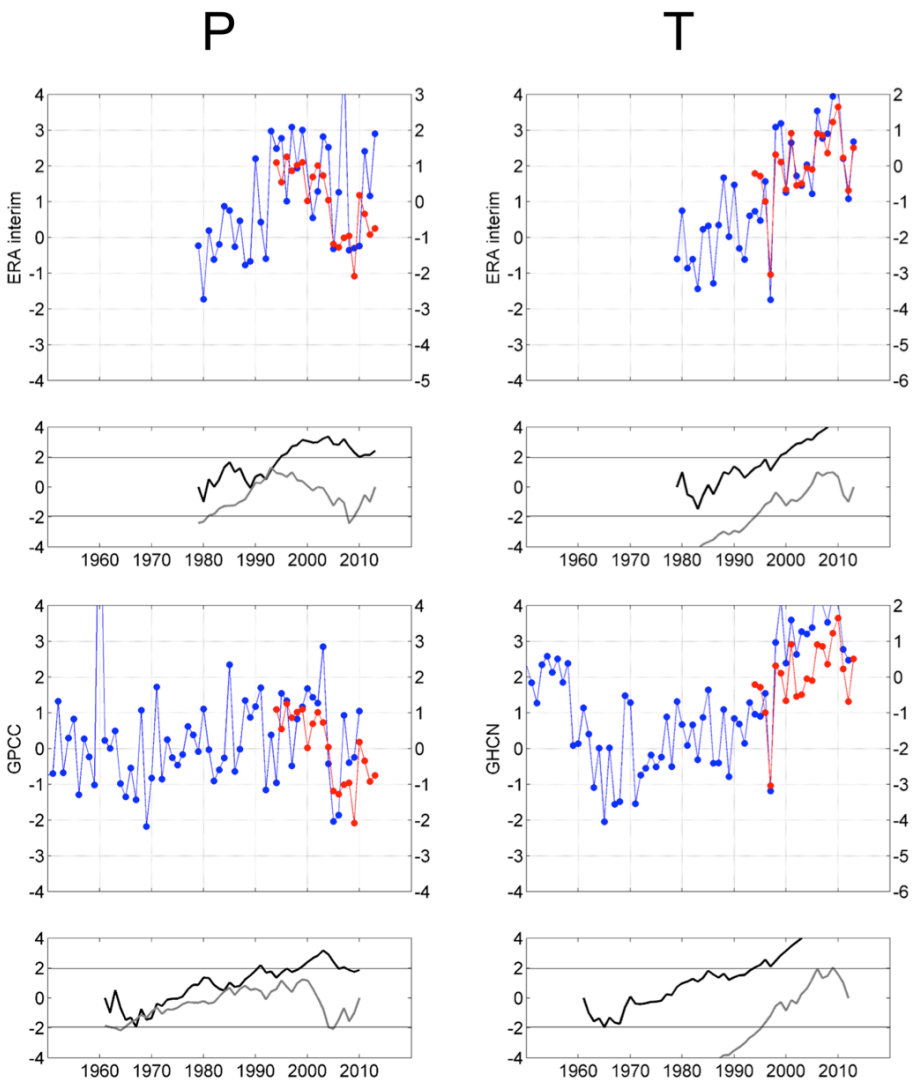

Figure 6. Comparison of the temperature (T) and precipitation (P) annual variability and associated non-stationarity between main gridded and reanalysis products and the Pyramid reconstruction. For each product, the upper plot present annual standardized anomalies (blue lines, left axis) compared with the Pyramid reconstruction anomalies (red line, right axis), while the lower plot reports the progressive (black line) and retrograde (grey line) sequential Kendall's tau coefficient of the gridded and reanalysis products starting in the 1960 when available.

The comparison of different gridded and reanalysis data for temperature and precipitation indicates that the ERA-Interim data does well reproduce the observe trend seasonality for temperature for both the Pyramid and the Koshi basin, while GPCC better reproduce precipitation trend seasonality (Fig. 7). ERA-Interim well reproduce most of the mean and minimum temperature trend seasonality and amplitude observed at Pyramid during the past two decades, as the relatively stationary during the warmer month (monsoon) and the warming during the pre-monsoon period until April, but underestimates the post mooson trend in particular, in November and December. Moreover, the observed relative lower trends in maximum temperature than mean and minimum are well reproduced, even if slightly anticipated during the pre-mooson.

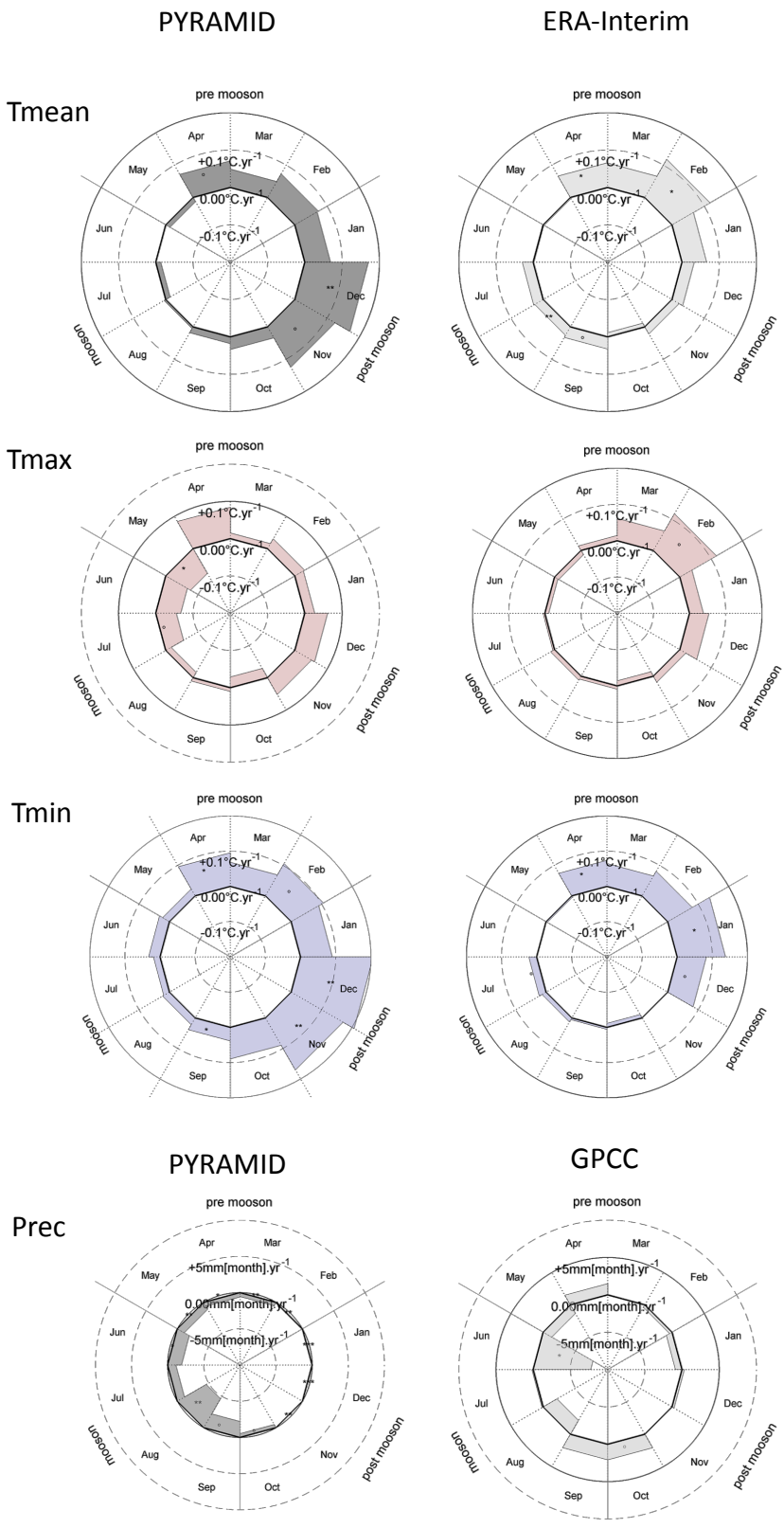

Figure 7. Polar plots of Monthly Sen's slope (SS) for mean, maximum, and minimum temperature (Tmean, Tmax, and Tmin, respectively), and precipitation (Prec) from reconstructed Pyramid series and the closest ERA-Interim (for temperature) and GPCC (for precipitation) nodes over the past two decades (1994–2013).

2.4.2 Downscaling and Evaluation of Temperature Data

The gridded and reanalysis data have a coarse grid resolution (ranging from 0.25 to 0.75°). As a result, they have bias over our study area (Table 3) and unable to represent directly local scale characteristics and such series cannot be applied for quantitative analysis, for instance, glacier melt computation. Thus, ERA-Interim and APHRODITE temperature series are statistically downscaled over the Dudh Koshi basin (670) using the monthly quantile mapping (e.g., Guyennon et al., 2013). The downscaling results for ERA-Interim temperature (Minimum, Maximum, and Mean) are presented for the period 1994-2013 (Fig. 8). Each downscaled time series are compared in term of monthly quantiles for validation.

(a) Minimum temperature

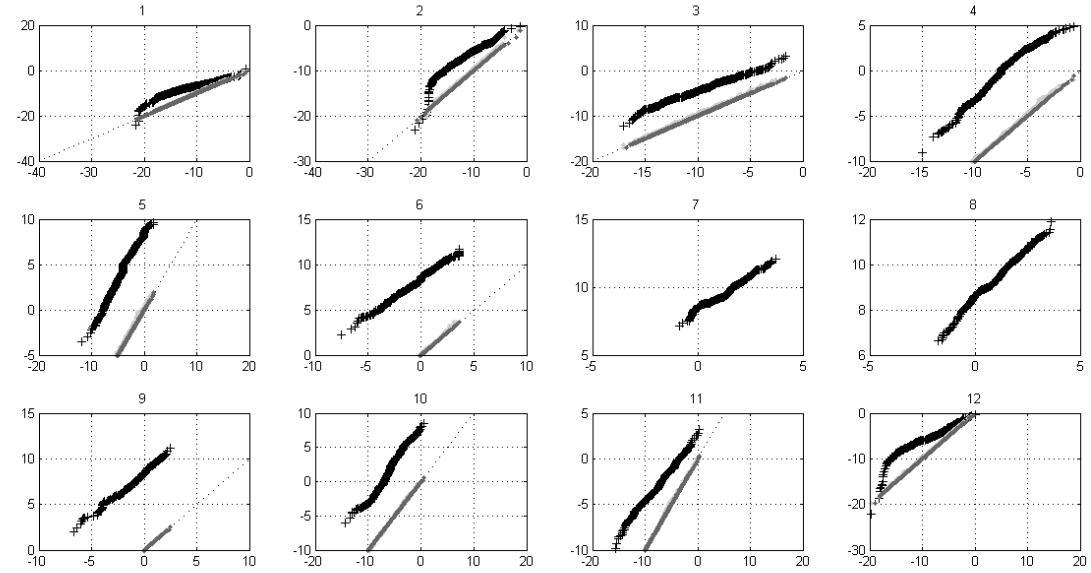

(b) Maximum temperature

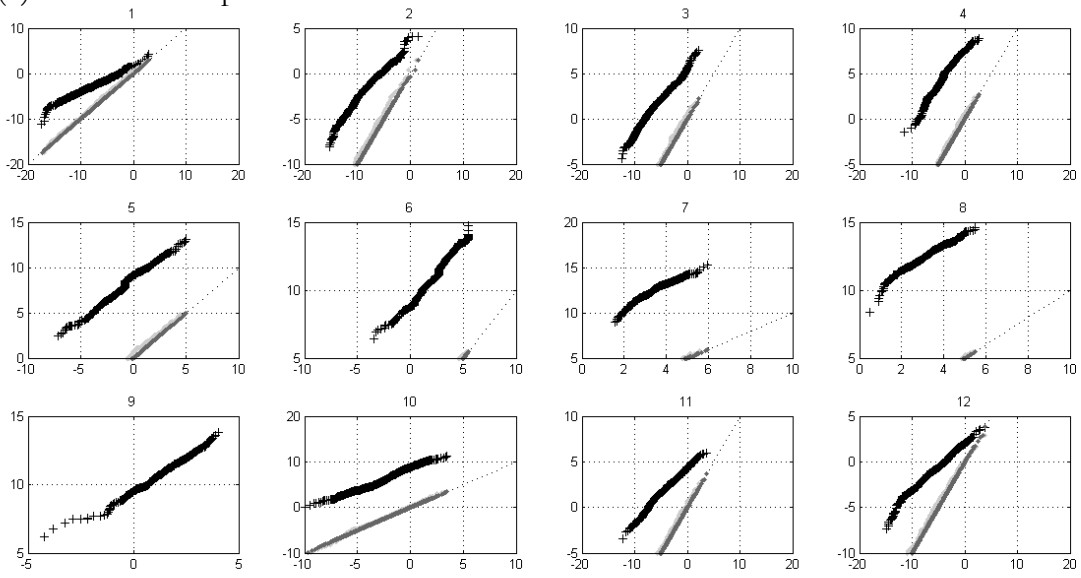

Figure 8. To be continued in next page.

(c) Mean temperature

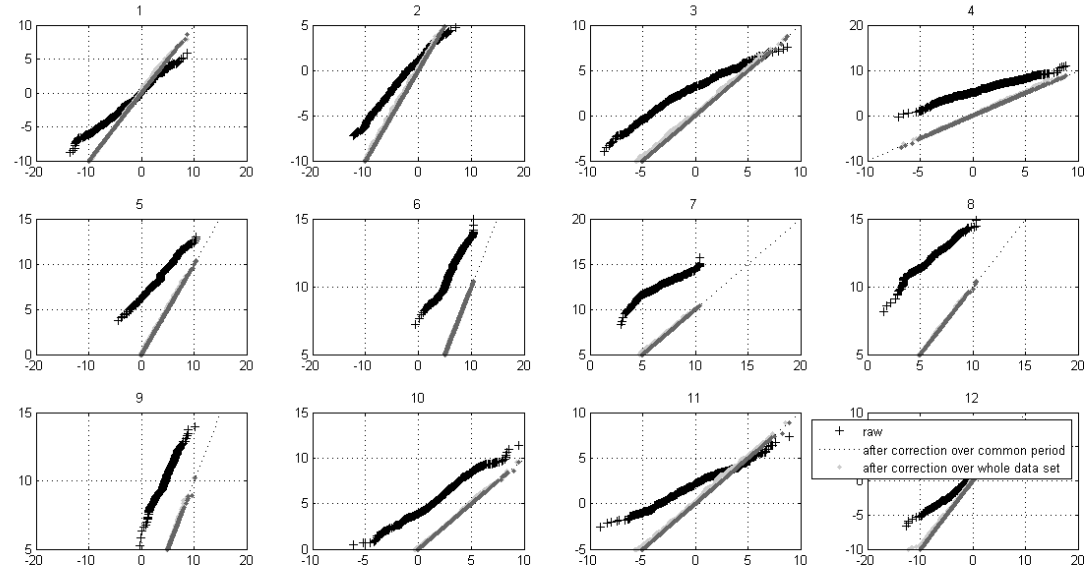

(d) Reconstructed Pyramid and ERA-Interim

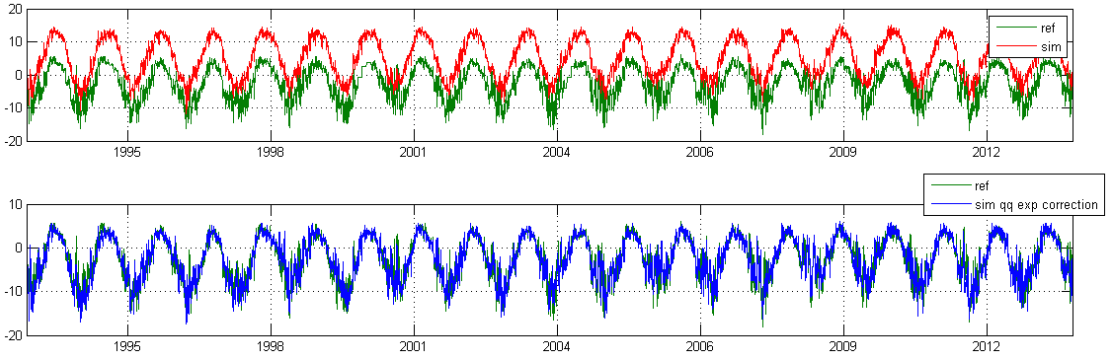

Figure 8. Downscaling of ERA-Interim temperature for Dudhkoshi (670). Monthly quantile comparison of the downscaled ERA-Interim time series with the reconstructed daily mean tempearature series of Pyramid: **(a)** Minimum Temperature; **(b)** Maximum Temperature; and **(c)** Mean Temperature; Months are reported as 1 (January) to 12 (December); **(d)** Reconstructed daily mean temperature series of Pyramid and the ERA-Interim.

2.4.3 Temperature and Precipitation Trends and Variabilities

Table 4. Temperature trends for ERA-Interim and APHRODITE (APH). Significance levels: ° $p = 0.1$; * $p = 0.05$; ** $p = 0.01$; *** $p = 0.001$.

Period	ERA min	ERA max	ERA mean	APH mean	PYRAMID
1961-1978				0.088*	
1979-1993	0.029	0.000	0.028	-0.051	
1994-2013	0.053*	0.033°	0.052*		0.044*
1994-2007				0.070*	
1979-2013	0.029**	0.031**	0.052***		
1961-2007				0.016*	

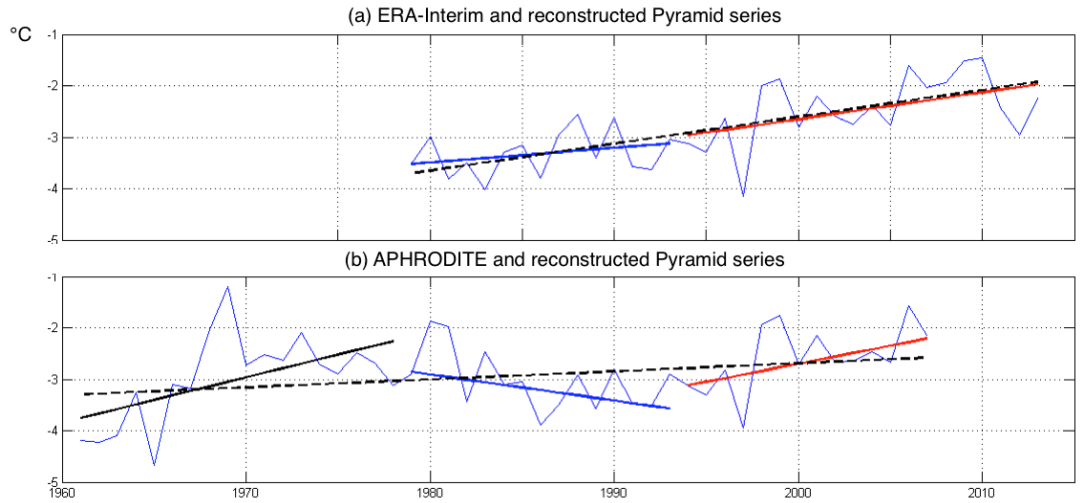

Figure 9. Temperature trends computed from reconstructed Pyramid, ERA-Interim, and APHRODITE.

The ERA-Interim (minimum, maximum, and mean) and APHRODITE (mean) temperature both show and increased temperature in all periods, except by APHRODITE in 1979–1993. The ERA-Interim as demonstrated earlier is a representative than other for temperature in this region, indicates a significant increasing of mean temperature 0.052 °C a^{-1} in 1994–2013, close to the value of Pyramid reconstruction 0.044 °Ca^{-1} in 1994–2013. This further shows that the mean temperature increased by 0.052 °C between 1979–2013, exactly same as in 1994–2013, suggesting that there was no difference in the temperature increase rate during the analysed period, while APHRODITE show an increase of mean temperature of 0.016 °C a^{-1} (0.736 °C) in 1961–2007, but with varying rates over time (Table 4; Fig. 9).

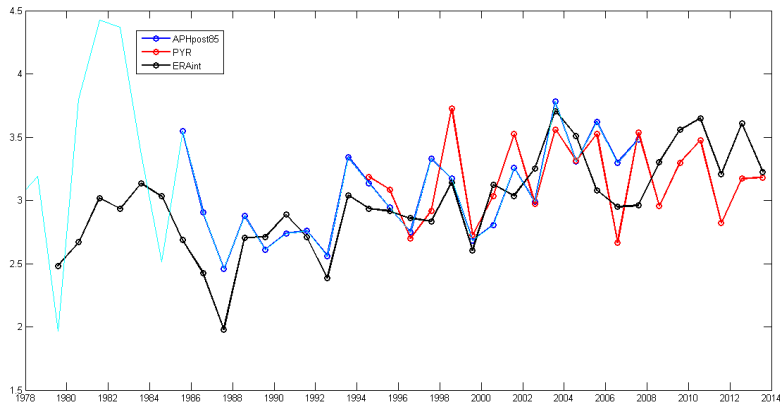

Figure 10. Interannual variation of August temperature for reconstructed Pyramid, ERA-Interim (ERAint), and APHRODITE after 1985 (APHpost85).

Except for APHRODITE, the rates of increase are often higher in the last decades compared to the previous. The APHRODITE shows an increase of the 0.088 °C a^{-1} in 1961–1978, which is dubious due to the data sources used for producing APHRODITE grids before 1980s. The APRHODITE data show the highest temperature records during August before 1985 (Fig. 10) when it shows substantially high temperature. In general, in

our region of interest, the analysis suggests an increasing trend of temperature over the whole analysis period, but for precipitation trend, we find an increasing trend until the beginning of 1990s and significantly decreasing trend that afterwards.

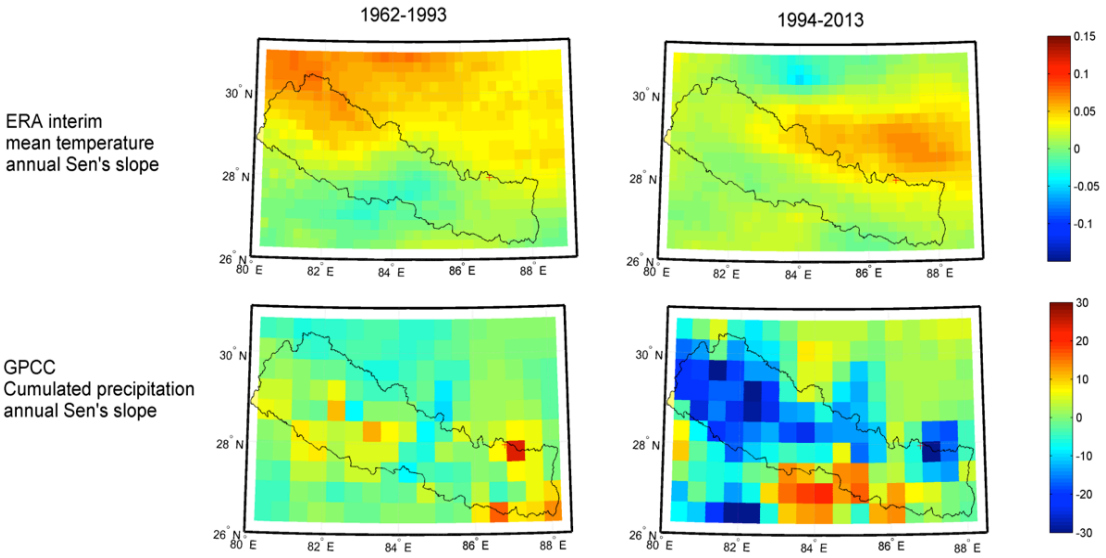

Figure 11. Spatial trend (Sen's slope) observed from the ERA-Interim temperature and GPCC precipitation. The ERA-Interim shows a global increase in temperature, higher in the North Slope compared to the South. The GPCC precipitation shows a decreasing trend in the South and stationarity in the North Slope.

In Figure 11, the spatial pattern of temperature and precipitation trends for two periods, 1962–1993 and 1994–2013, are presented for ERA-Interim and GPCC, respectively. The figure implies that temperature has increased for the first period (1962–1993) significantly on the northwestern part of the central Himalaya (Nepal) and beyond towards the Tibetan plateau. In both periods, temperature has continued to increase in Mt. Everest region. The increasing trend of temperature is slightly higher in the second period compared to first. The annual precipitation exhibited no any trend in the first period, although the tendency was toward slightly increasing annual precipitation in the southern part of the Himalayan ridge. In the second period, annual precipitation exhibited strongly decreasing spatial trend in the south of the Himalayan ridge. In particular, in Mt. Everest region, the figure clearly indicates an increasing precipitation trend in the first period and decreasing trend in the second period.

In this chapter, we presented the recent climate trends and variability without dealing with the issue of possible causes of the change – natural or human-induced – in the Mt. Everest region. Continuously, increasing of annual temperature from the 1960s and slightly increasing precipitation from 1960s to 1990s and decreasing precipitation after 1990s are confirmed, however, due to the spatial representativeness, some discrepancies exist between different gridded and reanalysis climate data products. We conclude by underlining that the observed changes in the climate, temperature and precipitation, is expected to have significant impacts on the glaciers and hydrological processes that is essential to explore further.

3

Recent Variation of Glaciers

3.1 Introduction

Glaciers are good indicators of ongoing climate change in high mountains. Any changes in the climate system are, thus, reflected into the glacier geometry (Kuhn, 1981; Oerlemans, 1994). Climate influences glaciers, most directly by changing the net inflow or outflow of mass– the mass balance. The changes in the climate system are expected to pose considerable threat to the glaciers (Kuhn, 1981; Beniston, 2003; Cuffey and Paterson, 2010).

The Himalaya glaciers are becoming of a key interest since last decade due to uncertainties about their status and the role they play in the water resources (Kaser et al., 2010; Immerzeel et al., 2010). The retreat of these glaciers could reduce the availability of water, but yet, we are still unable to quantify how much glacier variation is available in the Himalaya and at local-small scales with acceptable accuracy. A very few studies exist on the historical glacier variations in the Himalaya due to inaccessibility and the harsh weather conditions that limits the extensive field activities. After the release of the 4th assessment report of the IPCC in 2007, there were notable disagreements about the status of the Himalayan glacier shrinkage (Cogley et al., 2010; Bagla, 2009), but to some extend, progress has been achieved to improve the knowledge on them by involvements and interests of the global scientific community on their study (IPCC, 2013). Most of those studies are based on the remote sensing approach (Racoviteanu et al., 2008; Bolch et al., 2012; Yao et al., 2012) that offers an opportunity to cover a large area and a number of glaciers in a time efficient way. The glacier studies used a variety of remote sensing data that included topographic maps, aerial photography, satellite imagery, laser altimetry, and limited field-based measurements.

An increasing number of studies based on data from remote sensing and in situ observations suggest that the glacier shrinkage has been prevailing over the Himalaya in the past decades (e.g., Fujita and Nuimura, 2011; Bolch et al., 2012; Yao et al., 2012; Kääb et al., 2012; Gardelle et al., 2013). It has raised a major concern over their impact on hydrological process and water supplies to about 1.4 billion people in Asia (Immerzeel

et al., 2010). Furthermore, it is also expected to have concern for their impact on the global sea level rise (Jacob et al., 2012; Gardner et al., 2013).

In central Himalaya, in particular, in Mt. Everest region the glacier studies had begun in the 1960s (Müller 1959), but until early 2000s, there were only a few studies existing. Müller (1970) reported an inventory of glaciers in Mt. Everest region, which can be considered as a pioneering work in this field. The work was undertaken using map of the late 1950s on 1:50,000 scale (Schneider, 1967). After this work, Fujii and Higuchi (1977) elaborated further using the base inventory of Müller (1970). In 2001, the International Center for Integrated Mountain Development (ICIMOD; Mool et al., 2001) constructed a glacier inventory for whole Nepal, and thus also for SNP using multi-source data (satellite images, aerial photographs and maps). However, the inventory too, proved unsuitable as a basis of area comparison due to the multiplicity of their data sources and thus, cannot be attributed to a precise historical period.

In last decades, some studies have been carried out concerning the change detection, particularly, using remote sensing techniques, on glaciers properties in terms of elevation change (Bolch et al., 2011; Nuimura et al., 2012; Gardelle et al., 2013), flow velocity (Scherler et al., 2008; Bolch et al., 2008b; Quincey et al., 2009; Peters et al., 2010), and glacier surface area (*Surf*) and terminus (e.g., Salerno et al., 2008; Bolch et al., 2008a; Nie et al., 2010). In particular, Bolch et al. (2011) studied the mass change for 10 glaciers in the south of Mt. Everest and found that the glaciers have exhibited significant mass loss of 0.32 ± 0.08 m a^{-1} w.e. for 1970–2007 and 0.79 ± 0.52 m a^{-1} w.e. for 2002–2007. However, Gardelle et al. (2013) found less mass loss (0.41 ± 0.21 m a^{-1} w.e.) for 1999–2011.

Salerno et al. (2008), using the topographic maps of the late 1950s and early 1990s, prepared the glacier inventory and computed the glacier surface area change ($\Delta Surf$) in the SNP. They adopted the glacier codes proposed by the ICIMOD for tracing the glaciers extension at the end of the 1950s and early 1990s based on the Khumbu–Himal map (scale 1:50,000, Schneider, 1967), published in 1978 and the current Official Nepali map (scale 1:50,000, Survey Department of His Majesty's Government of Nepal, 1997), respectively. They reported 4.9 % surface area loss from 403.9 to 384.6 km^2. Their study further asserted that the large glacier facing south had experienced the increase in the glacier accumulation area. Some other studies based on field measurements have confirmed in this region that shrinkage of individual glaciers considerably since the 1970s (Higuchi et al., 1980; Yamada et al., 1992; Kodota et al., 1993; Fujita et al., 2001; Wagnon et al., 2013).

Therefore, with an effort to improve the knowledge on the glaciers status, we investigated variations of the glaciers since the 1960s to recent year in the SNP using optical satellite imagery and topographic maps.

3.2 Data and Methods

The minutiae on datasets and the methods implemented for the glacier study in Mt. Everest region is presented in *Article II and III*.

3.3 Summary of Article II

Tracing glacier changes since the 1960s on the south slope of Mt. Everest (central Southern Himalaya) using optical satellite imagery

Even though there are few previous studies existing on the glacier variations in the Mt. Everest region, none of them has considered a long time period and addressed sufficiently large geographic area for characterizing the basin's glaciers. Bolch et al. (2008a), for selected glaciers, and Salerno et al. (2008), using topographic maps of 1950s and 1990s, has analysed the surface area change ($\Delta Surf$).

In this paper, we have provide a comprehensive picture of the glacier changes by examining the different glacier variables on the southern slope of Mt. Everest from 1962 to 2011 considering five intermediate periods. We considered the 1960s as a beginning time for this study because data are mainly available from that time and most of the studies have indicated that climate change sensations was started from that time and thus, the glaciers are subject to change under such situation. We further evaluated the climatic and topographic control to the changes. The multi-temporal optical satellite imagery from different sensors (declassified Corona KH-4/KH-4B, Landsat MSS/TM/ETM/OLI, ALOS AVINIR 2, all available topographic maps, and the ASTER GDEM ver. 2 (30 m spatial resolution) were used to analyse the glacier changes. The most recent and established glacier analysis tools and techniques were applied for the glacier change study. The glacier change variables, 1) surface area (*Surf*), b) terminus, c) Snow-Line Altitude (*SLA*), and d) debris-covered area were investigated.

The investigated glaciers cover ~400 km^2 and present among the largest debris coverage (32 %) and the highest elevations (5720 m) of the world. We found an overall surface area loss of 13.0 ± 3.1 % (median 0.42 ± 0.06 % a^{-1}), an upward shift of 182 ± 22 m (3.7 ± 0.5 m a^{-1}) in Snow-Line Altitude (*SLA*), a terminus retreat of 403 ± 9 m (median 6.1 ± 0.2 m a^{-1}), and an increase of 17.6 ± 3.1 % (median 0.20 ± 0.06 % a^{-1}) in debris coverage between 1962 and 2011. The recession process of glaciers has been relentlessly continuous over the past 50 years (e.g., Fig. 12 & 13). Moreover, we observed that (i) glaciers with increased debris cover have experienced a reduced termini retreat. (ii) negative mass balances (i.e., upward shift of *SLA*) induce increases of debris coverage; (iii) slight, but statistically insignificant acceleration of the surface area loss since early

1990s; but a significant loss for the largest glaciers (> 10 km^2) that have accumulation zones at higher elevations and along the preferable South–North direction of the monsoon; (iv) a significant changes in SLA. Moreover, the largest glaciers present median upward shifts of the *SLA* that is nearly double than that of the smallest. To evaluate the role of climate drivers in the glacier response, we used a simple ELA-climate model (Kuhn, 1981). Using this model we estimated that for the observed 182 m upward shift of SLA in the 1962–2011 period, a temperature increase of 1.1 °C, or a precipitation decrease of 543 mm, or a solar radiation radiation increase of 1.8 MJ m^{-2} d^{-1} is required. Reviewing the previous studies on the temperature, precipitation, and solar radiation trends, we argued that the reported temperature increase in the period cannot justify the upward shift of SLA, but instead, the reported precipitation decrease in the last decades could have contributed in the SLA shift. Thus, we cocluded that Mt. Everest glaciers are shrinking continuously, not only due to warming temperatures, but also as a result of weakening Asian monsoons registered over the last few decades.

In the paper, we compared our findings on glacier surface and terminus changes with other studies in the high mountain Asia. The shrinkage of the glaciers in south of Mt. Everest is less than that western and eastern Himalaya, and southern and eastern Tibetan Plateau. The glacier's positions in higher elevations have likely reduced the impact of warming on these glaciers, but have not been excluded from a relentlessly continuous and slow recession process over the past 50 years.

3.4 Summary of Article III

Increased Imja Lake expansion as response to reduced Imja Glacier flow velocity (Mt. Everest region, Nepal)

In this paper, taking the reference for Imja Glacier and Imja Lake, we seek the nexus between contemporary variation of glacier properties and the lakes surface evolution. We selected Imja as case study considering that Imja Lake is one of the most potentially dangerous proglacial lakes (Yamada, 1998; Bajracharya et al., 2007; Fujita et al., 2009) and only lake that has shown a unique characteristic by continuous growth since early 1960s in the SNP (Somos-Valenzuela et al., 2014). We link increased Imja Tsho (Lake) with changes in Imja Glacier (area: ~25 km^2) under the effect of climate change.

The multi-temporal satellite imagery from different sensors (declassified Corona KH-4/KH-4B, Landsat MSS/TM/ETM/OLI, ALOS AVINIR 2, all available topographic maps, and the ASTER GDEM ver. 2 (30 m spatial resolution) were used to analyse the Imja Glacier and Imja Lake. Besides, these data, we used reconstructed Pyramid climate data (*Article I*). In additional to glacier change variables used in *Article II*, we further more studied (a) glacier elevation (thickness) change for 2001–2014 using ASTER stereo

scences (Paul and Haeberli, 2008; Bolch et al., 2011) and (b) flow velocity for 1992–2013 using Landsat scences (Kääb and Vollmer, 2000; Paul and others, 2013). For Imja Lake, detailed inter-annual and intra-annual surface area variations are examined. Furthermore, the temporal evolutions of supraglacial lakes on Imja Glacier were investigated.

Between 1962 and 2013, Imja Lake has expanded from 0.029 ± 0.010 km^2 to 1.352 ± 0.054 km^2 (0.026 ± 0.001 km^2 a^{-1}). Overall, surface area of Imja Glacier has decrease by 12.1 % (28.1 ± 0.5 km^2 to 24.7 ± 0.6 km^2) between 1962 and 2013, with an accelerated shrinkage after 1992 (0.04 ± 0.03 km^2 a^{-1} in 1962–1992 period, while 0.11 ± 0.05 km^2 a^{-1} in 1992–2013 period). Due to growth of Imja Lake, the glacier terminus has retreated more than 2200 m (~ 44 m a^{-1}). Despite the glacier terminus retreat and surface area loss, the glaciers have experienced the thickness loss and decreasing flow velocities. The evaluated glacier ablation areas indicate very low flow velocity or stagnant. The flow velocity of the glacier has decreased in the last period, compared to the previous period. The average glacier flow velocity was 37 ± 30 m a^{-1} in 1992–93; 31 ± 15 m a^{-1} in 2000–01, and 21 ± 15 m a^{-1} in 2013-14, indicating a reduction in the glacier velocity. An average glacier elevation change of -1.59 ± 0.71 m a^{-1} observed for 2001–14 period with a rate of -1.78 ± 0.80 m a^{-1} in 2008–14 and -1.40 ± 0.63 m a^{-1} in 2001–08 (Fig. 12).

The decreasing glacier flow velocity could be related to negative mass balance of the glacier. We underline that the decrease in velocity is mainly associated with reduced accumulation due to significantly decreasing precipitation in the last decades and increased ablation due to increasing of maximum temperature that effectively impact the glacier during the post-monsoon months. The decreasing glacier flow velocities and the increasing mass losses induce the formation and subsequent expansion of glacial lakes under a favourable topography as a boundary condition.

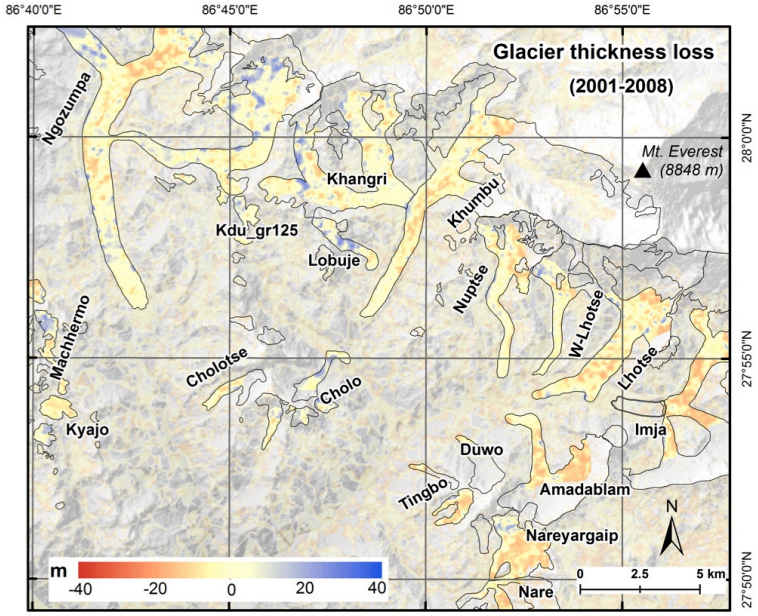

Figure 12. Elevation changes for the glaciers in 2001–2008.

3.5 Some More on Glacier Changes

3.5.1 Glacier Surface Area Change and Elevation

Despite the study presented in the foregoing two sections, some other glacier analysis results are the present in the following section.

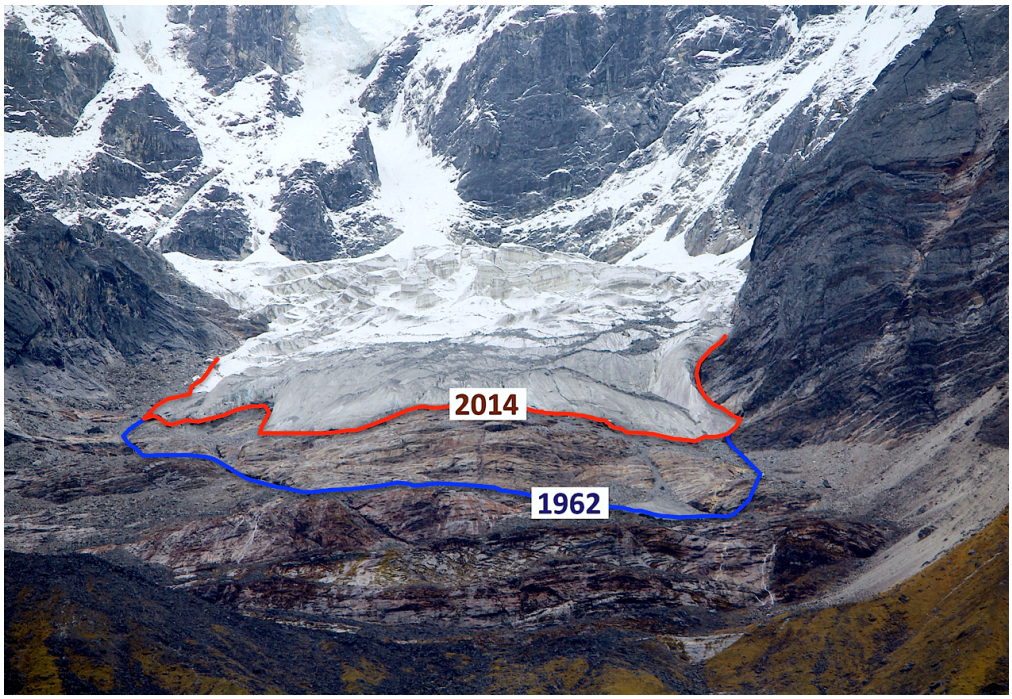

Figure 13. Glacier terminus position change: An example of a small-sized glacier (picture taken during a field work in September 2014). The tentative position of terminus is marked based on evaluation with Corona KH-4 image of 15 December 1962. The glaciers in this region have retreated in an average by ~ 400 m in the last 50 years (*Artcle II*).

Accumulation Area Ratio of glaciers had decreased from 0.66 to 0.58 between 1962 and 2011. Based on the slopes change along the glaciers' length, the glaciers in this region are characterized by two glacier zones: the lower glacier zone with gentle slope (Down_area), corresponding nearly to debris-covered ablation part, and upper glacier part with steep slopes (Up_area), corresponding nearly to accumulation area. The Up_areas of glaciers have decreased at an accelerated rate in the last two decades (Fig. 14).

Figure 15 presents the glacier $\Delta Surf$ of the SNP by elevation for two periods: 1962-1992 and 1992-2011. The comparison between them stresses an opposite trend: for 1962-1992, the main surface area reductions are below 5850 m, while there is an increasing surface area at higher elevation. For 1992-2011, a clearly decreasing of glacier surface area observed at all elevations. The decreasing glacier $\Delta Surf$ only in the lower elevation before 1990s and also along the higher elevation after 1990s, could be explained by the observed temperature and precipitation behaviours during those periods. In the first period (1962-

1992), the glacier area loss in the lower elevation could be a result of an increasing temperature, while an increasing precipitation favoured glaciers above 5850 m. In the second period (1992-2011), although loss of *Surf* in lower elevation was continued due to increasing temperature, a significant decreasing precipitation could have resulted the decreasing *Surf* in the higher elevations (above 5850 m). Exactly the same behaviour has been observed in individual case study of Imja Glacier (*Article III*). In conclusion, before 1990s, the glacier *Surf* has decreased mainly due to temperature, but after 1990s, the precipitation has augmented *Surf* loss impacting the accumulation area.

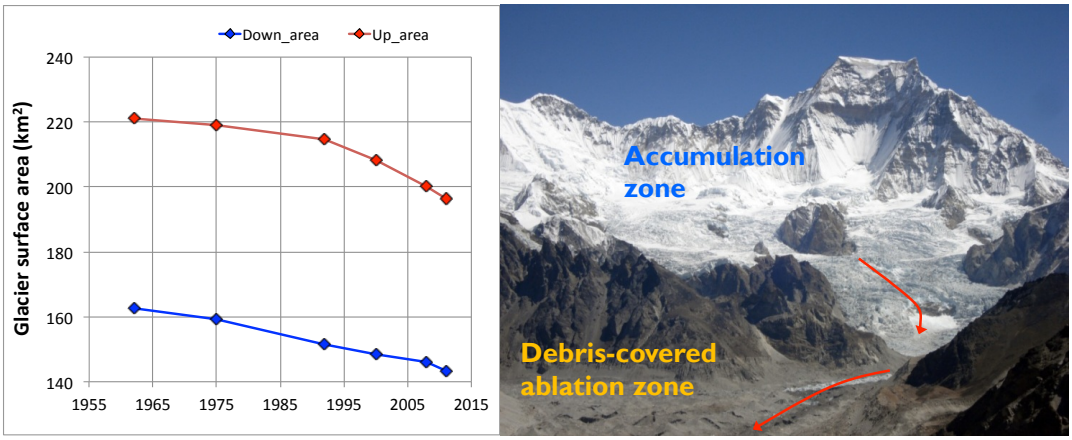

Figure 14. Accumulation and Debris-covered ablation zone. **(a)** Changes of upper and lower glacier zones (separated by slope change point); **(b)** Ngozumpa glacier: showing the accumulation and debris-covered ablation areas.

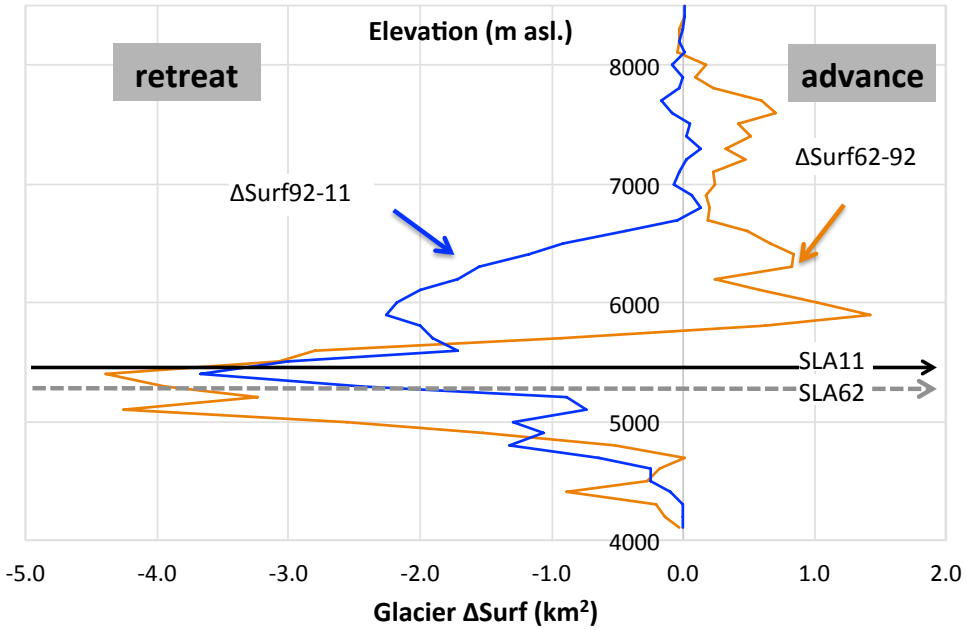

Figure 15. Glacier surface area changes (Δ*Surf*) by elevation in two periods: 1962–1992 and 1992–2011.

Here, we have to remember the response time of the glaciers, but unfortunately we don't have a known response time of the Himalayan glaciers yet investigated. The changes in climate, temperature and precipitation, influence the balance of the glaciers on a year-to-year basin, and ultimately determine glacier area through ice flow dynamics (Bahr et al., 1998; Cuffey and Paterson, 2010). The major changes in the glaciers in our case study were around the snow-line and in accumulation zone, in particular in the area above the abrupt slope change point of glaciers (Fig. 14). We assume that the glacier in these zones quickly response to the climate perturbations.

3.5.2 Glacier Change and Climate Nexus

The role of climate to shrinking glaciers has been issue of crucial interest to understand the future of glaciers. Following the main objective of exploring the nexus between the different components, we have examined and discussed the possible climatic drivers and the glacier shrinkage in specific details in *Article I, II,* and *III.*

In *Article I* possible connections are discussed between the observed shrinkage of glaciers, (Article II), the observed temperature increases, and precipitation decrease has been discussed. In the *Article II,* possible realationship between the SLA, a proxy for providing indications of local climate variability has been discussed. Climatic variables, such as temperature, precipitation, and solar radiation (e.g., Kuhn, 1981, Cuffey and Paterson, 2010), and the local topographic settings (e.g., Scherler et al., 2011; Pedersen and Egholm, 2013) influence the distribution of glaciers and their variations. The deviation in the individual glacier characteristics and variation can be attributed to the topographic control, while the general trend of shrinking glaciers implies the climatic impacts on the glaciers. In *Article III,* we discussed on the decreasing of glacier flow velocities as a result of decreased precipitation and increased ablation as a result of increased maximum temperature, triggered to the subsequent expansion of glacial lakes. In summary, we have observed an increasing temperature mainly during the pre-monsoon and winter months and increasing tendency of precipitation from 1960s to early 1990s and substantially decreasing afterward. On the other hand, the glaciers were shrinking continuously from 1960s to recent years, with an accelerated rate after 1990s. In this regards, the glaciers in the Mt. Everest region is not only impacted due to increasing temperature, but also as a result of the significant decreasing precipitation observed over the last few decades.

In this chapter, we presented the recent glacier variation in the SNP. The studies of different glacier properties in the Mt. Everest region suggest a worsening condition of the glaciers status in the past decades. We underline that it is further expected to continue these glacier shrinkage trends, if the observed past climatic trends would prevail in the future unless an abrupt change in climate occurs. Such shrinkage of glaciers in the region and over the Himalaya may have both climatic and hydrological implications.

4

Recent Evolution of Glacial Lakes

4.1 Introduction

Studies of abundance, size distribution, and changes of glacial lakes play a significant role in assessing the glacier and snow melt, biogeochemical cycles, and ongoing climate change (Shijin and Tao, 2014). Three types of glacial lakes can be distinguished, according to Ageta et al. (2000), in Mt. Everest region. They are (a) Supraglacial lakes, which develop on the surface of the glacier, (b) Proglacial lakes, which are moraine-dammed lakes and are in contact with glacier front, and (c) Unconnected glacial lakes, which are not directly connected with glaciers, but may have a glacier located in their basin (Fig. 16). Gardelle et al. (2011), considering supraglacial and proglacial lakes, noted that the southern side of Mt. Everest is the region that is most characterized by glacial lakes in the Himalaya. Little is known about the condition of formation, distribution, and evolution of these three types of glacial lakes in this region, even though they are considered as a suitable indicator for evaluating the impact of climate change at high elevation (Richardson and Reynolds, 2000; Benn et al., 2001).

Previous studies in Mt. Everest region addressed the evolution of lakes (Tartari et al., 2008; Gardelle et al., 2011; Lamsal et al., 2011; Somos-Valenzuela et al., 2014), their potential GLOF hazard or risk (Yamada, 1998; Bolch et al., 2008b; Bajracharya and Mool, 2009; Watanabe et al., 2009; Benn et al., 2012), and condition of formation (Benn et al., 2001; Fujita et al., 2009; Sakai et al., 2010) using field and remote sensing methods. Tartari et al. (2008) provided a complete review of the limnological studies carried out in Mt. Everest region. After the first pioneering work by Löffler (1969) in the 1960s, other studies focused on these lake environments only after the late 1980s. The research activities were initially addressed on the hydro-geochemical characterization of the lakes over a wide spatial extent (Tartari et al., 1998; Bortolami, 1998; Smiraglia, 1998). In seven expeditions conducted between 1989 and 1997, 48 lakes were visited (Tartari et al., 1998), leading to the identification of many temporary water bodies.

A first cartographic study was carried out to compile a lake cadastre using the Mount Everest map (scale 1:50,000, National Geographic Society, Washington D.C., 1988), which represented the lakes morphology of the Northeastern sector of the SNP in

December 1984 (Tartari et al., 1998). This initial cadastre was after 10 years integrated for the same territory with the Official Nepali map (scale 1:50,000, Survey Department of His Majesty's Government of Nepal, 1997) dated December 1992 (Tartari et al., 2008). Including this study of Tartari et al. (2008), some other studies revealed that areas of proglacial lakes increased on the south slopes of Mt. Everest (central Himalaya) since the early 1960s (Tartari et al., 2008; Bolch et al., 2008b; Bajracharya and Mool, 2009; Gardelle et al., 2011). Gardelle et al. (2011) found that strong increasing of lake surface area in this region (33 % in 1990 to 2009).

Studies have indicated that the current moraine-dammed or ice-dammed lakes are the consequences of coalesce and the growth of supraglacial lakes (Sakai et al., 2000; Fujita et al., 2009; Watanabe et al., 2009; Thompson et al., 2012). These growths of lakes pose a potential threat of the GLOFs (Reynolds, 2000; Richardson and Reynolds, 2000; Bajracharya et al., 2007; Benn et al., 2012) with the potential consequent loss of human life and property in the downstream valley. One of such proglacial lakes in Mt. Everest region, Imja Tsho (lake; hereafter referred as 'Imja Lake'), that evolved and in the continuing growth since the early 1960s, has been of great research interest due to its potential GLOF risk (e.g., Yamada, 1998; Mool et al., 2001; Bajracharya et al., 2007; Fujita et al., 2009).

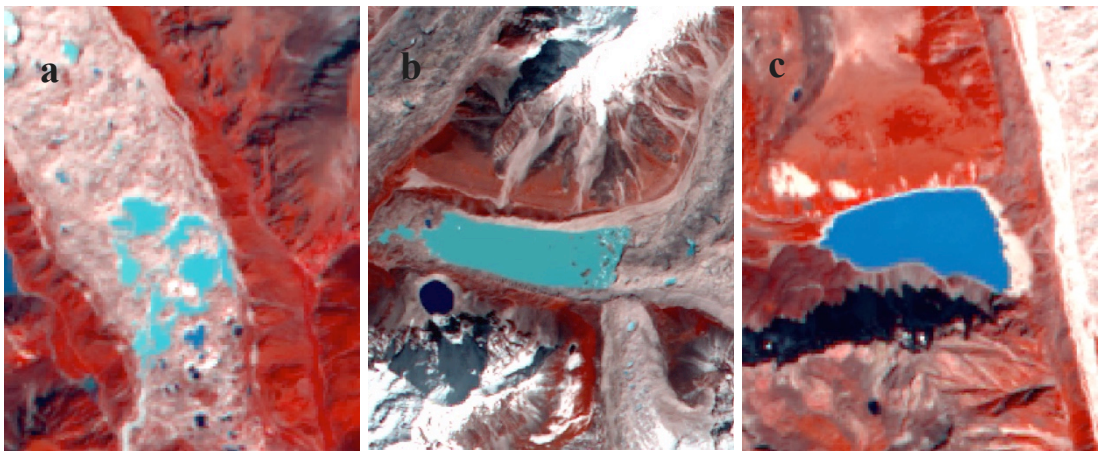

Figure 16. Three types of glacial lakes: **(a)** Supraglacial, **(b)** Proglacial, and **(c)** Unconnected lakes in the Sagarmatha National Park (SNP), as seen from Landsat 8 OLI image of 10 October 2013.

Considering these issues, in this study, we studied the distribution, condition of formation, and evolution of glacier lakes for the last 50 years, based on the satellite data and available topographic maps.

4.2 Data and Methods

The same datasets (satellite imagery from different sensors and topographic maps) as in the glacier study were used for lake mapping and their change detection in Mt. Everest region. Using these data, we were able to analyse the temporal evolution of unconnected, supraglacial, and proglacier lakes between 1960s and 2013. The ASTER GDEM ver. 2 was used for extracting morphometric information on lakes parameters.

The mapping of glacier lakes was conducted with both manual and semi-automatic methods. In *Article IV*, the manual method was used for lake delineation, while in subsequent analysis, semi-automatic method was used. In the semi-automatic method, the lake outlines were identified first, using the Normalized Difference Water Index (NDWI; [NIR - BLUE]/[NIR + BLUE], originally proposed by McFeeters (1996) and successfully applied by Bolch et al. (2008b) in our study region, then, applied manual post-correction for shadowed area and ice parts. When the NDWI method was not appropriate (like in, topographic map and panchromatic images), the lake boundaries were manually digitized.

We computed lake morphometric characteristics and surface area variation of lakes. In each analysis, a particular emphasize was provided for introducing the uncertainties of the measurements.

4.3 Summary of Article IV

Glacial lake distribution in the Mount Everest region: Uncertainty of measurement and conditions of formation

Glacial lakes show better, visible, and quick response to climate, making it possible to map long-term impact of climate change on glaciers and water resources. Following to previous work by Tartari et al. (2008), in this article, we made a complete mapping of the glacial lakes using a medium-high resolution ALOS imagery (October 2008) within the Sagarmatha (Mt. Everest) National Park (SNP). Supraglacial lakes were excluded in Tartari et al. (2008) cadastres because they were not deemed ecological relevant, in light of their rapid evolution and recent formation. In fact, such water bodies can be better defined as ice-melt ponds rather than fully-fledged lakes. Contrary to previous study, considering the accelerated process of deglaciation in the last decades, in this new cadastre (LCN 2008), we regarded it right to take a census also of supraglacial lakes and group them together according to the glacier they belong to.

In this paper, the attention was focused on the condition of formation of lakes, the greatest evidence of climate change impact at high altitude characterized by debris-covered glaciers. Such analyses are essential in studies of the impact of recent climate

change, and therefore the uncertainty of measurements is discussed with the aim of creating a reference study for use when glaciers and lakes are delineated using remote sensing imagery. A total of 29 glaciers (size > 1 km^2) with a surface area of 356.2 (±2 %) km^2 and 624 lakes of 7.43 (±18 %) km^2 surface areas were delineated. We examined in depth the underlining capability of the satellite imagery to properly characterize 64 % of lakes (error < 15 %) in terms of surface, whereas, concerning glaciers, this sensor allows correctly characterizing the whole resource (±2 %).

Regarding the formation process of supraglacial lakes, our findings confirm that the slope of the glacier where lakes are located is primarily responsible for the low flow velocity of this zone. Otherwise, this study is novel in its identification of a further boundary condition. The slope of the glacier upstream is able to influence both the low flow velocity and the high ablation rates at the glacier terminus. In fact, the imbalance between the two glacier zones generates the down- slope passage of debris, snow and ice. We found the slope of the glacier upstream to be inversely correlated with the relevant total surface of the lakes downstream. The multiple regression model developed in this study, considering the slopes of the two glacier areas distinctly, have been able to predict 90 % of the supraglacial lake surfaces. Concerning the surfaces of lakes not directly connected with glaciers (unconnected glacial lakes), we found they are correlated with the dimensions of their drainage basin, whereas no correlation was found with the glacier cover in the basin. Considering that the evaporation/precipitation ratio at these altitudes is approximately 0.34, the evolution of these lakes appears to be a helpful sign for detecting the precipitation trend of these high-altitude regions. In this paper, we further pointed out that changes in the flow velocities are one possible trigger for the formation of glacial lakes.

4.4 Temporal Evolution of Glacial Lakes

Table 5. Lake evolution in the 1963–2011 period.

Lake type	Number			Surface area (km^2)			
	1963	*1992*	*2011*	*1963*	*1992*	*2011*	*Uncertainty*
Supraglacial	216	252	453	1.373	1.344	1.555	±45 %
Proglacial	19	17	18	0.305	1.882	2.043	±7 %
Unconnected	102	126	155	4.394	4.153	4.131	±14 %
Total	337	395	626	6.047	7.378	7.789	±18 %

Note: Proglacial and Unconnected lake changes are presented until 2013 in the text.

Overall, the surface area of glacial lakes in the SNP has increased by 1.742 km^2 (28.9 %) from a total area of 6.047 km^2 in 1963 to 7.789 km^2 in 2011 (Table 5). Moreover, the numbers of lake are enormously increased from 337 to 626 (by 86 %). The new lakes have appeared at higher elevations (42 m higher than the lakes in the 1960s) following the glaciers retreat.

4.4.1 Supraglacial Lake

The debris-covered ablation part of glaciers in the Mt. Everest region holds many supraglacial lakes. Such lakes are very small in size, but numerous. Both numbers and surface areas of supraglacial lakes have increased (109.7 % and 13.3 %, respectively) in the SNP during the 1960s to 2011 (Table 5; Fig. 17). Due to their very small sizes, the associated uncertainties are large (±45 %). Such supraglacial lakes are ephemeral and very unstable in space and time as they can suddenly drain when they reach the sub-glacial drainage system (Benn et al., 2001). However, total surface area of the lakes was more or less stationary until 2000, but then after has increased rapidly.

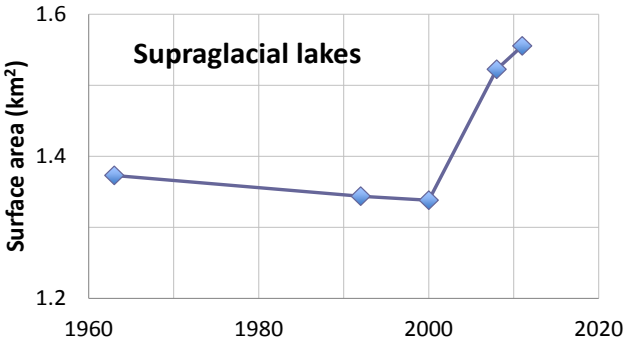

Figure 17. Temporal surface area change of supraglacial lakes in the Sagarmatha National Park (SNP) from 1963 to 2011.

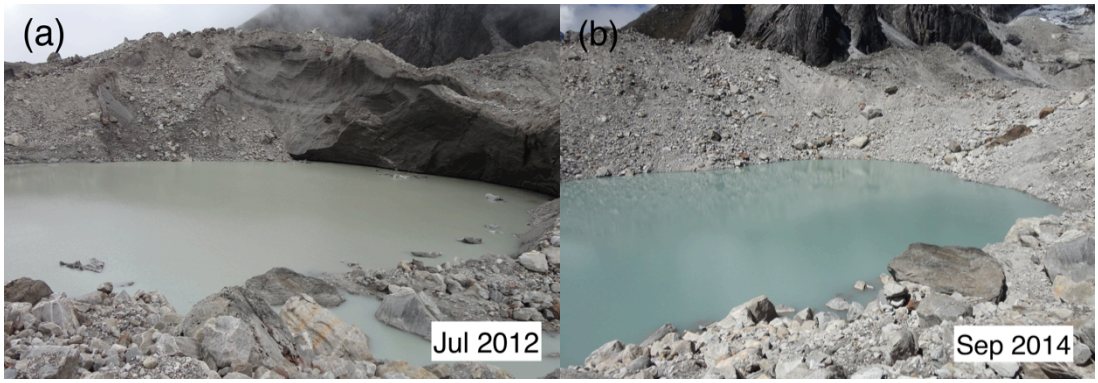

Figure 18. An example of glacier mass loss: Supra-glacier lake in Lobuje Glacier. **(a)** July 2012 and **(b)** September 2014, indicating substantial mass loss of debris-covered ice. Glaciers are extensively losing mass in last few years, particularly those glacier which have lakes on their surface. The evolutions of lakes on surface of glaciers are increasing the loss of glaciers ice mass, primarily by ice calving.

The increasing of the lakes in the last decade can be associated to the glacier flow velocities decrease, as we presented in *Article III,* caused by reduced precipitation and increased ablation of glacier ice. The reduced precipitation induces and increased ablation of the glacier ice lowers ice velocities and trigger evolution of such lakes. Furthermore, as

a feedback, evolutions of the supraglacial lakes on the surface make glacier susceptible to enhanced mass loss (Fig. 18).

4.4.2 Proglacial Lake

The surface area of the proglacial lakes has remained quite stationary, except Imja Lake. (Fig. 19a). For a group of lakes that were proglacial in the past (before 1990s) and became Unconnected lakes recently, we observed that their surface area have decreased continuously (Fig. 19b). The lakes that are appeared as proglacial lakes recently have increased in their surface area (Fig., 19c). Small number of lakes were becoming unconnected (leaving the glacier) and a similar number of small lakes became the proglacial lake, without changing the total surface area. Just four proglacial lakes, except Imja Lake, in the last 50 years continued to be proglacial lakes independently to the glacial they belong. They increased in the first period (1963–1992) and then remain constant (Fig. 19d).

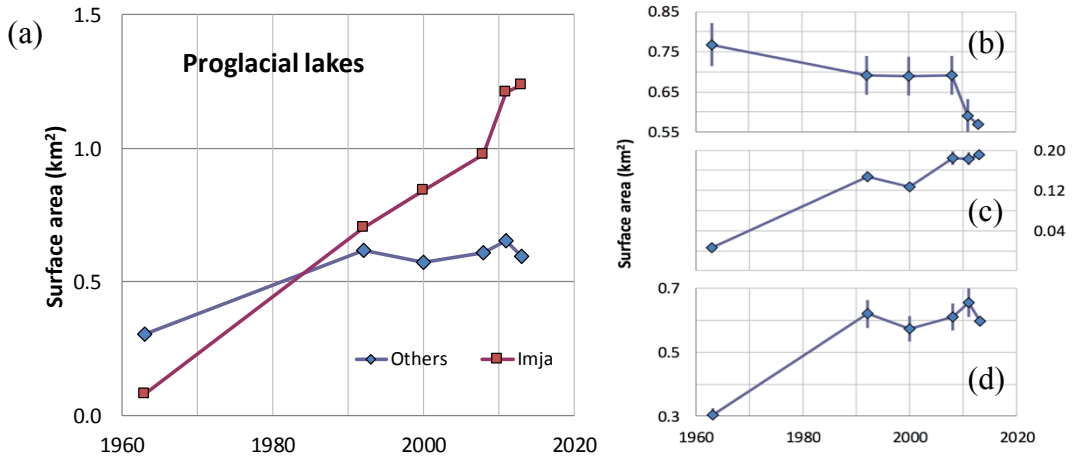

Figure 19. Temporal trends of proglacial lakes in the SNP from 1963 to 2013. **(a)** A comparison between Imja Lake and other proglacial lakes for their surface area change. Surface area change for **(b)** the lakes that were proglacial before 2000s and no more proglacial now, **(c)** recent new proglacial lakes those were not present in past, and **(d)** the lakes that remained always proglacial lake.

Imja was the only proglacial lake that has increased continuously from 0.029 ± 0.010 km^2 in 1963 to 1.352 ± 0.054 km^2 in 2013. No significant changes in the surface areas for other proglacial lakes were found. As a case study to Imja Lake, we demonstrated that continuous increasing of the lake is associated with decreasing flow velocities of Imja Glacier and increased elevation of zero degree isotherms of Maximum temperature (*Article III* in details). Flow velocities of Imja Glacier have significantly decreased from 1992 to 2013. The isotherm line has crossed the current location of Imja Lake (Fig. 20).

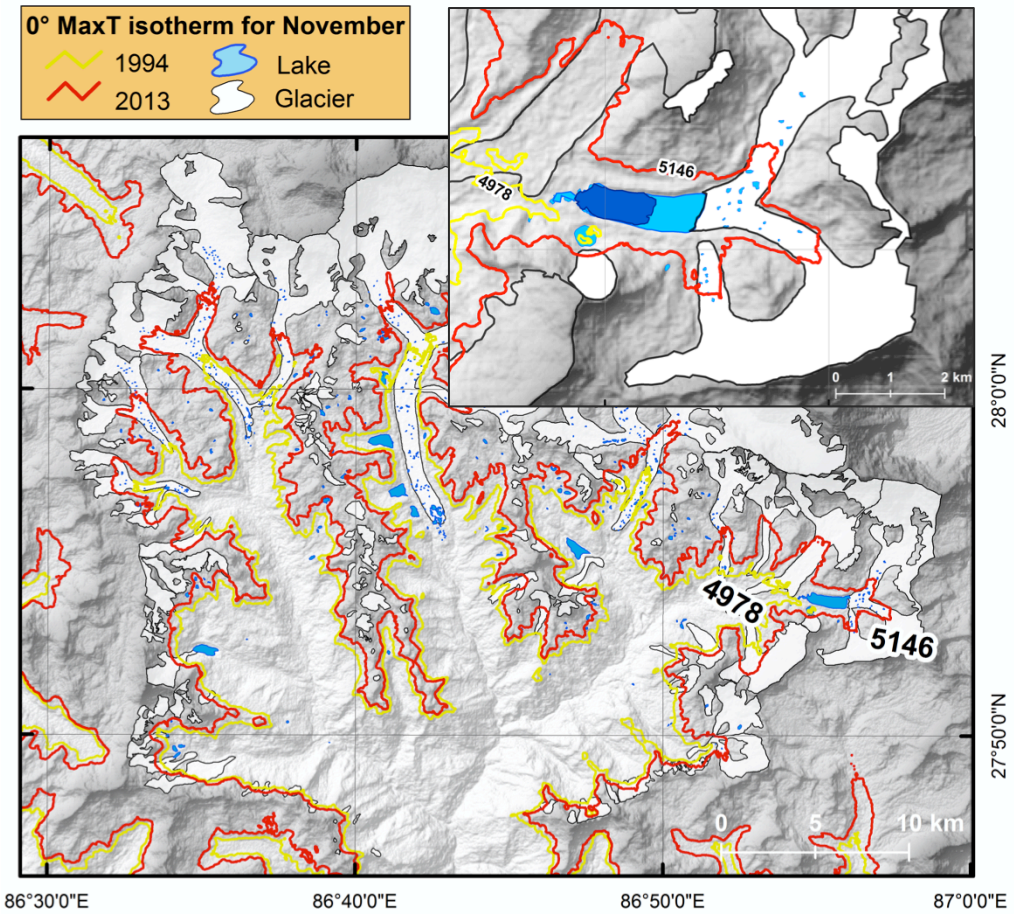

Figure 20. The 0 °C isotherms of November maximum temperature (MaxT) in the 1994 and 2013. Inset map is focused for Imja Lake and Imja Glacier.

In this thesis, with a case study of Imja Lake and Imja Glacier, we analysed and indicated that glaciers velocities and mass loss controls the glacial lake evolution, however, to find reasons for the differential behaviour of other proglacial lakes in relation to mass loss and velocity changes, we emphasize a need for further evaluation of conditions at other different situations.

4.4.3 Unconnected Lake

The surface area of unconnected lakes has increased from 1960s to 1990s (4.3 %) and decreased (10.9 %) of the surface area from 1990s to 2013 (Table 5; Fig. 21a) with an overall decreasing by 7.2 % (from 4.395 to 4.080 km^2). This observation is in line with slightly increased precipitation until the beginning of 1990s and a significantly reduced precipitation then after.

The surface areas of the unconnected lakes are strongly dependent on their basin area (R = 0.70; p < 0.001; Fig. 21b). There are no correlations with the glacier surface area (Fig. 21c). In Figure 21d, the glacier surface areas are plotted against the lake area. It indicates that the lake surfaces are slightly correlated with the glacier area (R = 0.46), but it is due

to autocorrelation, because the glacier surface is a function of the basin (R = 0.65; Fig. 21e). We demonstrate in Figure 21d that there are no correlation between the ratios, Lake/Basin area and Glacier area/Basin area (R = 0.02). Thus, considering that the evaporation/precipitation ratio at these altitudes is approximately 0.34, we underline that the evolution of such lakes acts as an indicator of precipitation trend of these high-altitude regions.

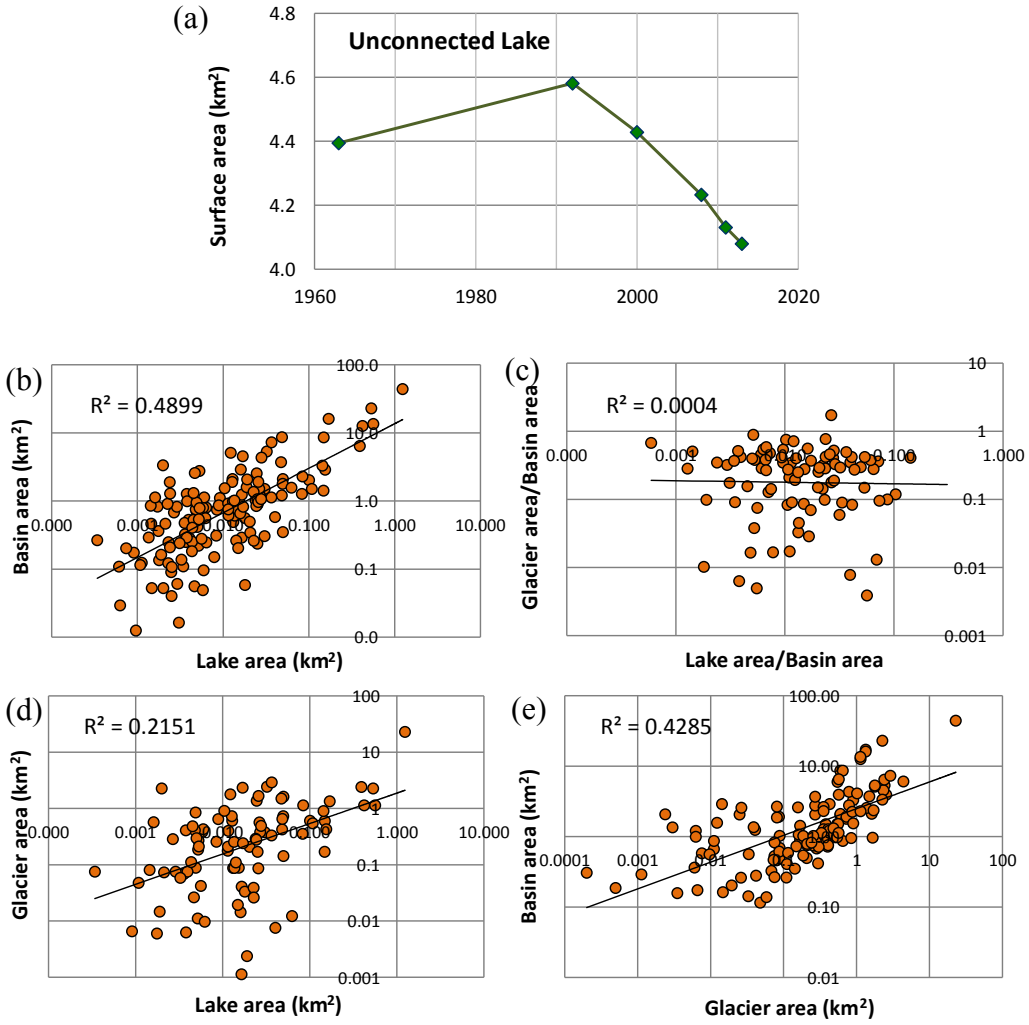

Figure 21. Unconnected lakes. **(a)** Temporal trend of average surface area in 1963–2013 period; **(b–e)** Relationships between lake surface area, their basin surface area, and glacier area in the basin, indicating that Unconnected lake act as an indicator of precipitation trend at high-altitude.

In this chapter, we described the recent evolution of three types of glacial lakes in the SNP. We conclude by underlining that the three types of lakes are capable of representing the unique condition of glaciers and climate variations in the region. Unconnected lakes have been observed a good indicator of the precipitation change in the region.

5

River Flow and Glacio-Hydrological Simulation

5.1 Introduction

Glaciers and snow play important roles in meltwater production and regulation of mountain hydrological processes (e.g., Beniston, 2003; Cuffey and Paterson, 2010; Immerzeel et al., 2010; Collin et al., 2013; Fig. 22). The observed accelerated glacier shrinkage in past decades and foreseen future of glaciers under climate change (IPCC, 2013) has raised concerns about the role of the Himalayan glaciers (Kaser et al., 2010; Collin et al., 2013; Lutz et al., 2014) on water resources. A better understanding of glacio-hydrology associated with climate change can be achieved by contemporary analysis of temporal changes of glaciers, climate, and river runoff. We observed a continuous shrinkage of glaciers, changes in both the temperature, and precipitation in the last 50 years in the upper part of the Dudh Koshi basin, as presented in previous chapters, which have an increasing concern about runoff and downstream water supplies.

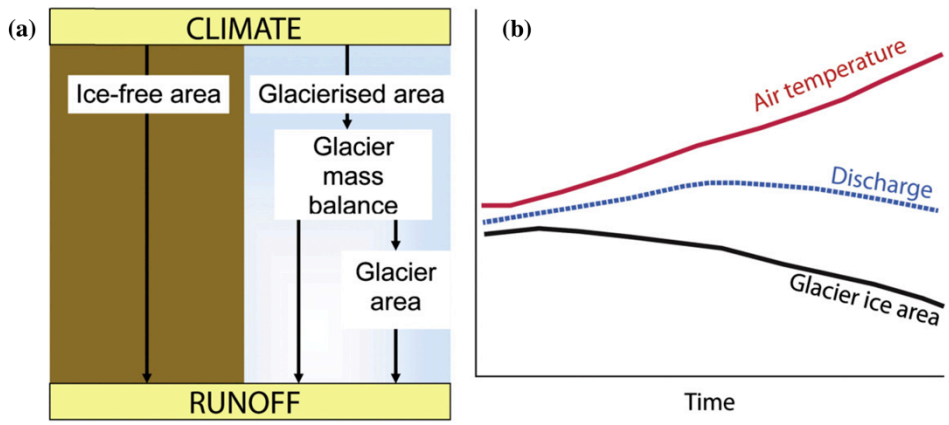

Figure 22. Climate-discharge nexus. **(a)** Showing climatic influence on runoff in ice-free and partially-glaciarised area; **(b)** Expected relationship between increasing temperature, discharge, and glacier surface area over time. Adopted from Collin et al. (2013).

River runoffs from basins without the presence of glaciers represent the behaviour of precipitation, unless an anthropic activity interfers the process. In the glacierized basins,

runoffs are subject to response with a combination of climatic factors, like temperature and precipitation (Barnett et al., 2005). Glaciers and snow provide meltwater to river runoff when air temperature is above melting point (> 0 °C). In glacierized basins, under the effect of increasing temperature, runoffs are expected to be increased initially due to glaciers melt, over time the decreasing of the glacier surface area offsets the increasing melting during warm period. A "deglaciation discharge dividend" is added to the basin runoff from depletion of the glacier surface over time (Collins, 2008), but this process cannot go on forever as glaciers disappear. On the other side, the changes in the precipitation form and amount can have a direct as well as an indirect influence (through glacier mass balance) on runoffs (Collin et al., 2013; Fig. 22).

The estimations of the hydrological response in the mountain region are complicated by heterogeneity, lack of adequate ground station data, and the uncertainties remaining in glaciers and snow behaviour (Beniston, 2003). An increasing number of studies, attempting to understand the hydrological dynamics in the central Himalaya, have addressed the glaciers and snow components at the basin-scale using various models (e.g., Racovitanau et al., 2013; Neupane et al., 2013; Immerzeel et al., 2012 & 2013; Nepal et al., 2014; Lutz et al., 2014). Most of these studies did not use the higher elevation (where the glaciers are located) climate data and information on glacier change over time. In this study, we use the new knowledge obtained from our own analysis on glaciers and climate (previous Chapters), and try to explore the variability in river flow as a response of glaciers retreat in the Dudh Koshi basin. We, first, examine the river discharge series through stochastic frequency analysis and then, simulate the discharge to explore the impacts of glaciers and precipitation change. In addition to these, we estimate the contribution of glacier melt to river discharge and different flow components.

We simulate and evaluate melt contribution to river flow through coupling the Soil Water Assessment Tool (SWAT), a physically-based model with the Temperature index (T-index), and a physical energy balance method in the Dudh Koshi basin (area: 3717 km^2) located on the south slope of Mt. Everest region. We further use a multilinear regression to represent relationships between precipitation regime and the discharge. The models were enforced using hydro-meteorological, Digital Elevation Model (DEM), land cover, and soil data. The basin charateristics are provided in Figure 24.

5.2 Data and Methods

5.2.1 Data Sources

Hydro-meteorological data

The data from meteorological ground stations in the Koshi basin (same as used in the climate studies, in Chapter 2), discharge series from (1) the Dudh Koshi river (670) for

the 1964–2010 period, (2) Khimti Khola (650) for 1995–2008 period, and (3) Tamor river (690) for 1964–2008 period, and hourly radiation data from the AWS Pyramid station from 2002–2012 are used. Here, numbers in parenthesis (670, 650, and 690) represent the station indices from the DHM Nepal. The locations of these stations in the Koshi basin are presented in Figure 23.

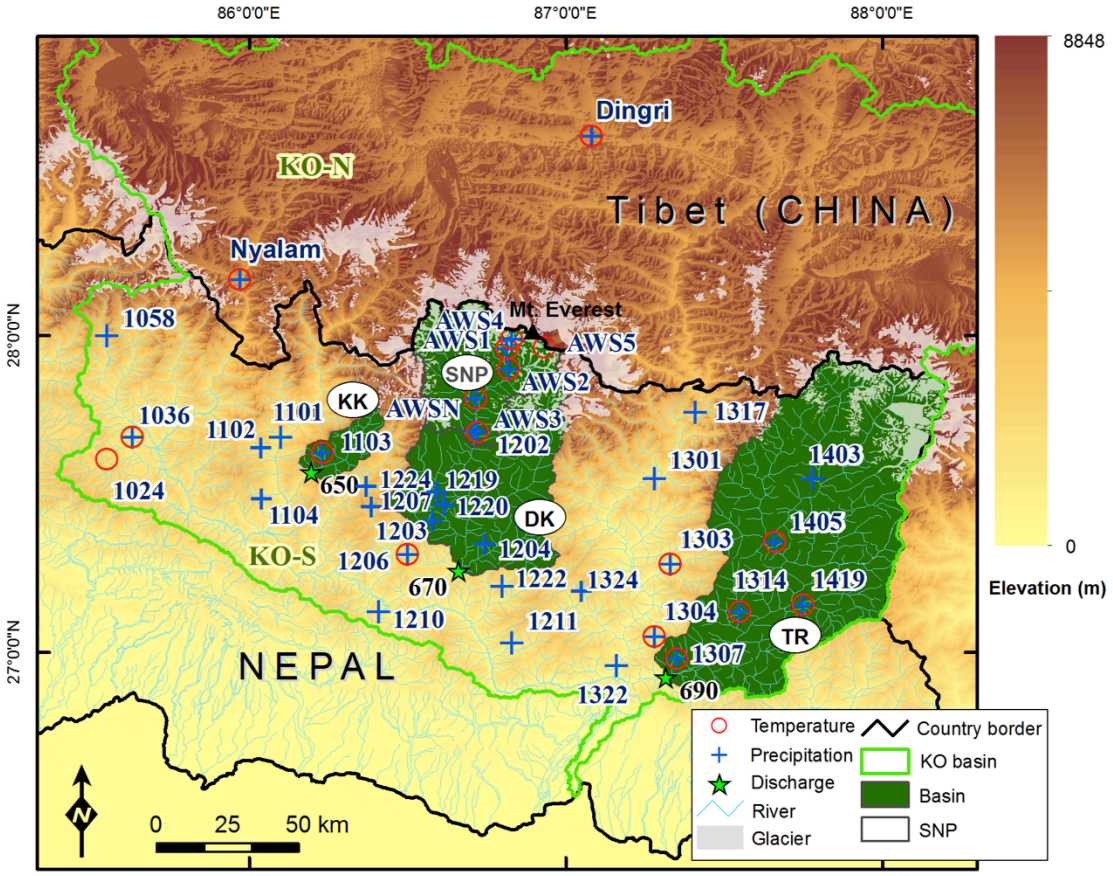

Figure 23. Location of hydro-meteorological sations in the Koshi (KO) basin. Further, the location of Dudh Koshi (DK), Khimti Khola (KK), and Tamor (TR) basins are also indicated.

Spatial data

The DEM, landuse, and soil data are used in additional for hydrological simulation in the SWAT (Table 6).

5.2.2 River Discharge Analysis

The stochastic frequency analysis is performed by using Continuous Wavelet Transform (CWT; Torrence and Compo, 1998) to detect the stationarity pattern of dominant spectral modes in the daily time series of the Dudh Koshi discharge (at Rabuwa bazaar) extending from 1964 to 2010. The wavelet transform is a method to decompose a time series to

explore the signals in the time and frequency domain. The CWT applied in this study is the Morlet transform (Torrence and Compo, 1998; Salerno and Tartari, 2009).

The CWT of a time series $x(t)$ is expressed as,

$$W_\psi(x)(a,b) = \frac{1}{\sqrt{a}} \int_{-\infty}^{\infty} x(t)\psi\left(\frac{t-b}{a}\right) dt \quad (1)$$

Where, $x(t)$ is time series, ψ is a continuous wavelets function (Morlet function) with length that is much shorter than the time series $x(t)$, W_ψ is wavelet coefficients, a is scale factor that determines the frequency (scale) so that varying a gives rise to spectrum, b is related to the shift of the analysis window in time so that varying b represents the sliding method of the wavelet over $x(t)$.

The analysis was executed in the MATLAB®.

5.2.3 Soil Water Assessment Tool (SWAT)

The physically based semi-distributed hydrological model, the SWAT was applied for a glacierized Dudh Koshi basin, including both the snowmelt and glacier melt processes. The SWAT is well established and most commonly applied tool for watershed research and management. Some studies have already used this tool successfully on the glacierized mountain basins for hydrological simulation (e.g., Rahman et al., 2012; Neupane et al., 2013).

The hydrologic balance in the SWAT (Neitsch et al., 2011) is represented by,

$$SW_t = SW_0 + \sum_{i=1}^{t} (R_{day} - Q_{surf} - E_a - w_{seep} - Q_{gw}) \quad (2)$$

In this equation, SW_t = the final soil water content (mm H2O); SW_0 = the initial soil water content (mm H2O); t = the time (days); R_{day} = the amount of precipitation on day *i* (mm H_2O); Q_{surf} = the amount of surface runoff on day *i* (mm H_2O); E_a = the amount of evapotranspiration on day *i* (mm H_2O); w_{seep} = the amount of percolation and bypass flow exiting the soil profile bottom on day *i* (mm H_2O); Q_{gw} = the amount of return flow on day *i* (mm H_2O)

ArcSWAT 2012 was used for model set up and the simulation run. In Figure 25, overall SWAT implementation procedure is presented. For delineating the basin, sub-basins, and Hydrological Response Units (HRUs) characteristics, the SWAT needs DEM, soil, and landuse data. The details of data and their sources are presented in Table 6.

The SWAT was applied both with and without glacier and snowmelt modules. The SWAT includes an inbuilt snowmelt module, but not the glacier melt module. For glacier, T-index method (presented in following Section 5.4.2) was used to compute the meltwater outside the SWAT and incorporated to the simulation output.

Table 6. The datasets used for SWAT and their sources.

Data type	Data source
DEM	ASTER GDEM ver 2 (30 m) *www.jspacesystems.or.jp/ersdac/GDEM/E/4.html* A product of METI and NASA.
Landuse map	Land Cover Map of Himalayan Region (2009) *www.fao.org/geonetwork/srv/en/metadata.show?id=37286&currTab=simple* The database was produced under the Global Land Cover Network– Regional Harmonization Programme (FAO) using 2000 Landsat Land satellite imagery as reference and covers the Himalaya Region.
Soil map	1) Soil Map of Nepal (2008) *http://rds.icimod.org/Home/DataDetail?metadataId=1889&searchlist=True* The dataset was developed by the ICIMOD based on Zonal Maps (1:250,000 scale) published by Department of Survey Nepal in 1988. 2) Digital Soil Map of the World (2007) *www.fao.org/geonetwork/srv/en/metadata.show?id=14116&currTab=distribution* Produced by FAO-UNESCO (1:5,000,000 scale).
Weather and discharge data	Data from network of Pyramid Observatory stations and the DHM Nepal.

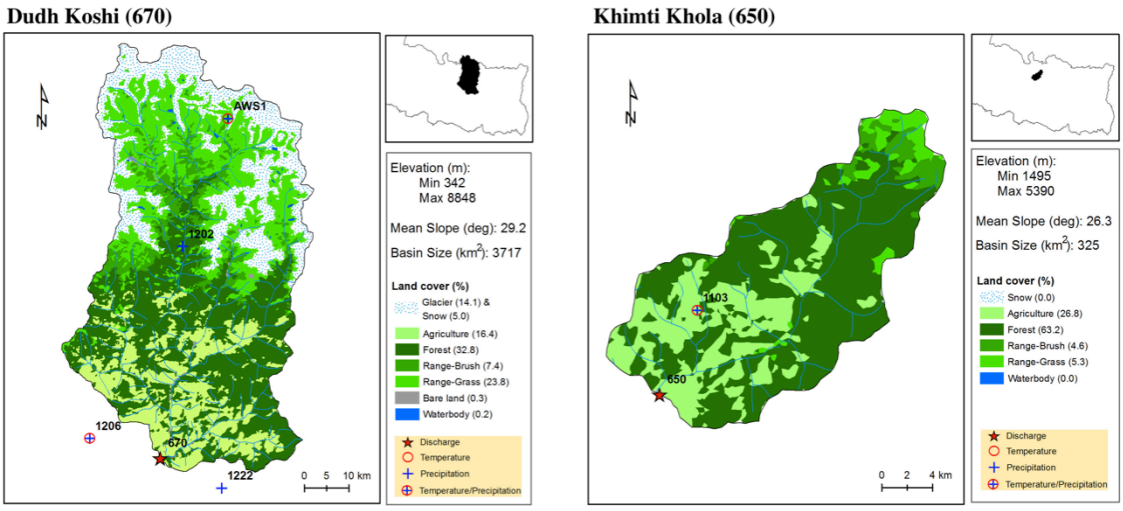

Figure 24. Characteristics of the Dudh Koshi and the Khimti-Khola basins.

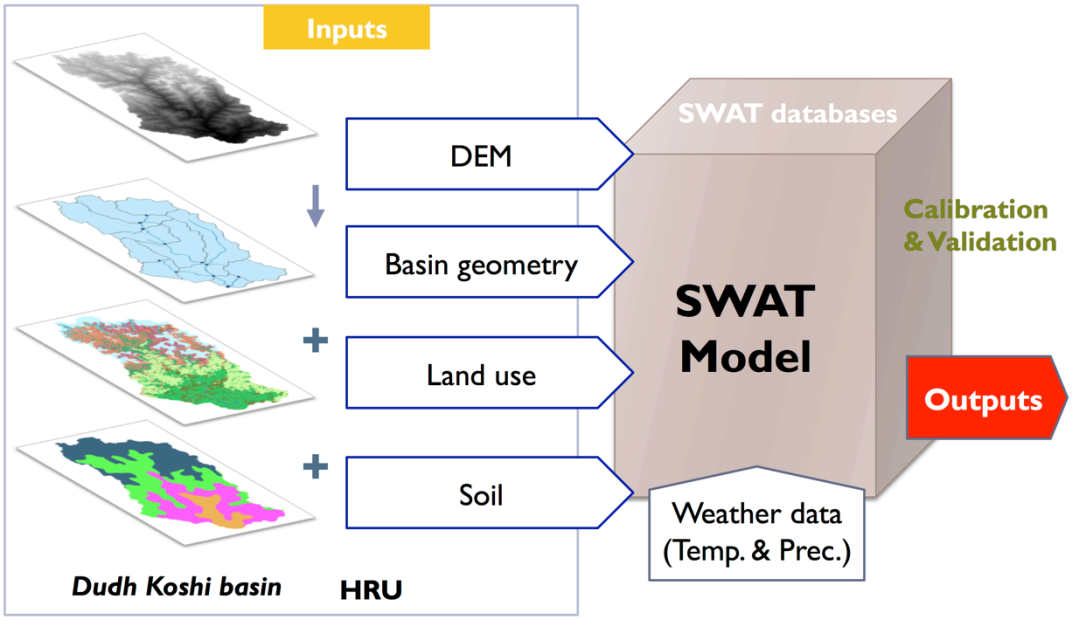

Figure 25. Schematic diagram of hydrological simulation in the SWAT.

SWAT Calibration, Validation, and Application

The SWAT model is calibrated (through trial and error method; Table 7) and validated (Arnold et al., 2012) in the Khimti Khola basin (650), a basin without glacier and permanent snow cover, lying close to the Dudh Koshi basin (670) (Fig. 23). The model was calibrated in 1995–2001 and validated in 2002–2008 period at daily-scale. Then, the model is applied to our glaciarized Dudh Koshi basin (670) for understanding the glaciers and snowmelt in the basin. A total of 9 subbasins and 39 HRUs were created for the calibration and validation basin, while 23 subbasins and 168 HRUs was implemented in the Dudh Koshi basin.

The model was applied using elevation bands and considering the temperature and precipitation lapse rates. Activating default snowmelt routing and applying elevation bands, improved the simulation results. Subbasins were divided into different elevation bands of 1000 m and fraction of surface area calculated for each elevation band. In that way, a maximum of four elevation bands used in subbasins of the Khimti-Khola basin, while it was up to eight elevation bands in the Dudh Koshi basin. The ArcSWAT interface, used for running SWAT, allows inserting single lapse rate for each temperature and precipitation. In order to incorporate two precipitation lapse rates, the SWAT source codes are modified in FORTRAN and compiled. A common temperature lapse rate (TLAPS) rate -5.9 °C km^{-1}, and precipitation lapse rate (PLAPS) rate 1340 mm km^{-1} below 2800 m, and an additional PLAPS rate -204 mm km^{-1} above 2800 m elevation, were applied. The performance of SWAT with two lapse rates was better than one lapse rate.

Table 7. SWAT calibration and set up parameters.

Parameter	Description	Default*	Calibration/Set up
Cn2	SCS runoff curve number for moisture condition 2	x	x-40
Sol_AWC	Groundwater "revap" coefficient.	y	y-0.004
ESCO	Soil evaporation compensation factor	0.95	0.9
Recharge_dp	Deep aquifer percolation fraction [fraction]	0.05	0
SURLAG	Surface runoff lag time [days]	4	2
SFTMP	Snowfall temperature (°C)	1	0
SMFMX	Maximum snowmelt rate (mm/°C-day)	4.5	7
TLAPS	Temperature lapse rate °C/km)	0	-5.9
PLAPS	Precipitation lapse rate (mm/km) (< 2700 m elevation)	0	1160
PLAPS1	Precipitation lapse rate second (mm/km) (> 2700 m elevation)	0	-204
PET	Potential evapotranspiration (mm H_2O)	Hargreaves method	

* Here, x and y represents the multiple default values.

Evaluation of Model Performance

The SWAT calibration and validation performance was evaluated using Nash-Sutcliffe (NS) efficiency coefficient, Absolute Error (AE), and Coefficient of Determination (R^2) (Nash and Sutcliffe, 1970; Legates and McCabe, 1999).

The computation formulas for each index are defined below.

$$NS = 1 - \frac{\sum_{i=1}^{n}(Qobs_i - Qsim_i)^2}{\sum_{i=1}^{n}(Qobs_i - \overline{Qobs})^2} \quad (3)$$

$$AE = \frac{\sum_{i=1}^{n}|Qsim_i - Qobs_i|}{n} \frac{1}{\overline{Qobs}} \quad (4)$$

$$R^2 = \left[\frac{\sum_{i=1}^{n}(Qobs_i - \overline{Qobs}) * (Qsim_i - \overline{Qsim})}{\left[\sum_{i=1}^{n}(Qobs_i - \overline{Qobs})^2\right]^{0.5} * \left[\sum_{i=1}^{n}(Qsim_i - \overline{Qsim})^2\right]^{0.5}}\right]^2 \quad (5)$$

Where, $Qobs_i$ = the observed discharge

$Qsim_i$ = the daily simulated discharge

$\overline{Qobs}$ = the average of the observed discharge

$\overline{Qsim}$ = mean of simulated discharge

n = the number of observations during the considered period

NS can range from ∞ to 1; AE can be greater than or equal to 0; and R^2 value ranges from 0 to 1.

5.2.4 Temperature Index (T-index)

In order to compute the glacier melt, currently existing methods are simple T-index, enhanced T-index, and energy balance model (Hock, 2003 and 2005; Pellicciotti et al., 2005). We used a simple T-index or degree-day melt method for estimating ablation from glaciers (Hock, 2003). Other methods demand more data for their application. T-index could be the only option for a long-term computation of melt due to only possibility of obtaining temperature data. The T-index method uses the relationship between glacier melting (melt factor or degree-day factor) and air temperature and is given by,

$$M = \begin{cases} M_f(T_d - T_0), & T_d > T_0 \\ 0, & T_d \leq T_0 \end{cases} \quad (6)$$

Where, M is daily-melt; T_d is daily mean temperature; T_0 is a threshold temperature beyond which ice melt is assumed to occur (0 °C), and M_f is a melt factor. T-index melt model was applied to each 100 m elevation band, using temperature data for each band separately, calculated by using varying monthly lapse rates (Fig. 26) derived from the ground station data.

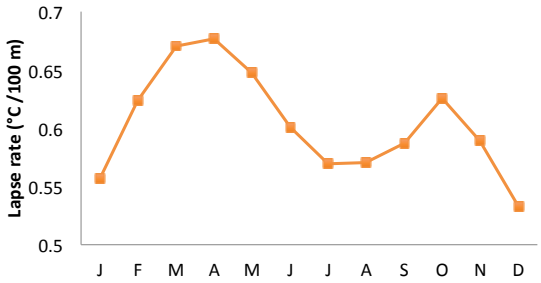

Figure 26. Variation of temperature lapse rate, from January (J) to December (D).

The M_f value 0.0087 m d^{-1} $°C^{-1}$, provided by Kayastha et al. (2000) from the field measurement (Glacier AX010) in the Dudh Koshi basin, was used. Moreover, we computed glacier melts also separately for the debris-covered and debris-free glacier area using the M_f values provided by Lutz et al. (2014). We computed glacier meltings both by using the constant glacier surface area of 2013 and the change of glacier surface over the period due to glacier surface loss.

Daily glacier meltwaters were calculated by T-index method using reconstructed Pyramid (1994-2013) and downscaled ERA-Interim (1979-2013) temperature series. Furthermore, non-parametric sequential monthly Mann Kendall test was performed to evaluate significance of monthly discharge trend and Sen's slope estimator computed for discharge trends.

5.2.5 Surface Energy Balance (SEB)

The physical Surface Energy Balance (SEB) approach was also used for estimation of the glacier melt at the elevation of weather station location for evaluating the melts calculated by T-index method. The SEB method is usually considered the best one for accurate computation of ablation if sufficient data are available, but the availability of data normally limits its application. The ice and snow melt at the temperature 0 °C, but it is not necessary that at air temperature equal or greater than 0 °C. The melting depends on the energy available around the surface and various other weather and surface conditions.

The general surface energy balance (Hock, 2005) is expressed as,

$$Q_m = Q_N + Q_H + Q_L + Q_G + Q_R \quad (7)$$

In this equation, Q_m = energy available for melting, Q_N = net radiation, Q_H = sensible heat flux, Q_L = latent heat flux, Q_G = ground heat flux, and Q_N = sensible heat flux supplied by rain incoming shortwave radiation. We used SEB according to Brock and Arnold (2000) neglecting the Q_G and Q_R as they are negligible compared to other heat fluxes (Hock, 2005).

When the positive energy is available, it is assumed that the available energy is used for melting and thus converted to meltwater as,

$$Meltwater = Q_m/L_m * \rho \quad \text{[mm w.e.]} \quad (8)$$

Here, L_m = latent heat of melting and ρ = density of water

The SEB was computed using hourly radiation data (2002–2012) from AWS station close to the ablation area at an altitude of 5050 m, above the average terminus elevation (~4800 m). The total meltwater for a 100 m elevation band estimated by generalizing the point SEB to make comparison with melting by T-index method.

The albedo of glacier ice is assumed to be 0.2 based on the field observed data on Asian glaciers (Takeuchi and Li, 2008; Fujita and Sakai, 2014). We used other standard coefficients as provided by Brock and Arnold (2000).

5.2.6 Multilinear Regression: Precipitation–Discharge (SPI–Q)

To represent the relationship between the precipitation regime and the discharge, a simple multilinear regression has been computed at monthly scale using a least-square method as,

$$Q(m,i) = a_{SPI2}(m).SPI2(i) + a_{SPI3}(m).SPI3(i) + a_{SPI9}(m).SPI9(i) + a_0(m) \qquad (9)$$

Where, $Q(m,i)$ is the observed discharge for the m month and i year; $SPI2(i)$, $SPI3(i)$, and $SPI3(i)$ are the Standardized Precipitation Indices (SPIs), whose original formulation was proposed by McKee et al. (1993), computed at Chaurikhark (station 1202) for the m month, i year on the precipitations accumulated over 2, 3 and 9 months; $a_{SPI2}(m)$, $a_{SPI3}(m)$, $a_{SPI9}(m)$, and $a_0(m)$ are the coefficients from the multilinear regression of $SPI2$, $SPI3$, $SPI9$, and a known term, respectively (computed for each m month).

Of course, the choice to consider the SPIs at Chaurikhark station (2600 m) is reliable only if the station is representative of the whole basin in term of inter-annual variability. *Article I* identified a maximum in precipitation occurring around 2500 m, followed by an exponential reduction. Thus, the Chaurikark observation is likely more representative of the overall amount of precipitation than higher altitude (and thus, lower amount of precipitation) observation. Moreover, with respect to the Pyramid reconstruction, Chaurikark is the only long-term precipitation station available in the basin.

5.3 Hydrological Dynamics of the Dudh Koshi River

5.3.1 The SWAT Simulation Outputs

Figure 27 shows the calibration and validation results of the hydrological simulation in the SWAT. The simulation was performed at daily time scale. The model calibrated (1995–2001; NS = 0.68, *AE* = 0.37, R^2 = 0.69) and validated (2002–2008; NS = 0.69, *AE* = 0.38, R^2 = 0.71) in the Khimti-Khola basin (650) close to the Dudh Koshi basin (Fig. 23), having no glaciers and permanent snow cover.

The SWAT simulation was able to capture the variations in the river discharge, providing a reasonable estimation of the runoff in the catchment (Fig. 27) in the 650 basin. Then, the model applied to the glacierized Dudh Koshi basin (Fig. 28). The application of the model in the Dudh Koshi is able to capture the seasonality, due to strong monsoon domination, but unable to capture the high discharges. Figure 29 reports water balance computed from the application of the model in the Dudh Koshi basin.

Percentage bias was less than 1 for both calibration and validation periods. Without glacier and snowmelt, we found 28.6 % deficit in water balance compared to observed annual discharge in the Dudh Koshi basin. While applying the snowmelt module and

glacier melt by the T-index method, we found addition of 2.3 % and 12.8 % water from snow and glacier melt, respectively. But still there was 13.5 % of water deficit in water balance. We assume that this amount could be associated with the uncertainties to the glacier and snow melt.

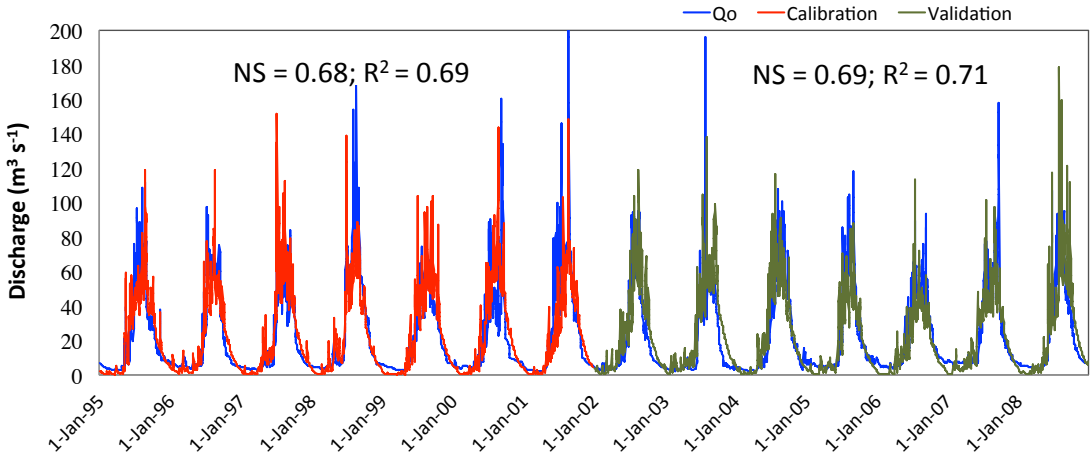

Figure 27. Calibration (1995-2001) and validation (2002-2008) of the SWAT model in the Khimti-Khola basin (650)

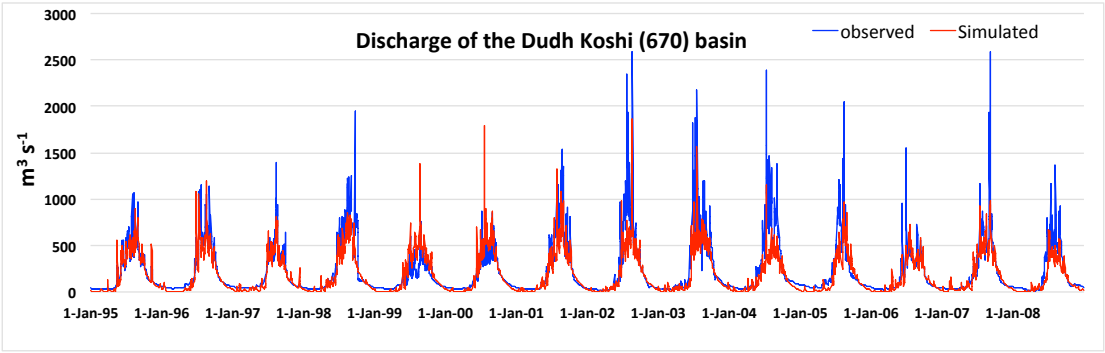

Figure 28. Application of SWAT to Dudh Koshi basin without glacier melts.

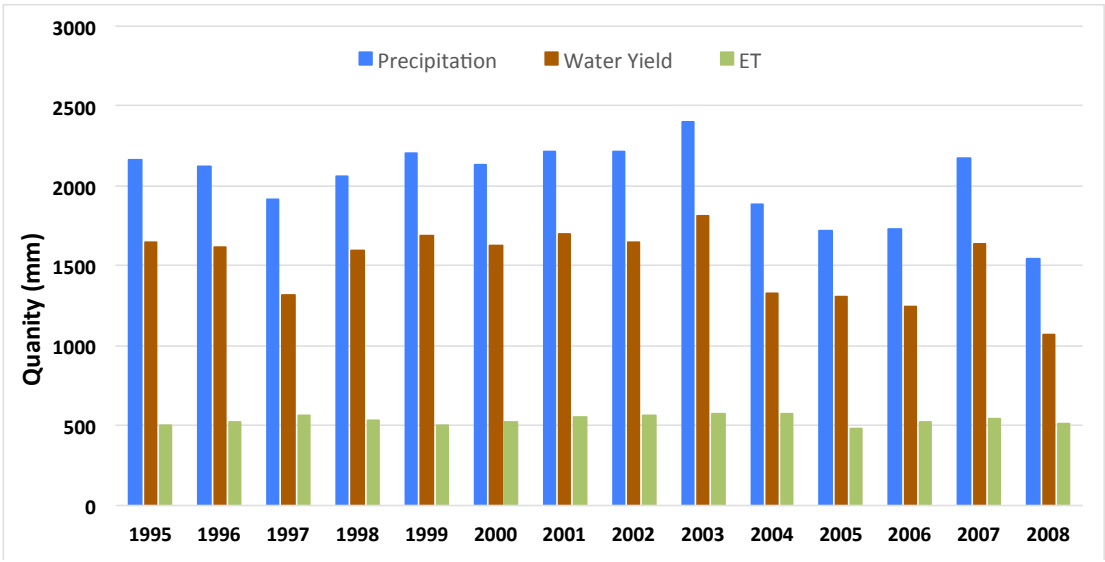

Figure 29. Annual water balance for the Dudh Koshi basin.

The estimated annual quantity of glacier meltwater considering a constant glacier surface area (2013) over all years was less by an average 3.8 % compared to estimated meltwater by using changes of glacier surface over time, indicating that melt water has decreased with decreasing glacier surface area. For this computation, the glacier surface area change information from our glaciers analysis was used. A single melt factor M_f of 0.0087 m d^{-1} $°C^{-1}$ reduced the negative bias, compared to using two melt factors. The estimation of glacier melts using two melt factors (for debris-covered and debris-free part) indicated that 40.5 % and 59.5 % share in the total melt from the debris-covered area and debris-free area, but produced significantly less (56 %) melt compared to single melt factor over the glaciers. This suggests that the choice of melt factor is very essential for reliable estimation of the glacier and snow melt.

T-index is a simple approach requiring only the temperature and melt factor; however, while using mean daily temperature data for calculations, such model underestimated the glacier melt. The diurnal ranges of temperature in the study site are large. Even though the mean daily temperature is below the melting point (0 °C), temperatures in certain hours of the day are positive. The simulated melting by the T-index method using the maximum temperature was much better than using mean daily data compared to the observed station discharge (produced meltwater nearly 100 % more and significantly reduced the bias). Further, first result from an experiment using SEB indicated much higher rate of glacier melt, confirming that T-index method significantly underestimated the glacier melt (Fig. 30). Results indicated that the melting of glaciers continues until 3 °C below the average mean temperature, suggesting that in such high altitude, the solar radiation can play vital role in the melting of glaciers and snow.

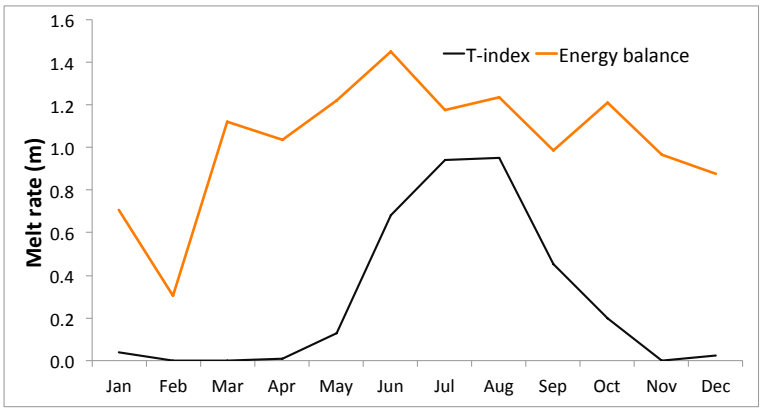

Figure 30. Comparison of the melt from T-index and surface energy balance (SEB) for the location of weather station.

In conclusion, the radiative energy dominates energy exchanges at the glacier-atmosphere interface, due to the variation in the net shortwave radiation. In fact, Senese et al. (2014) indicated that the threshold temperature for ablation of snow can be a minimum daily air temperature of -4.6 °C.

5.3.2 Glacier Melt Contribution to River Flow

In Figure 31, different components of discharge are presented based on the application of the model. For the Dudh Koshi basin, using daily mean temperature in T-index method provided 12.8 % of glacier meltwater, and 2.3% snowmelt outside the glacier area, accounting for a total of 15.1 %. But considering the water deficit in annual water balance and observed much higher quantity of meltwater by T-index using maximum temperature and by the SEB, we expect that the percentage of meltwater contribution to river flow could be much higher (15.1 to 28.7 %). The observed bias could be mainly related to the uncertainty in meltwater quantity. Previous studies have values ranging from 7.4 to 34.0 % contribution from glacier and snowmelt to the Dudh Koshi using different models. Racovitanau et al. (2013), using the ice ablation model, indicated that glacier melt provides 7.4 % water to the Dudh Koshi river. Nepal et al. (2014), using J2000 model, reported 17 % glacier and 17 % snowmelt, in total 34 % contributing to river runoff. Lutz et al. (2014) estimated 18.8 % of contribution from glacier and 4.8 % from snowmelt in the Dudh Koshi river. Immerzeel et al. (2010) estimated about 10% of snow and glacier melt to the river runoff in the Ganges river basin. However, we have to keep in mind that with increasing distance from the glacier downstream, the melt contribution decreases (Kaser et al., 2010).

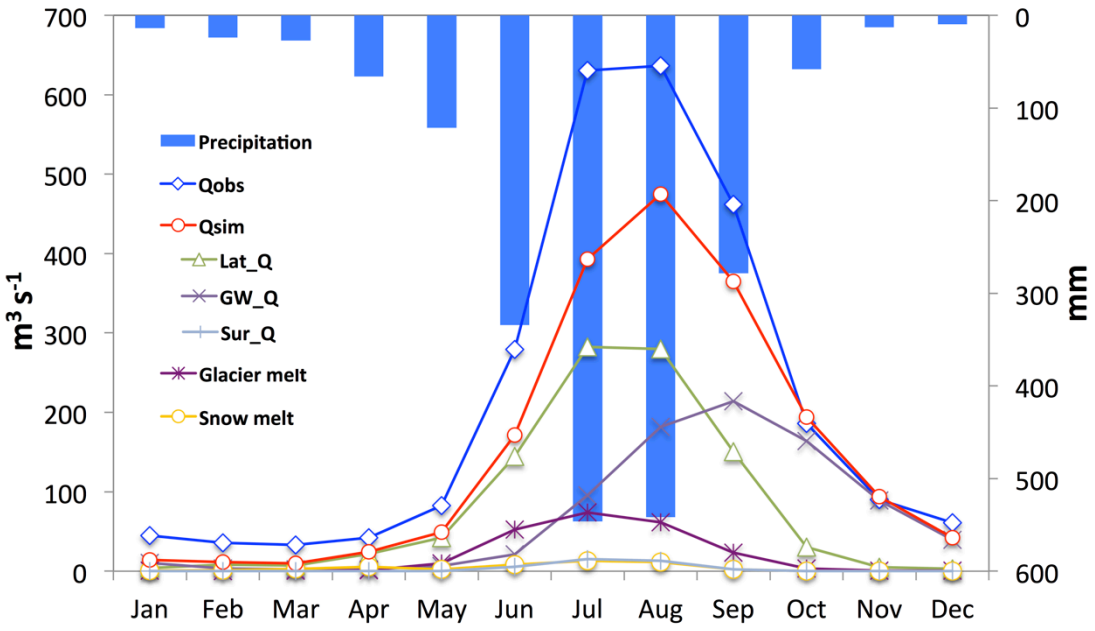

Figure 31. Annual hydrograph for the 1995–2008 period at Dudh Koshi river. The observed station discharge and the SWAT simulated discharge including three components (lateral, ground, and surface) and glacier melt using T-index are indicated.

5.3.3 Temporal Changes of Glacier Meltwater

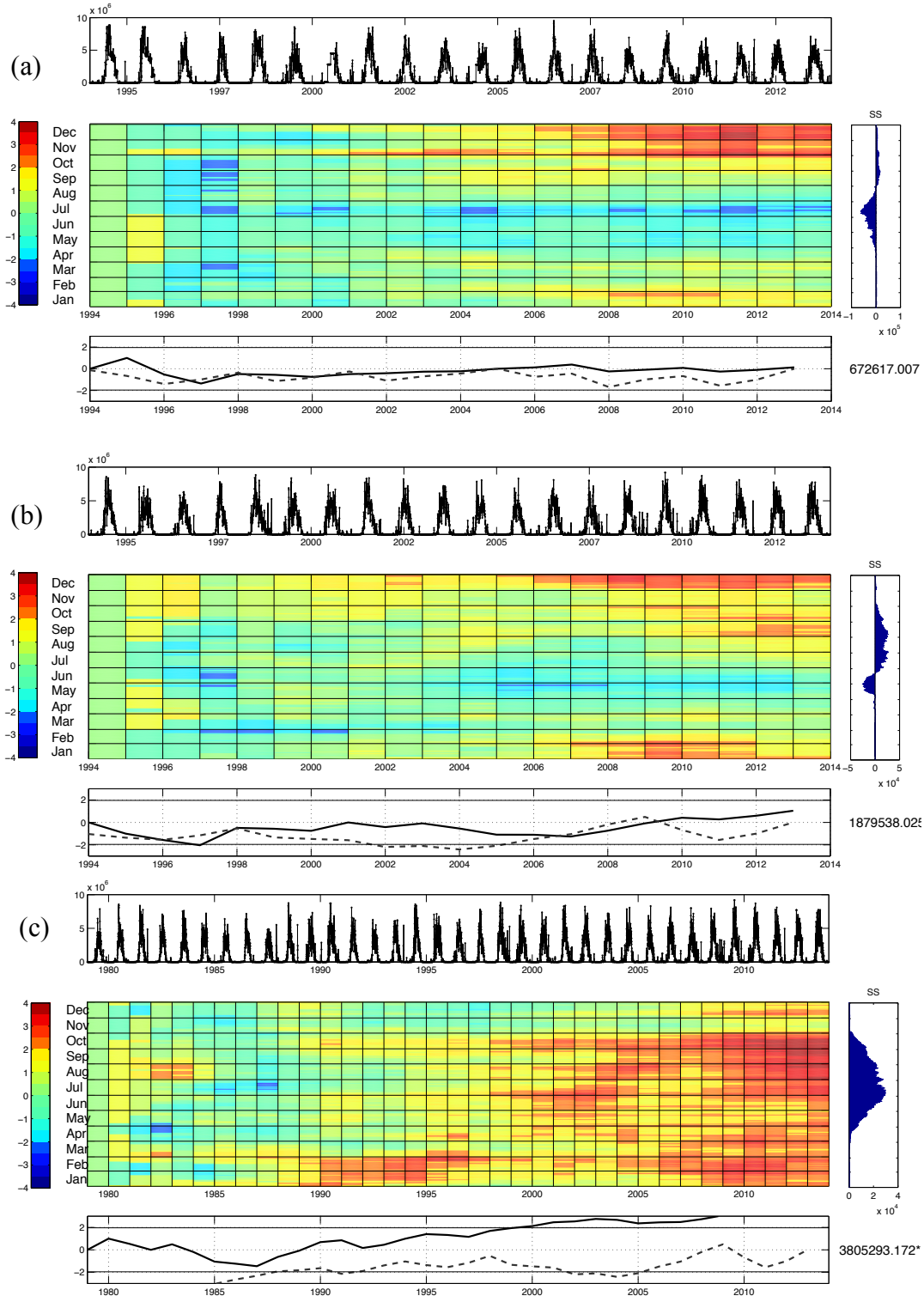

Figure 32. Trend analysis for glacier melts (volume m³) computed by T-index method using **(a)** the reconstructed Pyramid mean temperature and **(b)** ERA-Interim mean temperature in the DK basin for 1994–2013; **(c)** The melt calculated for all year (1979–2013) by ERA-Interim temperature. In each plot (a–c), the top graph represents the calculated daily glacier melt. The central grid displays the results of the sequential Mann–

Kendall (seqMK) test applied at the monthly level. On the left, the color bar represents the normalized Kendall's tau coefficient $\mu(T)$. The color tones below 1.96 and above 1.96 are significant at $p = 0.05$. On the right, the monthly Sen's slopes presented. The bottom graph plots the progressive (black line) and retrograde (dotted line) $\mu(T)$ applied on the annual scale. On the right, the annual Sen's slope is shown for the analysis period.

The glacier melt calculated using reconstructed Pyramid mean temperature indicated that a significant increasing of the glacier melts from early 2000s during the post monsoon and winter months and decreasing during pre-monsoon and monsoon months (April–August), indicating an increased total annual glacier meltwater by 6.7 $x10^5$ $m^3 a^{-1}$ (Fig. 32a), but not statistically significant. Also, the glacier melt computed by the ERA-Interim mean temperature have shown a good agreement with the glacier melt computed by reconstructed Pyramid temperature (Fig. 32b), confirming an increasing trend of melting during the post monsoon and winter months, while some decreasing trend in the summer months in last decades (1990s to 2013). However, the increasing rate computed by ERA-Interim temperature is more than double (18.7 $x10^5$ $m^3 a^{-1}$). Considering the glacier melt calculation from 1980s by using the ERA-Interim mean temperature (Fig. 32c), the result indicates that the increasing glacier melt are becoming significant over a more months in last two decades due to effect of the length of the analysis period. It suggests that the there are also an increase in temperature in the monsoon months compared to beginning of 1980s, but mainly on post-monsoon and winter months in last decade (after 1990s).

5.3.4 Dudh Koshi River Discharge

In Figure 33a, the wavelet analysis results for discharge series of the Dudh Koshi River (670) is presented. We can observe a significant annual signal (red band between the period 256 and 512 days) due to the dominance of monsoon precipitation. No any significant change in the river discharge signal observed until 2000, but we observed non-stationary discharge behaviour after 2000 with an appearance of an additional discharge peak (red band between the period 128 and 256 days). Initially, we suspected that the non-stationary behaviour could be associated with a result of a Tam Pokhari GLOF event that occurred on 3 September 1998 (Osti and Egashira, 2009).

To evaluate if the observed phenomenon is associated with the GLOF or not, first we checked for the updates on rating curves that the DHM Nepal used to estimate the river discharge. The DHM Nepal regularly calibrates and updates the rating curve for estimating river discharge in each of their stations and the recalibration was performed several times after the GLOFs (Nepal et al., 2014). Furthermore, we analysed the discharge from another closest Tamor river basin (690) with similar characteristics to the Dudh Koshi basin, in terms of percentage of glacier coverage, basin size, elevation distribution, etc. The basin (690) discharge revealed a similar behaviour of discharge as in the Dudh Koshi basin (Fig. 33b), confirming that the non-stationarity is not associated with GLOF event.

We further supposed the phenomena could be due to glacier or precipitation dynamics during that period. Despite the observed precipitation decrease we observed and increase in discharge and non-stationary after 2000s. To examine, if the observed phenomenon is due to the precipitation or Cryospheric process, we analysed the residual between the annual and monthly-observed discharge with (a) SWAT simulated discharge without the glacier melt (Fig. 34) and (b) Stochastically estimated discharge using multilinear regression (Fig. 35).

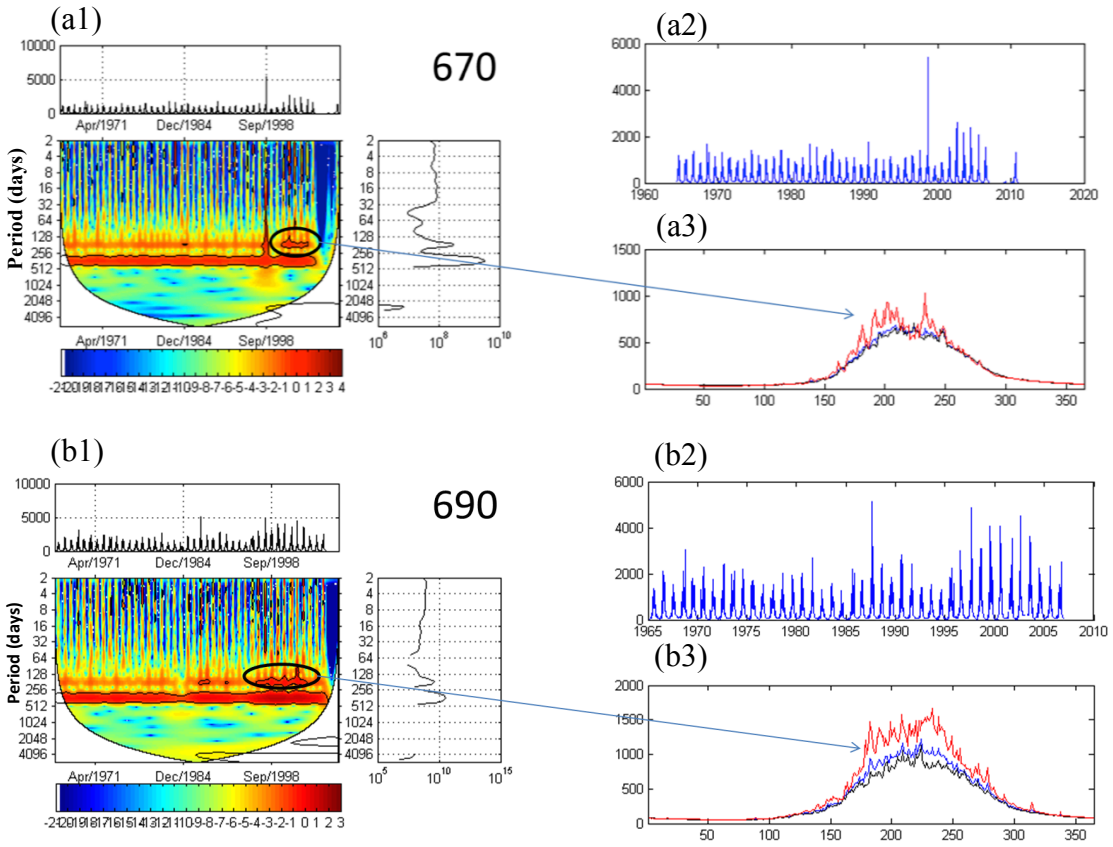

Figure 33. River discharge analysis for **(a)** Dudh Koshi river (670) from 1964 to 2010 and **(b)** Tamor river (690) from 1964 to 2008. For each river discharge series (a & b), **(1)** Continuous Wavelet Transform (CWT, left main plot) along with a plot of daily discharge series (upper) and a plot for cumulative discharge (right). Variance in wavelet power spectrum (colour scale) in CWT is plotted as a function of time and period. The black line encircling the red-noise indicates the significance at α = 0.05; **(2)** Daily discharge time series; **(3)** Average daily discharge plot from all years (black line), for highlighted years (red line), for only for before period (overall minus the highlighted parts; blue line).

In Figure 34, a comparison is made between the observed discharge and simulated discharge in SWAT without glacier melt component. The simulated discharge without glacier represents the precipitation behaviour. There was a systematic underestimation of discharge over the whole period, but higher underestimation after 2000, compared to previous years. This is evident in both the annual and monthly comparisons of series (Fig. 34a–b). In comparing the before and after 1998 (when GLOF occurred), the high

underestimation occurs during the monsoon months for the period after 1998 as can be seen from the monthly mean bias (MB) and monthly mean absolute error (MAE; Fig. 34c–d).

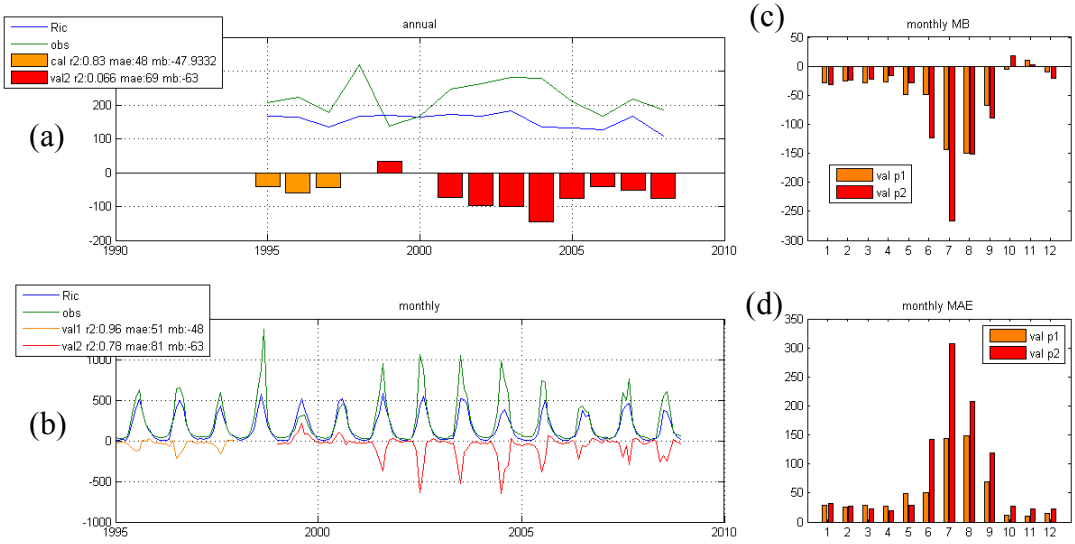

Figure 34. Residual analysis of the observed discharge (obs) and the simulated discharge (without glacier melt) in SWAT (Ric). **(a)** Discharge at annual aggregation (line) with residue of observed and simulated series (lower bar) for period before 1998 (orange) and for period after 1998 (red); **(b)** Monthly aggregation; **(c)** Monthly mean bias (MB), and **(d)** Monthly mean absoulute errors (MAE).

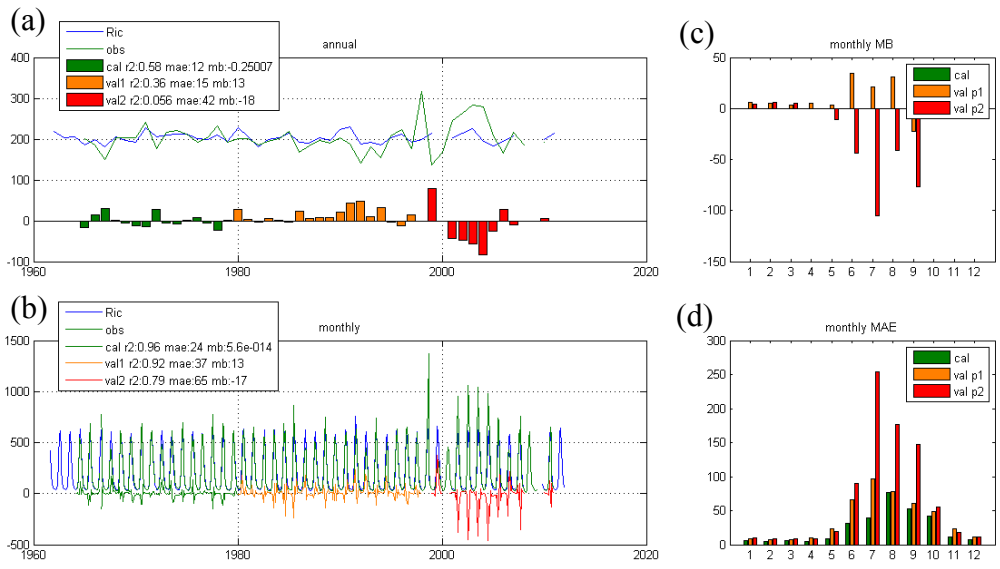

Figure 35. Residual analysis of the observed discharge (obs) and estimated discharge using multilinear regression, SPI-Q (Ric). **(a)** Discharge at annual aggregation (line) with residue of observed and estimated series (lower bars) for calibration (green), validation 1 (orange), and validation 2 (red) periods. **(b)** Monthly aggregation; **(c)** Monthly mean bias (MB), and **(d)** Monthly mean absoulute errors (MAE).

Similarly, in Figure 35, the estimated discharge series through multilinear regression (between SPI and discharge, SPI-Q) and the observed station discharges are plotted for 1964–2010. The multilinear regression coefficients were computed over the 1965-1980 period. Consequently, the resulting estimated discharge considers the mean response of the basin to precipitation during the 1965-1980 period for all the involved processes (runoff, eventual groundwater, Cryosphere, and evapotranspiration). Thus, the resulting stochastic relationship will not be able to reproduce eventual non-stationarity in one or more of these processes outside of the calibration period. The calibration gives good results in terms of MAE, MB, and R^2 (12, -0.25, and 0.58, respectively). The stochastically estimated discharge series also shows the slightly improved, but similar behaviour with that of SWAT simulated discharge, indicating higher differences during the last period (after 1998) for both annual and monthly comparison and show the highest bias during the monsoon months (June to September). These residual analyses confirm that the precipitation cannot explain the observed non-stationarity in the river discharge in the last decade. The only thing that can have such impact could be from the changes in cryospheric part.

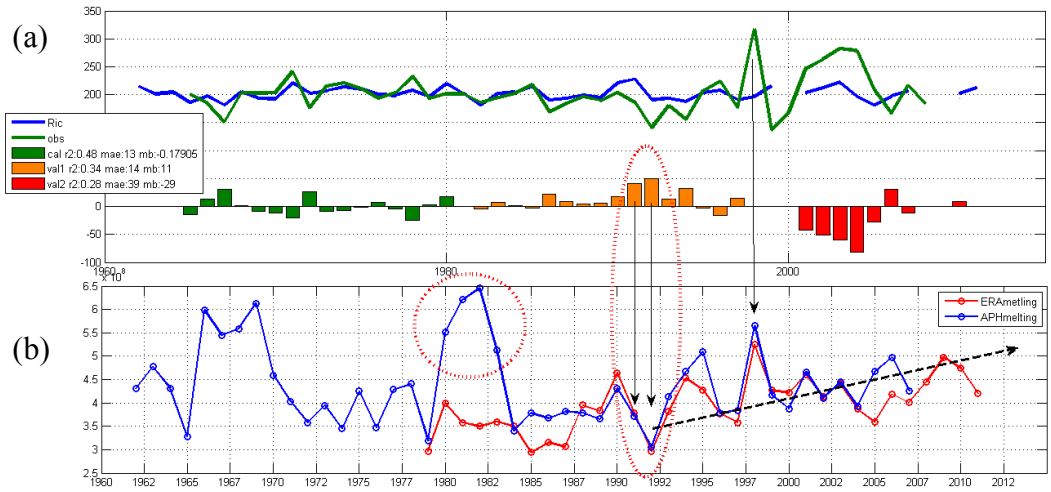

Figure 36. River discharge and glacier melt. **(a)** Comparison of the observed (Obs) discharge and estimated (Ric) annual discharge using multilinear regression of standardized precipitation indices (SPIs). Lower bar plot shows the residual between Obs and Ric series for calibration (green), validation 1 (orange), and validation 2 (red) periods. **(b)** Annual glacier melts (m3) computed by T-index method using ERA-Interim and APHRODITE mean temperature.

Human activities (e.g., land use) may impact on surface runoff, groundwater, or evapotraspiration processes and occurrence of major seismic events can disturb the groundwater processes. In the Dudh Koshi basin (670), there were extremely low urbanization and anthropic activities as well as no any recorded major seismic events during the period under study to explain the discharge behaviour. For this reason, the residues between the estimated and the observed discharge are attributable to non-stationarity in the Cryosphere component. Moreover, the eventual change in surface

water retention capacity (and thus, non-stationarity in the runoff process) due to glacial lake surface change are considered irrelevant because of limited water volumes. Finally, considering these residues at the annual scale does remove eventual impact of non-stationarity on the seasonal snow pack and may, thus, fully be attributable to non-stationarity in the Cryosphere component (glacier processes).

The glacier meltwater computed by ERA and APHRODITE fits well after the late 1980s (Fig. 36). The figure further indicates that the meltwater from the APHRODITE in 1980-1983 and second half of the 1960s, due to inherent high temperature records in the APHRODITE series. The glacier melt waters from both series are increasing after 1990s. Some signals (indicated by arrows in the figure) corresponding to both observed discharge and calculated glacier melts suggest an influence of temperature to the anomaly in the river discharge and can be justifiable why the simulated discharge has higher bias on that year.

Another evidence that we have, is the reduction of precipitation at ~5000 m that is accelerating after 2000. Probably, the reduced precipitation can involve a reduce cloud cover, and thus increases incoming radiation. As discussed on the SEB at the end of section 5.3.2, the results signify the radiation as a main energy sources for melting of the glaciers in this region. From another perspective, in the higher elevation, precipitation appears in the form of snow as temperatures are below zero. The previous studies indicate that precipitation in the form of snow, when apprears, prevent the melting of glaciers due to increased surface albedo, while the decrease in the snowfall can decrease surface albedo and as a consequence increased glacier melting. This means that the decrease in precipitation significantly alters the glacier ablation by increasing the discharge.

Finally, in this chapter, we presented the recent conditions of river flow trends linked with glacier melt and eventually, linked with climate change. The potential climatic impacts on hydrology under the climate change in the Himalayan basins needs better assessment for management of water resources. In case of catchments hosting several glaciers, the hydrological response is a function of the combined effect of different glacier volume changes, and is therefore more variable in space and time.

6

Conclusion and Perspectives

This thesis work made use of the existing datasets from multiple sources and studied climate variables, in particular, temperature and precipitation at high elevation of the south slopes of Mt. Everest and examined the possible impacts to a) glaciers variables, b) glacial lake surface, and c) frequency of daily river discharge. Distinct climatic trends are established for the high elevation (~ 5000 m) at the location of the glaciers ablation area and glacial lakes. This study confirmed in the southern slope of Mt. Everest an increasing temperature and decreasing precipitation trend in the last decades with subsequent impacts on glacier melt and evolution of glacial lakes.

A continuously increasing trend of annual temperature has been found since the 1960s to 2013 in the high elevation (~ 5000 m). The increasing temperature trend occurred mainly in the winter months and secondarily in spring, but not during the summer months. All the other ground stations confirm this pattern. We confirmed for the higher elevation (~ 5000 m) a generalized weakening of the monsoon implied by some previous studies. The precipitation increased slightly from 1960s to 1990s, but decreased significantly after 1990s, accounting for nearly 50 % of reduction in monsoon precipitation in the last 20 years.

The glaciers here are following a general trend of shrinking over the Himalaya, but less than that of others in the western and eastern Himalaya, and southern and eastern Tibetan Plateau. Their position in higher elevations has likely reduced the impact of warming on these glaciers, but have not excluded from a relentlessly continuous and slow recession process over the past 50 years. The surface areas have decreased from 1960s to recent time with an accelerated rate in the last two decades. The shrinkages of glaciers are with the highest rate in the accumulation zone compared to ablation in the last two decades, attributable to decreasing precipitation quantity in the higher elevation. The accelerated increasing number and surface area of supragracial lakes in the last decade confirms the acceleration of the mass loss of glaciers, might be due to reduced glacier flow velocities caused by decreased precipitation. Unconnected lakes have increased from 1960s to early 1990s and decreased afterward, reflecting precisely the observed precipitation trend.

River runoff moderately increased in the last decade, while it was more or less stationary before. The increase in the river runoff was concentrated during the post-monsoon and winter months. The increasing of the discharge is affected by an accelerated glacier melting as observed through the glacier shrinkage, but could not directly justifiable by the observed weakening monsoon. However, we suspect that a strong reduced accumulation (weaker precipitation) which probably induced lower ice velocities of debris covered tongues and a consequent higher melting, or resulted the least cloud cover permitting more radiation to the glacier surface, and ultimately augmenting the melting.

The shrinkage of glaciers is usually attributed to temperature increase during the summer; while in our study area, we observed a stationary trend during the warmer months. Consequently, the role of precipitation becomes central in the climate change impact studies of the region. The accelerated shrinkage of glaciers observed in the last two decades can be ascribed to the regional monsoon weakening. This study was conducted through the best available datasets in this region. We underline that for addressing the need of more accurate investigation of the climate and their future possible impacts, it is necessary to continue and prioritize the production of good quality and high-resolution climate, glaciological and hydrological data. In subsequent research, it is important investigate the variation of solar radiation at high elevation and to look for improvement in the glacier melt computation with consideration of assuring radiation data to better understand climate-glacier-river flow nexus and to understand the behavior of river discharge under climate change. Application of this approach to investigate in other basins could also provide a regional perspective on the hydrological behaviour of the river system.

7

References

Ageta, Y. and K. Fujita (1996) Characteristics of mass balance of summer-accumulation type glaciers in the Himalayas and Tibetan Plateau. *Z. Gletscherkd, Glazialgeol.,* 32, 61–65, 1996.

Ageta, Y., S. Iwata, H. Yabuki, N. Naito, A. Sakai, C. Narama, and T. Karma (2000) Expansion of glacier lakes in recent decades in the Bhutan Himalayas. *IAHS Publ.*, 264, 165–175.

Arnold, J. G., D. N. Moriasi, P. W. Gassman, K. C. Abbaspour, M. J. White, R. Srinivasan, C. Santhi, R. D. Harmel, A. van Griensven, M. W. Van Liew, N. Kannan, and M. K. Jha (2012) SWAT: Model use, calibration, and validation. *Trans. ABASE*, 55(4), 1491–1058.

Ashfaq, M., Y. Shi, W. Tung, R. J. Trapp, X. Gao, J. S. Pal, and N. S. Diffenbaugh (2009) Suppression of south Asian summer monsoon precipitation in the 21st century. *Geophys. Res. Lett.,* 36, 1704–1709, doi: 10.1029/2008GL036500.

Bagla, P. (2009) No sign yet of Himalayan meltdown, Indian report finds. *Science*, 326, 924–925.

Bahr, D. B., W. T. Pfeffer, C. Sassolas, and M. F. Meier (1998) Response time of glaciers as a function of size and mass balance: 1. Theory. *J. Geophys. Res.,* 103, B5, 9777–9782.

Bajracharya, B., K. Uddin, N. Chettri, B. Shrestha, and S. A. Siddiqui (2010) Understanding land cover change using a harmonized classification system in the Himalayas: A case study from Sagarmatha National Park, Nepal. *Mt. Res. Dev.,* 30 (2), 143–156.

Bajracharya, S. R. and P. Mool (2009) Glaciers, glacial lakes and glacial lake outburst floods in the Mount Everest region, Nepal. *Ann. Glaciol.,* 50, 81–86.

Bajracharya, S. R., P. K. Mool, and B. R. Shrestha (2007) Impact of climate change on Himalayan glaciers and glacial lakes: Case studies on GLOF and associated hazards in Nepal and Bhutan. Pp. 119, Kathmandu: ICIMOD.

Barnett, T. P., J. C. Adam, and D. P. Lettenmaier (2005) Potential impacts of a warming climate on water availability in snow-dominated regions. *Nature,* 438, 303–309.

Beniston, M. (2003) Climatic change in mountain regions: a review of possible impacts. *Climatic Change*, 59, 5-31.

Benn, D. I., T. Benn, K. Hands, J. Gulley, A. Luckman, L. I. Nicholson, D. Quincey, S. Thompson, R. Toumi, and S. Wiseman (2012) Response of debris-covered glaciers in the Mount Everest region to recent warming, and implications for outburst flood hazards. *Earth-Sci. Rev.,* 114, 156–174.

Benn, D., S. Wiseman, and K. Hands (2001) Growth and drainage of supraglacial lakes on debris-mantled Ngozumpa Glacier, Khumbu Himal, Nepal. *J. Glaciol.,* 47 (159), 626–638.

Benn, D.I., and L.A. Owen (1998) The role of the South Asian summer monsoon and the mid-latitude westerlies in controlling Himalayan glacial cycles: Review and speculative discussion. *J. Geological Society* London, 155, 353–363.

Bolch, T., A. Kulkarni, A. Kääb, C. Huggel, F. Paul, J. G. Cogley, H. Frey, J. S. Kargel, K. Fujita, M. Scheel, S. Bajracharya, and M. Stoffel (2012) The state and fate of Himalayan glaciers. *Science,* 336, 310–314.

Bolch, T., M. Buchroithner, T. Pieczonka, and A. Kunert (2008a) Planimetric and volumetric glacier changes in the Khumbu Himalaya since 1962 using Corona, Landsat TM and ASTER data. *J. Glaciol.,* 54, 592–600.

Bolch, T., M. F. Buchroithner, J. Peters, M. Baessler, and S. Bajracharya (2008b) Identification of glacier motion and potentially dangerous glacial lakes in the Mt. Everest region/Nepal using spaceborne imagery. *Nat. Hazards Earth Syst. Sci.,* 8, 1329–1340.

Bolch, T., T. Pieczonka, and D. I. Benn (2011) Multi-decadal mass loss of glaciers in the Everest area (Nepal Himalaya) derived from stereo imagery. *The Cryosphere,* **5**, 349-358, doi: 10.5194/tc-5- 349-2011.

Bollasina, M. A., Y. Ming, and V. Ramaswamy (2011) Anthropogenic aerosols and the weakening of the South Asian summer monsoon. *Science,* 334, 502–505.

Bookhagen, B. and D. W. Burbank (2010) Toward a complete Himalayan hydrological budget: Spatiotemporal distribution of snowmelt and rainfall and their impact on river discharge. *J. Geophys. Res.,* 115, F03019, doi: 10.1029/2009JF001426.

Bortolami, G. (1998) Geology of Khumbu Region, Mt. Everest, Nepal. In: Lami, A. and G. Giussani (Eds), *Limnology of high altitude lakes in the Mt. Everest Region (Nepal). Mem. Ist. ital. Idrobiol.*, 57, 41-49.

Brock, B. W. and N. S. Arnold (2000) A spreadsheet-based (Microsoft Excel) point surface energy balance model for glacier and snow melt studies, Technical Communication. *Earth Surf. Process. Landforms, 25*, 649-658.

Cogley, J. G., J. S. Kargel, G. Kaser, and C. J. Van der Veen (2010) Tracking the source of glacier misinformation. *Science*, 327, 522.

Collin, D. N., J. L. Davenport, M. Stoffel (2013) Climatic variation and runoff from partially-glacierized Himalayan tributary basins of the Ganges. *Sci. Total Environ.,* S48–S59, 468–469.

Collins, D. (2008) Climatic warming, glacier recession and runoff from Alpine basins after the Little Ice Age maximum. *Ann. Glaciol.,* 48, 119–124.

Cuffey, K. M. and W. S. B. Paterson (2010) The Physics of Glaciers. 4th edition, Elsevier, Inc. pp. 704.

Dee, D. P., M. Balmaseda, G. Balsamo, R. Engelen, A. J. Simmons, and J.-N. Thepaut (2014) Toward a consistent reanalysis of the climate system. *BAMS,* 1235–1248, doi: 10.1175/BAMS-D-13-00043-1.

Déqué, M. (2007) Frequency of precipitation and temperature extremes over France in an anthropogenic scenario: Model results and statistical correction according to observed values. *Global Planet. Change*, 57, 16–26, doi: 10.1016/j.gloplacha.2006.11.030.

Fan, Y. and H. van den Dool (2008) A global monthly land surface air temperature analysis for 1948-present. *J. Geophys. Res.,* 113, D01103, doi: 10.1029/2007JD008470.

Fowler, H. J., S. Blenkisop, and C. Tebaldi (2007) Review Linking climate change modelling to impacts studies: recent advances in downscaling techniques for hydrological modelling. *Int. J. Climatol.,* 27, 1547–1578, 2007.

Frìas, M. D., E. Zorita, J. Fernàndez, and C. Rodrìguez-Puebla (2006) Testing statistical downscaling methods in simulated climates. *Geophys. Res. Lett.,* 33, L19807, doi: 10.1029/2006GL027453.

Fujii, Y. and K. Higuchi (1977) Statistical analysis of the forms of the glaciers in the Khumbu Himal. *J. Jap. Soc. Snow Ice,* 39, 7–14.

Fujita, K. and A. Sakai (2014) Modelling runoff from a Himalayan debris-covered glacier. *Hydrol. Earth Syst. Sci.,* 18, 2679–2694, doi: 10.5194/hess-18-2679–2014.

Fujita, K. and T. Nuimura (2011) Spatially heterogeneous wastage of Himalayan glaciers. *Proc. Natl. Acad. Sci.* USA, 108, 14011– 14014.

Fujita, K., A. Sakai, T. Nuimura, S. Yamaguchi, and R. R. Sharma (2009) Recent changes in Imja Glacial Lake and its damming moraine in the Nepal Himalaya revealed by in situ surveys and multi-temporal ASTER imagery. *Environ. Res. Lett.,* 4, 045205, doi: 10.1088/1748-9326/4/4/045205.

Fujita, K., T. Kadota, B. Rana, R. B. Kayastha, and Y. Ageta (2001) Shrinkage of Glacier AX010 in Shorong region, Nepal Himalayas in the 1990s. *Bull. Glaciol. Res.,* 18, 51–54.

Fushimi, H., K. Ikegami, K. Higuchi, and K. Shankar, (1985) Nepal case study: Catastrophic floods. *IAHS Publication*, 149, 125–130.

Gardelle, J., E. Berthier, Y. Arnaud, and A. Kääb (2013) Region-wide glacier mass balances over the Pamir-Karakoram-Himalaya during 1999–2011. *The Cryosphere*, 7, 1263–1286, doi: 10.5194/tc-7-1263-2013.

Gardelle, J., Y. Arnaud, and E. Berthier (2011) Contrasted evolution of glacial lakes along the Hindu Kush Himalayan mountain range between 1990 and 2009. *Global Planet. Change*, 75, 47-55.

Gardner, A. S., G. Moholdt, J. G. Cogley, B. Wouters, A. A. Arendt, J. Wahr, E. Berthier, R. Hock, W. T. Pfeffer, G. Kaser, S. R. M Ligtenberg, T. Bolch, M. J. Sharp, J. O. Hagen, M. R. van den Broeke, and F. Paul (2013) A reconciled estimate of glacier contributions to Sea level rise: 2003 to 2009. *Science,* 340, 852–857.

Guyennon, N., E. Romano, I. Portoghese, F. Salerno, S. Calmanti, A. B. Petrangeli, G. Tartari, and D. Copetti (2013) Benefits from using combined dynamical-statistical downscaling approaches – lessons from a case study in the Mediterranean region. *Hydrol. Earth Syst. Sci.,* 17, 705-720, doi: 10.5194/hess-17-705-2013.

Harris, I., P. D. Jones, T. J. Osborn, and D. H. Lister (2014) Updated high-resolution grids of monthly climatic observations – the CRU TS3.10 Dataset. *Int. J. Climatol.,* 34, 623–642.

Hewitson, B. C. and R. G. Crane (1996) Climate downscaling: techniques and application. *Clim. Res.,* 7, 85–95.

Higuchi, K., H. Fushimi, T. Ohata, S. Takenaka, S. Iwata, K. Yokoyama, H. Higuchi, A. Nagoshi, and T. Iozawa (1980) Glacier inventory in the Dudh Kosi region, East Nepal. World Glacier Inventory–Inventraire mondial des Glaciers (Proceedings of the Riederalp Workshop, September 1978), *IAHS–AISH Publ.* 126, 1980.

Hock, R. (2003) Temperature index melt modelling in mountain areas. *J. Hydrol.,* 282, 1-4, 104– doi: 115.10.1016/S0022-1694(03)00257-9.

Hock, R. (2005) Glacier melt: a review of processes and their modeling. *Prog. Phys. Geography*, 29, 3, 362–391. doi: 10.1191/0309133305pp453ra.

Ichiyanagi, K., M. D. Yamanaka, Y. Muraji, and B. K. Vaidya (2007) Precipitation in Nepal between 1987 and 1996. *Int. J. Climatol.,* 27, 1753–1762.

Immerzeel, W. W., F. Pellicciotti, and M. F. P. Bierkens (2013) Rising river flows throughout the twenty-first century in two Himalayan glacierized watersheds. *Nature Geosci.,* 6, 1–4, doi: 10.1038/ngeo1896.

Immerzeel, W. W., L. P. H. van Beek, M. Konz, A. B. Shrestha, and M. F. P. Bierkens (2012) Hydrological response to climate change in a glacierized catchment in the Himalayas. *Clim. Change,* 110, 721–736, doi: 10.1007/s10584-011-0143-4.

Immerzeel, W. W., L. P. Van Beek, and M. F. P. Bierkens (2010) Climate change will affect the Asian water towers. *Science,* 328, 1382–5.

IPCC (2013) Climate Change 2013: The Physical Science Basis. Contribution of Working Group I to the Fifth Assessment Report of the Intergovernmental Panel on Climate Change [Stocker, T.F., D. Qin, G.-K. Plattner, M. Tignor, S.K. Allen, J. Boschung, A. Nauels, Y. Xia, V. Bex and P.M. Midgley (Eds.)]. Cambridge University Press, Cambridge, United Kingdom and New York, NY, USA, pp. 1535.

Jacob, T., J. Wahr, W. T. Pfeffer, and S. Swenson (2012) Recent contributions of glaciers and ice caps to sea level rise. *Nature,* 482, 514–518.

Kääb, A. and M. Vollmer (2000) Surface geometry, thickness changes and flow fields on creeping mountain permafrost: Automatic extraction by digital image analysis. *Permafrost Periglac. Process.,* 11, 315-326.

Kääb, A., E. Berthier, C. Nuth, J. Gardelle, and Y. Arnaud (2012) Contrasting patterns of early twenty-first-century glacier mass change in the Himalayas. *Nature*, 488, 495-498, doi: 10.1038/natue11324.

Kadota, T., K. Seko, and Y. Ageta (1993) Shrinkage of glacier AX010 since 1978, Shorong Himal, east Nepal. *IAHS Publ.* 218 (Symposium at Kathmandu, 1992 – Snow and Glacier Hydrology), 145–154.

Kang, I.-S., K. Jin, B. Wang, K.-M. Lau, J. Shukla, V. Krishnamurthy, S. D. Schubert, D. E. Wailser, W. F. Stern, A. Kitoh, G. A. Meehl, M. Kanamitsu, V. Y. Galin, V. Satyan, C.-K. Park, and Y. Liu (2002) Intercomparison of the climatological variations of Asian summer monsoon precipitation simulated by 10 GCMs. *Climate Dyn.,* 19, 383–395.

Kaser, G., M. Grosshauser, and B. Marzeion (2010) Contribution potential of glaciers to water availability in different climate regimes. *Proc. Natl Acad. Sci.* USA, 107, 47, 20223–20227.

Kattel, D. B. and T. Yao (2013) Recent temperature trends at mountain stations on the southern slope of the central Himalayas. *J. Earth Syst. Sci.,* 122, 215–227. doi: 10.1007/s12040-012-0257-8.

Kayastha, R. B., Y. Ageta, and M. Nakawo (2000) Positive degree-day factors for ablation on glaciers in the Nepalese Himalayas: Case study on Glacier AX010 in Shorong Himal, Nepal. *Bull. Glaciol. Res.,* 17, 1–10.

Kendall, M. G. (1975) Rank Correlation Methods, Oxford University Press, New York.

Kuhn, M. (1981) Climate and Glaciers. In: Allison, I. (Ed.) *Sea Level, Ice, and Climate Change* (Proc. Canberra Sym., December 1979), IAHS Publ. 131, 3–20 .

Kumar, K. R., A. K. Sahai, K. K. Kumar, S. K. Patwardhan, P. K. Mishra, J. V. Revadekar, K. Kamala, and G. B. Pant (2006) High-resolution climate change scenarios for India for the 21st century. *Curr. Sci.,* 90, 3, 334–345.

Lamsal, D., T. Sawagaki, and T. Watanabe (2011) Digital terrain modelling using Corona and ALOS PRISM data to investigate the distal part of Imja glacier, Khumbu Himal, Nepal. *J. Mt. Sci.* [China], 8(3), 390–402, doi: 10.1007/s11629-011-2064-0.

Legates, D. and G. J. McCabe (1999) Evaluating the use of "goodness-of-fit" measures in hydrologic and hydroclimatic model validation. *Water Resour. Res.,* 35, 233– 241.

Löffler, H. (1969) High altitude lakes in Mt. Everest region. *Verh. int. Ver. Limnol.*, 17, 373-385.

Lutz, A. F., W. W. Immerzeel, A. B. Shrestha, and M. F. P. Bierkens (2014) Consistent increase in High Asia's runoff due to increasing glacier melt and precipitation. *Nature Climate Change,* doi: 10.1038/NCLIMATE2237.

McFeeters, S. K. (1996) The use of the Normalized Difference Water Index (NDWI) in the delineation of open water features. *Int. J. Remote Sens.,* 17(7), 1425-1432.

McKee, T. B., N. J. Doesken, and K. Kleist (1993) The relationship of drought frequency and duration to time scale. In: *Proc. 8th Conference on Applied Climatology, 17–22 January, Anaheim, CA*. American Meteorological Society, Boston, MA. 179–184.

Mool, P. K., S. R. Bajracharya, and S. P. Joshi (2001) Inventory of Glaciers, Glacial Lakes and Glacial Lake Outburst Floods, Mon- itoring and Early Warning Systems in the Hindu Kush-Himalaya Region, ICIMOD, Nepal.

Müller, F. (1970) A pilot study for an inventory of the glaciers in the eastern Himalayas: inventory of glaciers in the Mount Everest region. In: Perennial ice and snow masses: a guide for compilation and assemblage of data for a world inventory. Paris: UNESCO/International Association of Scientific Hydrology, 47– 59. (Technical Papers in Hydrology 1.)

Nash, J. E. and J. Sutcliffe (1970) River flow forecasting through conceptual models: part 1. A discussion of principles. *J. Hydrol.,* 10 (3), 282–290.

Neitsch, S. L., J. G. Arnold, J. R. Kiniry, and J. R. Williams (2011) Soil and Water Assessment Tool Theoretical Documentation. Texas Water Resources Insitute Technical Report No. 406, Agriculture Research Service and Texas A&M Univerisity, Texas, pp. 647.

Nepal, S., P Krause, W.-A. Flügel, M. Fink, and C. Fischer (2014) Understanding the hydrological system dynamics of a glaciated alpine catchment in the Himalayan region using the J2000 hydrological model. *Hydrol. Process.,* 28, 1329–1344.

Neupane, R. P., J. Yao, and J. D. White (2013) Estimating the effects of climate change on the intensification of monsoonal-driven stream discharge in a Himalayan watershed. *Hydrol. Process.,* doi: 10.1002/hyp.10115.

Nie, Y., Y. Zhang, L. Liu, and J. Zhang (2010) Glacial change in the vicinity of Mt. Qomolangma (Everest), central high Himalayas since 1976. *J. Geogr. Sci.,* 20, 667–686.

Nuimura, T., K. Fujita, S. Yamaguchi, and R. R. Sharma (2012) Elevation changes of glaciers revealed by multitemporal digital elevation models calibrated by GPS survey in the Khumbu region, Nepal Himalaya, 1992–2008. *J. Glaciol.,* 58, 648–656.

Oerlemans, J. (1994) Quantifying global warming from the retreat of glaciers. *Science,* 264, 243–245.

Osti, R. and S. Egashira (2009) Hydrodynamic characteristics of the Tam Pokhari Glacial Lake outburst flood in the Mt. Everest region, Nepal. *Hydrol. Process.,* 23, 2943–2955, doi: 10.1002/hyp.7405.

Owen, L. A. and D. I. Benn (2005) Equilibrium-line altitudes of the Last Glacial Maximum for the Himalaya and Tibet: An assessment and evaluation of results. *Quatern. Int.,* 138–139, 55–78.

Palazzi, E., J. von Hardenberg, and A. Provenzale (2013) Precipitation in the Hindu-Kush Karakoram Himalaya: observations and future scenarios. *J. Geophys. Res.-Atmos.*, 118, 85–100, doi: 10.1029/2012JD018697.

Paul, F. and W. Haeberli (2008) Spatial variability of glacier elevation changes in the Swiss Alps obtained from two digital elevation models. *Geophys. Res. Lett.,* 35, L21502, doi: 10.1029/2008GL034718.

Paul, F. et al. (2013) The glaciers climate change initiatives: Methods for creating glacier area, elevation change and velocity products. *Rem. Sens. Environ.,* In Press, doi: 10.1016/j.rse.2013.07.043.

Pedersen, V. K. and D. L Egholm (2013) Glaciations in response to climate variations preconditioned by evolving topography. *Nature,* 493, 206–210, doi: 10.1038/nature11786.

Pellicciotti, F., B. Brock, U. Strasser, P. Burlando, M. Funk, and J. Corripio (2005) An enhanced temperature-index glacier melt model including the shortwave radiation balance: development and testing for Haut Glacier d'Arolla, Switzerland. *J. Glaciol.,* 51(175), 573–587.

Pepin, N. C. and J. D. Lundqist (2008) Temperature trends at high elevations: patterns across the globe. *Geophys. Res. Lett.,* 35, L14701, doi: 10.1029/2008GL034026.

Peters, J., T. Bolch, M. F. Buchroithner, and M. Bäßler (2010) Glacier surface velocities in the Mount Everest area/Nepal using ASTER and Ikonos imagery. Proceeding of 10th International Symposium on High Mountain Remote Sensing Cartography, Kathmandu, Nepal, 313-320.

Quincey, D. J., A. Luckman, and D. Benn (2009) Quantification of Everest region glacier velocities between 1992 and 2002, using satellite radar interferometry and feature tracking. *J. Glaciol.,* 55, 192, 596–606.

Quincey, D. J., S. D. Richardson, A. Luckman, R. M. Lucas, J. M. Reynolds, M. J. Hambrey, and N. F. Glasser (2007) Early recognition of glacial lake hazards in the Himalaya using remote sensing datasets. *Global Planet. Change,* 56, 137-152.

Racoviteanu, A. E., M. Williams, and R. Barry (2008) Optical remote sensing of glacier characteristics: A review with focus on the Himalaya. *Sensors,* 8, 3355–3383, 2008.

Racoviteanu, A. E., R. Armstrong, and M. W. Williams (2013) Evaluation of an ice ablation model to estimate the contribution of melting glacier ice to annual discharge in the Nepal Himalaya. *Water Resour. Res.,* 49, 5117–5133.

Rahman, K., C. Maringanti, M. Beniston, F. Widmer, K. Abbaspour, and A. Lehmann (2012) Streamflow modeling in a highly managed mountainous glacier watershed using SWAT: The upper Rhone river watershed case in Switzerland. *Water Resour. Manage.,* doi: 10.1007/s11269-012-0188-9.

Ramanathan, V., C. Chung, D. Kim, T. Bettge, L. Buja, J. T. Kiehl, W. M. Washington, Q. Fu, D. R. Sikka, and M. Wild (2005) Atmospheric brown clouds: Impacts on South Asian climate and hydrological cycle. *Proc. Natl Acad. Sci.* USA, 102, 5326–5333.

Rangwala, I. and J. R. Miller (2012) Climate change in mountains: a review of elevation-dependent warming and its possible causes. *Climatic Change,* 114, 527–547.

Rao, Y. P. (1976) Southwest Monsoon. India Meteorological Department. Meteorological Monograph, New Delhi, pp. 366.

Reynolds, J. M. (2000) On the formation of supraglacial lakes on debris-covered glaciers. *IAHS Publ.,* 264 (Symposium at Seattle 2000 – Debris-Covered Glaciers), 153–161.

Richardson, S. D. and J. M. Reynolds (2000) An overview of glacial hazards in the Himalayas. *Quatern. Int.,* 65/66(1), 31–47.

Rood, R. B. and M. G. Bosilovich (2010) Reanalysis: Data assimilation for scientific investigation of climate. In: Data Assimilation, Making Sense of Observations. Part IV, 623–646, Springer, doi: 10.1007/978-3-540-74703-1_23

Saha, S. et al. (51 others) (2010) The NCEP Climate Forcast System Reanalysis. *BAMS*, American Meteorological Society, 1015–1057.

Sakai, A. and K. Fujita (2010) Formation conditions of supraglacial lakes on debris-covered glaciers in the Himalaya. *J. Glaciol.,* 56 (195), 177-181.

Sakai, A., N. Takeuchi, K. Fujita, and M. Nakawo (2000) Role of supraglacier ponds in ablation process of a debris-covered glacier in the Nepal Himalaya. *IAHS* Publ., 264, 119-130.

Salerno, F. and G. Tartari (2009) A coupled approach of surface hydrological modelling and Wavelet Analysis for understanding the baseflow components of river discharge in karst environments. *J. Hydrol.,* 376, 295–306.

Salerno, F., E. Buraschi, G. Bruccoleri, G. Tartari, and C. Smiraglia (2008) Glacier surface-area changes in Sagarmatha National Park, Nepal, in the second half of the 20th century, by comparison of historical maps. *J. Glaciol.,* 54 (187), 738–752.

Schaner, N., N. Voisin, B. Nijssen, and D. P. Lettenmaier (2012) The contribution of glacier melt to streamflow. *Environ. Res. Lett.,* 7, 034029.

Scherler, D., B. Bookhagen, and M. R. Strecker (2011) Hillslope-glacier coupling: The interplay of topography and glacial dynamics in High Asia. *J. Geophys. Res.,* 116, F02019, doi: 10.1029/2010JF001751.

Scherler, D., B. Bookhagen, and M. R. Strecker (2011) Spatially variable response of Himalayan glaciers to climate change affected by debris cover. *Nat. Geosci.,* 4, 156–159, doi: 10.1038/ngeo1068.

Scherler, D., S. Leprince, and M. R. Strecker (2008) Glacier-surface velocities in alpine terrain from optical satellite imagery - Accuracy improvement and quality assessment. *Remote Sens. Environ.,* 112, 10, 3806–3819.

Schneider, E. (1967) Begleitworte zur Karte Khumbu Himal und zur Namensgebung. In: Hellmich, W. (Ed.) Khumbu Himal. Universitasverlag Wagner, Innsbruck, (Ergebnisse des Forschungsunternehmens Nepal Himalaya Band 1, Lieferung 5.), 430–446.

Schneider, T. (2001) Analysis of incomplete climate data: estimation of mean values and covariance matrices and imputation of missing values. *J. Climate,* 14, 853–871, doi: 10.1175/1520-0442(2001)014<0853:AOICDE>2.0.CO;2.

Schneider, U., A. Becker, P. Finger, A. Meyer-Christoffer, M. Ziese, and B. Rudolf (2013) GPCC's new land surface precipitation climatology based on quality-controlled in situ data and its role in quantifying the global water cycle. *Theor. Appl. Climatol.,* doi: 10.1007/s00704-013-0860-x.

Sen, P. K. (1968) Estimates of the regression coefficient based on Kendall's Tau. *J. Am. Stat. Assoc.,* 63, 1379–1389, doi: 10.2307/2285891.

Senese, A., M. Maugeri, E. Vuillermoz, C. Smiraglia, and G. Diolaiuti (2014) Using daily air temperature thresholds to evaluate snow melting occurange and amount on Alpine glaciers by T-index models: the case study of the Forni Glacier (Italy). *The Cryosphere,* 8, 1921–1933, doi: 10.5194/tc-8-1921-2014.

Sharma, K. P., B. Moore, and C. J. Vorosmarty (2000) Anthropogenic, climatic, and hydrologic trends in the Kosi basin, Himalaya. *Clim. Change,* 47, 141–165.

Shijin, W., and T. Zhang (2014) Spatial change detection of glacial lakes in the Koshi River basin, the Central Himalayas. *Environ. Earth Sci.,* doi: 10.1007/s12665-014-3338-y.

Shrestha, A. B., C. P. Wake, P. A. Mayewski, and J. E. Dibb (1999) Maximum temperature trends in the Himalaya and its vicinity: An analysis based on temperature records from Nepal for the period 1971-94. *J. Clim.,* 12, 2775–2786.

Smiraglia, C. (1998) Glaciers and glaciology of Himalaya. In: Baudo, R., G. Tartari, and M. Munawar (Eds.), Top of the World Environmental Research: Mount Everest – Himalayan Ecosystem. *Ecovision World Monograph Series*, Backhuys Publ., Leiden, 65-100.

Somos-Valenzuela, M. A., D. C. McKinney, D. R. Rounce, and A. C. Byers (2014) Changes in Imja Tsho in the Mount Everest region of Nepal. *The Cryosphere,* 8, 1661–1671, doi: 10.5194/tc-8-1661-2014.

Takeuchi, N. and Z. Li (2008) Characteristics of surface dust on Ürümqi Glacier No. 1 in the Tien Shan Mountains, China. *Arct. Antarct. Alp. Res.,* 40(4), 744–750.

Tartari, G., F. Salerno, E. Buraschi, G. Bruccoleri, and C. Smiraglia (2008) Lake surface area variations in the north-eastern sector of Sagarmatha National Park (Nepal) at the end of the 20th century by comparison of historical maps. *J. Limnol.,* 67, 139–154.

Tartari, G., G. Verza, and L. Bertolami (2002) Meteorological data at the Pyramid Observatory Laboratory (Khumbu Valley, Sagarmatha National Park, Nepal). In: Lami, A. and G. Giussani (Eds.) Limnology of high altitude lakes in the Mt. Everest Region (Nepal). *Mem. Ist. Ital. Idrobiol.,* 57, 23–40.

Tartari, G., L. Previtali, and G. A. Tartari (1998) Genesis of the lake cadastre of Khumbu Himal Region (Sagarmatha National Park, East Nepal). In: Lami, A. and G. Giussani (Eds.), Limnology of high altitude lakes in the Mt. Everest Region (Nepal). *Mem. Ist. ital. Idrobiol.,* 57: 139-149.

Themeßl, M. J., A. Gobiet, and G. Heinrich (2012) Empirical-statistical downscaling and error correction of regional climate models and its impact on the climate change signal. *Climatic Change,* 112, 449–468, doi: 10.1007/s10584-011-0224-4.

Thompson, S. S., D. I. Benn, K. Dennis, and A. Lukman (2012) A rapidly growing moraine-dammned glacial lake on Ngozumpa Glacier, Nepal. *Geomorphology,* 145-146, 1-11.

Torrence, C. and G.P. Compo (1998) A practical guide to wavelet analysis. *Bull. Am. Meteorol. Soc.,* 79, 61–78.

Viviroli, D., D. R. Archer, W. Buytaert, H. J. Fowler, G. B. Greenwood, A. F. Hamlet, Y. Huang, G. Koboltschnig, M. I. Litaor, J. I. López-Moreno, S. Lorentz, B. Schädler, H. Schreier, K. Schwaiger, M. Vuille, and R. Woods (2011) Climate change and mountain water resources: overview and recommendations for research, management and policy. *Hydrol. Earth Syst. Sci.,* 15, 471–504, doi: 10.5194/hess-15-471-2011.

Vuille, M. (2011) Climate variability and high altitude temperature and precipitation. In: Singh, V. P., P. Singh, and U. K. Haritashya (Eds.) *Encyclopedia of Snow, Ice and Glaciers*. Springer, the Netherlands, 153–156.

Wagnon, P., C. Vincent, Y. Arnaud, E. Berthier, E. Vuillermoz, S. Gruber, M. Ménégoz, A. Gilbert, M. Dumont, J. M. Shea, D. Stumm, and B. K. Pokhrel (2013) Seasonal and annual mass balances of Mera and Pokalde glaciers (Nepal Himalaya) since 2007. *The Cryosphere*, 7, 1769–1786, doi: 10.5194/tc-7-1769- 2013.

Watanabe, T., D. Lamsal, and J. D. Ives (2009) Evaluating the growth characteristics of a glacial lake and its degree of danger of outburst flooding: Imja-Lhotse Shar glacier, Khumbu Himal, Nepal. *Norsk Geogr. Tidssk.,* 63, 255–267.

Yamada, T. (1998) Glacier lake and its outburst flood in the Nepal Himalaya. Monograph No. 1, Data Center for Glacier Research. Japanese Society of Snow and Ice, pp. 96.

Yamada, T. and C. K. Sharma (1993) Glacier lakes and outburst floods in Nepal Himalaya. *Snow and Glacier Hydrology*, IAHS Publication, 218, 319–330.

Yamada, T. T. Shiraiwa, H. Iida, T. Kadota, T. Watanabe, B. Rana, Y. Ageta, and H. Fushimi (1992) Fluctuations of the glaciers from the 1970s to 1989 in the Khumbu, Shorong and Langtang regions, Nepal Himalayas. *Bull. Glacier Res.,* 10, 11–19.

Yao, T., L. Thompson, W. Yang, W. Yu, Y. Gao, X. Guo, X. Yang, K. Duan, H. Zhao, B. Xu, J. Pu, A. Lu, Y. Xiang, D. B. Kattel, and D. Joswiak (2012) Different glacier status with atmospheric circulations in Tibetan Plateau and surroundings. *Nat. Clim. Change,* 2, 663–667.

Yasutomi, N., A. Hamada, and A. Yatagai (2011) Development of a long-term daily gridded temperature dataset and its application to rain/snow discrimination of daily precipitation. *Global Environ. Res.,* V15N2, 165–172.

Yatagai, A., K. Kamiguchi, O. Arakawa, A. Hamada, N. Yasutomi, and A. Kitoh (2012) APHRODITE: Constructing a Long-term Daily Gridded Precipitation Dataset for Asia based on a Dense Network of Rain Gauges. *BAMS,* doi: 10.1175/BAMS-D-11-00122.1.

8

Peer-Reviewed Articles

Article I

8.1 Article I

Salerno, F., N. Guyennon, S. Thakuri, G. Viviano, E. Romano, E. Vuillermoz, P. Cristofanelli, P. Stocchi, G. Agrillo, Y. Ma, and G. Tartari (2014) Weak precipitation, warm winters and springs impact glaciers of south slopes of Mt. Everest (central Himalaya) in the last two decades (1994-2013). *The Cryosphere Discuss.,* **8, 5911–5959, doi: 10.5194/tcd-8-5911–2014.**

The Cryosphere Discuss., 8, 5911–5959, 2014
www.the-cryosphere-discuss.net/8/5911/2014/
doi:10.5194/tcd-8-5911-2014

The Cryosphere Discussions
Open Access

Weak precipitation, warm winters and springs impact glaciers of south slopes of Mt. Everest (central Himalaya) in the last two decades (1994–2013)

F. Salerno[1,4], N. Guyennon[2], S. Thakuri[1,4], G. Viviano[1], E. Romano[2], E. Vuillermoz[4], P. Cristofanelli[3,4], P. Stocchi[3], G. Agrillo[3], Y. Ma[5], and G. Tartari[1,4]

[1]National Research Council, Water Research Institute, Brugherio (IRSA-CNR), Italy
[2]National Research Council, Water Research Institute, Roma (IRSA-CNR), Italy
[3]National Research Council, Institute of Atmospheric Sciences and Climate (ISAC-CNR) Bologna, Italy
[4]Ev-K2-CNR Committee, Via San Bernardino, 145, Bergamo 24126, Italy
[5]Institute of Tibetan Plateau Research, Chinese Academy of Science, China

Received: 22 September 2014 – Accepted: 5 November 2014 – Published: 1 December 2014

Correspondence to: F. Salerno (salerno@irsa.cnr.it)

Published by Copernicus Publications on behalf of the European Geosciences Union.

Abstract

Studies on recent climate trends from the Himalayan range are limited, and even completely absent at high elevation. This contribution specifically explores the southern slopes of Mt. Everest (central Himalaya), analyzing the minimum, maximum, and mean temperature and precipitation time series reconstructed from seven stations located between 2660 and 5600 m a.s.l. over the last twenty years (1994–2013). We complete this analysis with data from all the existing ground weather stations located on both sides of the mountain range (Koshi Basin) over the same period. Overall we observe that the main and more significant increase in temperature is concentrated outside of the monsoon period. At higher elevations minimum temperature ($0.072 \pm 0.011\,^{\circ}\mathrm{C\,a^{-1}}$, $p < 0.001$) increased far more than maximum temperature ($0.009 \pm 0.012\,^{\circ}\mathrm{C\,a^{-1}}$, $p > 0.1$), while mean temperature increased by $0.044 \pm 0.008\,^{\circ}\mathrm{C\,a^{-1}}$, $p < 0.05$. Moreover, we note a substantial precipitation weakening ($9.3 \pm 1.8\,\mathrm{mm\,a^{-1}}$, $p < 0.01$ during the monsoon season). The annual rate of decrease at higher elevation is similar to the one at lower altitudes on the southern side of the Koshi Basin, but here the drier conditions of this remote environment make the fractional loss much more consistent (47 % during the monsoon period). This study contributes to change the perspective on which climatic driver (temperature vs. precipitation) led mainly the glacier responses in the last twenty years. The main implications are the following: (1) the negative mass balances of glaciers observed in this region can be more ascribed to less accumulation due to weaker precipitation than to an increase of melting processes. (2) The melting processes have only been favored during winter and spring months and close to the glaciers terminus. (3) A decreasing of the probability of snowfall has significantly interested only the glaciers ablation zones (10 %, $p < 0.05$), but the magnitude of this phenomenon is decidedly lower than the observed decrease of precipitation. (4) The lesser accumulation could be the cause behind the observed lower glacier flow velocity and the current stagnation condition of tongues, which in turn could have trigged melting processes under the debris glacier coverage, leading to the formation of numerous

supraglacial and proglacial lakes that have characterized the region in the last decades. Without demonstrating the causes that could have led to the climate change pattern observed at high elevation, we conclude by listing the recent literature on hypotheses that accord with our observations.

1 Introduction

The current uncertainties concerning the glacial shrinkage in the Himalayas are mainly attributed to a lack of measurements, both of the glaciers and of climatic forcing agents (e.g., Bolch et al., 2012). Recent results underline the need for a fine scale investigation, especially at high altitude, to better model the hydrological dynamics in this area. However, there are few high elevation weather stations in the world where the glaciers are located (Tartari et al., 2009). This can be attributed to the remote location of glaciers, the rugged terrain, and a complex political situation, all of which make physical access difficult (Bolch et al., 2012). As a consequence of the remoteness and difficulty in accessing many high elevation sites combined with the complications of operating automated weather stations (AWSs) at these altitudes, long-term measurements are challenging (Vuille, 2011). However, nearly all global climate models report increased sensitivity to warming at high elevations (e.g., Rangwala and Miller, 2012), while observations are less clear (Pepin and Lundqist, 2008). Moreover, changes in the timing or amount of precipitation are much more ambiguous and difficult to detect, and there is no clear evidence of significant changes in total precipitation patterns in most mountain regions (Vuille, 2011).

The need for a fine scale investigation is particularly evident on the south slope of Mt. Everest (central Southern Himalaya, CH-S) as it is one of the heavily glaciated parts of the Himalaya (Salerno et al., 2012; Thakuri et al., 2014). Nevertheless, these glaciers have the potential to build up moraine-dammed lakes storing large quantities of water, which are susceptible to GLOFs (glacial lake outburst floods) (e.g., Salerno et al., 2012; Fujita et al., 2013). Gardelle et al. (2011) noted that this region is most characterized

by glacial lakes in the Hindu Kush Karakorum Himalaya. Recently, Thakuri et al. (2014) noted that the Mt. Everest glaciers experienced an accelerated shrinkage in the last twenty years (1992–2011), as underlined by an upward shift of the Snow Line Altitude (SLA) with a velocity almost three times greater than the previous period (1962–1992). Furthermore Bolch et al. (2011) and Nuimura et al. (2012) found a higher mass loss rate during the last decade (2000–2010). Anyway, to date, there are not continuous meteorological time series able to clarify the causes of the melting process to which the glaciers of these slopes are subjected.

In this context, since the early 1990s, PYRAMID Observatory Laboratory (5050 m) was created by the Ev-K2-CNR Committee (www.evk2cnr.org). This observatory is located at the highest elevation at which weather data has ever been collected in the region and thus represents a valuable dataset with which to investigate the climate change in CH-S (Tartari et al., 2002; Lami et al., 2010). However, the remoteness and the harsh conditions of the region over the years have complicated the operations of the AWSs, obstructing long-term measurements from a unique station.

In this paper, we mainly explore the small scale climate variability of the south slopes of Mt. Everest by analyzing the minimum, maximum, and mean air temperature (T) and precipitation (Prec) time series reconstructed from seven AWSs located from 2660 to 5600 m a.s.l. over the last couple of decades (1994–2013). Moreover, we complete this analysis with all existing weather stations located on both sides of the Himalayan range (Koshi Basin) for the same period. In general, this study has the ultimate goal of linking the climate change patterns observed at high elevation with the glacier responses over the last twenty years, during which a more rapid glacier shrinkage process occurred in the region of investigation.

2 Region of investigation

The current study is focused on the Koshi (KO) Basin which is located in the eastern part of central Himalaya (CH) (Yao et al., 2012; Thakuri et al., 2014). To explore pos-

sible differences in the surroundings of Mt. Everest, we decided to consider the north and south parts of CH (with the suffixes -N and -S, respectively) separately (Fig. 1a). The KO River (58 100 km^2 of the basin) originates in the Tibetan Plateau (TP) and the Nepali highlands. The area considered in this study is within the latitudes of 27° and 28.5° N and longitudes of 85.5° and 88° E. The altitudinal gradient of this basin is the highest in the world, ranging from 77 to 8848 m a.s.l., i.e., Mt. Everest. We subdivide the KO Basin into the northern side (KO-N), belonging to the CH-N, and southern side (KO-S), belonging to the CH-S. The southern slopes of Mt. Everest are part of the Sagarmatha (Everest) National Park (SNP) (Fig. 1b), where the small scale climate variability at high elevation is investigated. The SNP is the world's highest protected area, with over 30 000 tourists in 2008 (Salerno et al., 2013). The park area (1148 km^2), extending from an elevation of 2845 to 8848 m a.s.l., covers the upper Dudh Koshi (DK) Basin (Manfredi et al., 2010; Amatya et al., 2010). Land cover classification shows that almost one-third of the territory is characterized by glaciers and ice cover (Salerno et al., 2008; Tartari et al., 2008), while less than 10 % of the park area is forested (Bajracharya et al., 2010). The SNP presents a broad range of bioclimatic conditions with three main bioclimatic zones: the zone of alpine scrub; the upper alpine zone, which includes the upper limit of vegetation growth; and the Arctic zone, where no plants can grow (UNEP and WCMC, 2008). Figure 1c shows the glacier distribution along the hypsometric curve of the SNP. We observe that the glacier surfaces are distributed from 4300 to above 8000 m a.s.l., with more than 75 % of the glacier surfaces lying between 5000 and 6500 m a.s.l. The 2011 area-weighted mean elevation of the glaciers was 5720 m a.s.l. (Thakuri et al., 2014). These glaciers are identified as the summer accumulation-type fed mainly by summer Prec from the South Asian monsoon system, whereas the winter Prec caused by the mid-latitude westerly wind is minimal (Yao et al., 2012). The prevailing direction of the monsoons is S–N and SW–NE (e.g., Ichiyanagi et al., 2007). The climate is influenced by the monsoon system because the area is located in the subtropical zone with nearly 90 % of the annual Prec falling in the months of June to September (this study). Heavy autumn and winter snowfalls can occur in

association with tropical cyclones and westerly disturbances, respectively, and snow accumulation can occur at high elevations at all times of the year (Benn, 2012). Bollasina et al. (2002) have demonstrated the presence of well-defined local circulatory systems in the Khumbu Valley (SNP). The local circulation is dominated by a system of mountain and valley breezes. The valley breeze blows (approximately 4 m s^{-1}) from the south every day from sunrise to sunset throughout the monsoon season, pushing the clouds that bring Prec northward.

3 Data

3.1 Weather stations at high elevation

The first automatic weather station (named hereafter AWS0) at 5050 m a.s.l. near PYRAMID Observatory Laboratory (Fig. 1c), and beginning in October 1993, it has run continuously all year round (Bertolani et al., 2000). The station, operating in extreme conditions, had recorded long-term ground-based meteorological data, and the data are considered valid until December 2005. Due to the obsolescence of technology, the station was disposed of in 2006. A new station (named hereafter AWS1) was installed just a few tens of meters away from AWS0 and has been operating since October 2000. Other stations were installed in the following years in the upper DK Basin in the Khumbu Valley (Table 1). In 2008, the network included the sixth monitoring point, the highest weather station of the world, located at South Col of Mt. Everest (7986 m a.s.l.). The locations of all stations are presented in Fig. 1b. We can observe in Fig. 1c that this meteorological network represents the climatic conditions of the SNP glaciers well: AWS0 and AWS1 (5035 m a.s.l.) characterize the glacier fronts (4870 m a.s.l.), AWS4 (5600 m a.s.l.) represents the mean elevation of glaciers (5720 m a.s.l.), and AWS5, the surface station at South Col (7986 m a.s.l.), characterizes the highest peaks (8848 m a.s.l.).

All stations, except AWS5, record at least T and Prec. This dataset presents some gaps (listed in Table 1) as a consequence of the complications of operating AWS at these altitudes. The list of measured variables for each stations and relevant data can be downloaded from http://geonetwork.evk2cnr.org/. Data processing and quality checks are performed according to the international standards of the WMO (World Meteorological Organization).

The Prec sensors at these locations are tipping buckets usually used for rainfall measurements and may not fully capture the solid Prec. Therefore, Prec is probably underestimated, especially in winter. In this regard, according to both Fujita and Sakai, 2014 and field observations (Ueno et al., 1994), the precipitation phase has been taken into account assuming that the probability of snowfall and rainfall depends on mean daily temperature, using – as proposed by the aforementioned authors – as thresholds 0 and 4 °C, respectively. In Fig. 2 we first of all observe that at 5050 m a.s.l. 90 % of precipitation is concentrated during June–September and that the probability of snowfall is very low (4 %), considering that the mean daily temperature during these months is above 0 °C. On a yearly basis, this probability reaches 20 % of the annual cumulated precipitation.

3.2 Other weather stations at lower altitude in the Koshi Basin

In KO-S Basin (Nepal), the stations are operated by the Department of Hydrology and Meteorology (DHM) (www.dhm.gov.np/). For daily T and Prec, we selected 10 stations for T and 19 stations for Prec considering both the length of the series and the monitoring continuity (< 10 % of missing daily data). The selected stations cover an elevation range between 158 and 2619 m a.s.l. (Table 3). In KO-N Basin (TP, China), the number of ground weather stations (operated by the Chinese Academy of Science, CAS), selected with the same criteria mentioned above, is considerably smaller, just two, but these stations have a higher elevation (4302 m for the Dingri station and 3811 m a.s.l. for the Nyalam station).

4 Methods

We define the pre-monsoon, monsoon, and post-monsoon seasons as the months from February to May, June to September, and October to January, respectively. The minT, maxT, and meanT are calculated as the minimum, maximum, and mean daily air temperature. For total precipitation (Prec), we calculate the mean of the cumulative precipitation for the analyzed period.

4.1 Reconstruction of the daily temperature and precipitation time series at high elevation

The two stations named AWS0 and AWS1 in the last twenty years, considering the extreme weather conditions of these slopes, present a percentage of missing daily values of approximately 20 % (Table 1). The other stations (hereafter named secondary stations) were used here for infilling the gaps according to a priority criteria based on the degree of correlation among data. AWS1 was chosen as the reference station given the length of the time series and that it is currently still operating. Therefore, our reconstruction (hereafter named PYRAMID) is referred to an elevation of 5035 m a.s.l.

The selected infilling method is a simple regression analysis based on quantile mapping (e.g., Déqué, 2007; Themeßl et al., 2012). This simple regression method has been preferred to more complex techniques, such as the fuzzy rule-based approach (Abebe et al., 2000) or the artificial neural networks (Abudu et al., 2010; Coulibaly and Evora, 2007), considering the peculiarity of this case study. In fact, all stations are located in the same valley (Khumbu Valley). This aspect confines the variance among the stations to the altitudinal gradient of the considered variable (T or Prec), which can be easily reproduced by the stochastic link created by the quantile mapping method. In case all stations registered a simultaneous gap, we apply a multiple imputation technique (Schneider, 2001) that uses some other proxy variables to fill the remaining missing data. Details on the reconstruction procedure and the computation of the associated uncertainty are provided in Supplement 1.

4.2 The trends analysis: the Sequential Mann–Kendall test

The Mann–Kendall (MK) test (Kendall, 1975) is widely adopted to assess significant trends in hydro-meteorological time series (e.g., Carraro et al., 2012a, b; Guyennon et al., 2013). This test is non-parametric, thus being less sensitive to extreme sample values, and is independent of the hypothesis about the nature of the trend, whether linear or not. The MK test verifies the assumption of the stationarity of the investigated series by ensuring that the associated normalized Kendall's tau coefficient, $\mu(\tau)$, is included within the confidence interval for a given significance level (for $\alpha = 5\,\%$, the $\mu(\tau)$ is below −1.96 and above 1.96). In the sequential form (seqMK) (Gerstengarde and Werner, 1999), $\mu(\tau)$ is calculated for each element of the sample. The procedure is applied forward starting from the oldest values (progressive) and backward starting from the most recent values (retrograde). If no trend is present, the patterns of progressive and retrograde $\mu(\tau)$ vs. time (i.e., years) present several crossing points, while a unique crossing period allows the approximate location of the starting point of the trend (e.g., Bocchiola and Diolaiuti, 2010).

In this study, the seqMK is applied to monthly vectors. Monitoring the seasonal non-stationarity, the monthly progressive $\mu(\tau)$ is reported with a pseudo color code, where the warm colors represent the positive slopes and cold colors the negative ones. Color codes associated with values outside of the range (−1.96 to 1.96) possess darker tones to highlight the trend significance (Salerno et al., 2014). Moreover, to monitor the overall non-stationarity of the time series, both the progressive and the retrograde $\mu(\tau)$ at the annual scale are reported. We used the Sen's slope proposed by Sen (1968) as a robust linear regression allowing the quantification of the potential trends revealed by the seqMK (e.g., Bocchiola and Diolaiuti, 2010). The significance level is established for $p < 0.05$. We define a slight significance for $p < 0.10$. The uncertainty associated with the Sen's slopes (1994–2013) is estimated through a Monte Carlo uncertainty analysis (e.g., James and Oldenburg, 1997), described in detail in Supplement 1.

5 Results

5.1 Trend analysis at high elevation

Figure 3 shows the reconstructed PYRAMID time series for minT, maxT, meanT, and Prec resulting from the overall infilling process explained in Supplement 1. Figure 4 analyzes the monthly trends of T and Prec from 1994 to 2013 for PYRAMID.

5.1.1 Minimum air temperature (minT)

November ($0.17\,^{\circ}\mathrm{C\,a^{-1}}$ $p < 0.01$) and December ($0.21\,^{\circ}\mathrm{C\,a^{-1}}$, $p < 0.01$) present the highest increasing trend, i.e., both these two months experienced about even +4 °C over twenty years (Fig. 4a). In general, the post- and pre-monsoon periods experience higher and more significant increases than during the monsoon. In particular, we note the significant and consistent increase of April ($0.10\,^{\circ}\mathrm{C\,a^{-1}}$, $p < 0.05$). At the annual scale, the bottom graph shows a progressive $\mu(\tau)$ trend parallel to the retrograde $\mu(\tau)$ one for the entire analyzed period, i.e., a continuous tendency of minT to rise, which becomes significant in 2007, when the progressive $\mu(\tau)$ assumes values above +1.96. On the right, the Sen's slope completes the analysis, illustrating that minT is increasing at annual level by $0.072 \pm 0.011\,^{\circ}\mathrm{C\,a^{-1}}$, $p < 0.001$, i.e., $+1.44 \pm 0.22\,^{\circ}\mathrm{C}$ over twenty years.

5.1.2 Maximum air temperature (maxT)

The post- and pre-monsoon months show larger increases in maxT, but with lower magnitudes and significance than we observe for minT (Fig. 4b). The highest increases occurs also for this variable in April, November and December. Less expected is the decrease of maxT in May ($0.08\,^{\circ}\mathrm{C\,a^{-1}}$, $p < 0.05$) and during the monsoon months from June to August ($0.05\,^{\circ}\mathrm{C\,a^{-1}}$, $p < 0.1$). On the annual scale, the bottom graph shows a continuous crossing of the progressive and retrograde $\mu(\tau)$ trends until 2007, i.e., a general stationary condition. From 2007 until 2010, the trend significantly increased,

while 2012 and 2013 register a decrease, bringing the progressive $\mu(\tau)$ near the stationary condition. In fact, on the right, the Sen's slope confirms that maxT is at annual level stationary over the twenty years ($+0.009 \pm 0.012\,^{\circ}\mathrm{C\,a^{-1}}$, $p > 0.1$).

5.1.3 Mean air temperature (meanT)

Figure 4c, as expected, presents intermediate conditions for meanT than for minT and maxT. All months, except May and the monsoon months from June and August, register a positive trend (more or less significant). December presents the highest a more significant increasing trend ($0.17\,^{\circ}\mathrm{C\,a^{-1}}$, $p < 0.01$), while April shows the highest and a more significant increase ($p < 0.10$) during the pre-monsoon period. On the annual scale, the bottom graph shows that the progressive $\mu(\tau)$ trend has always increased since 2000 and that it becomes significant beginning in 2008. On the right, the Sen's slope concludes this analysis, showing that meanT has been significantly increasing by $0.044 \pm 0.008\,^{\circ}\mathrm{C\,a^{-1}}$, $p < 0.05$, i.e., $+0.88 \pm 0.16\,^{\circ}\mathrm{C}$ over twenty years.

5.1.4 Total precipitation (Prec)

In the last years, all cells are blue, i.e., we observe for all months an overall and strongly significant decreasing trend of Prec (Fig. 4d). In general, the post- and pre-monsoon periods experience more significant decreases, although the monsoon months (June–September) register the main Prec losses (e.g. August registers a Prec loss of even $4.6\,\mathrm{mm\,a^{-1}}$). On the annual scale, the bottom graph shows a continuous decreasing progressive $\mu(\tau)$ trend since 2000 that becomes significant beginning in 2005. On the right, the Sen's slope notes that the decreasing Prec trend is strongly high and significant at annual level ($13.7 \pm 2.4\,\mathrm{mm\,a^{-1}}$, $p < 0.001$).

The precipitation reduction is mainly due to a reduction in intensity. However during the early and late monsoon rather show a reduction in duration (see further details in Supplement 2).

5.2 Trend analysis in the Koshi Basin

Table 2 provides the descriptive statistics of the Sen's slopes for minT, maxT, meanT, and Prec for the 1994–2013 period for the Koshi Basin. The stations located on the two sides of the Himalayan range are listed separately. For the southern ones (KO-S), we observe that for minT less than half of the stations experience an increasing trend and just three are significant with $p < 0.1$. In general, the minT on the southern side can be defined as stationary ($+0.003\,^{\circ}\mathrm{C\,a^{-1}}$). Conversely, the maxT shows a decidedly non-stationary condition. All stations present an increasing trend, and even six of the ten are on the significant rise with at least $p < 0.1$. The mean trend is $+0.060\,^{\circ}\mathrm{C\,a^{-1}}$ ($p < 0.10$). Similarly, the meanT shows a substantial increase. Also in this case, six of the ten stations are on the significant rise with at least $p < 0.1$. The mean trend is $+0.029\,^{\circ}\mathrm{C\,a^{-1}}$ ($p < 0.10$). In regards to Prec, we observe that on the KO-S, 14 of the 19 stations present a downward trend. Among them, eight decrease significantly with at least $p < 0.1$. The mean trend is $-11.1\,\mathrm{mm\,a^{-1}}$, i.e., we observe a decreasing of 15 % (222 mm) of precipitation fallen in the basin during the 1994–2013 period (1527 mm on average).

The two stations located on the northern ridge (KO-N) show a singularly slight significant rise for minT ($0.034\,^{\circ}\mathrm{C\,a^{-1}}$, $p < 0.10$ on average) and for maxT ($0.039\,^{\circ}\mathrm{C\,a^{-1}}$, $p < 0.10$ on average), recording a consequent mean increase of meanT equal to $0.037\,^{\circ}\mathrm{C\,a^{-1}}$, $p < 0.05$. As for Prec, we observe that on the KO-N both stations maintain stationary conditions ($-0.1\,\mathrm{mm\,a^{-1}}$).

Table 3 provides the descriptive statistics of the Sen's slopes on a seasonal base. The stations analyzed here are the same as those considered in Table 2. We begin our description with PYRAMID, already analyzed in detail in Fig. 4. We confirm with this seasonal grouping that the main and significant increases of minT, maxT, and meanT are completely concentrated during the post-monsoon period (e.g., $0.124\,^{\circ}\mathrm{C\,a^{-1}}$, $p < 0.01$ for meanT). The pre-monsoon period experienced a slighter and not significant increase (e.g., 0.035, $p > 0.1$ for meanT). In general, during the mon-

soon period, T is much more stationary for all three variables (e.g., 0.015, $p > 0.1$ for meanT). Considering the other KO-S stations, the main increasing and significant trends of meanT occurred during the pre-monsoon ($0.043\,^{\circ}\mathrm{C\,a^{-1}}$) and post-monsoon ($0.030\,^{\circ}\mathrm{C\,a^{-1}}$) season, while the increase during the monsoon is slighter ($0.020\,^{\circ}\mathrm{C\,a^{-1}}$). The KO-N stations confirm that the main increasing trend of meanT occurred outside the monsoon period that is stationary ($+0.013\,^{\circ}\mathrm{C\,a^{-1}}$).

As for Prec, PYRAMID and the other KO-S stations show that the magnitude of the Sen's slopes is higher during the monsoon season ($-9.3\,\mathrm{mm\,a^{-1}}$ and $-8.6\,\mathrm{mm\,a^{-1}}$, respectively), when precipitation is more abundant. The relatively low snowfall phase of monsoon Prec at PYRAMID (as specified above) makes the decreasing trend observed during the summer more robust than the annual one as devoid of possible undervaluation of snowfall. The northern stations show slight significant decreasing Prec during the winter ($-3.3\,\mathrm{mm\,a^{-1}}$, $p < 0.05$).

5.3 Lapse rates in the southern Koshi Basin

5.3.1 Air temperature gradient

This study, aiming to create a connection between the climate drivers and cryosphere in the Koshi Basin, which presents the highest altitudinal gradient of the world (77 to 8848 m a.s.l.), offers a unique opportunity to calculate T and Prec lapse rates before analyzing their spatial trends. It is worth noting that the T lapse rate is one of the most important variables for modeling meltwater runoff from a glacierized basin using the T-index method (Hock, 2005; Immerzeel et al., 2014). It is also an important variable for determining the form of Prec and its distribution characteristics (e.g., Hock, 2005). Figure 5a presents the lapse rate of the annual meanT in the KO Basin (Nepal) along the altitudinal range of well over 7000 m (865 to 7986 m a.s.l.). We found an altitudinal gradient of $-0.60\,^{\circ}\mathrm{C}\,(100\,\mathrm{m})^{-1}$ on the annual scale with a linear trend ($r^2 = 0.98$, $p < 0.001$). It is known that up to altitudes of approximately 8–17 km a.s.l. in the lower regions of the atmosphere, T decreases with altitude at a fairly uniform rate (Washington and Parkinson, 2005). Kattel and Yao (2013) recently found a lower annual lapse rate for the overall CH-S, but until 4000 m a.s.l.: $-0.52\,^{\circ}\mathrm{C}\,(100\,\mathrm{m})^{-1}$.

Considering that the lapse rate is mainly affected by the moisture content of the air (Washington and Parkinson, 2005), we also calculated the seasonal gradients (not shown here). We found a dry lapse rate of $-0.65\,^{\circ}\mathrm{C}\,(100\,\mathrm{m})^{-1}$ ($r^2 = 0.99$, $p < 0.001$) during the pre-monsoon season when AWS1 registers a mean relative humidity of 62 %. A saturated lapse rate during the monsoon season is $-0.57\,^{\circ}\mathrm{C}\,(100\,\mathrm{m})^{-1}$ ($r^2 = 0.99$, $p < 0.001$) with a mean relative humidity of 96 %. During the post-monsoon period, we found a lapse rate equal to that registered during the monsoon: $-0.57\,(100\,\mathrm{m})^{-1}$ ($r^2 = 0.98$, $p < 0.001$) even if the relative humidity is decidedly lower in these months (44 %). Kattel and Yao (2013) explain this anomalous low post-monsoon lapse rate as the effect of strong radiative cooling in winter.

5.3.2 Precipitation gradient

As for Prec, its relationship with elevation helps in providing a realistic assessment of water resources and hydrological modeling of mountainous regions (Barros et al., 2004). In recent years, the spatial variability of Prec has received attention because the mass losses of the Himalayan glaciers can be explained with an increased variability in the monsoon system (e.g., Yao et al., 2012; Thakuri et al., 2014). Some previous studies of the Himalayas have considered orographic effects on Prec (Singh and Kumar, 1997; Ichiyanagi et al., 2007). Ichiyanagi et al. (2007), using all available Prec stations operated by DHM, of which < 5 % of stations are located over 2500 m and just one station is over 4000 m a.s.l., observed that in the CH-S region, the annual Prec increases with altitude below 2000 m a.s.l. and decreases for elevations ranging between 2000 and 3500 m a.s.l., but with no significant gradient. A broad picture of the relationship between Prec and topography in the Himalayas can be derived from the precipitation radar onboard the Tropical Rainfall Measuring Mission (TRMM). Some authors found an increasing trend with elevation characterized by two distinct maxima along two elevation bands (950 and 2100 m a.s.l.). The second maximum is much higher than the

first, and it is located along the Lesser Himalayas. Over these elevations, the annual distribution follows an approximate exponentially decreasing trend (Bookhagen and Burbank, 2006).

Figure 5b shows the altitudinal gradient for the total annual Prec in the Koshi Basin. We observe a clear rise in Prec with elevation until approximately 2500 m a.s.l., corresponding to the Tarke Ghyang station (code 1058), registering an annual mean of 3669 mm (mean for the 2004–2012 period). A linear approximation ($r = 0.83$, $p < 0.001$) provides a rate of $+1.16\,\mathrm{mm\,m^{-1}}$. At higher elevations, we observe an exponential decrease (ae^{bx}, with $a = 21\,168\,\mathrm{mm\,m^{-1}}$ and $b = -9 \times 10^{-4}\,\mathrm{m^{-1}}$, where x is the elevation expressed as m a.s.l.) until observing a minimum of 132 mm (years 2009 and 2013) for the Kala Patthar station (AWS4) at 5600 m a.s.l., although, as specified above, at these altitudes the contribution of winter snowfall could be underestimated. The changing point between the two gradients can be reasonably assumed at approximately 2500 m a.s.l., considering that the stations here present the highest interannual variability, belonging in this way, depending on the year, to the linear increase or to the exponential decrease. The clear outlier along the linear gradient is the Num Station (1301) located at 1497 m a.s.l., which recorded 4608 mm of precipitation. This station has been excluded for the linear approximation because, as reported by Montgomery and Stolar (2006), the station is located in the Arun Valley, which acts as a conduit for northward transport of monsoonal precipitation. The result is that local precipitation within the gorge of the Arun River is several times greater than in surrounding areas.

5.4 Spatial distribution of air temperature and precipitation trends in the Koshi Basin

Figure 6 presents the spatial distribution of the Sen's slopes in the Koshi Basin for minT (Fig. 6a), maxT (Fig. 6b), meanT (Fig. 6c), and Prec (Fig. 6d) during the 1994–2013 period. The relevant data are reported in Table 2. The Chainpur (East) station shows T trends in contrast with the other stations (see also Table 2); therefore, we consider this station as a local anomaly and do not discuss it further in the following sections.

In regards to minT, we observe an overall stationary condition in KO-S, as noted above. The only two stations showing a significant increasing trend are both located at East. The high elevation stations (PYRAMID and both those located on the north ridge) differ from the general pattern of the southern basin by showing a significant increasing trend. Even for maxT, we observe a higher increase in the southeastern basin. The central and western parts of the KO-S seem to be more stationary. PYRAMID follows this stationary pattern, while the northern stations (KO-N) show large and significant increases. As a consequence, meanT shows increasing trends for all the Koshi Basin, especially on the southeast and northern sides.

The decrease of precipitation in the southern Koshi Basin presents a quite homogeneous pattern from which the highly elevated PYRAMID is not excluded. The pattern is different on the north ridge, where it is stationary.

6 Discussion

6.1 Temperature trends of the Koshi Basin compared to the regional pattern

Kattel and Yao (2013) analyzed the annual minT, maxT, and meanT trends from stations ranging from 1304 to 2566 m a.s.l. in CH-S (corresponding to all stations in Nepal) during the 1980–2009 period. They found that the magnitude of warming is higher for maxT ($0.065\,^{\circ}\mathrm{C\,a^{-1}}$), while minT ($0.011\,^{\circ}\mathrm{C\,a^{-1}}$) exhibits larger variability, such as positive, negative or no change; meanT was found to increase at an intermediate rate of $0.038\,^{\circ}\mathrm{C\,a^{-1}}$. These authors extended some time series and confirmed the findings of Shrestha et al. (1999) that, analyzing the 1971–1994 period, found a maxT increase of $0.059\,^{\circ}\mathrm{C\,a^{-1}}$ for all of Nepal. Furthermore, warming in the winter was more pronounced compared to other seasons in both studies. These results are consistent with the pattern reported in WH (e.g., Bhutiyani et al., 2007; Shekhar et al., 2010), in EH, and in the rest of India (e.g., Pal and Al-Tabbaa, 2010) for the last three decades.

The trend analysis carried out in this study for the last two decades in KO-S shows full consistency with the pattern of change occurring in these regions over the last three decades in terms of a higher increase in maxT ($0.060\,^{\circ}\mathrm{C\,a^{-1}}$) than in minT ($0.003\,^{\circ}\mathrm{C\,a^{-1}}$), a seasonal pattern (more pronounced during the pre- and post-monsoon months), and the magnitudes of the trends (e.g., the meanT trend is $+0.030\,^{\circ}\mathrm{C\,a^{-1}}$). Therefore, at low elevations of KO-S, we observe an acceleration of warming in the recent years compared to the rate of change reported by Kattel and Yao (2013) and Shrestha et al. (1999) in the previous decades.

Different conditions have been observed on the TP, where the warming of minT is more prominent than that of maxT (e.g., Liu et al., 2006, 2009). In particular, for stations above 2000 m a.s.l. during the 1961–2003 period, Liu et al. (2006) found that minT trends were consistently greater ($+0.041\,^{\circ}\mathrm{C\,a^{-1}}$) than those of maxT ($+0.018\,^{\circ}\mathrm{C\,a^{-1}}$), especially in the winter and spring months. Yang et al. (2012), focusing their analysis on CH-N (which corresponds to the southern TP) in a more recent period (1971–2007), showed a significant increase of $0.031\,^{\circ}\mathrm{C\,a^{-1}}$ for meanT. Yang et al. (2006) analyzed five stations located in a more limited area of CH-N: the northern side of Mt. Everest (therefore, including the two stations also considered in this study) from 1971 to 2004. The warming is observed to be influenced more markedly by the minT increase.

The trend analysis carried out in this study for KO-N over the last two decades agrees with these studies in regards to both the considerable increase of minT ($0.034\,^{\circ}\mathrm{C\,a^{-1}}$) and the seasonal consistency of trends, related to all three *T* variables, outside the monsoon months. However, we observe that in recent years, maxT is increasing more than the rest of the TP ($0.039\,^{\circ}\mathrm{C\,a^{-1}}$). In general we observed an increase of meanT ($0.037\,^{\circ}\mathrm{C\,a^{-1}}$) comparable to that reported by Yang et al. (2012) ($0.031\,^{\circ}\mathrm{C\,a^{-1}}$) in the 1971–2007 period.

With all these regional studies, PYRAMID shares the higher *T* trends outside the monsoon period. However, in contrast with studies located south of the Himalayan ridge, which observed a prevalence of maxT increase, PYRAMID experienced a consistent minT increase ($0.072\,^{\circ}\mathrm{C\,a^{-1}}$ for PYRAMID vs. $0.003\,^{\circ}\mathrm{C\,a^{-1}}$ for KO-S stations), while the maxT increase is decidedly weaker ($0.009\,^{\circ}\mathrm{C\,a^{-1}}$ for PYRAMID vs. $0.060\,^{\circ}\mathrm{C\,a^{-1}}$ for KO-S stations). The remarkable minT trend of PYRAMID is higher, but more similar to the pattern of change commonly described on the TP, in particular in CH-N, and also in this study ($0.072\,^{\circ}\mathrm{C\,a^{-1}}$ for PYRAMID vs. $0.034\,^{\circ}\mathrm{C\,a^{-1}}$ for KO-N stations), while the maxT increase is weaker ($0.009\,^{\circ}\mathrm{C\,a^{-1}}$ for PYRAMID vs. $0.039\,^{\circ}\mathrm{C\,a^{-1}}$ for KO-N stations).

6.2 Elevation dependency of temperature trends

Figure 7 shows *T* trends in the KO Basin for minT, meanT, and maxT relative to the elevation during the 1994–2013 period. No linear pattern emerges. However, we can observe the minT trend of the three stations located at higher altitude (PYRAMID and KO-N stations), which increases more than that of the lower stations (Fig. 7a, see also Table 2). Reviewing the most recent studies in the surroundings, we found that they are quite exclusively located on CH-N. These studies often show contradictory elevation dependencies (Rangwala and Miller, 2012). A recent study by You et al. (2010) did not find any significant elevation dependency in the warming rates of meanT between 1961 and 2005. However, considering mostly the same stations, Liu et al. (2009) found that the warming rates for minT were greater at higher elevations. Observations from CH-S are much rarer. Shrestha et al. (1999) found elevation dependency in the rate at which maxT were increasing in the Nepali Himalayas (CH-S), with higher rates at higher elevations, but this study exclusively considered stations under 3000 m a.s.l.

Furthermore we did not find for the Koshi Basin any significant elevation dependency in the weakening rates of Prec.

6.3 Precipitation trends of the Koshi Basin compared to the regional pattern

Turner and Annamalai (2012), using the all-India rainfall data based on a weighted mean of 306 stations, observed a negative precipitation trend since the 1950s in South Asia. According to Yao et al. (2012), using the Global Precipitation Climatology Project

(GPCP) data, there is strong evidence that precipitation from 1979 to 2010 decreased even in the Himalayas. In eastern CH-S, where the Koshi Basin is located, they estimated a loss of 173 mm, showing a real decreasing trend starting from the early 1990s (mean value between grid 9 and 11 in Fig. S18 of their paper).

On the TP, the observed pattern of change is opposite that of the monsoon weakening described by the authors cited above. Liu et al. (2010) described an increase in precipitation in CH-N for the period of the 1980s to 2008. Su et al. (2006) described a marked precipitation increase in the Yangtze River Basin (eastern CH-N). In a similar way to the *T* analysis, Yang et al. (2006) considered 5 stations located on the northern side of Mt. Everest (therefore, including the two stations also considered in this study) from 1971 to 2004 and observed an increasing, but not significant Prec trend. The higher stationarity we observed is confirmed since 1971 for the two KO-N stations considered in this study.

Different from the north side of Mt. Everest and from the general TP, we confirm the general monsoon weakening in the KO-S, observing a substantial Prec decrease of 15 % ($-11.1\,\mathrm{mm\,a^{-1}}$, 222 mm), but that is not significant for all stations. At PYRAMID, the annual loss is relatively comparable with that of the KO-S ($13.7\,\mathrm{mm\,a^{-1}}$, 273 mm), but at these high elevations, as we observed in Table 2, the weather is much more drier (449 and 1527 mm, respectively). Therefore, the fractional loss is more than 3 times (52 %) that of the KO-S. Considering that the decreasing trend observed during the summer is more robust than the annual one (see above), the fractional loss of Prec during the monsoon is 47 %, which means that currently, on average, the precipitation at PYRAMID is the half of what it was twenty years ago.

6.4 Mechanisms responsible for temperature warming and precipitation weakening

According to Rangwala and Miller (2012), there are a number of mechanisms that can cause enhanced warming rates at high elevation, and they often have strong seasonal dependency. These mechanisms arise from either elevation based differential changes

in climate drivers, such as snow cover, clouds, specific humidity, aerosols, and soil moisture, or differential sensitivities of surface warming to changes in these drivers at different elevations. This study does not aim to either realize a comprehensive review or to demonstrate the causes that could have led to the climate change pattern observed at PYRAMID, but our intent here is just to note the recent hypotheses advanced in the literature that fit with our observations for the region of investigation.

Snow/ice albedo is one of the strongest feedbacks in the climate system (Rangwala and Miller, 2012). Increases in minT are possible if decreases in snow cover are accompanied by increases in soil moisture and surface humidity, which can facilitate a greater diurnal retention of the daytime solar energy in the land surface and amplify the longwave heating of the land surface at night (Rangwala et al., 2012). For the Tibetan Plateau, Rikiishi and Nakasato (2006) found that the length of the snow cover season declined at all elevations between 1966 and 2001. Moreover, minT can be enhanced by nighttime increases in cloud cover. However, assessing changes in clouds and quantifying cloud feedbacks will remain challenging in the near term. For the Tibetan Plateau, Duan and Wu (2006) found that low level nocturnal cloud cover increased over the TP between 1961 and 2003 and that these increases explain part of the observed increases in minT.

The maxT increase observed here during April ($p < 0.05$ in 2011, Fig. 4b) fits with the warming reported by Pal and Al-Tabbaa (2010) which observed that within the pre-monsoon season only April shows significant changes in maxT in all Indian regions and WH (1901–2003 period). According to Ramanathan et al. (2007), Gautam et al. (2010) argued that the observed warming during the pre-monsoon period (April–June) can be ascribed not only to the global greenhouse warming, but also to the solar radiation absorption caused by the large amount of aerosol (mineral dust mixed with other carbonaceous material) transported over the Gangetic-Himalayan region. As recently reported by Marinoni et al. (2013), April represents the month for which the transport of absorbing carbonaceous aerosol (i.e. black carbon) is maximized in our region of investigation (Khumbu Valley). At this regards Putero et al. (2013) show evidences for

a possible influence of open fire occurrence in South Asia particular abundant during this period of the year. However the significant decreasing of maxT observed in May ($p < 0.05$) and the slight significant decreasing during the monsoon months from June to August ($p < 0.10$) appear to deviate from the scenario proposed for April. In this respect it should be kept in mind that the radioactive dynamical interactions of aerosol with the monsoon cycle are extremely complex and different processes can interact with each other. As an instance, as reported by Qian et al. (2011), the deposition of absorbing aerosol on snow and the snow albedo feedback processes can play a prominent role in Himalayas and TP inducing large radioactive flux changes and surface temperature perturbation.

Recent studies associate the precipitation decrease over India during the second half of 20th century (e.g., Ramanathan et al., 2005; Lau and Kim, 2006) to the significant tropospheric warming over the tropical area from the Indian Ocean to the western Pacific (e.g., Wu, 2005), while westerlies are strengthening (Zhao et al., 2012). Other authors (e.g., Bollasina et al., 2011) attribute the monsoon weakening to human-influenced aerosol emissions. In fact an increase of aerosols over South Asia has been well documented (Ramanathan et al., 2005; Lau and Kim, 2006) and climate model experiments suggest that sulfate aerosol may significantly reduce monsoon precipitation (Mitchell and Johns, 1997). Despite a historical weakening of the monsoon circulation, most studies project an increase of the seasonal monsoon rainfall under global warming. At this regards Levy II et al., 2013 find that the dramatic emission reductions (35–80 %) in anthropogenic aerosols and their precursors projected by Representative Concentration Pathway (RCP) 4.5 (Moss et al., 2010) result an increasing trend by the second half of the 21st century in South Asia and in particular over the Himalaya (Palazzi et al., 2013).

6.5 Linking climate change patterns observed at high elevation with glacier responses

6.5.1 Impact of temperature increase

Air temperature and precipitation are the two factors most commonly related to glacier fluctuations. However, there still exists a seasonal gap in order to explain the shrinking of summer accumulation-type glaciers (typical of CH) due to large temperature increases observed in the region during winter (Ueno and Aryal, 2008), as is the case for the south slopes of Mt. Everest. Furthermore, in this study we noted a slightly significant decline in summer maxT and stationary meanT. The real increase of T has been observed for minT, but given the mean elevation of glaciers (5695 m a.s.l. in 1992) and the mean elevation range of glacier fronts (4568–4817 m a.s.l. in 1992, mean 4817 m a.s.l., 249 m of SD) (Thakuri et al., 2014), this increase for minT can be most likely considered ineffective for melting processes, since T is still less than 0 °C. This inference can be ascertained analyzing Fig. 8, created in order to link temperature increases and altitudinal glacier distribution (data from Thakuri et al., 2014). The 0 °C isotherms, corresponding to the mean monthly minT and maxT, are plotted for 1994 and 2013. The elevation of each 0 °C isotherm is calculated according to the accurate lapse rates computation carried out in this study and the observed monthly T trends. We can note that in 1994 the 0 °C isotherm for minT reached the elevation band characterizing the glacier fronts only from June to September. However, twenty years later, the upward of the 0 °C isotherm is modest (92 m) during these months, compared to the huge but ineffective rise for melting processes (downstream from the glacier fronts) of December–November (even 854 m). The maxT has obviously a greater potential impact on glaciers. In fact the 0 °C isotherm for of all months except January and February crosses the elevation bands within which the glacier fronts are located ever since 1994. In this regard we observe that only April (224 m), December (212 m), and November (160 m) experienced an upward of the 0 °C isotherm able to enhance the melting processes, but only close to the glaciers fronts. We therefore point out that the impact caused by the increased tem-

perature occurring in April most likely plays an important role not only in relation to this case study, but also at the level of the Himalayan range. In fact, as mentioned above, Pal and Al-Tabbaa (2010), observed that within the pre-monsoon season, only April showed significant changes in maxT in all Indian regions and WH (1901–2003 period).

6.5.2 Impact of precipitation decrease

As regards the precipitation, in this study we noted a strong and significant decreasing Prec trend for all months, corresponding to a fractional loss of 47 % during the monsoon season which indicates that, on average, the precipitation at PYRAMID is currently half of what it was twenty years ago. This climate change pattern confirms and clarifies the observation of Thakuri et al. (2014), who noted that the southern Mt. Everest glaciers experienced a shrinkage acceleration over the last twenty years (1992–2011), as underlined by an upward shift of SLA with a velocity almost three times greater than the previous period (1962–1992). The authors, without the support of climatic data, proposed the hypothesis that Mt. Everest glaciers are shrinking faster since the early 1990s mainly as a result of a weakening of precipitation over the last decades. In fact they observed a double upward shift in the SLA of the largest glaciers (south-oriented and with a higher altitude accumulation zone): a clear signal of a significant decrease in accumulation. Wagnon et al. (2013) have recently reached the same conclusion, but also in this case without the support of any climatic studies. Bolch et al. (2011) and Nuimura et al. (2012) registered a higher mass loss rate during the last decade (2000–2010).

Furthermore Quincey et al. (2009) and Peters et al. (2010) observed lower glacier flow velocity in the region over the last decades. Many studies highlight how the present condition of ice stagnation of glaciers in the Mt Everest region, and in general in CHS, is attributable to low flow velocity generated by generally negative mass balances (Bolch et al., 2008; Quincey et al., 2009; Scherler et al., 2011). Our observations allow attributing the lower glacier flow velocity to lower accumulation due to weaker precipitation, which can thus be considered the main climatic factor driving the current ice

stagnation of tongues. In this regard we need to keep in mind that changes in velocity are among the main triggers for the formation of supraglacial and proglacial lakes (Salerno et al., 2012; Quincey et al., 2009), which we know to be susceptible to GLOFs.

6.5.3 Trend analysis of annual probability of snowfall

Figure 9 analyses how the changes observed for the meanT at PYRAMID have affected the probability of snowfall on total cumulated annual precipitation in the last twenty years. The increase of meanT observed outside the monsoon period, when the precipitation is almost completely composed by snow (Fig. 2), brought a significant decrease of solid phase ($0.7\,\%\,a^{-1}$, $p < 0.05$). Extending this analysis to the elevation bands characterizing the glaciers distribution (see Fig. 8), through the temperature lapse rate calculated here, we observe that at the level of the mean glaciers (5695 m a.s.l.) the probability of snowfall is stationary ($+0.04\,\%\,a^{-1}$), while it decreases at the mean elevation of SLAs (5345 m a.s.l. in 1992, Thakuri et al., 2014), but not significantly ($-0.38\,\%\,a^{-1}$, $p > 0.1$). The reduction becomes significant at lower altitudes. In particular, at the mean elevation of glacier fronts (4817 m a.s.l.) the probability of snowfall is $-0.56\,\%\,a^{-1}$ ($p < 0.05$), i.e. at these altitudesthe probability of snow on annual base is currently 11 % ($p < 0.05$) less than twenty years ago. We can conclude this analysis summarizing that a significant change in precipitation phase has occurred close to the terminal portions of glaciers, corresponding broadly to the glaciers ablation zones (around 10 %, $p < 0.5$), while the lower temperature of the upper glaciers zones has so far guaranteed a stationary condition.

7 Conclusion

Most relevant studies on temperature trends were conducted on the Tibetan Plateau, the Indian subcontinent (including the WH) and the Upper Indus Basin, while studies on the mountainous regions along the southern slope of the central Himalayas in Nepal

(CH-S) are limited. Although Shrestha et al. (1999) analyzed the maximum temperature trends over Nepal during the period 1971–1994, studies on recent temperature trends over CH-S are still lacking and, before this study, completely absent as regards high elevation. This paper addresses seasonal variability of minimum, maximum, and mean temperatures and precipitation at high elevation onthe southern slopes of Mt. Everest. Moreover, we complete this analysis with data from all the existing weather stations located on both sides of the Himalayan range (Koshi Basin) for the 1994–2013 period, during which a rapider glacier mass loss occurred.

At high elevation on the southern slopes of Mt. Everest, we observed the following:

1. The main increases in air temperature are almost completely concentrated during the post-monsoon months. The pre-monsoon period experienced a slighter and insignificant increase, while the monsoon season is generally stationary. This seasonal temperature change pattern is shared with the entire Koshi Basin, and it is also observed in the regional studies related to the northern and southern slopes of the Himalayan range. Surprisingly, at high elevation the maximum temperature decreases significantly in May and slightly during the monsoon months from June to August.

2. The minimum temperature increased much more than the maximum temperature. This remarkable minimum temperature trend is more similar to the pattern of change commonly described on the Tibetan Plateau and confirmed in this study in the northern Koshi Basin. However, this trend is in contrast with studies located south of the Himalayan ridge. As proved by this study, the southern Koshi Basin experienced a prevalence of maximum temperature increases. No linear pattern emerges in the elevation dependency of temperature trends. We only observed higher minimum temperature trends at higher altitudes.

3. The total annual precipitation has considerably decreased. The annual rate of decrease at high elevation is similar to the one at lower altitudes on the southern side of the Koshi Basin, but the drier conditions of this remote environment make

the fractional loss relatively more consistent. The precipitation at high elevation during the monsoon period is currently half of what it was twenty years ago. These observations confirm the monsoon weakening observed by previous studies in India and even in the Himalayas since the early 1980s. As opposed to the northern side of the Koshi Basin that shows in this study certain stability, as positive or stationary trends have been observed by previous studies on the TP and more specifically in northern central Himalaya.

4. There is a significantly lower probability of snowfall in the glaciers ablation zones, while the lower temperature of the upper glaciers zones have so far guaranteed a stationary condition.

In general, this study contributes to change the perspective on how the climatic driver (temperature vs. precipitation) led the glacier responses in the last twenty years. to a change perspective related to the climatic driver (temperature vs. precipitation) led the glacier responses in the last twenty years.

Without demonstrating the causes that could have led to the climate change pattern observed at the PYRAMID, we simply note the recent literature on hypotheses that accord with our observations. for the case study.

In conclusion, we have here observed that weather stations at low elevations are not able to suitably describe the climate changes occurring at high altitudes and thus correctly interpret the impact observed on the cryosphere. This consideration stresses the great importance of long-term ground measurements at high elevation.

The Supplement related to this article is available online at doi:10.5194/tcd-8-5911-2014-supplement.

Author contributions. G. Tartari, Y. Ma and E. Vuillermoz designed research; F. Salerno performed research; F. Salerno, N. Guyennon, S. Thakuri, G. Viviano and E. Romano analyzed data; F. Salerno, N. Guyennon, E. Romano and G. Tartari wrote the paper. P. Cristofanelli, P. Stocchi, N. Guyennon and G. Agrillo data quality check.

Acknowledgements. This work was supported by the MIUR through Ev-K2-CNR/SHARE and CNR-DTA/NEXTDATA project within the framework of the Ev-K2-CNR and Nepal Academy of Science and Technology (NAST). Sudeep Thakuri is recipient of the IPCC Scholarship Award under the collaboration between the IPCC Scholarship Programme and the Prince Albert II of Monaco Foundation's Young Researchers Scholarships Initiative.

References

Abebe, A., Solomatine, D., and Venneker, R.: Application of adaptive fuzzy rule based models for reconstruction of missing precipitation events, Hydrolog. Sci. J., 45, 425–436, doi:10.1080/02626660009492339, 2000.

Abudu, S., Bawazir, A. S., and King, J. P.: Infilling missing daily evapotranspiration data using neural networks, J. Irrig. Drain. E.-ASCE, 136, 317–325, doi:10.1061/(ASCE)IR.1943-4774.0000197, 2010.

Amatya, L. K., Cuccillato, E., Haack, B., Shadie, P., Sattar, N., Bajracharya, B., Shrestha, B., Caroli, P., Panzeri, D., Basani, M., Schommer, B., Flury, B. Salerno, F., and Manfredi, E. C.: Improving communication for management of social-ecological systems in high mountain areas: development of methodologies and tools – the HKKH Partnership Project, Mt. Res. Dev., 30, 69–79, doi:10.1659/MRD-JOURNAL-D-09-00084.1, 2010.

Bajracharya, B., Uddin, K., Chettri, N., Shrestha, B., and Siddiqui, S. A.: Understanding land cover change using a harmonized classification system in the Himalayas: a case study from Sagarmatha National Park, Nepal, Mt. Res. Dev., 30, 143–156, doi:10.1659/MRD-JOURNAL-D-09-00044.1, 2010.

Barros, A. P., Kim, G., Williams, E., and Nesbitt, S. W.: Probing orographic controls in the Himalayas during the monsoon using satellite imagery, Nat. Hazards Earth Syst. Sci., 4, 29–51, doi:10.5194/nhess-4-29-2004, 2004.

Benn, D. I., Bolch, T., Hands, K., Gulley, J., Luckman, A., Nicholson, L. I., Quincey, D., Thompson, S., Toumi, R., and Wiseman, S.: Response of debris-covered glaciers in the Mount

Everest region to recent warming, and implications for outburst flood hazards, Earth-Sci. Rev., 114, 156–174, doi:10.1016/j.earscirev.2012.03.008, 2012.

Bertolani, L., Bollasina, M., and Tartari, G.: Recent biannual variability of meteorological features in the eastern Highland Himalayas, Geophys. Res. Lett., 27, 2185–2188, doi:10.1029/1999GL011198, 2000.

Bhutiyani, M. R., Kale, V. S., and Pawar, N. J.: Long-term trends in maximum, minimum and mean annual air temperatures across the Northwestern Himalaya during the twentieth century, Climatic Change, 85, 159–177, doi:10.1007/s10584-006-9196-1, 2007.

Bocchiola, D. and Diolaiuti, G.: Evidence of climate change within the Adamello Glacier of Italy, Theor. Appl. Climatol., 100, 351–369, doi:10.1007/s00704-009-0186-x, 2010.

Bolch, T., Buchroithner, M., Pieczonka, T., and Kunert, A.: Planimetric and volumetric glacier changes in the Khumbu Himal, Nepal, since 1962 using Corona, Landsat TM and ASTER data, J. Glaciol., 54, 592–600, doi:10.3189/002214308786570782, 2008.

Bolch, T., Pieczonka, T., and Benn, D. I.: Multi-decadal mass loss of glaciers in the Everest area (Nepal Himalaya) derived from stereo imagery, The Cryosphere, 5, 349–358, doi:10.5194/tc-5-349-2011, 2011.

Bolch, T., Kulkarni, A., Kääb, A., Huggel, C., Paul, F., Cogley, J. G., Frey, H., Kargel, J. S., Fujita, K., Scheel, M., Bajracharya, S., and Stoffel, M.: The state and fate of Himalayan glaciers, Science, 336, 310–314, doi:10.1126/science.1215828, 2012.

Bollasina, M. A., Ming, Y., and Ramaswamy, V.: Anthropogenic aerosols and the weakening of the south Asian summer monsoon, Science, 334, 502–505, doi:10.1126/science.1204994, 2011.

Bookhagen, B. and Burbank, D. W.: Topography, relief, and TRMM-derived rainfall variations along the Himalaya, Geophys. Res. Lett., 33, L08405, doi:10.1029/2006GL026037, 2006.

Carraro, E., Guyennon, N., Hamilton, D., Valsecchi, L., Manfredi, E. C., Viviano, G., Salerno, F., Tartari, G., and Copetti, D.: Coupling high-resolution measurements to a three-dimensional lake model to assess the spatial and temporal dynamics of the cyanobacterium Planktothrix rubescens in a medium-sized lake, Hydrobiologia, 698, 77–95, doi:10.1007/s10750-012-1096-y, 2012a.

Carraro, E., Guyennon, N., Viviano, G., Manfredi, E. C., Valsecchi, L., Salerno, F., Tartari, G., and Copetti, D.: Impact of global and local pressures on the ecology of a medium-sized prealpine lake, in: Models of the Ecological Hierarchy, edited by: Jordan, F. and Jorgensen, S. E., Elsevier, 259–274, doi:10.1016/B978-0-444-59396-2.00016-X, 2012b.

Coulibaly, P. and Evora, N.: Comparison of neural network methods for infilling missing daily weather records, J. Hydrol., 341, 27–41, doi:10.1016/j.jhydrol.2007.04.020, 2007.
Déqué, M.: Frequency of precipitation and temperature extremes over France in an anthropogenic scenario: model results and statistical correction according to observed values, Global Planet. Change, 57, 16–26, doi:10.1016/j.gloplacha.2006.11.030, 2007.
Duan, A. and Wu, G.: Change of cloud amount and the climate warming on the Tibetan Plateau, Geophys. Res. Lett., 33, L22704, doi:10.1029/2006GL027946, 2006.
Dytham, C.: Choosing and Using Statistics: a Biologist's Guide, John Wiley & Sons, New York, USA, 2011.
Fujita, K. and Sakai, A.: Modelling runoff from a Himalayan debris-covered glacier, Hydrol. Earth Syst. Sci., 18, 2679–2694, doi:10.5194/hess-18-2679-2014, 2014.
Fujita, K., Sakai, A., Takenaka, S., Nuimura, T., Surazakov, A. B., Sawagaki, T., and Yamanokuchi, T.: Potential flood volume of Himalayan glacial lakes, Nat. Hazards Earth Syst. Sci., 13, 1827–1839, doi:10.5194/nhess-13-1827-2013, 2013.
Ganguly, N. D. and Iyer, K. N.: Long-term variations of surface air temperature during summer in India, Int. J. Climatol., 29, 735–746, doi:10.1002/joc.1748, 2009.
Gardelle, J., Arnaud, Y., and Berthier, E.: Contrasted evolution of glacial lakes along the Hindu Kush Himalaya mountain range between 1990 and 2009, Global Planet. Change, 75, 47–55, doi:10.1016/j.gloplacha.2010.10.003, 2011.
Gautam, R., Hsu, N. C., and Lau, K. M.: Premonsoon aerosol characterization and radiative effects over the Indo-Gangetic plains: implications for regional climate warming, J. Geophys. Res., 115, D17208, doi:10.1029/2010JD013819, 2010.
Gerstengarbe, F. W. and Werner, P. C.: Estimation of the beginning and end of recurrent events within a climate regime, Clim. Res., 11, 97–107, 1999.
Guyennon, N., Romano, E., Portoghese, I., Salerno, F., Calmanti, S., Petrangeli, A. B., Tartari, G., and Copetti, D.: Benefits from using combined dynamical-statistical downscaling approaches – lessons from a case study in the Mediterranean region, Hydrol. Earth Syst. Sci., 17, 705–720, doi:10.5194/hess-17-705-2013, 2013.
Hock, R.: Glacier melt: a review of processes and their modeling, Prog. Phys. Geog., 29, 362–391, doi:10.1191/0309133305pp453ra, 2005.
Ichiyanagi, K., Yamanaka, M. D., Muraji, Y., and Vaidya, B. K.: Precipitation in Nepal between 1987 and 1996, Int. J. Climatol., 27, 1753–1762, doi:10.1002/joc.1492, 2007.

Immerzeel, W. W., Petersen, L., Ragettli, S., and Pellicciotti, F.: The importance of observed gradients of air temperature and precipitation for modeling runoff from a glacierized watershed in the Nepal Himalayas, Water Resour. Res., 50, 2212–2226, doi:10.1002/2013WR014506, 2014.
James, A. L. and Oldenburg, C. M.: Linear and Monte Carlo uncertainty analysis for subsurface contaminant transport simulation, Water Resour. Res., 33, 2495–2508, doi:10.1029/97WR01925, 1997.
Kattel, D. B. and Yao, T.: Recent temperature trends at mountain stations on the southern slope of the central Himalayas, J. Earth Syst. Sci., 122, 215–227, doi:10.1007/s12040-012-0257-8, 2013.
Kendall, M. G.: Rank Correlation Methods, Oxford University Press, New York, 1975.
Kivekäs, N., Sun, J., Zhan, M., Kerminen, V.-M., Hyvärinen, A., Komppula, M., Viisanen, Y., Hong, N., Zhang, Y., Kulmala, M., Zhang, X.-C., Deli-Geer, and Lihavainen, H.: Long term particle size distribution measurements at Mount Waliguan, a high-altitude site in inland China, Atmos. Chem. Phys., 9, 5461–5474, doi:10.5194/acp-9-5461-2009, 2009.
Lami, A., Marchetto, A., Musazzi, S., Salerno, F., Tartari, G., Guilizzoni, P., Rogora, M., and Tartari, G. A.: Chemical and biological response of two small lakes in the Khumbu Valley, Himalayas (Nepal) to short-term variability and climatic change as detected by long-term monitoring and paleolimnological methods, Hydrobiologia, 648, 189–205, doi:10.1007/s10750-010-0262-3, 2010.
Lau, K.-M. and Kim, K.-M.: Observational relationships between aerosol and Asian monsoon rainfall, and circulation, Geophys. Res. Lett., 33, L21810, doi:10.1029/2006GL027546, 2006.
Lavagnini, I., Badocco, D., Pastore, P., and Magno, F.: Theil-Sen nonparametric regression technique on univariate calibration, inverse regression and detection limits, Talanta, 87, 180–188, doi:10.1016/j.talanta.2011.09.059, 2011.
Levy II, H., Horowitz, L. W., Schwarzkopf, M. D., Ming, Y., Golaz, J. C., Naik, V., and Ramaswamy, V.: The roles of aerosol direct and indirect effects in past and future climate change, J. Geophys. Res., 118, 1–12, doi:10.1002/jgrd.50192, 2013.
Liu, J., Yang, B., and Qin, C.: Tree-ring based annual precipitation reconstruction since AD 1480 in south central Tibet, Quatern. Int., 236, 75–81, doi:10.1016/j.quaint.2010.03.020, 2010.
Liu, K., Cheng, Z., Yan, L., and Yin, Z.: Elevation dependency of recent and future minimum surface air temperature trends in the Tibetan Plateau and its surroundings, Global Planet. Change, 68, 164–174, doi:10.1016/j.gloplacha.2009.03.017, 2009.

Liu, X. D. and Chen, B. D.: Climatic warming in the Tibetan Plateau during recent decades, Int. J. Climatol., 20, 1729–1742, doi:10.1002/1097-0088(20001130)20:14<1729::AID-JOC556>3.0.CO;2-Y, 2000.

Liu, X. D., Yin, Z. Y., Shao, X., and Qin, N.: Temporal trends and variability of daily maximum and minimum, extreme temperature events, and growing season length over the eastern and central Tibetan Plateau during 1961–2003, J. Geophys. Res., 111, D19109, doi:10.1029/2005JD006915, 2006.

Manfredi, E. C., Flury, B., Viviano, G., Thakuri, S., Khanal, S. N., Jha, P. K., Maskey, R. K., Kayastha, R. B., Kafle, K. R., Bhochhibhoya, S., Ghimire, N. P., Shrestha, B. B., Chaudhary, G., Giannino, F., Carteni, F., Mazzoleni, S., and Salerno, F.: Solid waste and water quality management models for Sagarmatha National Park and Buffer Zone, Nepal: implementation of a participatory modeling framework, Mt. Res. Dev., 30, 127–142, doi:10.1659/MRD-JOURNAL-D-10-00028.1, 2010.

Marinoni, A., Cristofanelli, P., Laj, P., Putero, D., Calzolari, F., Landi, T. C., Vuillermoz, E., Maione, M., and Bonasoni, P.: High black carbon and ozone concentrations during pollution transport in the Himalayas: five years of continuous observations at NCO-Prec global GAW station, J. Environ. Sci., 25, 1618–1625, doi:10.1016/S1001-0742(12)60242-3, 2013.

Mitchell, J. F. B. and Johns, T. C.: On the modification of global warming by sulphate aerosols, J. Climate, 10, 245–267, 1997.

Montgomery, D. R. and Stolar, D. B.: Reconsidering Himalayan river anticlines, Geomorphology, 82, 4–15, doi:10.1016/j.geomorph.2005.08.021, 2006.

Moss, R. H., Edmonds, J. A., Hibbard, K. A., Manning, M. R., Rose, S. K., van Vuuren, D. P. , Carter, T. R., Emori, S., Kainuma, M., Kram, T. , Meehl, G. A., Mitchell, J. F. B., Nakicenovic, N., Riahi, K., Smith, S. J., Stouffer, R. J., Thomson, A. M., Weyant, J. P., and Wilbanks, T. J.: The next generation of scenarios for climate change research and assessment, Nature, 463, 747–756, doi:10.1038/nature08823, 2010.

Nuimura, T., Fujita, K., Yamaguchi, S., and Sharma, R. R.: Elevation changes of glaciers revealed by multitemporal digital elevation models calibrated by GPS survey in the Khumbu region, Nepal Himalaya, 1992–2008, J. Glaciol., 58, 648–656, doi:10.3189/2012JoG11J061, 2012.

Pal, I. and Al-Tabbaa, A.: Long-term changes and variability of monthly extreme temperatures in India, Theor. Appl. Climatol., 100, 45–56, doi:10.1007/s00704-009-0167-0, 2010.

Palazzi, E., von Hardenberg, J., and Provenzale, A.: Precipitation in the Hindu-Kush Karakoram Himalaya: observations and future scenarios, J. Geophys. Res.-Atmos., 118, 85–100, doi:10.1029/2012JD018697, 2013.

Pepin, N. C. and Lundqist, J. D.: Temperature trends at high elevations: patterns across the globe, Geophys. Res. Lett., 35, L14701, doi:10.1029/2008GL034026, 2008.

Peters, J., Bolch, T., Buchroithner, M. F., and Bäßler, M.: Glacier Surface Velocities in the Mount Everest Area/Nepal using ASTER and Ikonos imagery, in: Proceeding of 10th International Symposium on High Mountain Remote Sensing Cartography, Kathmandu, Nepal, 8–11 September 2008, 313–320, 2010.

Putero, D., Landi, T. C., Cristofanelli, P., Marinoni, A., Laj, P., Duchi, R., Calzolari, F., Verza, G. P., and Bonasoni, P.: Influence of open vegetation fires on black carbon and ozone variability in the southern Himalayas (NCO-P, 5079 m a.s.l.), Environ. Pollut., 184, 597–604, doi:10.1016/j.envpol.2013.09.035, 2013.

Qian, Y., Flanner, M. G., Leung, L. R., and Wang, W.: Sensitivity studies on the impacts of Tibetan Plateau snowpack pollution on the Asian hydrological cycle and monsoon climate, Atmos. Chem. Phys., 11, 1929–1948, doi:10.5194/acp-11-1929-2011, 2011.

Quincey, D. J., Luckman, A., and Benn, D.: Quantification of Everest region glacier velocities between 1992 and 2002, using satellite radar interferometry and feature tracking, J. Glaciol., 55, 596–606, doi:10.3189/002214309789470987, 2009.

Ramanathan, V., Chung, C., Kim, D., Bettge, T., Buja, L., Kiehl, J. T., Washington, W. M., Fu, Q., Sikka, D. R., and Wild, M.: Atmospheric brown clouds: impacts on South Asian climate and hydrological cycle, P. Natl. Acad. Sci. USA, 102, 5326–5333, doi:10.1073/pnas.0500656102, 2005.

Ramanathan, V., Li, F., Ramana, M. V., Praveen, P. S., Kim, D., Corrigan, C. E., Nguyen, H., Stone, E. A., Schauer, J. J., Carmichael, G. R., Adhikary, B., and Yoon, S. C.: Atmospheric brown clouds: hemispherical and regional variations in long-range transport, absorbtion, and radiative forcing, J. Geophys. Res., 112, D22S21, doi:10.1029/2006JD008124, 2007.

Rangwala, I. and Miller, J. R.: Climate change in mountains: a review of elevation-dependent warming and its possible causes, Climatic Change, 114, 527–547, doi:10.1007/s10584-012-0419-3, 2012.

Rangwala, I., Barsugli, J., Cozzetto, K., Neff, J., and Prairie, J.: Mid-21st century projections in temperature extremes in the southern Colorado Rocky Mountains from regional climate models, Clim. Dynam., 39, 1823–1840, doi:10.1007/s00382-011-1282-z, 2012.

Rikiishi, K. and Nakasato, H.: Height dependence of the tendency for reduction in seasonal snow cover in the Himalaya and the Tibetan Plateau region, 1966–2001, Ann. Glaciol., 43, 369–377, doi:10.3189/172756406781811989, 2006.

Salerno, F., Buraschi, E., Bruccoleri, G., Tartari, G., and Smiraglia, C.: Glacier surface-area changes in Sagarmatha National Park, Nepal, in the second half of the 20th century, by comparison of historical maps, J. Glaciol., 54, 738–752, 2008.

Salerno, F., Thakuri, S., D'Agata, C., Smiraglia, C., Manfredi, E. C., Viviano, G., and Tartari, G.: Glacial lake distribution in the Mount Everest region: uncertainty of measurement and conditions of formation, Global Planet. Change, 92–93, 30–39, doi:10.1016/j.gloplacha.2012.04.001, 2012.

Salerno, F., Viviano, G., Mangredi, E. C., Caroli, P., Thakuri, S., and Tartari, G.: Multiple Carrying Capacities from a management-oriented perspective to operationalize sustainable tourism in protected area, J. Environ. Manage., 128, 116–125, doi:10.1016/j.jenvman.2013.04.043, 2013.

Salerno, F., Gambelli, S., Viviano, G., Thakuri, S., Guyennon, N., D'Agata, C., Diolaiuti, G., Smiraglia, C., Stefani, F., Bochhiola, D., and Tartari, G.: High alpine ponds shift upwards as average temperature increase: a case study of the Ortles-Cevedale mountain group (Southern alps, Italy) over the last 50 years, Global Planet. Change, 120, 81–91, doi:10.1016/j.gloplacha.2014.06.003, 2014.

Scherler, D., Bookhagen, B., and Strecker, M. R.: Spatially variable response of Himalayan glaciers to climate change affected by debris cover, Nature Geosci., 4, 156–159, doi:10.1038/ngeo1068, 2011.

Schneider, T.: Analysis of incomplete climate data: estimation of mean values and covariance matrices and imputation of missing values, J. Climate, 14, 853–871, doi:10.1175/1520-0442(2001)014<0853:AOICDE>2.0.CO;2, 2001.

Sellegri, K., Laj, P., Venzac, H., Boulon, J., Picard, D., Villani, P., Bonasoni, P., Marinoni, A., Cristofanelli, P., and Vuillermoz, E.: Seasonal variations of aerosol size distributions based on long-term measurements at the high altitude Himalayan site of Nepal Climate Observatory-Pyramid (5079 m), Nepal, Atmos. Chem. Phys., 10, 10679–10690, doi:10.5194/acp-10-10679-2010, 2010.

Sen, P. K.: Estimates of the regression coefficient based on Kendall's Tau, J. Am. Stat. Assoc., 63, 1379–1389, doi:10.2307/2285891, 1968.

Shekhar, M. S., Chand, H., Kumar, S., Srinivasan, K., and Ganju, A.: Climate-change studies in the western Himalaya, Ann. Glaciol., 51, 105–112, doi:10.3189/172756410791386508, 2010.

Shrestha, A. B., Wake, C. P., Mayewski, P. A., and Dibb, J. E.: Maximum temperature trends in the Himalaya and its vicinity: an analysis based on temperature records from Nepal for the period 1971–94, J. Climate, 12, 2775–5561, doi:10.1175/1520-0442(1999)012<2775:MTTITH>2.0.CO;2, 1999.

Singh, P. and Kumar, N.: Effect of orography on precipitation in the western Himalayan region, J. Hydrol., 199, 183–206, doi:10.1016/S0022-1694(96)03222-2, 1997.

Su, B. D., Jiang, T., and Jin, W. B.: Recent trends in observed temperature and precipitation extremes in the Yangtze River basin, China, Theor. Appl. Climatol., 83, 139–151, doi:10.1007/s00704-005-0139-y, 2006.

Tartari, G., Verza, P., and Bertolami, L.: Meteorological data at PYRAMID Observatory Laboratory (Khumbu Valley, Sagarmatha National Park, Nepal), in: Limnology of High Altitude Lakes in the Mt. Everest Region (Nepal), edited by: Lami, A., and Giussani, G., Mem. Ist. Ital. Idrobiol, 57, 23–40, 2002.

Tartari, G., Salerno, F., Buraschi, E., Bruccoleri, G., and Smiraglia, C.: Lake surface area variations in the North-Eastern sector of Sagarmatha National Park (Nepal) at the end of the 20th Century by comparison of historical maps, J. Limnol., 67, 139–154, doi:10.4081/jlimnol.2008.139, 2008.

Tartari, G., Vuillermoz, E., Manfredi, E. C., and Toffolon, R.: CEOP High Elevations Initiative, GEWEX News, Special Issue, 19, 4–5, 2009.

Thakuri, S., Salerno, F., Smiraglia, C., Bolch, T., D'Agata, C., Viviano, G., and Tartari, G.: Tracing glacier changes since the 1960s on the south slope of Mt. Everest (central Southern Himalaya) using optical satellite imagery, The Cryosphere, 8, 1297–1315, doi:10.5194/tc-8-1297-2014, 2014.

Themeßl, M. J., Gobiet, A., and Heinrich, G.: Empirical-statistical downscaling and error correction of regional climate models and its impact on the climate change signal, Climatic Change, 112, 449–468, doi:10.1007/s10584-011-0224-4, 2012.

Turner, A. G. and Annamalai, H.: Climate change and the South Asian summer monsoon, Nat. Clim. Change, 2, 587–595, doi:10.1038/nclimate1495, 2012.

Ueno, K. and Aryal, R.: Impact of tropical convective activity on monthly temperature variability during non monsoon season in the Nepal Himalayas, J. Geophys. Res., 113, D18112, doi:10.1029/2007JD009524, 2008.

Ueno, K., Endoh, N., Ohata, T., Yabuki, H., Koike, M., and Zhang, Y.: Characteristics of precipitation distribution in Tangula, Monsoon, 1993, B. Glaciol. Res., 12, 39–46, 1994.

UNEP (United Nations Environment Programme)/WCMC (World Conservation Monitoring Centre): Sagarmatha National Park, Nepal, in: Encyclopedia of Earth, edited by: McGinley, M., and Cleveland, C. J., Environmental Information Coalition, National Council for Science and the Environment, Washington, DC, available at: http://www.eoearth.org/view/article/155820 (last access: 28 November 2014), 2008.

Venzac, H., Sellegri, K., Laj, P., Villani, P., Bonasoni, P., Marinoni, A., Cristofanelli, P., Calzolari, F., Fuzzi, S., Decesari, S., Facchini, M. C., Vullermoz, E., and Verza, G. P.: High frequency new particle formation in the Himalayas, P. Natl. Acad. Sci. USA, 105, 15666–15671, doi:10.1073/pnas.0801355105, 2008.

Vuille, M.: Climate variability and high altitude temperature and precipitation, in: Encyclopedia of Snow, Ice and Glaciers, edited by: Singh, V. P., Singh, P., and Haritashya, U. K., Springer, the Netherlands, 153–156, 2011.

Wagnon, P., Vincent, C., Arnaud, Y., Berthier, E., Vuillermoz, E., Gruber, S., Ménégoz, M., Gilbert, A., Dumont, M., Shea, J. M., Stumm, D., and Pokhrel, B. K.: Seasonal and annual mass balances of Mera and Pokalde glaciers (Nepal Himalaya) since 2007, The Cryosphere, 7, 1769–1786, doi:10.5194/tc-7-1769-2013, 2013.

Washington, W. M. and Parkinson, C. L.: An Introduction to Three-Dimensional Climate Modeling, 2nd edn., University Science Books, Sausalito, 2005.

Wu, B.: Weakening of Indian summer monsoon in recent decades, Adv. Atmos. Sci., 22, 21–29, doi:10.1007/BF02930866, 2005.

Yang, J., Tan, C., and Zhang, T.: Spatial and temporal variations in air temperature and precipitation in the Chinese Himalayas during the 1971–2007, Int. J. Climatol., 33, 2622–2632, doi:10.1002/joc.3609, 2012.

Yang, X., Zhang, Y., Zhang, W., Yan, Y., Wang, Z., Ding, M., and Chu, D.: Climate change in Mt. Qomolangma region since 1971, J. Geogr. Sci., 16, 326–336, doi:10.1007/s11442-006-0308-7, 2006.

Yao, T., Thompson, L., Yang, W., Yu, W., Gao, Y., Guo, X., Yang, X., Duan, K., Zhao, H., Xu, B., Pu, J., Lu, A., Xiang, Y., Kattel, D. B., and Joswiak, D.: Different glacier status with atmo-

spheric circulations in Tibetan Plateau and surroundings, Nat. Clim. Change, 2, 663–667, doi:10.1038/nclimate1580, 2012.

You, Q., Kang, S., Pepin, N., Flügel, W., Yan, Y., Behrawan, H., and Huang, J.: Relationship between temperature trend magnitude, elevation and mean temperature in the Tibetan Plateau from homogenized surface stations and reanalysis data, Global Planet. Change, 71, 124–133, doi:10.1016/j.gloplacha.2010.01.020, 2010.

Zhao, H., Xu, B., Yao, T., Wu, G., Lin, S., Gao, J., and Wang, M.: Deuterium excess record in a southern Tibetan ice core and its potential climatic implications, Clim. Dynam., 38, 1791–1803, doi:10.1007/s00382-011-1161-7, 2012.

Table 1. List of surface stations belonging to PYRAMID Observatory Laboratory network located along the south slopes of Mt. Everest (upper DK Basin).

Station ID	Location	Latitude °N	Longitude °E	Elevation m a.s.l.	Sampling Frequency	Data Availability From	To	% of daily missing data Air Temperature	Precipitation
AWS3	Lukla	27.70	86.72	2660	1 h	2 Nov 2004	31 Dec 2012	23	20
AWSN	Namche	27.80	86.71	3570	1 h	27 Oct 2001	31 Dec 2012	21	27
AWS2	Pheriche	27.90	86.82	4260	1 h	25 Oct 2001	31 Dec 2013	15	22
AWS0	Pyramid	27.96	86.81	5035	2 h	1 Jan 1994	31 Dec 2005	19	16
AWS1	Pyramid	27.96	86.81	5035	1 h	1 Jan 2000	31 Dec 2013	10	21
ABC	Pyramid	27.96	86.82	5079	1 h	1 Mar 2006	31 Dec 2011	5	1
AWS4	Kala Patthar	27.99	86.83	5600	10 min	1 Jan 2009	31 Dec 2013	28	38
AWS5	South Col	27.96	86.93	7986	10 min	1 May 2008	31 Oct 2011	39	100

Table 2. List of ground weather stations located in the Koshi Basin and descriptive statistics of the Sen's slopes for minimum, maximum, and mean air temperatures and total precipitation for the 1994–2012 period. The annual mean air temperature, the total annual mean precipitation, and the percentage of missing daily values is also reported.

						Air Temperature					Precipitation		
	ID	Station Name	Latitude °N	Longitude °N	Elevation m a.s.l.	Annual mean °C	Missing values %	MinT trend °C a^{-1}	MaxT trend °C a^{-1}	MeanT trend °C a^{-1}	Annual total mm	Missing values %	Prec trend mm a^{-1}
KO-S (NEPAL)	1024	DHULIKHEL	27.61	85.55	1552	17.1	2	−0.012	0.041	0.026			
	1036	PANCHKHAL	27.68	85.63	865	21.4	10	0.038	0.051^{b}	0.038^{a}	1191	10	−25.0^{b}
	1058	TARKE GHYANG	28.00	85.55	2480						3669	10	−21.9
	1101	NAGDAHA	27.68	86.10	850						1369	3	−1.4
	1103	JIRI	27.63	86.23	2003	14.4	1	0.013	0.020	0.014^{a}	2484	4	6.6
	1202	CHAURIKHARK	27.70	86.71	2619						2148	2	1.3
	1206	OKHALDHUNGA	27.31	86.50	1720	17.6	2	−0.017	0.042	0.000	1786	3	−5.1
	1210	KURULE GHAT	27.13	86.41	497						1017	2	−23.4^{a}
	1211	KHOTANG BAZAR	27.03	86.83	1295						1324	4	15.9
	1222	DIKTEL	27.21	86.80	1623						1402	6	10.4
	1301	NUM	27.55	87.28	1497						4537	6	−54.3^{c}
	1303	CHAINPUR (EAST)	27.28	87.33	1329	19.1	0	−0.127^{b}	0.024	−0.064^{a}	1469	0	−1.1
	1304	PAKHRIBAS	27.05	87.28	1680	16.7	0	−0.005	0.036^{b}	0.015	1540	4	−3.7
	1307	DHANKUTA	26.98	87.35	1210	20.0	0	−0.002	0.153^{d}	0.071^{d}	942	6	−9.2^{a}
	1314	TERHATHUM	27.13	87.55	1633	18.2	10	0.033	0.066^{a}	0.049^{b}	1052	6	−13.1^{a}
	1317	CHEPUWA	27.46	87.25	2590						2531	5	−41.9^{b}
	1322	MACHUWAGHAT	26.96	87.16	158						1429	6	−22.9^{a}
	1403	LUNGTHUNG	27.55	87.78	1780						2347	1	2.6
	1405	TAPLEJUNG	27.35	87.66	1732	16.6	1	0.060^{b}	0.085^{c}	0.071^{c}	1966	3	−11.6
	1419	PHIDIM	27.15	87.75	1205	21.2	7	0.047^{b}	0.082^{c}	0.067^{c}	1287	2	−13.6^{b}
		MEAN	27.33	87.00	1587	17.9	2	0.003	0.060^{a}	0.029^{a}	1527	4	−11.1
		PYRAMID	27.96	86.81	5035	−2.4	0	0.072^{d}	0.009	0.044^{b}	449	0	−13.7^{d}
KO-N (TIBET)		DINGRI	28.63	87.08	4.302	3.5	0	0.037^{a}	0.041^{a}	0.037^{b}	309	0	−0.1
		NYALAM	28.18	85.97	3.811	4.1	0	0.032^{a}	0.036^{a}	0.036^{a}	616	0	−0.2
		MEAN	28.41	86.53	4.057	3.8	0.1	0.034^{a}	0.039^{a}	0.037^{b}	463	0	−0.1

Level of significance (^{a} p value = 0.1, ^{b} p value = 0.05, ^{c} p value = 0.01, and ^{d} p value = 0.001).

Table 3. Descriptive statistics of the Sen's slopes on a seasonal basis for minimum, maximum, and mean air temperatures and total precipitation of weather stations located in the Koshi Basin for the 1994–2012 period. The Nepali and Tibetan stations are aggregated as mean values.

Location	Minimum Temperature				Maximum Temperature				Mean Temperature				Total Precipitation			
	Pre-	Monsoon	Post-	Annual	Pre-	Monsoon	Post-	Annual	Pre-	Monsoon	Post-	Annual	Pre-	Monsoon	Post-	Annual
SOUTHERN KOSHI BASIN (KO-S,NEPAL)	0.012	−0.005	−0.001	0.003	0.076[a]	0.052	0.069[a]	0.060[a]	0.043	0.020	0.030	0.030[a]	0.8	−8.6	−2.5	−11.1
PYRAMID (NEPAL)	0.067[a]	0.041[a]	0.151[d]	0.072[d]	0.024	−0.028	0.049	0.009	0.035	0.015	0.124[c]	0.044[c]	−2.5[c]	−9.3[c]	−1.4[c]	−13.7[d]
NORTHERN KOSHI BASIN (KO-N,TIBET)	0.042[a]	0.019	0.086[b]	0.034[a]	0.023	0.030	0.071[b]	0.039[a]	0.042[a]	0.013	0.084[b]	0.037[b]	2.2	0.4	−3.3[b]	−0.1

Level of significance ([a] p value = 0.1, [b] p value = 0.05, [c] p value = 0.01, and [d] p value = 0.001). Annual and seasonal temperature trends are expressed as $^{\circ}C\,a^{-1}$. Annual precipitation trend is expressed as $mm\,a^{-1}$, while the seasonal precipitation trends are in mm (4 months) a^{-1}.

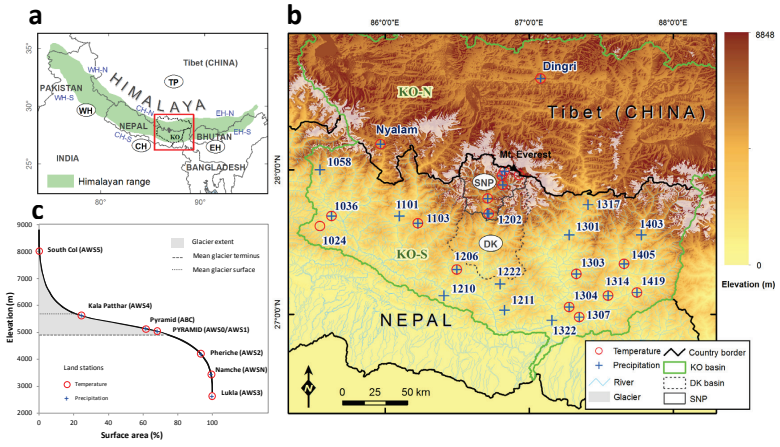

Figure 1. (a) Location of the study area in the Himalaya, where the abbreviations WH, CH, EH represents the Western, Central and Eastern Himalaya, respectively (the suffixes -N and -S indicate the northern and southern slopes). **(b)** Focused map on the spatial distribution of all meteorological stations used in this study, where KO and DK stand for the Koshi and Dudh Koshi Basins, respectively; SNP represents the Sagarmatha National Park. **(c)** Hypsometric curve of SNP (upper DK Basin) and altitudinal glacier distribution. Along this curve, the locations of meteorological stations belonging to PYRAMID Observatory Laboratory are presented.

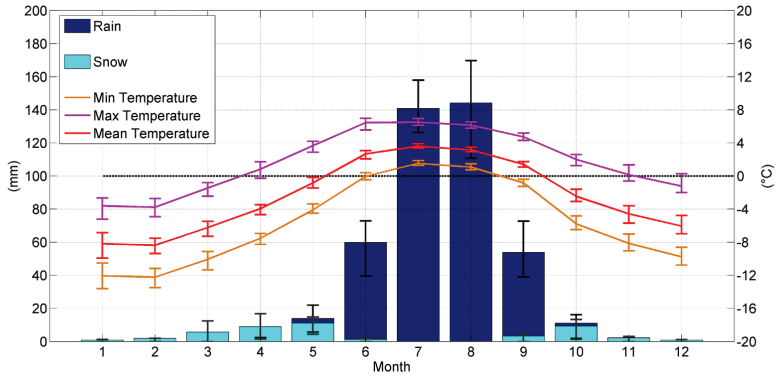

Figure 2. Mean monthly cumulated precipitation subdivided into snowfall and rainfall and minimum, maximum, and mean temperature at 5050 m a.s.l. (reference period 1994–2013). The bars represent the SD.

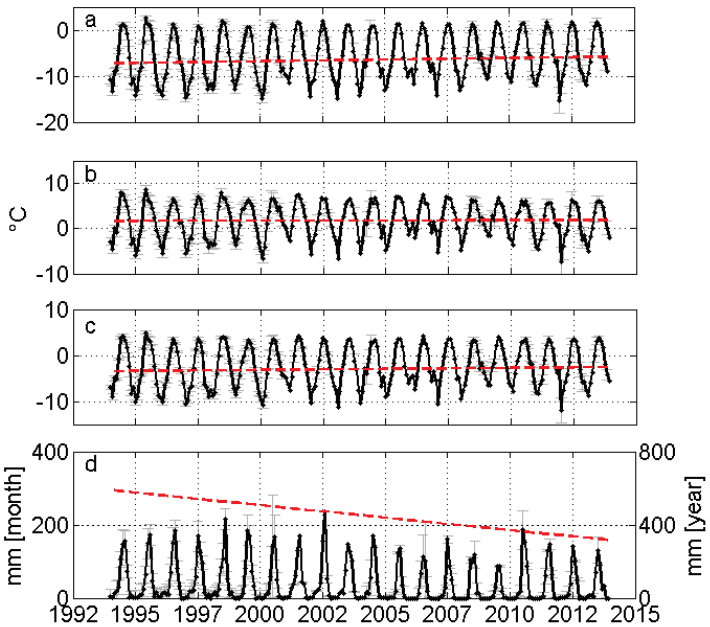

Figure 3. Temperature and precipitation monthly time series (1994–2013) reconstructed at high elevations of Mt. Everest (PYRAMID): minimum **(a)**, maximum **(b)**, and mean temperature **(c)**, and precipitation **(d)**. Uncertainty at 95 % is presented as gray bar. The red lines represents the robust linear fitting of the time series characterized by the associated Sen's slope. According to Dytham (2011), the intercepts are calculated by taking the slopes back from every observation to the origin. The intercepts used in here represent the median values of the intercepts calculated for every point (Lavagnini et al., 2011). For precipitation the linear fitting refers at the right axis.

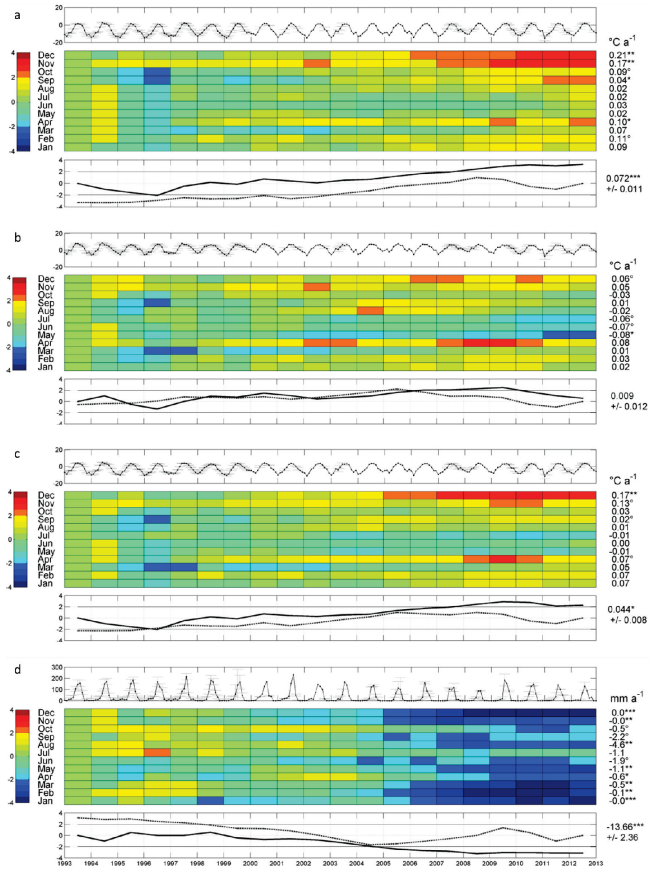

Figure 4. Trend analysis for **(a)** minimum, **(b)** maximum, and **(c)** mean air temperatures and **(d)** total precipitation in the upper DK Basin. The top graph of each meteorological variable shows the monthly trend (dark line) and uncertainty due to the reconstruction process (gray bars). The central grid displays the results of the sequential Mann–Kendall (seqMK) test applied at the monthly level. On the left, the color bar represents the normalized Kendall's tau coefficient $\mu(\tau)$. The color tones below −1.96 and above 1.96 are significant ($\alpha = 5\,\%$). On the right, the monthly Sen's slopes and the relevant significance levels for the 1994–2013 period ($^{\circ}$ p value = 0.1, * p value = 0.05, ** p value = 0.01, and *** p value = 0.001). The bottom graph plots the progressive (black line) and retrograde (dotted line) $\mu(\tau)$ applied on the annual scale. On the right, the annual Sen's slope is shown for the 1994–2013 period.

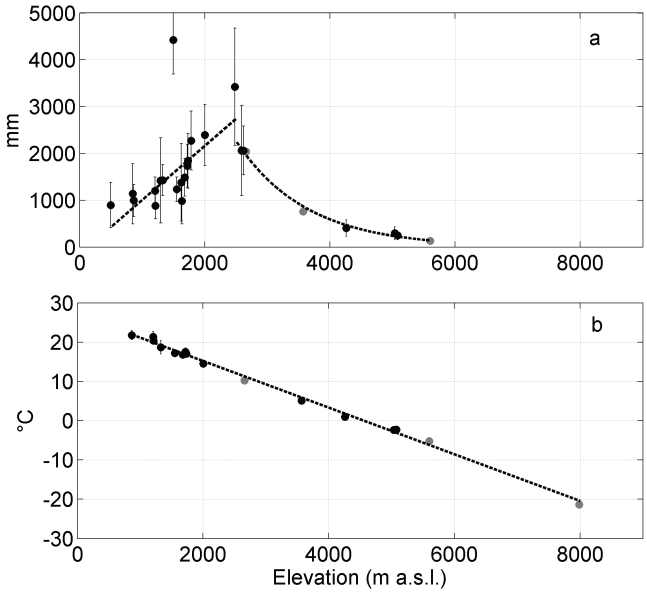

Figure 5. Lapse rates of **(a)** mean annual air temperature and **(b)** total annual precipitation in the Koshi Basin for the last 10 years (2003–2012). The daily missing data threshold is set to 10 %. Only stations presenting at least 5 years of data (black points) are considered to create the regressions (the bars represent two SD). Gray points indicate the stations presenting less than 5 years of data.

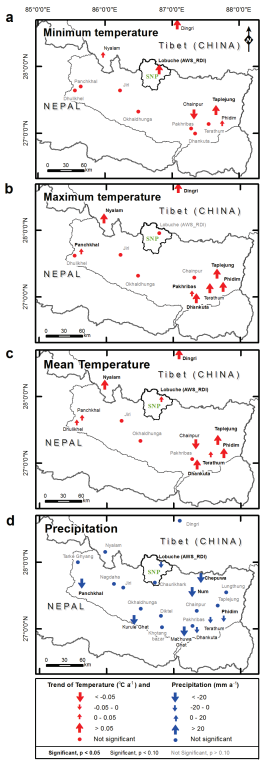

Figure 6. Spatial distribution of the Sen's slopes in the Koshi Basin for minimum **(a)**, maximum **(b)**, and mean **(c)** air temperature and **(d)** total precipitation for the 1994–2013 period. Data are reported in Table 2.

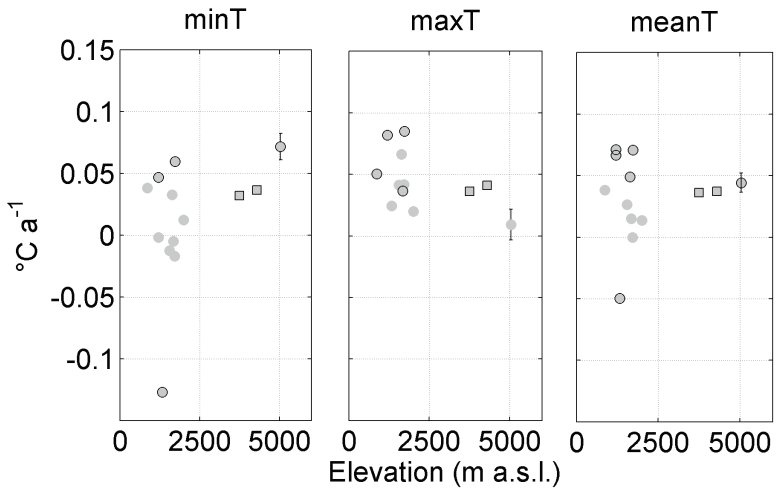

Figure 7. Elevation dependency of minimum **(a)**, maximum **(b)**, and mean **(c)** air temperatures with the Sen's slopes for the 1994–2013 period. The circle indicates stations with less than 10 % of missing daily data, and the star indicates stations showing a trend with p value < 0.1. The red marker represents the trend and the associated uncertainty (two SD) referred to the reconstructed time series for the AWS1 station (Pyramid). Data are reported in Table 2.

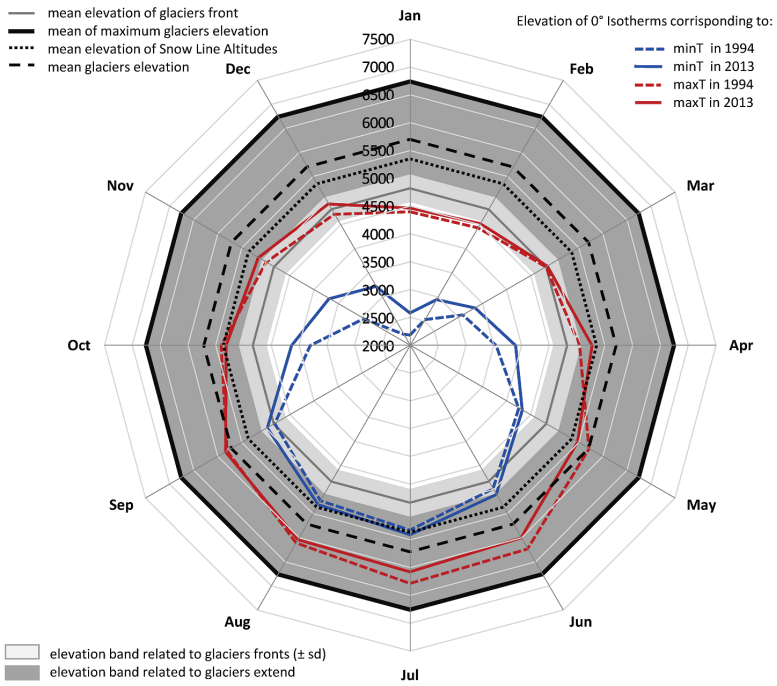

Figure 8. Linkage between the temperature increases and altitudinal glacier distribution. The 0 °C isotherms corresponding to the mean monthly minimum and maximum temperature are plotted for the 1994 and 2013 years according the observed T trends and lapse rates.

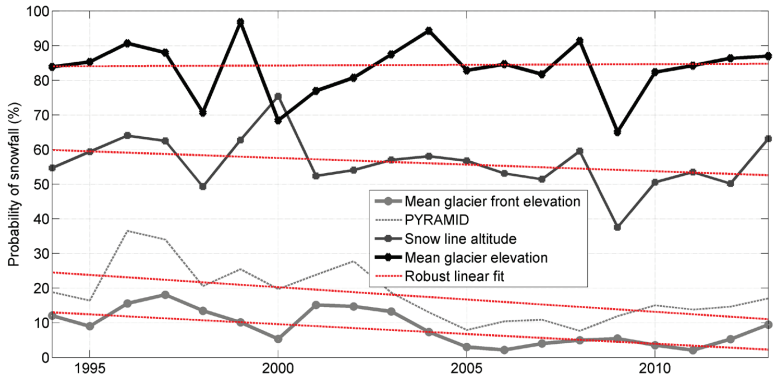

Figure 9. Trend analysis of annual probability of snowfall on total cumulated precipitation. The red lines represents the robust linear fitting of the time series characterized by the associated Sen's slope (more details in the caption of Fig. 3).

Supplement of The Cryosphere Discuss., 8, 5911–5959, 2014
http://www.the-cryosphere-discuss.net/8/5911/2014/
doi:10.5194/tcd-8-5911-2014-supplement

The Cryosphere Discussions
Open Access

Supplement of

Weak precipitation, warm winters and springs impact glaciers of south slopes of Mt. Everest (central Himalaya) in the last two decades (1994–2013)

F. Salerno et al.

Correspondence to: F. Salerno (salerno@irsa.cnr.it)

Supplementary Material 1

Reconstruction methods of the daily temperature and precipitation time series at Pyramid station (5035 m a.s.l.)

In the following, we describe the missing daily data reconstruction performed on daily T (minimum, maximum, and mean) and Prec time series collected at Pyramid (5035 m a.s.l.) for the 1994-2013 period. As already mentioned in the main text, we consider AWS1 as the reference station (REF) for the reconstruction, which has been operating continuously from 2000 to the present. This station replaced AWS0 (1994-2005). These two stations have a recorded percentage of missing daily values of approximately 20% over the last twenty years (Table 1). The other five stations (ABC, AWSKP, AWS2, AWSN and AWS3) taken into account for the reconstruction process will be referred to as secondary stations.

The time series reconstruction process considers four steps:

1) Pre-processing of data
2) Infilling method
3) Multiple imputation technique
4) Monthly aggregation of data

Step 1 – Pre-processing of data

Table 1 shows the sampling frequency of stations (ranging from 10 minutes to 2 hours). After an accurate data quality control according to Ikoma et al., 2007, a daily aggregation of the time series (temporal homogenization) is performed. Daily data have been computed only if the 100% of sub-daily data are available; otherwise, it is considered missing. These rules ensure a maximum quality of daily values with a loss of information limited to the first and last day of the failure events.

Step 2 – Infilling method

The selected daily infilling method is based on a quantile mapping regression (e.g. Déqué 2007). This method estimates a rescaling function F between two time series. This function ensures that the daily cumulated density function (cdf) of a secondary station reproduces the daily cdf of the REF over their over their common observation period. Applying the inverse function (F^{-1}) to each secondary station, a new time series is computed for each of them. In the following, these new time series with the systematic bias corrected are indicated as '*' (e.g., AWS0*, ABC*). In our case the bias is mainly due to the altitude gradient, all stations being located along the same valley (Fig. 1b).

A new time series (REF_filled) has been created merging REF and the * time series according to a priority criterion based on the degree of correlation among data (Fig. S1). The specific rules of computing are described below:

- all available data of REF are maintained in the final reconstruction without any further processing;

- the priority criterion for infilling is based on the magnitude of correlation coefficient (*r*) between REF and each secondary station, for each variable (Table S1); In case the daily data of the secondary station with higher *r* is missing the station with the slight lower r is selected.

We can observe from Table S1 that AWS0, located few tens of meters far from REF, presenting *r* = 0.99 and r = 0.97 for temperature and precipitation, respectively, has been the first choice. The 82% of missing daily values of temperature and 72% of precipitation are filled using the AWS0*. The second choice is ABC. Together these two stations cover more than the 90% of missing values; the whole infilling procedure allows for filling the 86% and the 91% of the overall missing values of temperature and precipitation, respectively.

Table S1. Correlation coefficients (r) between the reference station (REF) and the other secondary stations for temperature and precipitation. Furthermore the table reports the number of daily data (n) that each station has provided to the reconstruction of the time series.

Stations	Temperature		Precipitation	
	r	*n*	*r*	*n*
AWS0	0.99	2,144 (82.2%)	0.97	2,298 (72.2%)
ABC	0.98	254 (9.7%)	0.84	646 (20.3%)
AWSKP	0.96	48 (1.8%)	0.62	13 (0.4%)
AWS2	0.94	95 (3.6%)	0.81	145 (4.6%)
AWSN	0.92	66 (2.5%)	0.56	78 (2.5%)
AWS3	0.87	0 (0.0%)	0.53	3 (0.1%)
Total infilled missing values		2,607		3,183

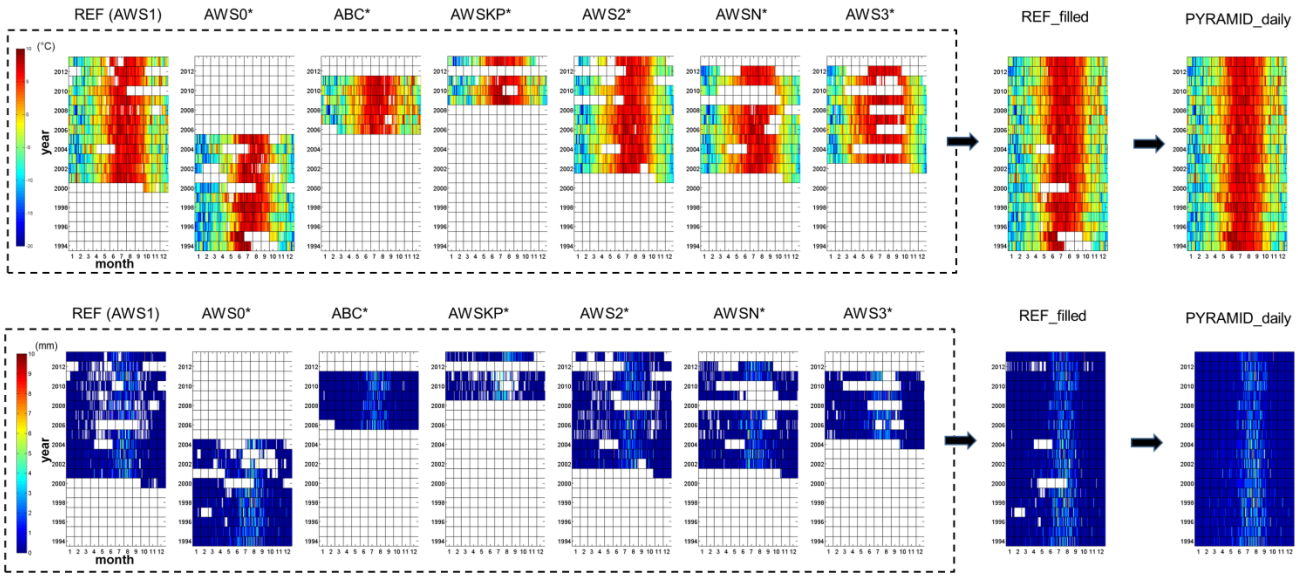

Figure S1. Scheme followed for the infilling process. Upper panel: daily mean temperature. Lower panel: precipitation. On the left, for each station, the daily data availability and the re-computed

*values, according to the quantile mapping procedure, are shown. On the right, a new time series (REF_filled) is created by merging REF (reference station) and the * time series, according to a priority criterion described in the text. In case all stations recorded some simultaneous gaps, a multiple imputation technique is applied to obtain the PYRAMID_daily time series.*

The uncertainty associated with REF_filled (σ_{REF_filled}) time series derives from the quantile mapping procedure and in particular from the miss-correlation and possible non stationarity in the quantile relationship.

In order to estimate the σ_{REF_filled}, the probability distribution of the residues between REF and *time series is considered. In order to take into account the possible seasonal variability of the uncertainty, residues have been analyzed on monthly basis.

The Kolmogorov-Smirnov test (Massey, 1951), applied to distribution of the residues, verifies their normality. As a consequence, the daily uncertainty σ_{REF_filled} is estimated as the standard deviation of the residues. The estimated daily uncertainties are reported in Table S2.

Table S2. Daily uncertainty (expressed as °C and mm for temperature and precipitation, respectively) for each station associated with the daily data infilled through the quantile mapping regression.

Minimum Temperature (minT)

	Jan	Feb	Mar	Apr	May	Jun	Jul	Aug	Sep	Oct	Nov	Dec
AWS0	0.95	0.98	0.72	0.65	0.49	0.48	0.29	0.35	0.49	0.77	1.09	0.86
ABC	0.82	0.79	1.6	1.29	0.9	0.58	0.66	0.45	0.56	1	0.87	0.89
AWSKP	1.41	1.3	2.25	1.62	1.54	0.84	0.84	0.71	0.65	1.29	1.18	1.61
AWS2	2.06	2.09	2.11	1.85	1.49	1.11	0.88	0.78	0.99	1.99	2.15	1.87
AWSN	2.8	2.44	1.98	1.3	1.14	0.81	0.62	0.72	0.79	1.89	2.95	2.96
AWS3	3.18	2.48	2.35	1.33	1.31	1.25	0.82	0.8	0.88	2.02	3.39	3.23

Maximum Temperature (maxT)

	Jan	Feb	Mar	Apr	May	Jun	Jul	Aug	Sep	Oct	Nov	Dec
AWS0	0.81	0.9	0.71	1.05	0.65	0.75	0.63	0.61	0.71	1.02	0.74	1.43
ABC	0.61	0.92	1.68	1.2	1.53	1	1.07	0.65	0.75	0.77	0.65	0.62
AWSKP	1.4	1.91	2	1.58	2.12	1.31	1.02	1.07	0.8	1.21	1.49	1.35
AWS2	2.2	2.05	2.07	1.71	1.62	1.13	1.06	0.99	1.12	1.47	1.91	1.9
AWSN	3.41	3.04	2.89	2.25	2.06	1.84	1.42	1.3	1.39	2.14	3.31	3.26
AWS3	4.08	4.11	3.99	2.68	2.6	2.55	2.2	2.23	2.62	3.11	4.15	3.91

Mean Temperature (meanT)

	Jan	Feb	Mar	Apr	May	Jun	Jul	Aug	Sep	Oct	Nov	Dec
AWS0	0.56	0.7	0.57	0.24	0.28	0.29	0.24	0.24	0.27	0.46	0.45	0.5
ABC	0.34	0.32	1.46	1.02	0.96	0.54	0.72	0.41	0.36	0.59	0.46	0.4
AWSKP	0.91	0.74	2.08	1.3	1.29	0.82	0.58	0.52	0.47	0.94	1.07	1.4
AWS2	1.8	1.88	1.71	1.38	1.1	0.66	0.5	0.43	0.57	1.56	1.88	1.53
AWSN	2.78	2.43	1.85	1.17	1.03	0.69	0.56	0.54	0.64	1.78	2.79	2.83
AWS3	3.09	2.44	2.43	1.41	1.25	1.15	0.75	0.79	1.03	1.91	3.16	3.06

Precipitation (P)

	Jan	Feb	Mar	Apr	May	Jun	Jul	Aug	Sep	Oct	Nov	Dec
AWS0	0.68	0.22	0.43	0.99	0.61	0.72	1.34	0.93	0.61	0.29	0.38	0.04
ABC	0.02	0.03	0.07	0.28	0.52	1.17	1.91	3.42	1.49	0.1	0.19	0.04
AWSKP	0.27	0.42	0.46	1.04	0.79	1.62	2.79	2.8	1.97	2.09	0.09	0.19
AWS2	0.31	0.15	0.22	0.42	0.7	2.36	4.71	3.68	2.04	1.93	0.6	0
AWSN	0.42	0.66	0.69	1.1	1.19	2.2	5.41	5.13	3.07	1.41	0.27	0.8
AWS3	0.14	0.29	0.43	0.68	0.44	2.06	5.35	5.11	4.57	0.88	0.43	0.11

Step 3 – Multiple imputation technique

Unfortunately, all stations recorded some simultaneous gaps for a given variable: 5.7% and 4.3% for temperature and precipitation, respectively. For these cases, we applied a multiple imputation technique (the Regularized Expectation Maximization algorithm, RegEM; Schneider, 2001) to obtain the final PYRAMID_daily time series (Fig. S1).

This algorithm considers more available meteorological variables. In our case, we feed the procedure with the minimum, maximum and mean temperatures, precipitation, atmospheric pressure and relative humidity. The additional two variables (atmospheric pressure and relative humidity) allowed for a reduction of the estimated uncertainty associated with the computing of these missing data (σ_{RegEM}).

RegEM has been applied to the daily missing data on a monthly basis, considering the possible seasonal effect on the uncertainty. Table S3 reports the number of days imputed to the complete PYRAMID_daily time series for each month and for each variable. The daily standard error σ_{RegEM} estimated by the RegEM algorithm (Table S4) has been associated with each imputed data filled into the complete and final time series reconstructions for daily minimum, maximum, and mean temperatures and precipitation.

Table S3. Number of days imputed through RegEM

Variable	Jan	Feb	Mar	Apr	May	Jun	Jul	Aug	Sep	Oct	Nov	Dec
minT	0	1	1	35	87	48	68	71	60	33	10	0
maxT	0	1	1	35	87	48	68	71	60	33	10	0
meanT	0	1	1	35	87	48	68	71	60	33	10	0
Prec	13	31	14	52	99	48	31	9	1	9	4	0

Table S4. Uncertainty (°C and mm for temperature and precipitation, respectively) associated to the daily imputed thought RegEM

Variable	Jan	Feb	Mar	Apr	May	Jun	Jul	Ago	Sep	Oct	Nov	Dic
minT	-	3.25	2.89	2.34	2.21	1.95	0.83	0.96	1.37	2.54	2.46	-
maxT	-	3.64	3.22	2.82	2.47	1.87	1.34	1.31	1.44	2.30	2.55	-
meanT	-	3.20	2.82	2.34	2.07	1.58	0.72	0.84	1.16	2.17	2.29	-
p	0.18	0.35	0.65	0.86	0.93	2.73	4.54	4.51	2.73	1.59	0.69	-

Step 4- Monthly aggregation

Finally, the PYRAMID_daily time series, for each variable, have been aggregated on the monthly scale (hereinafter referred to as PYRAMID). The uncertainty associated with each value of the PYRAMID (named σ_m) is estimated considering the propagation of the daily uncertainty to the monthly one through the computation of the mean (for temperature) or of the sum (for precipitation).

The propagation of the uncertainty from the daily data d_i to the monthly one is different if we consider the monthly average M_m (as for temperature) or the monthly accumulation M_c (as for precipitation):

$$\sigma_m = \sqrt{\sum_{j=1}^{N}\left(\frac{\partial M_m}{\partial d_j}\cdot\sigma_{d_j}\right)^2} = \sqrt{\sum_{j=1}^{N}\left(\frac{\partial\left(\frac{1}{N}\sum_{i=1}^{N} d_i\right)}{\partial d_j}\cdot\sigma_{d_j}\right)^2} = \sqrt{\frac{1}{N}\sum_{j=1}^{N}{\sigma_{d_j}}^2} \quad (1)$$

where $M_m = \frac{1}{N}\sum_{i=1}^{N} d_i$

and

$$\sigma_m = \sqrt{\sum_{j=1}^{N}\left(\frac{\partial Mc}{\partial d_j}\cdot\sigma_{d_j}\right)^2} = \sqrt{\sum_{j=1}^{N}\left(\frac{\partial \sum_{i=1}^{N} d_i}{\partial d_j}\cdot\sigma_{d_j}\right)^2} = \sqrt{\sum_{j=1}^{N}{\sigma_{d_j}}^2} \quad (2)$$

where $M_c = \sum_{i=1}^{N} d_i$

N is the number of days of a given month and σ_{d_j} the daily uncertainty as :

$$\begin{cases} \sigma_{d_j} = 0 & if\ the\ data\ \ belongs\ to\ the\ REF \\ \sigma_{d_j} = \sigma_{REF\_filled} & if\ the\ data\ \ is\ imputed\ through\ infilling\ step \\ \sigma_{d_j} = \sigma_{RegEM} & if\ the\ data\ is\ imputed\ through\ RegEM \end{cases}$$

Finally, we estimated the uncertainty associated with the annual Sen's slopes (1994-2013) of each time series through a Monte Carlo uncertainty analysis (e.g., James and Oldenburg 1997):

- For each month value, a random realization of the normal distribution with zero-mean and σ_m standard deviation is computed.
- This uncertainty is added to each monthly estimate coming from eq. (1) or (2), obtaining a time series perturbed by the uncertainty.
- The Sen's slope and associated p-value is computed.
- The process is repeated until the convergence of the mean value of the Sen's slope and the associated standard deviation. In these regards, we observed that approximately 5000 runs are enough to ensure the convergence with a threshold of 10^{-5} °C a^{-1} and 10^{-3} mm a^{-1} for temperature and precipitation, respectively.

Table S5 reports the Sen's slopes for the 1994-2013 period calculated for each reconstructed monthly time series (PYRAMID), associated intervals of confidence (95%), median p-value and the associated [5% and 95%] quantiles.

Table S5. Sen's slopes for the 1994-2013 period calculated for each reconstructed monthly time series (PYRAMID), associated intervals of confidence (95%), median p-value and the associated [5% and 95%] quantiles.

Time series	Sen's slope	Interval of confidence (95%)	p-value	quantiles [5% and 95%]
PYRAMID minT	0.072 °C a^{-1}	+/- 0.011	0.0021	[0.0001-0.0212]
PYRAMID maxT	0.009 °C a^{-1}	+/- 0.012	0.7212	[0.2843-0.9741]
PYRAMID meanT	0.044 °C a^{-1}	+/- 0.008	0.035	[0.0053-0.1443]
PYRAMID Prec	-13.66 mm a^{-1}	+/- 2.36	0.0021	[0.0002-0.0252]

REFERENCES

Ikoma, E., K. Tamagawa, T. Ohta, T. Koike, and M. Kitsuregawa (2007), QUASUR: Web-based quality assurance system for CEOP reference data, *J. Meteorol. Soc. JPN., 85A*, 461-473.

Massey, F. J. (1951), The Kolmogorov-Smirnov Test for Goodness of Fit, *J. Am. Stat. Assoc., 46*(253), 68–78.

Supplementary Material 2

Further analysis on the non-stationarity of the reconstructed daily precipitation time series at Pyramid station

The analysis described in the following aims at assessing whether the decreasing trend of precipitation observed for the daily time series reconstructed at Pyramid (1994-2013) is due to a reduction of duration or to a reduction of intensity.

To this goal we considered two different periods *p*, say *p1* = 1994-1998 and *p2* = 2009-2013, which correspond to the first and last five years of the whole analysis period *p0* = 1994-2013. For a given week *w*, the mean weekly-cumulated precipitation RR_w^p is defined as $RR_w^p = \left(\sum_{y=1}^{N} RR_{w,y}\right)/N$, where *N* is the number of years during the period *p*.

The difference between the mean weekly-cumulated precipitation RR_w^{p1} and RR_w^{p2} may be attributed to a change in the corresponding duration and/or intensity. To separate the relative contributions, we defined two descriptors:

1-The duration of precipitation for a given week *w* of the year *y* is described by the number of wet days $W_{w,y}$, where a "wet day" is defined by the threshold RR>1 mm. Then, the mean W_w^p over a given period *p* of *N* years is computed as:

$$W_w^p = \frac{1}{N}\sum_{y=1}^{N} W_{w,y} \qquad (1)$$

2- The daily intensity of precipitation for a given week *w* of the year *y* is computed as the cumulative precipitation $RR_{w,y}$ divided by the number of wet days $W_{w,y}$. Then, a mean intensity index $SDII_w^p$ over a given period *p* of *N* years is computed as:

$$SDII_w^p = \frac{1}{N}\sum_{y=1}^{N} \frac{RR_{w,y}}{W_{w,y}} \qquad (2)$$

An attempt to quantify the contribution to the variation in precipitation arising from variation in duration and/or intensity is to consider one of the two terms stationary over the whole period. This is a rough approximation as the non-stationarity may not be linear. However, an estimation of the relative contribution arising from the change in duration can be expressed considering the intensity of precipitation as stationary over the whole period p0 ($SDII_w^{p0}$) and computing the variation of precipitation due only to a variation in duration, i.e. $(W_w^{p2} - W_w^{p1}) * SDII_w^{p0}$. The relative contribution *RLD* to the total change $(RR_w^{p2} - RR_w^{p1})$ can be estimated as:

$$RLD = \frac{(W_w^{p2} - W_w^{p1}) * SDII_w^{p0}}{(RR_w^{p2} - RR_w^{p1})} * 100 \qquad (3)$$

The indexes proposed above are shown in figure S6 in dark blue area for the 1994-1998 period and light blue area for the 2009-2013 period for the W_w^p, $SDII_w^p$ and RR_w^p (panel a, b and c respectively). For each index, we defined as residues the difference between the two periods (red bar plot).

The *RLD* (shown in red on the right axis of the panel c) indicates that the early and late monsoon are more affected by the reduction in duration than intensity, while it is the opposite during the monsoon.

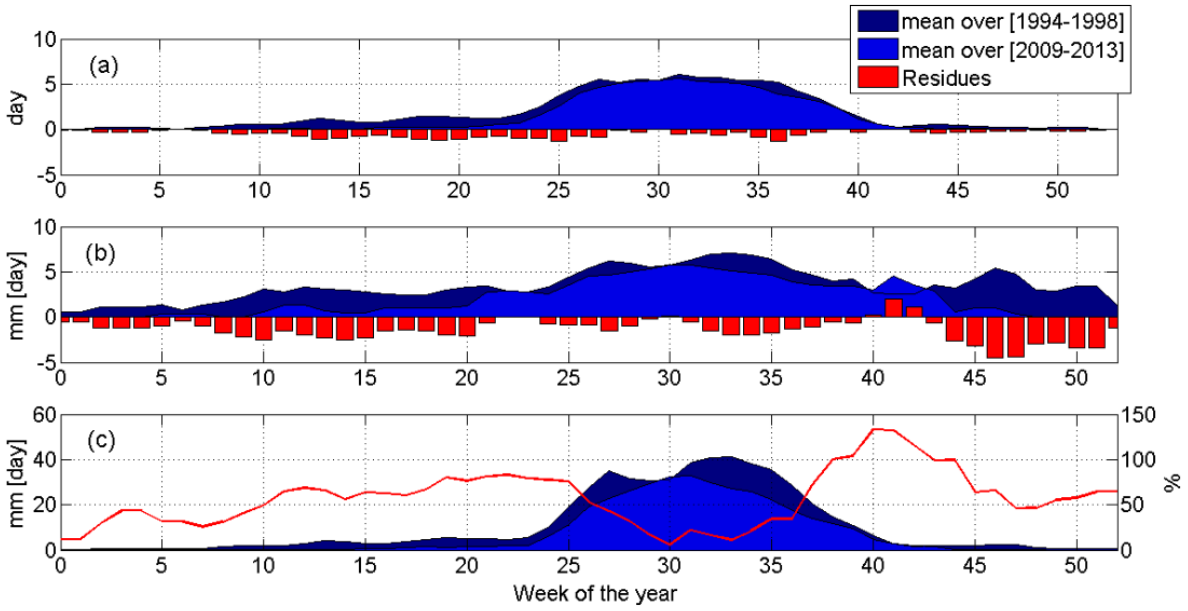

Figure S6. Panel a: Mean number of wet day per week W_w^p. Panel b: Mean daily precipitation intensity $SDII_w^p$ (mm). Panel c: Mean weekly-cumulated precipitation RR_w^p and relative contribution of the change in duration RLD in % (red line)

Article II

8.2 Article II

Thakuri, S., F. Salerno, C. Smiraglia, T. Bolch, C. D'Agata, G. Viviano, and G. Tartari (2014) Tracing glacier changes since the 1960s on the south slope of Mt. Everest (central Southern Himalaya) using optical satellite imagery. *The Cryosphere*, 8, 1297–1315, doi: 10.5194/tc-8-1297–2014.

The Cryosphere, 8, 1297–1315, 2014
www.the-cryosphere.net/8/1297/2014/
doi:10.5194/tc-8-1297-2014

The Cryosphere
Open Access

Tracing glacier changes since the 1960s on the south slope of Mt. Everest (central Southern Himalaya) using optical satellite imagery

S. Thakuri[1,3], F. Salerno[1,2], C. Smiraglia[3], T. Bolch[4,5], C. D'Agata[3], G. Viviano[1], and G. Tartari[1]

[1]National Research Council, Water Research Institute (IRSA-CNR), Brugherio, Italy
[2]Ev-K2-CNR Committee, Via San Bernardino, 145, Bergamo 24126, Italy
[3]Department of Earth Sciences "Ardito Desio", University of Milan, Milan, Italy
[4]Department of Geography, University of Zurich, Zurich, Switzerland
[5]Institute for Cartography, Technische Universität Dresden, Dresden, Germany

Correspondence to: S. Thakuri (thakuri@irsa.cnr.it)

Received: 1 September 2013 – Published in The Cryosphere Discuss.: 8 November 2013
Revised: 11 March 2014 – Accepted: 12 June 2014 – Published: 22 July 2014

Abstract. This contribution examines glacier changes on the south side of Mt. Everest from 1962 to 2011 considering five intermediate periods using optical satellite imagery. The investigated glaciers cover ~ 400 km^2 and present among the largest debris coverage (32 %) and the highest elevations (5720 m) of the world. We found an overall surface area loss of 13.0 ± 3.1 % (median 0.42 ± 0.06 % a^{-1}), an upward shift of 182 ± 22 m (3.7 ± 0.5 m a^{-1}) in snowline altitude (SLA), a terminus retreat of 403 ± 9 m (median 6.1 ± 0.2 m a^{-1}), and an increase of 17.6 ± 3.1 % (median 0.20 ± 0.06 % a^{-1}) in debris coverage between 1962 and 2011. The recession process of glaciers has been relentlessly continuous over the past 50 years. Moreover, we observed that (i) glaciers that have increased the debris coverage have experienced a reduced termini retreat ($r = 0.87$, $p < 0.001$). Furthermore, more negative mass balances (i.e., upward shift of SLA) induce increases of debris coverage ($r = 0.79$, $p < 0.001$); (ii) since early 1990s, we observed a slight but statistically insignificant acceleration of the surface area loss (0.35 ± 0.13 % a^{-1} in 1962–1992 vs 0.43 ± 0.25 % a^{-1} in 1992–2011), but an significant upward shift of SLA which increased almost three times (2.2 ± 0.8 m a^{-1} in 1962–1992 vs 6.1 ± 1.4 m a^{-1} in 1992–2011). However, the accelerated shrinkage in recent decades (both in terms of surface area loss and SLA shift) has only significantly affected glaciers with the largest sizes (> 10 km^2), presenting accumulation zones at higher elevations ($r = 0.61$, $p < 0.001$) and along the preferable south–north direction of the monsoons. Moreover, the largest glaciers present median upward shifts of the SLA (220 m) that are nearly double than that of the smallest (119 m); this finding leads to a hypothesis that Mt. Everest glaciers are shrinking, not only due to warming temperatures, but also as a result of weakening Asian monsoons registered over the last few decades. We conclude that the shrinkage of the glaciers in south of Mt. Everest is less than that of others in the western and eastern Himalaya and southern and eastern Tibetan Plateau. Their position in higher elevations have likely reduced the impact of warming on these glaciers, but have not been excluded from a relentlessly continuous and slow recession process over the past 50 years.

1 Introduction

The controversies concerning the possibly faster glacial shrinkage in the Himalaya than in any other part of the world (Cogley et al., 2010; Bagla, 2009) have focused global attention on necessity for a more comprehensive study in this region. Current uncertainties are mainly attributed to a lack of measurements, both of glaciers and of climatic forcing agents (Bolch et al., 2012). The need for a fine-scale investigation is particularly evident on the south slope of Mt. Everest, which is one of the most heavily glacierized parts of the Himalaya. Glaciers here are characterized by abundant debris coverage

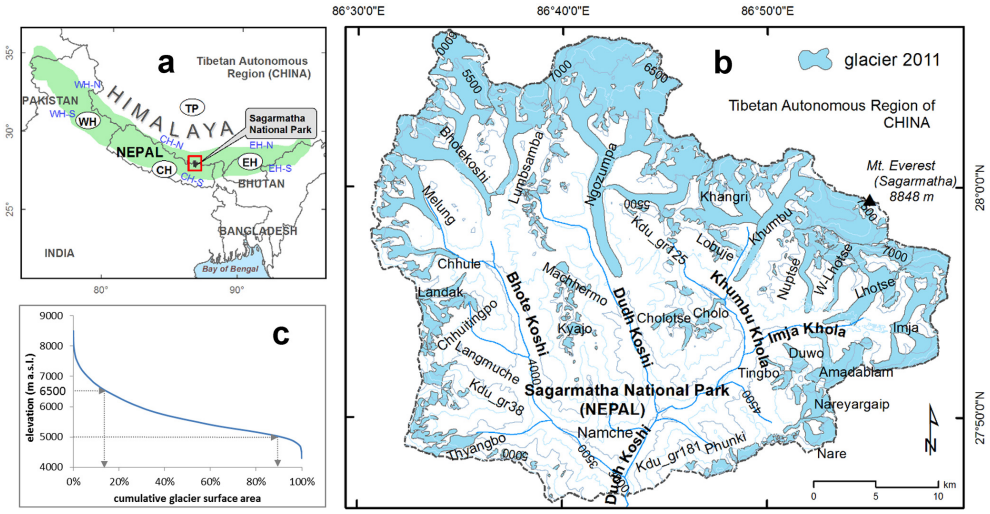

Figure 1. **(a)** Location of the study area: the Sagarmatha National Park (SNP), where the abbreviations CH, WH, EH, and TP represent the central Himalaya, the western Himalaya, the eastern Himalaya, and the Tibetan Plateau, respectively (suffixes -N and -S indicate the northern and southern slopes). **(b)** Focused map of the SNP in 2011 showing the distribution of 29 glaciers considered in this study with a surface area $> 1\,km^2$. **(c)** The hypsometric curve of the glaciers in 2011.

(Scherler et al., 2011; Salerno et al., 2012), an effect that has often been neglected in predictions of future water availability.

Some previous studies have discussed that debris-covered glaciers behave unlike clean glaciers (Nakawo et al., 1999; Benn et al., 2012). Scherler et al. (2011) studied debris-covered glaciers around the Himalayan range for a period of 2000–2008 and showed that heavy debris coverage influences terminus behaviors by stabilizing the terminus position change. However, Kääb et al. (2012), in a comprehensive study on the glacier mass change from 2003–2008 in the Himalaya, suggested that debris-covered ice thins at a rate similar to that of exposed ice. Significant mass loss despite thick debris cover was also reported by Bolch et al. (2011), Nuimura et al. (2012), and Pieczonka et al. (2013). Hence, the relation of length changes to mass balance is even weaker for debris-covered than for debris-free glaciers and there is a need for further assessment of the role of debris mantles.

This contribution examines the glacier changes on the south side of Mt. Everest as part of an effort to better define the glaciers status in the Himalaya. We extend the analysis of Salerno et al. (2008) carried out on the glacier surface area change (ΔSurf) on two historical maps (the period ranging from the 1950s to 1992). First of all, we cover a longer period (ranging from the 1960s to 2011) increasing furthermore the temporal resolution with six medium-high resolution satellite imagery, with the assistance of all available historical maps. Secondly, we make a complete analysis of terminus position change (ΔTerm), shift of snow-line altitude (ΔSLA), and changes in debris coverage (ΔDebrisCov). The results are compared with those obtained in previous studies in this area and along the Himalaya and the Tibetan Plateau range. We conclude by attempting to link the observed impacts with the climate change drivers.

2 Study area

The current study is focused on the Mt. Everest region, and in particular in the Sagarmatha (Mt. Everest) National Park (SNP) (27.75° to 28.11° N; 85.98° to 86.51° E) that lies in eastern Nepal in the southern part of the central Himalaya (CH-S) (Fig. 1a). The park area ($1148\,km^2$), extending from an elevation of 2845 m at Jorsale to 8848 m a.s.l., covers the upper catchment of the Dudh Koshi river (Manfredi et al., 2010; Amatya et al., 2010). Land cover classification shows that less than 10 % of the park area is forested (Salerno et al., 2010a; Bajracharya et al., 2010). The SNP is the world's highest protected area with over 30 000 tourists in 2008 (Salerno et al., 2010b, 2013). This region is one of the heavily glacierized parts of the Himalaya with almost one-third of the park territory characterized by ice cover. Bajracharya and Mool (2009) indicate that there are 278 glaciers in the Dudh Koshi Basin, with 40 glaciers accounting for most of the glacierized area (70 %) and all of these being valley-type. Most of the large glaciers are debris-covered type, with their ablation zone almost entirely covered by surface debris (Fig. 1b).

Several debris-covered glaciers have stagnant ice at their termini that have potential to develop widespread melting ponds and build up moraine-dammed lakes (Bolch et al., 2008b; Quincey et al., 2009). Gardelle et al. (2011) note that the southern side of Mt. Everest is the region that is most characterized by glacial lakes in the Hindu Kush Himalaya. Salerno et al. (2012) reported a total of 624 lakes in the

park including 17 proglacial lakes, 437 supraglacial lakes, and 170 unconnected lakes. In general, they observed that supraglacial lakes occupy from approximately 0.3 to 2 % of downstream glacier surfaces.

The glacier hypsometric curve plotted, using the glacier outlines of 2011 and the Advanced Spaceborne Thermal Emission and Reflection Radiometer Global Digital Elevation Model (ASTER GDEM, a product of METI and NASA), Version 2 indicates that the glacier surfaces are distributed from around 4300 m to above 8000 m a.s.l. with more than 75 % glacier surfaces lying between 5000 m and 6500 m a.s.l. (Fig. 1c); the area-weighted mean elevation of the glacier is 5720 m a.s.l in 2011. These glaciers are identified as summer-accumulation type fed mainly by summer precipitation from the South Asian monsoon system, whereas the winter precipitation caused by mid-latitude westerly wind is minimal (Ageta and Fujita, 1996; Tartari et al., 2002). The prevailing direction of the monsoons is S–N and SW–NE (Rao, 1976; Ichiyanagi et al., 2007). Based on the meteorological observations at the Pyramid Laboratory Observatory (5050 m a.s.l.), the mean annual air temperature is $-2.5 \pm 0.5\,^{\circ}\mathrm{C}$. In summer (June–September), air temperature is typically above 0 °C, the maximum occurs in July, and shows a typical variation associated with cloudiness. In contrast, thermal range is very high during winter owing to less cloudy conditions. In winter, the maximum daily temperature is usually below 0 °C, especially in February, the coldest month. Mean total annual precipitation is $516 \pm 75\,\mathrm{mm\,a^{-1}}$, with about 88 % of the annual amount recorded during the summer months (June–September). The vertical gradients of temperature, precipitation and solar radiation has been calculated using meteorological stations from 90 to 5600 m a.s.l. (data from Nepal Department of Hydrology and Meteorology – DHM – and Ev-K2-CNR Committee). We found a temperature lapse rate of $-0.0059\,^{\circ}\,\mathrm{m^{-1}}$, a solar radiation gradient of $+0.024\,\mathrm{W\,m^{-2}\,m^{-1}}$, valid for the 2800–5000 m a.s.l. elevation range, and for pre- and post-monsoon months, while the monsoon period is affected by high cloud cover. The precipitation increases with altitude by $+0.067$ mm [month] $\mathrm{m^{-1}}$ until around 2800 m a.s.l. afterwards it starts decreasing (-0.017 mm [month] $\mathrm{m^{-1}}$).

3 Data and methods

3.1 Data sources

The analyses of ΔTerm, ΔSurf, ΔSLA and ΔDebrisCov of Mt. Everest glaciers were performed from 1962 to 2011 using satellite imagery, with the assistance of all available historical maps (Table 1). We analyzed the glacier changes within five periods: 1962–1975, 1975–1992, 1992–2000, 2000–2008, and 2008–2011.

All satellite data were acquired after the monsoon season during the period from October-December. These images are characterized by low cloud cover and correspond to time just after the end of the snow accumulation and ablation period for that year; this allows for homogeneous comparisons (Paul et al., 2009). These months also coincides with the minimum ablation period on glaciers. The declassified Corona KH-4 (hereafter Corona-62) was used as a main data source for the base year of the analysis (1962). The Khumbu Himal map of late 1950s (Schneider, 1967; Salerno et al., 2008; hereafter KHmap-50s) and the topographic map of the Indian survey of 1963 (hereafter TISmap-63) were used to complement the results achieved using Corona-62 since the Corona-62 had the complex image geometry and absence of satellite camera specification for its rectification. The KHmap-50s has clear glacier boundaries, but the TISmap-63 has less discernible glacier outlines; thus, the first map was used for analysis related to ΔSurf, ΔTerm, and ΔSLA, while use of the TISmap-63 was limited to ΔTerm. The Corona KH-4B (Corona-70) image covers only a small portion of the northeast part of the study area. Therefore, the Landsat MultiSpectral Scanner (MSS) (1975) (Landsat-75) was used as the main data source, although its pixel resolution is significantly lower. Moreover, we compared the 1992 Landsat Thematic Mapper (TM) scene (Landsat-92) with the official topographic map of Nepal from same year (OTNmap-92). Concerning the more recent years, we used Landsat ETM+ scenes from 2000 (Landsat-00), 2011 (Landsat-11), and an ALOS AVNIR-2 scene (ALOS-08).

The ASTER GDEM, vers. 2 tiles for the Mt. Everest region were downloaded from http://gdem.ersdac.jspacesystems.or.jp. The vertical and horizontal accuracy of the GDEM are ∼ 20 m and ∼ 30 m, respectively (http://www.jspacesystems.or.jp/ersdac/GDEM/E/4.html). We decided to use the ASTER GDEM instead of the Shuttle Radar Topography Mission (SRTM) Digital Elevation Model (DEM) considering the higher resolution (30 m and 90 m, respectively) and the large data gaps of the SRTM DEM in this study area (Bolch et al., 2011). Furthermore, the ASTER GDEM shows better performance in mountain terrains (Frey et al., 2012).

3.2 Gap fill and pan-sharpening of Landsat SLC-off data

The problem of the scan line corrector failure (SLC-off) gap (Parkinson et al., 2006) in Landsat-11 was corrected using the IDL (Interactive Data Language) Extension-gap fill tool in ENVI® software that uses a local linear histogram matching algorithm in the application of another image from same year (Chen et al., 2011). The effect of the SLC-off gap in our study area can be assumed to be minimal due to the central location of our study area in the Landsat scene. More than 1/3 of our study area was not affected by the data gaps and the glaciers' boundaries were manually delineated taking the interpolation uncertainties into account. The Landsat-11 multispectral bands (30 m) were pan-sharpened for visual improvement (Rodriguez-Galiano et al., 2012) using the

Table 1. Data sources used in this study.

Abbreviation used in the text	Satellite image	Acquisition date	Spatial resolution (m)	Sensor	Scene ID
Corona-62	Corona	15 Dec 1962	~8	KH-4	DS009050054DF172_172 DS009050054DA174_174 DS009050054DA175_175
Corona-70	Corona	20 Nov 1970	~5	KH-4B	DS1112-1023DA163_163 DS1112-1023DF157_157
Landsat-75	Landsat 4	2 Nov 1975	60	MultiSpectral Scanner (MSS)	LM21510411975306AAA05
Landsat-92	Landsat 5	17 Nov 1992	30	Thematic Mapper (TM)	ETP140R41_5T19921117
Landsat-00	Landsat 7	30 Oct 2000	15[a]	Enhanced Thematic Mapper Plus (ETM+)	LE71400412000304SGS00
ALOS-08	Advanced Land Observation Satellite (ALOS)	24 Oct 2008	10	Advanced Visible and Near Infrared Radiometer type 2 (AVNIR-2)	ALAV2A146473040
Landsat-11	Landsat 7	30 Nov 2011	15[a, b]	ETM+	LE71400412011334EDC00
Abbreviation used in the text	**Topographic map**	**Acquisition date**	**Scale**	**Acquisition technique**	
KHmap-50s	Khumbu Himal map (Schneider Map)	late 1950s	1 : 50000	Photographic survey in 1921, terrestrial photogrammetric survey of 1935 and 1939, field survey and terrestrial photogrammetry in 1955–1963 (Schneider, 1967; Byers, 1997)	
TISmap-63	Topographic map of Indian survey	1963	1 : 50000	Vertical aerial photographic survey 1957–1959 and field survey in 1963 (Yamada, 1998)	
OTNmap-92	Official topographic map of Nepal	1992	1 : 50000	Aerial photogrammetry (1992) and field survey (1996), published in 1997 by Government of Nepal	

[a] Pan-sharpened images;
[b] SLC-off image.

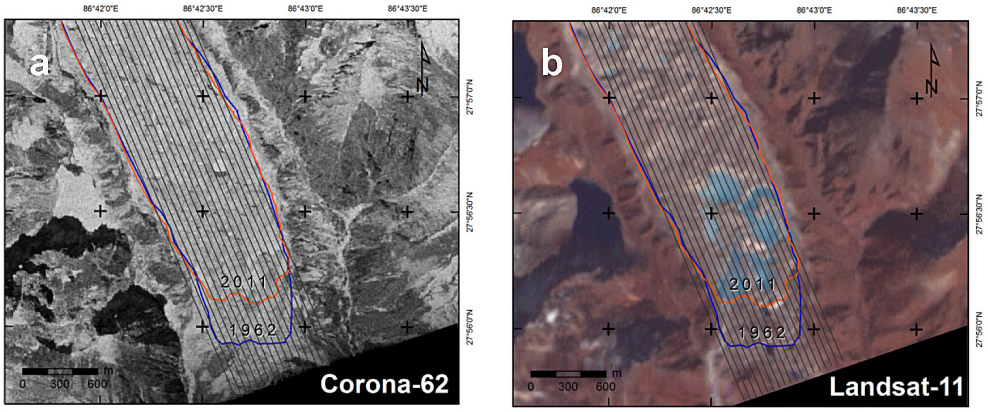

Figure 2. Glacier delineation in **(a)** panchromatic Corona-62; **(b)** SLC-off gap filled Landsat-11. The stripes in the images are meant for mean length change calculation.

panchromatic band (15 m) acquired by same satellite and on the same date.

3.3 Data registration

All of the imagery and maps were co-registered in the same coordinate system of WGS 1984 UTM Zone 45. The Landsat scenes were provided in standard terrain-corrected level (Level 1T) with the use of ground control points (GCPs) and necessary elevation data (https://earthexplorer.usgs.gov). The ALOS-08 image used here was orthorectified and corrected for atmospheric effects in Salerno et al. (2012). The Corona images were co-registered and rectified through the polynomial transformation and spline adjustment using more than 120 known GCPs obtained from the reference ALOS-08 image, including mountain peaks, river crossings, and identifiable rocks (Grosse et al., 2005; Lorenz, 2004). The polynomial transformation uses a least squares fitting algorithm and ensures the global accuracy of images (Rosenholm and Akerman, 1998), but does not guarantee local accuracy, whereas the spline adjustment improves for local accuracy, which is based on a piecewise polynomial that maintains continuity and smoothness between adjacent polynomials (Kresse and Danko, 2011). The overall root mean square error (RMSE) of GCPs in Corona registration was around 8 m. The ERDAS IMAGINE® software was used for processing the Corona image. The images were resampled to new pixel size (8 m) using the nearest neighbor method, most commonly applied resampling technique (Thompson et al., 2011; Brahmbhatt et al., 2012).

3.4 Interpretation and mapping of glacier features

The automated glacier mapping from satellite imagery is relatively accurate for clean ice, but it is hindered for the extensive debris-covered glaciers (Racoviteanu et al., 2008;

Paul et al., 2013). Though few automated approaches to map the debris-covered parts exist, the results are less accurate and need intensive manual post-correction (Paul et al., 2004; Bhambri et al., 2011; Rastner et al., 2013). In this study, the glacier outlines were manually delineated using an on-screen digitizing method based on visual interpretation and false-color composite (FCC) developed from multispectral bands and assisted by the GDEM (Fig. 2a and b). The well established the band ratio (TM4/TM5) technique (Paul et al., 2004) was used to obtain a clear vision of snow and ice portion that assisted in the manual digitization. In the ablation part of the glacier where debris mantles are present, the delineation of the outline was performed by identifying lateral and frontal moraine and using the thermal band for the Landsat TM and ETM images. Streams issuing from beneath glacier were used as additional indication of its boundary.

For the ΔTerm calculation, a band of stripes with a distance of 50 m between each stripe in the band was drawn parallel to the main flow direction of the glacier (Fig. 2), and the ΔTerm was calculated as the average length of the intersection of the stripes with the glacier outlines (cf. Koblet et al., 2010; Bhambri et al., 2012).

The snow lines were retrieved manually from each satellite image and map. The snow lines on glaciers were distinguished from the images as the boundary between the bright white snow and the darker ice by visual interpretation and using FCC (Karpilo, 2009). The kinematic "Hess method" (Hess, 1904) was used to identify the snow line in the KHmap-50s, which involves the delineation of the boundary between the accumulation and ablation zone in a glacier using the inflection of elevation contour lines on the topographic map (Leonard and Fountain, 2003). Then, the SLA, as a measure of equilibrium-line altitude (ELA; McFadden et al., 2011; Rabatel et al., 2012), was calculated as the average altitude of the identified snow line using the ASTER GDEM. The SLA derived from the "Hess method" for the map represents the long-term ELA and, thus, does not indicate the position of the snow line in a particular year. However, the snow line position obtained from satellite imagery represents the transient snow line of the year that varies along the year, but remains stable after the end of summer, corresponding to the end of the ablation season (Rabatel et al., 2005; Pelto, 2011). The map-based SLA was useful for understanding the representativeness of the snow line position derived from the Corona image, which has some limitations for accurately identifying the snow line because of its panchromatic nature.

The ASTER GDEM along with glacier outlines were used to derive morphological features (slope, aspect, elevation). The mean elevation, aspect, and slope of each glacier were computed as arithmetic mean of each pixel of the GDEM intersected by the glacier outline. Concerning the glacier identification and cataloging, we followed the classification of Salerno et al. (2008), which in turn is based on the inventory of the International Centre for Integrated Mountain Development (ICIMOD) (Mool et al., 2001). In agreement with this study, we named only those glaciers whose area exceeded a threshold of 1 km^2. In this way, we identified 29 glaciers, while the smaller glaciers ($< 1\,km^2$) were categorized into "other glaciers" group.

3.5 Uncertainty of measurement

The measurement accuracy of the position of a single point in the space using GIS (geographical information system) is limited by resolution of source data used (i.e., the scale factor for cartography and the pixel resolution for satellite image), defined as LRE (linear resolution error), and by the error of referencing (RE, registration error). This approach is usually adopted in studies of glacial front (ΔTerm) (Hall et al., 2003; Ye et al., 2006). Concerning the glacier surface and debris coverage, the uncertainty of measurement was calculated as a product of the LRE and the perimeter (l) (Salerno et al., 2012). Then, the uncertainty with ΔSurf and ΔDebrisCov was derived according to standard error propagation rule, root of sum of squares (RSS) of the mapping error for the single scene. The co-registration errors were approximated and adjusted during the measurement. For further details on methodology adopted here for uncertainty analysis, we refer to Tartari et al. (2008) and Salerno et al. (2012). The elevation error associated with ΔSLA was estimated as the RSS between of the pixel resolution combined with the mean surface slope (Pelto, 2011) and the vertical error associated to the GDEM (20 m). Concerning the uncertainty in the SLA estimation due to temporal variation of surface elevation, we consider them negligible as there was no significant elevation change around SLA (Bolch et al., 2011) compared to the GDEM vertical accuracy, and thus have no impact on the results (Rabatel et al., 2013).

In this study, the uncertainty of measurement ranges from 6 to 30 m for ΔTerm and from 21 to 35 m for ΔSLA. In both cases, as discussed below and shown in Fig. 3 and Table 2, the magnitude of the uncertainty is relatively low if compared with the observed changes, indicating good accuracy of the results. However, the errors associated with ΔSurf and ΔDebrisCov range from approximately 2 to 10 % for both of variables. In particular, Fig. 3 and Table 2 indicate that until early 1990s, this uncertainty, due to low sensor resolution, is high and needs to be carefully considered in the change evaluations.

3.6 The ELA-climate model

To evaluate the role of climatic drivers in the ΔSLA, we used the simple ELA-climate model by Kuhn (1981). This model has been widely used in the European Alps (Kerschner, 1997), New Zealand (Hoelzle et al., 2007) and the Himalaya (Kayastha and Harrison, 2008) to estimate the climate drivers changes required for explaining the observed SLA change. The model (Eq.1) requires temperature lapse

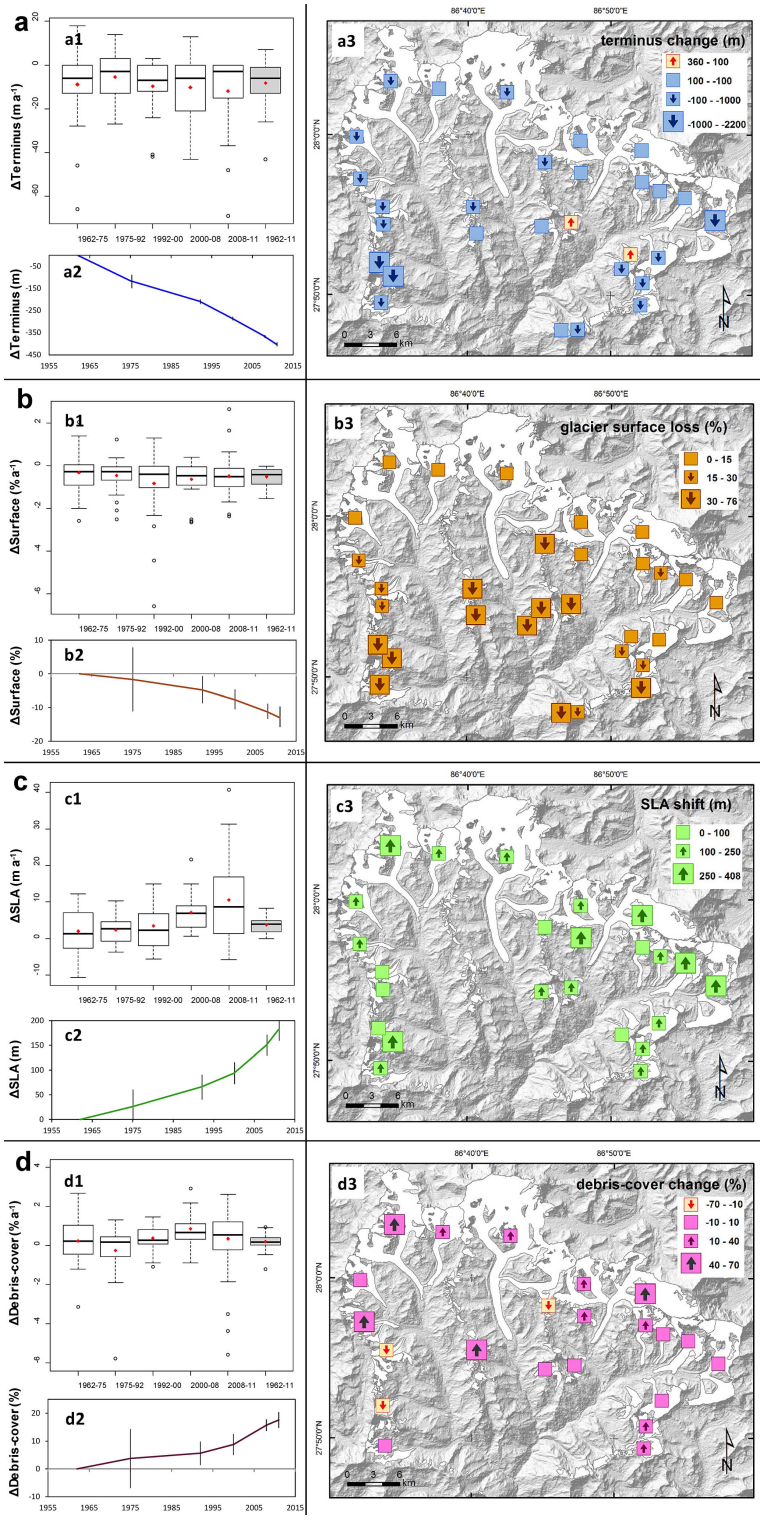

Figure 3. Spatio-temporal changes in Mt. Everest region; **(a)** terminus position change (ΔTerm), **(b)** surface area change (ΔSurf), **(c)** shift of snow-line altitude (ΔSLA), and **(d)** debris area coverage change (ΔDebrisCov). For each plot, upper left box plot represents the annual rates of change of the glaciers in the analyzed periods. The red point in the box indicates the mean. The lower left plot describes the cumulative changes with associated uncertainty. On the right side, the map represents the spatial variation of the glaciers. Data are in Table S1 of the Supplement. All percentages refer to the initial year of the analysis (1962).

Table 2. Glacier changes from 1962 to 2011 in the Mt. Everest region.

Period	Terminus position change (ΔTerm)		Surface area change (ΔSurf)			Snow-line altitude shift (ΔSLA)			Debris coverage change (ΔDebrisCov)		
	Cumulative length	Median annual rate	Cumulative area	Absolute rate	Median annual rate	Cumulative altitude	Mean annual rate	Median annual rate	Cumulative area	Absolute rate	Median annual rate
	(m)	($m\,a^{-1}$)	(%)	($km^2\,a^{-1}$)	(% a^{-1})	(m)	($m\,a^{-1}$)	($m\,a^{-1}$)	(%)	($km^2\,a^{-1}$)	(% a^{-1})
1962–1975	-116 ± 30	-6.0 ± 2.3	-1.7 ± 9.7	-0.51 ± 0.05	-0.27 ± 0.75	26 ± 35	2.0 ± 2.7	1.3 ± 2.7	3.8 ± 10.6	0.25 ± 0.01	0.22 ± 0.28
1975–1992	-208 ± 11	-2.6 ± 1.9	-4.8 ± 4.1	-0.75 ± 0.08	-0.29 ± 0.65	66 ± 25	2.4 ± 2.2	2.6 ± 2.2	5.7 ± 4.4	0.10 ± 0.01	0.19 ± 0.68
1992–2000	-285 ± 9	-7.0 ± 1.6	-7.7 ± 3.0	-1.48 ± 0.07	-0.39 ± 0.60	94 ± 22	3.5 ± 3.2	2.3 ± 3.2	8.8 ± 4.0	0.35 ± 0.02	0.28 ± 0.72
2000–2008	-367 ± 6	-5.8 ± 1.1	-11.3 ± 2.3	-1.83 ± 0.06	-0.46 ± 0.38	151 ± 21	7.1 ± 2.7	6.7 ± 2.7	15.8 ± 2.6	0.76 ± 0.03	0.68 ± 0.56
2008–2011	-403 ± 9	-3.0 ± 3.0	-13.0 ± 3.1	-2.30 ± 0.07	-0.52 ± 0.99	182 ± 22	10.6 ± 7.3	8.7 ± 7.3	17.6 ± 3.1	0.55 ± 0.02	0.55 ± 1.19
1962–2011	-403 ± 9	-6.1 ± 0.2	-13.0 ± 3.1	-1.08 ± 0.03	-0.42 ± 0.06	182 ± 22	3.7 ± 0.5	3.9 ± 0.5	17.6 ± 3.1	0.32 ± 0.01	0.20 ± 0.06

rate, mass balance and radiation gradients, latent heat of fusion and length of melting season.

The model is expressed as,

$$\frac{\partial b_w}{\partial z}\Delta h + \delta b_w = \frac{T}{L}\left[\frac{\partial R}{\partial z}\Delta h + \delta R + \gamma\left(\frac{\partial T_a}{\partial z}\Delta h + \delta T_a\right)\right], \quad (1)$$

where Δh = an observed change in ELA (m), T = length of melting season (d), L = latent heat of fusion (kJ kg^{-1}), γ = constant (MJ $m^{-2}\,d^{-1}\,K^{-1}$), $\partial b_w/\partial z$ = mass balance gradient (kg m^{-2} m^{-1}), $\partial T_a/\partial z$ = temperature lapse rate (K m^{-1}), $\partial R/\partial z$ = net radiation gradient (MJ $m^{-2}\,m^{-1}\,d^{-1}$), δT_a = bias in air temperature (K), δb_w = bias in mass balance (kg m^{-2}), and δR = bias in net radiation (MJ m^{-2} d^{-1}). We applied the model using the temperature lapse rate and the net radiation gradient calculated for this case study as described above, the mass balance gradient of 5 ± 1 mm w.e. $a^{-1}\,m^{-1}$ provided by Fujita et al. (2006), $T = 100$ d; $L = 334\,kJ\,kg^{-1}$, $\gamma = 1.7\,MJ\,m^{-2}\,d^{-1}\,K^{-1}$ as described in Kuhn (1981).

Concerning the limitations of this model, we need first of all to consider that the SLA as a proxy to ELA; we assume that there is little, or no ablation during winter season. Furthermore, this model just considers a single mass balance gradient value, while some authors, e.g., Wagnon et al. (2013) recently found an average mass balance gradient of 4.5 mm w.e. a^{-1} m^{-1} for Mera Glacier (in the Dudh Koshi Basin), similar to the gradient provided by Fujita et al. (2006), but point out its variability in relation to local topographic conditions.

3.7 Statistical analysis

The normality of the data is tested using the Shapiro–Wilk test. The null hypothesis for the Shapiro–Wilk test is that samples x1, x2....xn belong to a normally distributed population. If the p value $(p) > 0.05$, we consider the series to be normally distributed; otherwise, it is not normal (Shapiro and Wilk, 1965). We used the paired t test for comparing the means of two series. The null hypothesis is that the difference between paired observations is zero ($p < 0.05$) (Walford, 2011). If the series were not normal, we first used a log transformation to apply the paired t test for a normally distributed series. The parallelism between the regressions of SLAs time series is tested by the analysis of covariance (ANCOVA) (Dette and Neumeyer, 2001). All tests are implemented in the R software environment.

4 Results

Table 2 provides a general summary of the changes that occurred from 1962 to 2011. Our main findings, however, are visualized in Fig. 3, which has been subdivided into four sections (a–d), corresponding to four selected indicators of change (terminus, surface area, SLA, and debris coverage). The spatial differences are presented on the right side of each section, and the temporal changes are shown on the left side. On the left side, in the upper panel of each section, the box plots show the annual rates of change for the analyzed period, while the cumulative changes and their associated uncertainties are presented in the lower panels. All data presented and discussed in this paper are reported in Tables S1 and S2 of the Supplement.

4.1 Glacier terminus position change

Overall, the Mt. Everest glaciers experienced a ΔTerm of -403 ± 9 m ($\sigma = 533$ m) (Fig. 3a2 and Table 2) as the mean (-301 ± 9 m as median), corresponding to an annual mean rate of $-8.2 \pm 0.2\,m\,a^{-1}$ ($\sigma = 10.8\,m\,a^{-1}$) and a median value equal to $-6.1 \pm 0.2\,m\,a^{-1}$ from 1962 to 2011 (Fig. 3a1 and Table 2). We found that the distribution of the annual retreat rates in all observed periods (Shapiro–Wilk test) was always far from normal because a few glaciers experienced a retreat that was much higher than the retreat of others (see box plots in Fig. 3a1). Therefore, we consider the median values of ΔTerm to be more representative of the change.

Figure 3a2 depicts a generally continuous and constant retreat over the last 50 years. We thus tested these properties of the observed trend. First, we evaluated the continuity of the process, checking whether each period showed a retreat that was significantly different from zero. Second, we tested the possible acceleration of the retreat by comparing the annual rates of change between each period and previous. In both cases, we first provided a log transformation of the data to apply the paired t test for a normally distributed series. In the first case, we observed that the retreat of each period was always significantly different from zero

(the weakest significance was found in the 1962–1975 period). However, when evaluating the possible acceleration, we found no significant differences among the annual rates of change ($p > 0.1$). The result of this test can be further observed in Fig. 3a1, considering the distribution of the median annual rates. In fact, the retreat rate has decreased since 1992, although not significantly.

In Fig. 3a3, we can observe the spatial distribution for the overall period of analysis of 1962–2011. We observed that two glaciers (Duwo and Cholo) experienced an overall advance. These glaciers advanced until 1992, and then they began retreating, similarly to the other glaciers. Furthermore, we can observe that most of the western glaciers have retreated more than the eastern ones, except for the Imja Glacier.

As mentioned above, for the first years of the analysis, we used the Corona-62 with two topographic maps (KHmap-50s and TISmap-63). Comparing these data sources with the Landsat-75, we observed that the KHmap-50s ($6.1 \pm 1.9\,\mathrm{m\,a^{-1}}$) shows a closer mean retreat to the Corona-62 ($8.2 \pm 0.2\,\mathrm{m\,a^{-1}}$) than to the TISmap-63 ($13.3 \pm 2.6\,\mathrm{m\,a^{-1}}$), which seems to overestimate the ΔTerm, probably due to inaccurate representation of the glacier boundary in TISmap-63 as found for other topographic maps in the Himalaya (Bhambri and Bolch, 2009).

4.2 Glacier surface area change

The Mt. Everest glaciers experienced a ΔSurf of $-52.8 \pm 11.0\,\mathrm{km^2}$ (from 404.6 to 351.8 $\mathrm{km^2}$), corresponding to an overall change of $-13.0 \pm 3.1\,\%$ ($-0.27 \pm 0.06\,\%\,\mathrm{a^{-1}}$), from 1962 to 2011 (Fig. 3b2 and Table 2). The mean annual shrinkage rate calculated for each glacier in the period from 1962–2011 was $0.51 \pm 0.06\,\%\,\mathrm{a^{-1}}$ ($\sigma = 0.38$), and the median rate was $0.42 \pm 0.06\,\%\,\mathrm{a^{-1}}$ (Fig. 3b1). By testing the annual loss rate (Shapiro–Wilk test) of each glacier in each observed period, we observed (similarly to the terminus retreat) that it was never normally distributed (see box plots in Fig. 3b1). Therefore, in this case as well, we consider it to be more representative of change in the median values.

We can observe a continuous surface area loss since the 1960s that appears to have accelerated in recent years (Fig. 3b2). In fact, the rate of median annual area loss was $0.27 \pm 0.75\,\%\,\mathrm{a^{-1}}$ in 1962–1975 and has increased to the rate of loss of $0.48 \pm 0.55\,\%\,\mathrm{a^{-1}}$, in 2000–2011 period (Fig. 3b1). We thus tested these trend properties using same procedure that we had adopted for evaluating the ΔTerm. In this case, we again first provided a log transformation of the series. We observed that the surface area loss of each period was always significantly different from zero. The weakest significance was found in the 1962–1975 period. In fact, Fig. 3b2 and Table 2 show lower observed surface change (1.7 %) for this period, which, although significant, is associated with the highest uncertainty (9.7 %). However, in evaluating the possible acceleration of the surface area losses, we found slight but statistically insignificant acceleration of the surface area between the rates of area loss in the 1962–1992 period (median $0.35 \pm 0.13\,\%\,\mathrm{a^{-1}}$, $0.015\,\mathrm{km^2\,a^{-1}}$) and the 1992–2011 period (median $0.43 \pm 0.25\,\%\,\mathrm{a^{-1}}$, $0.039\,\mathrm{km^2\,a^{-1}}$) indicating that for the 1992–2011 period, each glacier is retreating on average at nearly the double rate than the previous period.

The area loss observed in the first period (1962–1975) using Corona-62 and Landsat-75 was robust using different data sources, as described in the methods section and shown in Table 1. Comparing the KHmap-50s with the Landsat-75, we obtain a glacier area loss of $0.22 \pm 0.64\,\%\,\mathrm{a^{-1}}$, which is very close to the value obtained using Corona-62 ($0.27\,\%\,\mathrm{a^{-1}}$). Moreover, for some glaciers, we were able to substitute high resolution Corona-70 with Landsat-75 to provide information about the accuracy of the Landsat data. The comparison of Corona-62 and Corona-70 provided a mean rate of $0.26\,\%\,\mathrm{a^{-1}}$, confirming that between late 1950s and early 1970s, the glacier surface losses were very small.

Figure 3b3 represents a distinct spatial pattern of glacier ΔSurf. All of the glaciers experienced surface area losses between 1962 and 2011. However, the southern glaciers lost higher surface area than the northern glaciers.

4.3 Snow Line Altitude change

Overall, from 1962 to 2011, the SLA of Mt. Everest glaciers shifted upward by 182 ± 22 m ($\sigma = 114$) from 5289 m to 5471 m a.s.l.; this increase corresponds to a mean annual rate of $3.7 \pm 0.5\,\mathrm{m\,a^{-1}}$ ($\sigma = 2.3$) (Fig. 3c1, 3c2, and Table 2). The distribution of the annual rate of the SLA shift in all of the observed periods is in this case normal (Shapiro–Wilk test; see box plots in Fig. 3c1). Therefore, the mean values are suitable for describing the ΔSLA.

In Fig. 3c2, the overall trend in ΔSLA shows a continuous upward shift in the last 50 years. In fact, in Fig. 3c1, we can observe that the mean annual upward rate of the SLA was $2.0 \pm 2.7\,\mathrm{m\,a^{-1}}$ in 1962–1975 and achieved the highest shift rate of $10.6 \pm 7.3\,\mathrm{m\,a^{-1}}$ in the 2008–2011 period. In this case, we tested the possible continuity and acceleration of trend following the same procedure applied above. We observed a statistically significant upward shift of the SLA ($p = 0.02$), except during the first period of 1962–1975. Moreover, we found significant differences ($p < 0.001$) in the annual upward shift of the SLA between periods 1962–1992 (mean $= 2.2 \pm 0.8\,\mathrm{m\,a^{-1}}$) and 1992–2011 (mean $= 6.1 \pm 1.4\,\mathrm{m\,a^{-1}}$).

Figure 3c3 represents the spatial distribution of the SLA for the overall 1962–2011 period. In this case, the spatial pattern is not distinct. The glaciers with the minimum and maximum SLA in 2011 are Cholo (5152 m) and Imja (5742 m), respectively.

Furthermore, as mentioned above, we calculated the SLA using the KHmap-50s with the "Hess method," which provides an average position of the average snow line for the 1950s. We observed the SLA at 5272 m a.s.l., which is not

very different from the SLA at 5289 m a.s.l., as derived from Corona-62.

4.4 Glacier debris-covered area change

Overall, the debris-covered area has increased by $17.6 \pm 3.1\,\%$ ($0.36 \pm 0.06\,\%\,a^{-1}$) (Fig. 3d2 and Table 2) from 1962 to 2011. The mean annual increase rate calculated for each glacier in the 1962–2011 period is $0.28 \pm 0.06\,\%\,a^{-1}$ ($\sigma = 0.34$), and the median rate is $0.20 \pm 0.06\,\%\,a^{-1}$ (Fig. 3d1). The debris-covered area was approximately 24.5 % of the total glacier area in 1962 and 32.0 % in 2011. In the same area, Nuimura et al (2012) reported 34.8 % of debris-covered area in 2003–2004. In correspondence of the increase of debris coverage we observed the consequent decreasing of debris free area (Fig. S2 in the Supplement). Testing the annual rate of ΔDebrisCov with the Shapiro–Wilk test, we observed that the increase of the debris-covered area is not normally distributed among all glaciers (Fig. 3d1). Therefore, we also consider the median values to be more representative of change in the case of ΔDebrisCov.

In Fig. 3d2, we present the overall ΔDebrisCov trend, which indicates a general continuous increase of debris cover area over the last 50 years. The debris cover increase began to be statistically significant for each glacier only after 2000 ($p < 0.01$) years. Evaluating the possible acceleration, we found no significant differences among the annual rates of changes ($p > 0.1$). The result of this test can be observed in Fig. 3d1, which considers the distribution of median annual rates. Since 2000, the rates of debris-covered area change appear to be decreasing, although not significantly. Furthermore, we observed a significant relationship between ΔDebrisCov and ΔSLA during the 1962–2011 period ($r = 0.79$, $p < 0.01$). In this regards, Bolch et al. (2008) observed that debris cover increases during periods of high ablation as more englacially stored debris is exposed. In Fig. 3d3, we can observe the spatial distribution of the debris-covered area (%) in the overall period of analysis of 1962–2011. We observe that the glaciers experienced an overall increase in the debris-covered area, except the glaciers Imja, Kdu_gr125, Langdak, and Langmuche for which local effects could have played important role.

5 Discussion

5.1 Comparison among terminus position change, surface area loss and the relevant mass budget observations

Mass budget measurements are the main index used for climate change impact studies on glaciers, as by Fujita et al. (2006), Bolch et al. (2011), Nuimura et al. (2012), and Gardelle et al. (2013) as this index can be directly linked to climate while length and area change show a delayed signal

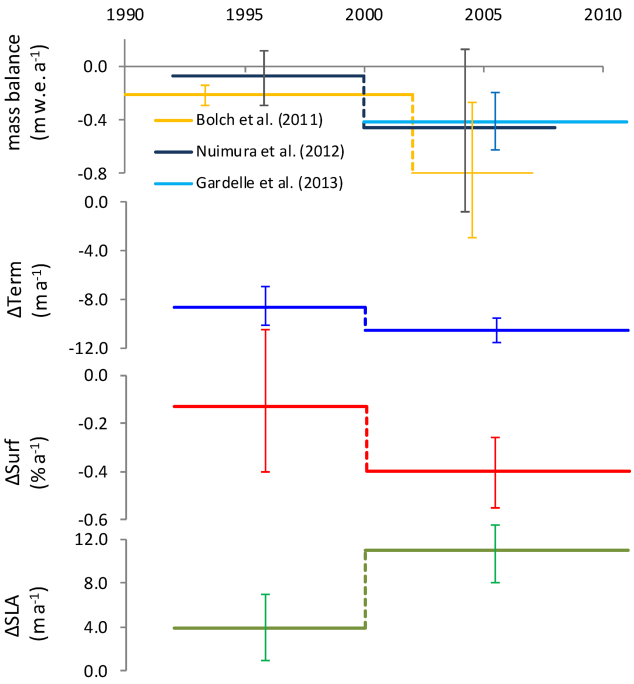

Figure 4. Comparison for 10 selected glaciers using the terminus position change (ΔTerm), glacier surface area loss (ΔSurf), and shift of snow-line altitude (ΔSLA) calculated in this study and relevant mass downwasting observations of Bolch et al. (2011), Nuimura et al. (2012). Furthermore, the mass balance data of Gardelle et al. (2013) are reported.

(Oerlemans, 2001). However, conducting mass-balance measurements is not a trivial task, due to the technical requirements and practical constraints (Bolch et al., 2012); these measurements are thus not often used in extensive studies. Most of the authors, in fact, analyze glacier terminus position and surface (Bolch et al., 2012; Yao et al., 2012; Kulkarni et al., 2011; Scherler et al., 2011). However, we need to consider the limitations of these variables especially for debris-covered glaciers, which experience more downwasting than area loss (Bolch et al., 2008; Tennant et al., 2012). In this regard, we decided to compare our findings in terms of ΔTerm, ΔSurf, and ΔSLA with the corresponding mass budget information provided by other authors to evaluate whether these factors are suitable indices in this context. We present here in Table 3 and Fig. 4 the mass balance data derived from geodetic methods for 10 glaciers located in our study area according to Bolch et al. (2011), Nuimura et al. (2012), and Gardelle et al. (2013). Bolch et al. (2011) and Nuimura et al. (2012) find a higher mass loss rate during the last decade. Furthermore, these estimations are reinforced by the rate provided in Gardelle et al. (2013) for the period (2000-2011).

Figure 4 shows that, for the same glaciers, we observed a ΔTerm that was only slightly higher in the second period (2000–2011) than in the previous one (1992–2000), while the ΔSurf and the ΔSLA were both approximately 4 times

Table 3. Rates of mass balance, ΔTerm, ΔSurf, and ΔSLA for 10 common glaciers.

Variable	Period	Change rate	Source
Mass balance (m w.e. a^{-1})	1970–2002	-0.21 ± 0.10	Bolch et al. (2011)
	2002–2007	-0.79 ± 0.52	
	1992–2000	-0.07 ± 0.20	Nuimura et al. (2012)
	2000–2008	-0.45 ± 0.60	
	2000-2011	-0.41 ± 0.21	Gardelle et al. (2013)
ΔTerm (m a^{-1})	1992-2000	-8.6 ± 1.6	This study
	2000–2011	-10.6 ± 1.0	
ΔSurf (% a^{-1})	1992–2000	-0.13 ± 0.30	
	2000–2011	-0.40 ± 0.15	
ΔSLA (m a^{-1})	1992–2000	3.9 ± 3.2	
	2000–2011	10.9 ± 2.8	

higher in the last decade, as observed using mass budget data. Such behavior is expected given the lag in response time because downwasting leads to more volume loss then retreat (Oerlemans, 2001; Hambrey and Alean, 2004). This comparison shows that, for this region, the glacier surface area loss and the shift of snow-line altitude (i.e., the shift of late summer snow line) can be considered suitable indicators for a broad description of glacial response to the recent climate change.

5.2 Comparison with other parts of the Himalaya and high-mountain Asia

Bolch et al. (2012) recently noted that length and surface area changes suggest that most Himalayan glaciers have been retreating since the mid-19th century. Yao et al. (2012) reported the glacier status over the past 30 years in the Himalaya and the Tibetan Plateau. They observed that the shrinkage generally decreases from the Himalaya to the continental interior, and it is most pronounced in the southeastern Himalayan region.

In Nepal, Yao et al. (2012) considered only three benchmark glaciers for evaluating the Term retreat during the 1974–1999 period and the same set of glaciers analyzed here (Koshi Basin) for evaluating the surface area loss, but for a shorter period (1976–2000) than in the present study. They reported a ΔTerm of 6.9 m a^{-1} based on the three glaciers located outside our study area. During a similar period (1975–2000), we calculated a median retreat of 4.4 ± 0.8 m a^{-1} for all 29 glaciers and a median retreat of 6.1 ± 0.2 m a^{-1} for the 1962–2011 period. Further, in comparing the same set of glaciers and during the same period we found a termini retreat rate (9 m a^{-1}) lower than the rate (19 m a^{-1}) provided by Bajracharya and Mool (2009), probably due to the higher resolution of data source used in this study (furthermore in Fig. S1 of the Supplement). Concerning the Surf area loss, Yao et al. (2012) reported a decrease of 0.15 % a^{-1}, while during a similar period (1975–2000), we calculate an area loss of 0.25 ± 0.40 % a^{-1}. We can observe that although the retreat rates are comparable between the studies, with regards to ΔSurf, we observed a greater area loss; this difference could be because both satellites used in 1975 and 1976 (Landsat MSS) had a broad resolution (60 m) leading to a large uncertainty in the estimates and, hence the studies take the uncertainty into account. Moreover, we sustain that the recent area loss estimation (0.63 % a^{-1}) provided by Shangguan et al. (2014) for the same set of glaciers analyzed here during the 1976–2009 period is overestimated probably for the misleading glacier boundary interpretation especially in the upper glacier area in 1976 due to the low resolution Landsat MSS image and adverse snow conditions, while our interpretation is reinforced by the higher resolution of Corona-70 image. Moreover, we point out that the present study corresponds to zone III of the analysis in Yao et al. (2012), defined by the authors as the central Himalaya and including both the north (Tibet) and south (Nepal) slopes of the Himalayan range, represented by the Mt. Qomolangma National Nature Preserve and the Koshi Basin, respectively. The average termini retreat and area loss rates for zone III have been established by the authors at 6.3 m a^{-1} and 0.41 % a^{-1}, respectively. However, the glacier behavior is not homogenous in the central Himalaya, so this mean loses significance, particularly considering the different area loss observed for the northern and southern parts. In fact, according to Nie et al. (2010) and as reported by Yao et al. (2012), the area loss rate is 0.50 % a^{-1} (1976–2006) in the north; during the same period in the south, the area loss rate is about half that, according to the present study, and one third of that, according to Yao et al. (2012). Likewise, an area loss of 0.3 % a^{-1} for the 1974-2008 period was provided by Ye et al. (2009) on the northern side, and 0.15 % a^{-1} for the period ranging from the 1950s to 1992 (similar to our observation 0.16 % a^{-1}

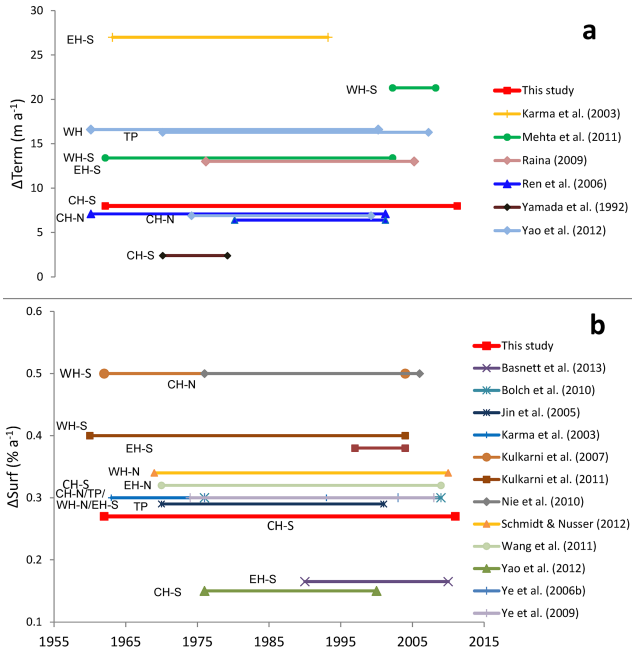

Figure 5. Recent studies on the variations of Himalayan glaciers concerning both the terminus retreat **(a)** and the surface area loss **(b)**. Data and references of this figure are presented Table S4 of the Supplement.

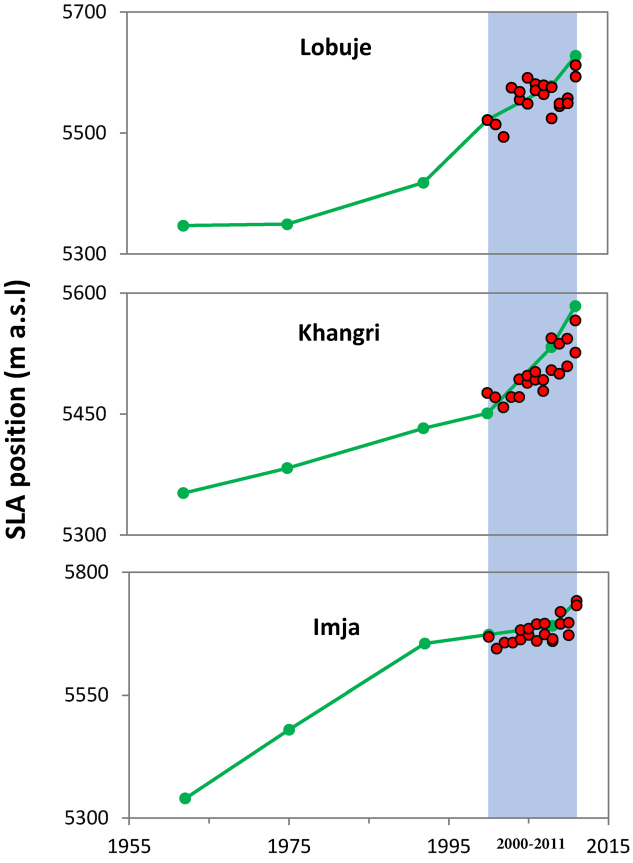

Figure 6. Validation of the SLA trend of 1962-2011 period (green line) for three selected glaciers (Lobuje, Khangri, and Imja) using the satellite imagery reported in Table 1 with additional 20 Landsat ETM+ imagery (red points) of 2000–2011 period (shaded region).

during 1962–1992) (Salerno et al., 2008) and 0.12 % a^{-1} for selected glaciers for the 1962–2005 period (Bolch et al., 2008a), both located in the southern side. Therefore, to explore possible differences in the surroundings of the south slopes of Mt. Everest, we decided to separately consider the northern and southern parts of the central, western and eastern Himalaya (CH, WH, and EH, respectively, with the suffixes -N and -S). Following this scheme, the present case study and all of Nepal are located in CH-S. Evidence from the Tibetan Plateau (TP) is presented separately (Fig. 1a).

Figure 5 reports the most recent studies on the changes of Himalayan glaciers concerning both the terminus retreat (Fig. 5a) and the area loss (Fig. 5b). In general, we can observe that the CH-S, in terms of both ΔTerm and ΔSurf,registered among the lowest changes of the entire Himalaya and the TP. The northern and the southern central Himalaya (CH-N and CH-S) share the lower termini retreat, while the record is held by the CH-S glaciers regarding the lowest area loss, if we consider that the recent study of Basnett et al. (2013) on Sikkim Himalaya, although this area is geographically part of EH-S, is adjacent to the eastern CH-S border. The lower ΔTerm and ΔSurf observed in CH-S region, compared with the other parts of the Himalaya and the TP, can be ascribed both to the abundance of debris cover (Scherler et al., 2011; Bolch et al., 2012) and to the altitude of these glaciers. Scherler et al. (2011) defined the southern central Himalaya as the region with the glaciers that contain the highest debris coverage (∼ 36 %) and considered the abundance of debris coverage to be a significant factor in reducing the melt rate of these glaciers, preserving their surfaces from further recession. In this regards, we observed a strong direct relationship between ΔDebrisCov and ΔTerm (divided by the length of the ablation area) ($r = 0.87$, $p < 0.01$ for 1962–2011 period) which means that the glaciers who have increased the debris coverage have experienced a reduced termini retreat. We remember here that, Bolch et al. (2008a, 2011) noted the highest rate of mass downwasting is located in the transition zone between the active and the stagnant glacier parts of the debris covered glaciers.

However, of no less importance is the altitude of these glaciers. In fact, as reported by Bolch et al. (2012), with a mean elevation of 5600 m a.s.l., the highest glaciers of the Himalayan range are located in CH. In this regards, Wagnon et al. (2013), in the same zone analyzed here (Dudh Koshi Basin) show that a low elevation glacier (Phokalde, 5430 to 5690 m a.s.l.) presents a more negative mass balance (0.72 ± 0.28 m w.e. a^{-1}) than a higher elevation one (Mera, 4940 to 6420 m a.s.l.) which experienced a mass balance rate of -0.23 ± 0.28 m w.e. a^{-1} between 2009 and 2012. On the

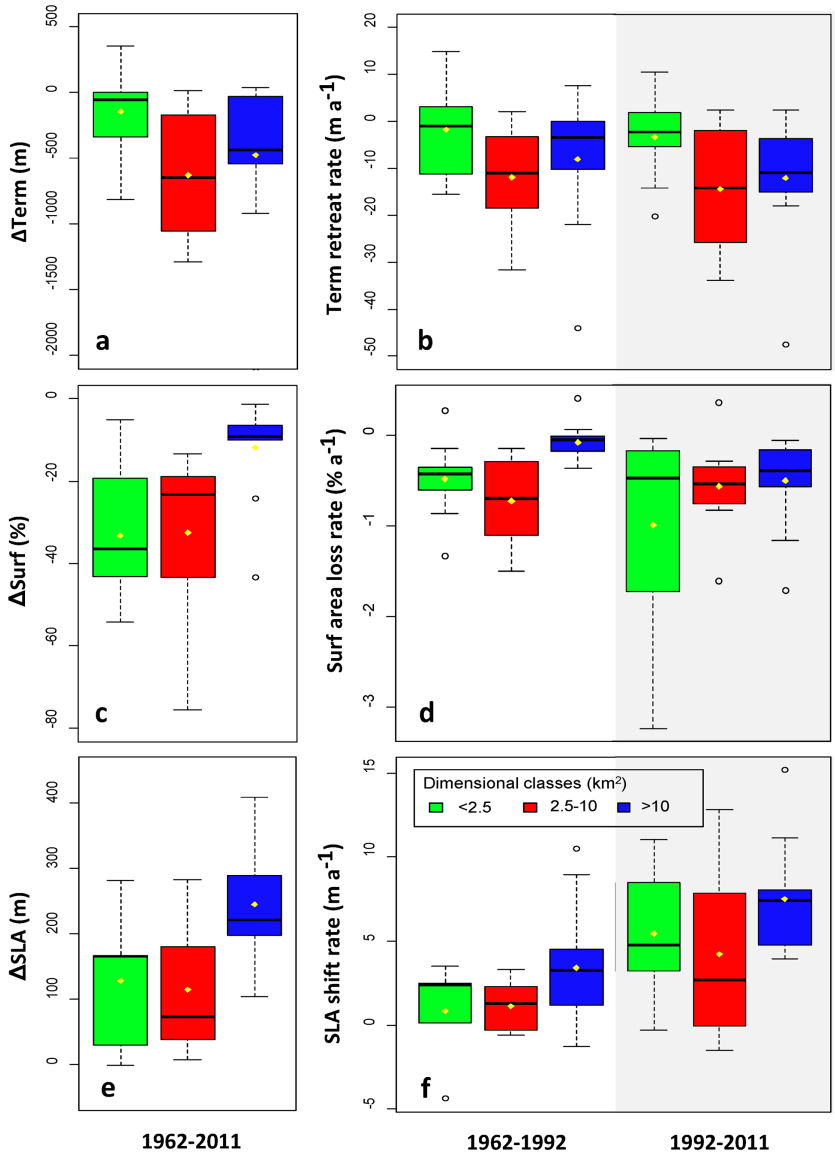

Figure 7. Differences among three-dimensional classes of glaciers ($< 2.5\,km^2$; 2.5–10 km^2; $> 10\,km^2$) in terms of cumulative changes in the overall 1962–2011 period: **(a)** terminus retreat (m); **(c)** surface area loss (%); **(e)** shift of SLA (m). Differences in terms of annual rate of change between 1962–1992 and 1992–2011 periods; **(b)** annual terminus retreat rate ($m\,a^{-1}$); **(d)** annual surface area loss rate ($\%\,a^{-1}$); **(f)** shift rate of SLA ($m\,a^{-1}$). All percentages refer to the initial year of the analysis (1962).

south slope of Mt. Everest, the area-weighted mean elevation of the glaciers is 5720 m a.s.l in 2011. Therefore, it is highly likely that the summit of the world has preserved these glaciers from excessive melting better than in the other parts of the Himalaya and the TP.

5.3 Snow-line altitude change and climate relation

The snow-line is characterized by seasonal fluctuations (Mernild et al., 2013; Pelto et al., 2013). To avoid the possible risk of introducing this variability into the inter-annual analysis, we enforced our 1962–2011 trend exploiting the availability of 20 Landsat ETM+ imagery for 2000–2011 period. Three glaciers were selected according to their size: Lobuje, Khangri and Imja (Table S3 in the Supplement). Figure 6 shows, for all three cases, that the trend estimated just using three time steps (year 2000, 2008, and 2011) (green line) represents correctly the upward shift of SLA described using all available imagery. We statistically ensure this statement testing the parallelism of SLAs time series. In all three cases, the test shows all three comparisons are significantly parallel ($F = 1.0$, $p > 0.3$; $F = 1.7$, $p > 0.2$; $F = 0.0$, $p > 0.9$ for Lobuje, Khangri, and Imja, respectively).

Bolch et al. (2012), considering the mean elevation as a rough proxy for the ELA, reported an ELA of about 5600 m a.s.l. in CH. For the south slope of the Mt. Everest region, Owen and Benn (2005) indicated an elevation of 5200 m a.s.l. for the 1980s, while Asahi (2010) noted an altitude of 5400 m a.s.l. in the early 1990s. In this study, comparing the same years, we observed a SLA position of 5315 m a.s.l. in 1975 and 5355 m a.s.l. in 1992, corresponding to a lower shift. Kayastha and Harrison (2008) observed an upward of ELA by $0.9 \pm 1.1\,\mathrm{m\,a^{-1}}$ (29 ± 35 m) during the 1959–1992 period using the toe-to-headwall altitude ratio (THAR) method with TISmap-63 and the aerial photos of 1992, from which the OTNmap-92 was delineated. In a comparable period (1962–1992), we calculated an upward shift of SLA by $2.2 \pm 0.8\,\mathrm{m\,a^{-1}}$ (66 ± 24 m) based on satellite data. The difference between the calculation of Kayastha and Harisson (2008) and our calculation is mainly due to different methodologies applied and the data set used. Surely, if a suitable scene is available, the SLA derived directly from the satellite imagery is more representative of a specific year than the map-based estimation.

The SLA trend qualitatively indicates the mass-balance variation of glaciers (Chinn et al., 2005). Variations in SLA derived from satellite imagery can be used as a proxy for providing indications of local climate variability (Fujita and Nuimura, 2011; McFadden et al., 2011, Rabatel et al., 2012). In this case study, the SLA is significantly moving upwards, with an accelerated rate after 1992, indicating that the glaciers in this region are experiencing an increasingly negative mass balance as it is suggested with the mass downwasting observations of Bolch et al. (2011) and Nuimura et al. (2012) (Fig. 4). The observed upward shift of the snow line could be interpreted as a direct response to high-temperature events, reduced precipitation, or increased solar radiation (Hooke, 2005). To evaluate the role of climatic drivers in the ΔSLA, we used the simple ELA-climate model by Kuhn (1981). Using this model, we estimated that for the observed 182 m upward shift of SLA in the 1962–2011 period, a temperature increase of 1.1 °C, or a precipitation decrease of 543 mm, or a solar imbalance increase of $1.8\,\mathrm{MJ\,m^{-2}\,d^{-1}}$ is required. By reacting to this climate perturbation, the SLA shifted by 182 m upward.

Concerning the temperatures, on the south slope of Mt. Everest, Diodato et al. (2012) established the longest temperature series (1901–2009) for this high elevation area, taking advantage of both land data obtained from the "Pyramid" meteorological observatory (5050 m) for the 1994–2005 period and gridded temperature data for extending the time series. They observed an increasing trend of $0.01\,^{\circ}\mathrm{C\,a^{-1}}$ in the last century (+0.9 °C), which can be attributed mainly to the 1980–2008 period ($0.03\,^{\circ}\mathrm{C\,a^{-1}}$, +0.8 °C). Likewise, Lami et al. (2010), using only the land data from the "Pyramid" stations (5050 m) for the 1992–2008 period, reported an increasing trend of $0.04\,^{\circ}\mathrm{C\,a^{-1}}$ (+0.7 °C). However, we need to consider that the recent global warming trend is more dominant in the winter season (Jones and Moberg, 2003). Cook et al. (2003) re-examined a longer Kathmandu mean temperature record and compared it with a gridded data set based on records from neighboring northern India; both showed a cooling trend in the monsoon season (June to September) for the 1901–1995 period. Summer cooling trends during the last few decades of the twentieth century have also been documented for the Tibetan Plateau (Liu and Chen, 2000). According to Diodato et al. (2012), the temperature in this zone increased by more than +0.8/+0.9 °C during our study period (1962–2011), corresponding to 70–80 % of the temperature increase required to justify the upward shift of SLA (+1.1 °C), even if, this rise has probably not occurred in the summer period when the ablation process is concentrated and thus, less impacting on glaciers shrinkage.

For the precipitation, Sharma et al. (2000) showed an increased tendency from 1948–1993 in the Dudh Koshi Basin. Additionally, Salerno et al. (2008) noted an increasing trend for higher elevations until the early 1990s. From these years of analysis, many researchers have highlighted a mainly decreasing trend in the Himalayan range (Wu, 2005; Thompson et al., 2006; Naidu et al., 2009). According to Yao et al. (2012), using the Global Precipitation Climatology Project (GPCP) data, the Asian monsoon lost 173 mm in this region for the 1979–2010 period, with a real decreasing trend starting from the early 1990s (mean value between grid 9 and 11 in Fig. S18 of their paper). We have already noted that we would have recorded a decrease of 543 mm if the only factor responsible for the higher SLA were the precipitation. Current knowledge shows that precipitation can be held responsible for approximately 30 % of the negative balance of glaciers in the study region (e.g., Yao et al., 2012; Palazzi et al., 2013).

Establishing the influence of solar radiation on the negative mass balance of these glaciers is much more difficult considering the complete global lack of long-term measurements of this variable at high elevations. For the Northern Hemisphere, Wild et al. (2005) reported a general decrease of sunlight over land surfaces, using the popular expression "global dimming," on the order of 2 to $5\,\mathrm{W\,m^{-2}}$ $\mathrm{decade^{-1}}$ (1960–1990 period), corresponding to a decline of 4 to 9 %. A partial recovery ("global brightening") has been registered more recently (1986–2000) at many locations ($2.2\,\mathrm{W\,m^{-2}\,decade^{-1}}$, corresponding to a rise of 2 %). According to Wild (2009), changes in solar radiation can be due to (1) changes in cloud cover and optical properties, (2) changes in water vapor, and (3) changes in the mass and optical properties of aerosols. However, sensitivity studies indicate that considerable changes in water vapor would be necessary to explain the observed solar radiation trends, while changes in cloud and aerosol characteristics are the dominant factors (Wild, 1997). Since early 1990s, reduced emissions have been registered in Asia, with a resulting decline of aerosol concentrations (Streets et al., 2009). This trend reversal in aerosol levels fits the general picture of a widespread

transition from dimming to brightening (Ramanathan et al., 2005). Furthermore, the weakness of the monsoon could correspond to minor cloud coverage; both factors are favorable for hypotheses of an increase in solar radiation in this region. Furthermore, the aerosol–cloud interactions cause an amplification of dimming and brightening trends in pristine environments (Kaufman et al., 2005; Wild, 2009). The average solar radiation at the 5050 m elevation is 12.4 MJ m^{-2} d^{-1} (143.5 W m^{-2}) (Tartari et al., 2002). The increase of nearly 15 % (1.8 MJ m^{-2} d^{-1} or 19.7 W m^{-2}) of solar radiation, according to the ELA-climate model, is large if compared with the 2 % of global rise reported for recent years, but it cannot be excluded, according to Kaufman et al. (2005) and Wild (2009), that the aerosol-cloud interactions cause an amplification of dimming and brightening trends in pristine environments.

5.4 Acceleration of the recession process

We observed clear signs of glacier changes since the 1960s on the south slope of the Mt. Everest region. All of the variables analyzed showed a continuing deglaciation trend. The phenomenon appears to be accelerated in recent decades, particularly with regards to the loss of surface area and the upward shift of the SLA. Based on this evidence, we decided to deepen the analysis to shed light on what may be the boundary conditions favoring the process and the possible drivers of change. Many authors (Salerno et al., 2008; Yao et al., 2012) have already shown that the glacier area loss rate is related to size of the glacier. Therefore, we divided the glaciers into three-dimensional classes ($< 2.5\,km^2$; 2.5–10 km^2; $> 10\,km^2$) that were defined to contain a similar number of glaciers in each class. For each variable, we analyzed the differences in cumulative changes in the overall period (1962–2011) (Fig. 7a, c, e) and the differences in the annual rate of change between two periods (1962–1992 and 1992–2011) (Fig. 7b, d, f).

In Fig. 7a, we observe that the cumulative terminus retreat, in the overall 1962–2011 period, is 55 m (median) for glaciers $< 2.5\,km^2$ and 433 m (median) for glaciers $> 10\,km^2$. If we compare these values with the length of the ablation area of the glacier we would get a percentage of terminus retreat double for the largest glaciers (2.3 %, 4.3 %, respectively for the 1962–2011 period). In order to understand this divergent glacier behavior we need to deepen the possible linkage between ΔTerm and the other variables of change. As discussed earlier, the terminus retreat of each glacier is strongly related to the increase of debris coverage ($r = 0.87$, $p < 0.001$ for ΔDebrisCov vs ΔTerm/length of the ablation zone). Although we did not find any significant correlation with the glacier elevation, the termini retreat is related to the ΔSLA ($r = 0.67$, $p < 0.01$ for ΔSLA vs ΔTerm/length of the ablation zone), that means more negative glacier mass balances induce an increasing of debris coverage ($r = 0.79$, $p < 0.01$ for ΔSLA vs ΔDebrisCov) (e.g., Chiarle et al., 2007; Rickenmann and Zimmermann, 1993) and a lower glacier retreat. As discussed below, we observed higher ΔSLA for larger glaciers ($r = 0.60$, $p < 0.01$) and thus, we can consider clarified the reason because larger glaciers experienced double terminus retreats.

We have already discussed that these glaciers, regardless of size, did not show a significant increase in the annual retreat rate. In Fig. 7b, we note that the annual retreat rate is increasing for all classes and especially for the glaciers of greater size, but these differences are not significant even considering the glaciers' size ($p = 0.41$, $p = 0.52$, $p = 0.13$, from small to large, respectively), which means that each class contains a significant number of glaciers that are not currently accelerating the process.

Regarding the glacier surface area losses, we showed a general decrease of 13.0 ± 3.1 % between 1962 and 2011. In Fig. 7c, we can observe that the percentage of area loss is 9.0 ± 3.3 % for the glaciers $> 10\,km^2$, but that this percentage rises to 36.0 ± 4.8 % for the glaciers $< 2.5\,km^2$. For the glaciers $< 1\,km^2$, this percentage rises to 42.0 ± 5.8 %. Comparing the annual rate of area loss, we note an interesting change (Fig. 7d): the rate is increasing in the 1992–2011 period from the previous period for all classes, but it is especially increasing for glaciers of larger size. By testing the significance of these differences, only the rate of glaciers $> 10\,km^2$ were significant between two periods. The p values were 0.13, 0.80, and 0.03, from small to large, respectively, compared to the overall significant area loss, as highlighted above.

A similar picture emerges if we consider the changes in the SLA (Fig. 7f). Significant differences were found between two periods only for glaciers $> 10\,km^2$ ($p = 0.15$, $p = 0.25$, and $p = 0.03$, from small to large, respectively) compared to a significant overall shift in SLA, as highlighted above. It is also interesting to note (Fig. 7e) that these glaciers presented median upward shifts equal to more than 220 m, while smaller glaciers showed increases of 119 m (approximately half).

Based on all these evidences, we can say that from the 1960s to today, the glaciers that have undergone the most climate impact are small ones, but it is also true that over the last 2 decades, the condition of larger glaciers has worsened much more. To find the reasons for this differential acceleration, first of all, we have to consider that the glaciers size is significantly correlated with the mean and the minimum (i.e., SLA) elevation of the accumulation zone ($r = 0.61$, $p < 0.01$; $r = 0.54$, $p < 0.01$), while it is not significantly correlated with the mean as well as the minimum elevation of ablation zone. Therefore, larger glaciers present accumulation zones at higher elevations. Moreover, we found the largest glaciers are mainly south oriented ($r = 0.62$, $p < 0.05$). In this regards, Salerno et al. (2008) observed that in the period ranging from the 1950s to 1992, larger glaciers decreased less in size and that some of them were on the rise. This divergent behavior was explained by considering the

increase of precipitation registered in those years that favored the south-oriented glaciers (along the preferential monsoon axis) and those that were located at higher elevations, thus less subjected to the temperature warming effects. This interpretation agrees with Fowler and Archer (2006), who examined the upper Indus Basin and found that the temperature change could play a pronounced effect on glaciers located at lower altitudes, while the precipitation change could be the main driver of mass balance and ΔSLA of glaciers located at higher altitudes, which have surface temperatures lower than the melting point. The veracity of this statement must match the present study because the glaciers of the south slopes of Mt. Everest are among the highest glaciers in the world, as mentioned above, and these altitudes have preserved these glaciers, more than the other parts of the Himalaya, from excessive melting. Therefore, the double upward shift of SLA of the largest glaciers (i.e., south-oriented and with higher altitude accumulation zone) compared to the smallest and the acceleration observed for these glaciers in term of shifts in SLA and surface area loss indicate the weakening of the Asian monsoon, which has led to a loss of 173 mm of precipitation in this region for the 1979–2010 period (e.g., Yao et al., 2012; Palazzi et al., 2013). Following the same reasoning for the acceleration observed from the 1990s, this loss could be mainly due to a minor accumulation that involved more large glaciers than an increase in melting at these elevations. Wagnon et al. (2013) recently arrived at the same conclusion. In fact, analyzing two glaciers in the Dudh Koshi Basin, they justify the observed negative mass balances mainly as the consequence of weakening of the Asian monsoon.

6 Conclusions

We have provided a comprehensive picture of the glacier changes to the south of Mt. Everest since the early 1960s. We considered five intermediate periods and analyzed available optical satellite imagery. An overall reduction in glacier area of 13.0 ± 3.1 % was observed, which was accompanied by an upward shift of the snow-line altitude (SLA) of 182 ± 22 m, a terminus retreat of 403 ± 9 m, and an increase of the debris coverage of 17.6 ± 3.1 %. Over the last 20 years, we noted an acceleration of the surface area loss and SLA. However, the increased recession velocity has only significantly affected the glaciers of the largest sizes. These glaciers present median upward shifts equal to more than 220 m, while the smaller ones have increases of about half of that. Temperature variations, despite being the primary cause eliciting glacier response, cannot alone account for why these glaciers, located at higher altitudes, reordered such a high upward shift of SLA and why their annual rate of area loss increased much more than that of the other glaciers. We propose that in the case of larger glaciers that have accelerated area loss processes, the effects of the current weakening of the Asian monsoon were added to the effects of increasing temperatures because the glaciers' orientation is aligned with the prevailing precipitation, which makes these glaciers more sensitive to variations in precipitation than to variations in temperatures.

Moreover, we noted that the shrinkage of these glaciers is lower than in the entire Himalayan range. Their location at higher elevations have reduced the warming impact, but have not been able to exclude these glaciers from a relentlessly continuous and slow recession process over the past 50 years.

The Supplement related to this article is available online at doi:10.5194/tc-8-1297-2014-supplement.

Acknowledgements. This work was supported by the Ministry of Education, Universities and Research (MIUR) through Ev-K2-CNR/SHARE and CNR-DTA/NEXTDATA projects within the framework of the Ev-K2-CNR and Nepal Academy of Science and Technology (NAST) collaboration in Nepal. S. Thakuri is recipient of the Intergovernmental Panel on Climate Change (IPCC) Scholarship Award under the collaboration between the IPCC Scholarship Programme and the Prince Albert II of Monaco Foundation's Young Researcher Scholarships Initiative. T. Bolch acknowledges funding through Deutsche Forschungsgemeinschaft (DFG).

Edited by: E. Larour

References

Ageta, Y. and Fujita, K.: Characteristics of mass balance of summer-accumulation type glaciers in the Himalayas and Tibetan Plateau, Z. Gletscherkd, Glazialgeol., 32, 61–65, 1996.

Amatya, L. K., Cuccillato, E., Haack, B., Shadie, P., Sattar, N., Bajracharya, B., Shrestha, B., Caroli, P., Panzeri, D., Basani, M., Schommer, B., Flury, B., Salerno, F., and Manfredi, E. C.: Improving Communication for Management of Social-ecological Systems in High Mountain Areas: Development of Methodologies and Tools – The HKKH Partnership Project, Mt. Res. Dev., 30, 69–79, 2010.

Asahi, K.: Equilibrium-line altitudes of the present and Last Glacial Maximum in the eastern Nepal Himalayas and their implications for SW monsoon climate, Quatern. Int., 212, 26–34, 2010.

Bagla, P.: No sign yet of Himalayan meltdown, Indian report finds, Science, 326, 924–925, 2009.

Bajracharya, B., Pradhan S., Shrestha B., and Salerno F.: An Integrated Decision Support Toolbox (DST) for the Management of Mountain Protected Areas. Mt. Res. Dev., 30, 94–102, 2010.

Bajracharya, S. R. and Mool, P.: Glaciers, glacial lakes and glacial lake outburst floods in the Mount Everest region, Nepal, Ann. Glaciol., 50, 81–86, 2009.

Basnett, S. Kulkarni, A., and Bolch, T.: The influence of debris cover and glacial lakes on the recession of glaciers in Sikkim Himalaya, India, J. Glaciol., 59, 1035–1046, 2013.

Benn, D. I., Benn, T., Hands, K., Gulley, J., Luckman, A., Nicholson, L. I., Quincey, D., Thompson, S., Toumi, R., and Wiseman,

S.: Response of debris-covered glaciers in the Mount Everest region to recent warming, and implications for outburst flood hazards, Earth-Sci. Rev., 114, 156–174, 2012.

Bhambri, R. and Bolch, T.: Glacier mapping: a review with special reference to the Indian Himalayas. Prog. Phys. Geog., 33, 672–704, 2009.

Bhambri, R., Bolch, T., Chaujar, R. K., and Kulshreshtha, S. C.: Glacier changes in the Garhwal Himalaya, India, from 1968 to 2006 based on remote sensing, J. Glaciol., 57, 543–556, 2011.

Bhambri, R., Bolch, T., and Chaujar, R. K.: Frontal recession of Gangotri glacier, Garhwal Himalayas, from 1965 to 2006, measured through high-resolution remote sensing data, Curr. Sci., 102, 489–494, 2012.

Bolch, T., Buchroithner, M., Pieczonka, T., and Kunert, A.: Planimetric and volumetric glacier changes in the Khumbu Himalaya since 1962 using Corona, Landsat TM and ASTER data, J. Glaciol., 54, 592–600, 2008a.

Bolch, T., Buchroithner, M. F., Peters, J., Baessler, M., and Bajracharya, S.: Identification of glacier motion and potentially dangerous glacial lakes in the Mt. Everest region/Nepal using spaceborne imagery, Nat. Hazards Earth Syst. Sci., 8, 1329–1340, 2008b,
http://www.nat-hazards-earth-syst-sci.net/8/1329/2008/.

Bolch, T., Pieczonka, T., and Benn, D. I.: Multi-decadal mass loss of glaciers in the Everest area (Nepal Himalaya) derived from stereo imagery, The Cryosphere, 5, 349-358, doi:10.5194/tc-5-349-2011, 2011.

Bolch, T., Kulkarni, A., Kääb, A., Huggel, C., Paul, F., Cogley, J. G., Frey, H., Kargel, J. S., Fujita, K., Scheel, M., Bajracharya, S., and Stoffel, M.: The state and fate of Himalayan glaciers, Science, 336, 310–314, 2012

Brahmbhatt, R. M., Bahuguna, I. M., Rathore, B. P., Kulkarni, A. V., Nainwal, H. C., Shah, R. D., and Ajai: A comparative study of deglaciation in two neighbouring basins (Warwan and Bhut) of Western Himalaya, Curr. Sci., 103, 298–304, 2012.

Byers, A. C.: Landscape change in Sagarmatha (Mt. Everest) National Park, Khumbu, Nepal, Himalayan Res. Bull., XVII, 31–41, 1997.

Chen, J., Zhu, X., Vogelmann, J. E., Gao, F., and Jin, S.: A simple and effective method for filling gaps in Landsat ETM+ SLC-off images, Remote Sens. Environ., 115, 1053–1064, 2011.

Chiarle, M., Lannotti, S., Mortara, G., and Deline, P.: Recent debris flow occurrences associated with glaciers in the Alps, Glob. Planet Change, 56, 123–136, 2007.

Chinn, T. J., Heydenrych, C., and Salinger, M. J.: Use of the ELA as a practical method of monitoring glacier response to climate in New Zealand's Southern Alps, J. Glaciol., 51, 85–95, 2005.

Cogley, J. G., Kargel, J. S., Kaser, G., and Van der Veen, C. J.: Tracking the source of glacier misinformation, Science, 327, p. 522, 2010.

Cook, E. R., Krusic, P. J., and Jones, P. D.: Dendroclimatic signals in long tree-ring chronologies from the Himalayas of Nepal, Int. J. Climatol., 23, 707–732, 2003.

Dette, H. and Neumeyer, N.: Nonparametric Analysis of Covariance, Ann. Stat., 29, 1361–1400. 2001,

Diodato, N., Bellocchi, G., and Tartari, G.: How do Himalayan areas respond to global warming?, Int. J. Climatol., 32, 975–982, 2012.

Fowler, H. J. and Archer, D. R.: Conflicting Signals of Climatic Change in the Upper Indus Basin, J. Clim., 19, 4276–4293, 2006.

Frey, H., Paul, F., and Strozzi, T.: Compilation of a glacier inventory for the western Himalayas from satellite data: methods, challenges and results, Remote Sens. Environ., 124, 832–843, 2012.

Fujita, K. and Nuimura, T.: Spatially heterogeneous wastage of Himalayan glaciers, Proc. Natl. Acad. Sci. USA, 108, 14011–14014, 2011.

Fujita, K., Thompson, L. G., Ageta, Y., Yasunari, T., Kajikawa, Y., Sakai, A., and Takeuchi, N.: Thirty-year history of glacier melting in the Nepal Himalayas, J. Geophys. Res., 111, D03109, doi:10.1029/2005JD005894, 2006.

Gardelle, J., Arnaud, Y., and Berthier, E.: Contrasted evolution of glacial lakes along the Hindu Kush Himalaya mountain range between 1990 and 2009, Global Planet. Change, 75, 47–55, 2011.

Gardelle, J., Berthier, E., Arnaud, Y., and Kääb, A.: Region-wide glacier mass balances over the Pamir-Karakoram-Himalaya during 1999-2011, The Cryosphere, 7, 1263–1286, doi:10.5194/tc-7-1263-2013, 2013.

Grosse, G., Schirrmeister, L., Kunitsky, V. V., and Hubberten, H. W.: The use of CORONA images in remote sensing of periglacial geomorphology: an illustration from the NE Siberian coast, Permafrost Periglac., 16, 163–172, 2005.

Hall, D. K., Bayr, K. J., Schoner, W., Bindschadler, R. A., and Chien, J. Y. L.: Consideration of the errors inherent in mapping historical glacier positions in Austria from the ground and space (1893–2001), Remote Sens. Environ., 86, 566–577, 2003.

Hambrey, M. and Alean, J.: Glaciers. 2nd ed., Cambridge University Press, 376 pp., 2004.

Hess, H.: Die Gletscher, Braunschweig, 406 pp., 1904.

Hewitt, K.: Tributary glacier surges: an exceptional concentration at Panmah Glacier, Karakoram Himalaya, J. Glaciol., 53, 181–188, 2007.

Hoelzle, M., Chinn, T., Stumm, D., Paul, F., Zemp, M., and Haeberli, W.: The application of inventory data for estimating past climate change effects on mountain glaciers: a comparison between the European Alps and the Southern Alps of New Zealand, Global Planet. Change, 56, 69–82, 2007.

Hooke, R. L.: Principles of Glacier Mechanics, Cambridge University Press, 429 pp., 2005.

Ichiyanagi, K., Yamanaka, M. D., Muraji, Y., and Vaidya, B. K.: Precipitation in Nepal between 1987 and 1996, Int. J. Climatol., 27, 1753–1762, 2007.

Jones, P. D. and Moberg, A.: Hemispheric and large-scale surface air temperature variations: an extensive revision and an update to 2001, J. Climate, 16, 206–223, 2003.

Kääb, A., Berthier, E., Nuth, C., Gardelle, J., and Arnaud, Y.: Contrasting patterns of early twenty-first-century glacier mass change in the Himalayas, Nature, 488, 495-498, 2012.

Karpilo, R. D. J.: Glacier monitoring techniques, in: Geological Monitoring, edited by: Young, R. and Norby, L., The Geological Society of America, Boulder, Colorado, 141–162, 2009.

Kattel, D. B. and Yao, T.: Recent temperature trends at mountain stations on the southern slope of the Central Himalayas, J. Earth Syst. Sci., 122, 215–227, 2013.

Kaufman, Y. J., Koren, I., Remer, L. A., Tanre, D., Ginoux, P., and Fan, S.: Dust transport and deposition observed from the Terra-moderate Resolution Imaging Spectroradiometer (MODIS) spacecraft over the Atlantic Ocean, J. Geophys. Res. – Atmos., 110, D10S12, doi:10.1029/2003JD004436, 2005.

Kayastha, R. B. and Harrison, S. P.: Changes of the equilibrium-line altitude since the little ice age in the Nepalese Himalaya, Ann. Glaciol., 48, 93–99, 2008.

Kerschner, H.: Statistical modelling of equilibrium-line altitudes of Hintereisferner, central Alps, Austria, 1859-present, Ann. Glaciol., 24, 111–115, 1997.

Koblet, T., Gartner-Roer, I., Zemp, M., Jansson, P., Thee, P., Haeberli, W., and Holmlund, P.: Reanalysis of multi-temporal aerial images of Storglaciaren, Sweden (1959–99) – Part 1: Determination of length, area, and volume changes, The Cryosphere, 4: 333–343, doi:10.5194/tc-4-333-2010, 2010.

Kresse, W. and Danko, D. M.: Springer Handbook of Geographic Information, Springer Verlag, 1120 pp., 2011.

Kuhn, M.: Climate and glaciers. Sea level, ice and climatic change, in: Proceedings of the Canberra Symposium, December 1979, edited by: Allison, I., December 1979, IASH Publ. 131, 3–20, 1981.

Kulkarni, A. V., Rathore, B. P., Singh, S. K., and Bahuguna, I. M.: Understanding changes in the Himalayan cryosphere using remote sensing techniques, Int. J. Remote Sens., 32, 601–615, 2011.

Lami, A., Marchetto, A., Musazzi, S., Salerno, F., Tartari, G., Guilizzoni, P., Rogora, M., and Tartari, G. A.: Chemical and biological response of two small lakes in the Khumbu Valley, Himalayas (Nepal) to short-term variability and climatic change as detected by long-term monitoring and paleolimnological methods, Hydrobiologia, 648, 189–205, 2010.

Leonard, K. C. and Fountain, A. G.: Map-based methods for estimating glacier equilibrium-line altitudes, J. Glaciol., 49, 329–336, 2003.

Liu, X. and Chen, B.: Climatic warming in the Tibetan Plateau during recent decades, Int. J. Climatol., 20, 1729–1742, 2000.

Lorenz, H.: Integration of Corona and Landsat Thematic Mapper data for bedrock geological studies in the high Arctic, Int. J. Remote Sens., 25, 5143-5162, 2004.

Manfredi, E. C., Flury, B., Viviano, G., Thakuri, S., Khanal, S. N., Jha P. K., Maskey, R. K., Kayastha, R. B., Kafle, K. R., Bhochhibhoya, S. B., Ghimire, N. P., Shrestha, B. B., Gyanendra, C., Giannino, F., Carteni, F., Mazzoleni, S., and Salerno, F.: Solid Waste and Water Quality Management Models for Sagarmatha National Park and Buffer Zone, Nepal: Implementation of a Participatory Modeling Framework, Mt. Res. Dev., 30, 127–142, 2010.

McFadden, E. M., Ramage, J., and Rodbell, D. T.: Landsat TM and ETM+ derived snowline altitudes in the Cordillera Huayhuash and Cordillera Raura, Peru, 1986–2005, The Cryosphere, 5, 419–430, doi:10.5194/tc-5-419-2011, 2011.

Mernild, S., Pelto, M., Malmros, J., Yde, J., Knudsen, N., and Hanna, E.: Identification of snow ablation rate, ELA, AAR and net mass balance using transient snowline variations on two Arctic glaciers, J. Glaciol., 59, 649–659, doi:10.3189/2013JoG12J221, 2013.

Mool, P. K., Bajracharya, S. R., and Joshi, S. P.: Inventory of Glaciers, Glacial Lakes and Glacial Lake Outburst Floods, Monitoring and Early Warning Systems in the Hindu Kush-Himalaya Region, ICIMOD, Nepal, 2001.

Naidu, C. V., Durgalakshmi, K., Muni Krishna, K., Ramalingeswara, S., Satyanarayan, G. C., Lakshminarayana, P., and Rao, L. M.: Is summer monsoon rainfall decreasing over India in the global warming era? J. Geophys. Res.-Atmos., 114, D24108, doi:10.1029/2008JD011288, 2009.

Nakawo, M., Yabuki, H., and Sakai, A.: Characteristics of Khumbu Glacier, Nepal Himalaya: recent change in the debris-covered area, Ann. Glaciol., 28, 118–122, 1999.

Nie, Y., Zhang, Y., Liu, L., and Zhang, J.: Glacial change in the vicinity of Mt. Qomolangma (Everest), central high Himalayas since 1976, J. Geogr. Sci., 20, 667–686, 2010.

Nuimura, T., Fujita, K., Yamaguchi, S., and Sharma, R. R.: Elevation changes of glaciers revealed by multitemporal digital elevation models calibrated by GPS survey in the Khumbu region, Nepal Himalaya, 1992–2008, J. Glaciol., 58, 648–656, 2012.

Oerlemans, J.: Glaciers and Climate Change, edited by: Oerlemans, J., A. A. Balkema Publishers, Rotterdam, 160 pp., 2001.

Ouimet, W., Whipple, K., and Granger, D.: Beyond threshold hillslopes: Channel adjustment to base-level fall in tectonically active mountain ranges, Geology, 37, 579–582, 2009.

Owen, L. A. and Benn, D. I.: Equilibrium-line altitudes of the Last Glacial Maximum for the Himalaya and Tibet: an assessment and evaluation of results, Quatern. Int., 138–139, 55–78, 2005.

Palazzi, E., von Hardenberg, J., and Provenzale, A.: Precipitation in the Hindu-Kush Karakoram Himalaya: observations and future scenarios, J. Geophys. Res.-Atmos. 118, 85–100, 2013.

Parkinson, C. L., Ward, A., and King, M. D.: Earth Science Reference Handbook, A Guide to NASA's Earth Science Program and Earth Observing Satellite Missions: National Aeronautics and Space Administration, 2006.

Paul, F., Barrand, N., Berthier, E., Bolch, T., Casey, K., Frey, H., Joshi, S. P., Konovalov, V., Le Bris, R., Molg, N., Nosenko, G., Nuth, C., Pope, A., Racoviteanu, A., Rastner, P., Raup, B., Scharrer, K., Steffen, S., and Winsvold, S.: On the accuracy of glacier outlines derived from remote sensing data. Ann. Glaciol., 54, 171–182, 2013.

Paul, F., Barry, R. G., Cogley, J. G., Frey, H., Haeberli, W., Ohmura, A., Ommanney, C. S. L., Raup, B., Rivera, A., and Zemp, M.: Recommendations for the compilation of glacier inventory data from digital sources, Ann. Glaciol., 50, 119–126, 2009.

Paul, F., Huggel, C., and Kääb, A.: Combining satellite multispectral image data and a digital elevation model for mapping debris-covered glaciers, Remote Sens. Environ., 89, 510–518, 2004.

Pelto, M.: Utility of late summer transient snowline migration rate on Taku Glacier, Alaska, The Cryosphere, 5, 1127–1133, doi:10.5194/tc-5-1127-2011, 2011.

Pelto, M., Kavanaugh, J., and McNeil, C.: Juneau Ice field Mass Balance Program 1946–2011, Earth Syst. Sci. Data, 5, 319–330, doi:10.5194/essd-5-319-2013, 2013.

Pieczonka, T., Bolch, T., Wei, J., and Liu, S.: Heterogeneous mass loss of glaciers in the Aksu-Tarim Catchment (Central Tien Shan) revealed by 1976 KH-9 Hexagon and 2009 SPOT-5 stereo imagery, Remote Sens. Environ., 130, 233–244, 2013.

Quincey, D. J., Luckman, A., and Benn, D.: Quantification of Everest region glacier velocities between 1992 and 2002, using satellite radar interferometry and feature tracking, J. Glaciol., 55, 596–606, 2009.

Rabatel, A., Letréguilly, A., Dedieu, J. P., and Eckert, N.: Changes in glacier equilibrium-line altitude in the western Alps from 1984 to 2010: evaluation by remote sensing and modeling of the morpho-topographic and climate controls, The Cryosphere, 7, 1455–1471, doi:10.5194/tc-7-1455-2013, 2013.

Rabatel, A., Bermejo, A., Loarte, E., Soruco, A., Gomez, J., Leonardini, G., Vincent, C., and Sicart, J. E.: Can the snowline be used as an indicator of the equilibrium line and mass balance for glaciers in the outer tropics?, J. Glaciol., 58, 1027–1036, 2012.

Rabatel, A., Dedieu, J. P., and Vincent, C.: Using remote-sensing data to determine equilibrium-line altitude and mass-balance time series: validation on three French glaciers, 1994–2002, J. Glaciol., 51, 539–546, 2005.

Racoviteanu, A., Williams, M., and Barry, R.: Optical Remote Sensing of Glacier Characteristics: A Review with Focus on the Himalaya, Sensors, 8, 3355–3383, 2008.

Ramanathan, V., Chung, C., Kim, D., Bettge, T., Buja, L., Kiehl, J. T., Washington, W. M., Fu, Q., Sikka, D. R., and Wild, M.: Atmospheric brown clouds: impacts on south Asian climate and hydrological cycle, Proc. Natl. Acad. Sci. USA, 102, 5326–5333, 2005.

Rao, Y. P.: Southwest Monsoon, India Meteorological Department. Meteorological Monograph, New Delhi, 366 pp., 1976.

Rastner, P., Bolch, T., Notarnicola, C., and Paul, F.: A comparison of pixel- and object based glacier classification with optical satellite images. IEEE J. Sel. Topics Appl. Earth Observ., doi:10.1109/JSTARS.2013.2274668, 2013.

Rickenmann, D. and Zimmermann, M.: The 1987 debris flows in Switzerland: documentation and analysis, Geomorphology, 8, 175–189, 1993.

Rodriguez-Galiano, V. F., Pardo-Iguzquiza, E., Chica-Olmo, M., Mateos, J., Rigol-Sanchez, J. P., and Vega, M.: A comparative assessment of different methods for Landsat 7/ETM+ pansharpening, Int. J. Remote Sens., 33, 6574–6599, 2012.

Rosenholm, D. and Akerman, D.: Digital orthophotos from IRS – production and utilization, in: IAPRS, edited by: Fritsch, D., Englich, M. and Sester, M., ISPRS Commission IV Symposium on GIS – Between Visions and Applications, Stuttgart, Germany, 32, 501–505, 1998.

Salerno, F., Buraschi, E., Bruccoleri, G., Tartari, G., and Smiraglia C.: Glacier surface-area changes in Sagarmatha National Park, Nepal, in the second half of the 20th century, by comparison of historical maps, J. Glaciol., 54, 738–752, 2008.

Salerno, F., Viviano, G., Thakuri, S., Flury, B., Maskey, R. K., Khanal, S. N., Bhuju, D., Carrer, M., Bhochhibhoya, S., Melis, M. T., Giannino, F., Staiano, A., Carteni, F., Mazzoleni, S., Cogo, A., Sapkota, A., Shrestha, S., Pandey, R. K., and Manfredi, E. C.: Energy, forest, and indoor air pollution models for Sagarmatha National Park and Buffer zone, Nepal: implementation of a participatory modeling framework, Mt. Res. Dev., 30, 113–126, 2010a.

Salerno, F., Cuccillato, E., Caroli, P., Bajracharya, B., Manfredi, E. C., Viviano, G., Thakuri, S., Flury, B., Basani, M., Giannino, F., and Panzeri, D.: Experience with a hard and soft participatory modeling framework for social ecological system management in Mount Everest (Nepal) and K2 (Pakistan) protected areas, Mt. Res. Dev., 30, 80–93, 2010b.

Salerno, F., Thakuri, S., D'Agata, C., Smiraglia, C., Manfredi, E. C., Viviano, G., and Tartari, G.: Glacial lake distribution in the Mount Everest region: Uncertainty of measurement and conditions of formation, Global Planet. Change, 92–93, 30–39, 2012.

Salerno, F., Viviano, G., Mangredi, E. C., Caroli, P., Thakuri, S., and Tartari, G.: Multiple Carrying Capacities from a management-oriented perspective to operationalize sustainable tourism in protected area, J. Environ. Manag., 128, 116–125, 2013.

Scherler, D., Bookhagen, B., and Strecker, M. R.: Spatially variable response of Himalayan glaciers to climate change affected by debris cover, Nat. Geosci., 4, 156–159, 2011.

Schneider, E.: Begleitworte zur Karte Khumbu Himal und zur Namensgebung, in: Khumbu Himal, edited by: Hellmich, W., Universitasverlag Wagner, Innsbruck, (Ergebnisse des Forschungsunternehmens Nepal Himalaya Band 1, Lieferung 5.), 430–446, 1967.

Shapiro, S. S. and Wilk, M. B.: An analysis of variance test for normality (complete samples), Biometrika, 52, 591–611, 1965.

Shangguan, D., Liu, S., Ding, Y., Wu, L., Deng, W., Guo, W., Wang, Y., Xu, J., Yao, X., Guo, Z., and Zhu, W.: Glacier changes in the Koshi River basin, central Himalaya, from 1976 to 2009, derived from remote-sensing imagery, Ann. Glaciol., 55, 61–68, 2014.

Sharma, K. P., Moore, B., and Vorosmarty, C. J.: Anthropogenic, climatic, and hydrologic trends in the Kosi basin, Himalaya, Clim. Change, 47, 141–165, 2000.

Streets, D. G., Yan, F., Chin, M., Diehl, T., Mahowald, N., Schultz, M., Wild, M., Wu, Y., and Yu, C.: Anthropogenic and natural contributions to regional trends in aerosol optical depth, 1980–2006, J. Geophys. Res.-Atmos., 114, D00D18, doi:10.1029/2008JD011624, 2009.

Tartari, G., Verza, G., and Bertolami, L.: Meteorological data at the Pyramid Observatory Laboratory (Khumbu Valley, Sagarmatha National Park, Nepal), in: Limnology of high altitude lakes in the Mt. Everest Region (Nepal), edited by: Lami, A. and Giussani, G., Mem. Ist. Ital. Idrobiol., 57, 23–40, 2002.

Tartari, G., Salerno, F., Buraschi, E., Bruccoleri, G., and Smiraglia, C.: Lake surface area variations in the North-Eastern sector of Sagarmatha National Park (Nepal) at the end of the 20th Century by comparison of historical maps, J. Limnol., 67, 139–154, 2008.

Tennant, C., Menounos, B., Ainslie, B., Shea, J., and Jackson, P.: Comparison of modeled and geodetically-derived glacier mass balance for Tiedemann and Klinaklini glaciers, southern Coast Mountains, British Columbia, Canada, Global Planet. Change, 82–83, 74–85, 2012.

Thompson, D., Tootle, G., Asce, M., Kerr, G., Sivanpillai, R., and Pochop, L.: Glacier Variability in the Wind River Range, Wyoming, J. Hydrol. Eng., 16, 798–805, doi:10.1061/(ASCE)HE.1943-5584.0000384, 2011.

Thompson, L. G., Thompson, E. M., Brecher, H., Davis, M., Leon, B., Les, D., Lin, P. N., Mashiotta, T., and Mountain, K.: Abrupt tropical climate change: Past and present, Proc. Natl. Acad. Sci. USA, 103, 10536–10543, 2006.

Wagnon, P., Vincent, C., Arnaud, Y., Berthier, E., Vuillermoz, E., Gruber, S., Ménégoz, M., Gilbert, A., Dumont, M., Shea, J. M., Stumm, D., and Pokhrel, B. K.: Seasonal and annual mass balances of Mera and Pokalde glaciers (Nepal Himalaya) since 2007, The Cryosphere, 7, 1769–1786, doi:10.5194/tc-7-1769-2013, 2013.

Walford, N.: Practical Statistics for Geographers and Earth Scientists, John Wiley and Sons, 440 pp., 2011.

Wild, M.: The heat balance of the Earth in GCM simulations of present and future climate, Zuercher Geografische Schriften No. 68, Verlag der Fachvereine, Zuerich, 188 pp., 1997.

Wild, M.: Global dimming and brightening: a review, J. Geophys. Res.-Atmos., 114, D00D16, doi:10.1029/2008JD011470, 2009.

Wild, M., Gilgen, H., Roesch, A., Ohmura, A., Long, C. N., Dutton, E. G., Forgan, B., Kallis, A., Russak, V., and Tsvetkov, A.: From dimming to brightening: decadal changes in solar radiation at Earth's surface, Science, 308, 847–850, 2005.

Wu, B.: Weakening of Indian summer monsoon in recent decades, Adv. Atmos. Sci., 22, 21–29, 2005.

Yamada, T.: Glacier lake and its outburst flood in the Nepal Himalaya, Tokyo, Japanese Society of Snow and Ice, Data Center for Glacier Research (Monograph 1), 1998.

Yao, T., Thompson, L., Yang, W., Yu, W., Gao, Y., Guo, X., Yang, X., Duan, K., Zhao, H., Xu, B., Pu, J., Lu, A., Xiang, Y., Kattel, D. B., and Joswiak, D.: Different glacier status with atmospheric circulations in Tibetan Plateau and surroundings, Nat. Clim. Change, 2, 663–667, 2012.

Ye, Q., Kang, S., Chen, F., and Wang, J.: Monitoring glacier variations on Geladandong mountain, central Tibetan Plateau, from 1969 to 2002 using remote-sensing and GIS technologies, J. Glaciol., 52, 537–545, 2006.

Ye, Q., Zhong, Z., Kang, S., Stein, A., Wei, Q., and Liu, J.: Monitoring glacier and supra-glacier lakes from space in Mt. Qomolangma region of the Himalayas on the Tibetan Plateau in China, J. Mt. Sci. China, 6, 211–220, 2009.

Supplement of The Cryosphere, 8, 1297–1315, 2014
http://www.the-cryosphere.net/8/1297/2014/
doi:10.5194/tc-8-1297-2014-supplement

The Cryosphere Open Access

Supplement of

Tracing glacier changes since the 1960s on the south slope of Mt. Everest (central Southern Himalaya) using optical satellite imagery

S. Thakuri et al.

Correspondence to: S. Thakuri (thakuri@irsa.cnr.it)

Table S1. A complete set of data on glacier surface area (Surf), terminus (Term), snow-line altitude (SLA) and debris cover area (DebrisCov) for all analysed glaciers.

Glacier	Surface area (km^2)						Terminus difference (m)						SLA (m a.s.l.)						Debris-cover area (%)					
	1962	1975	1992	2000	2008	2011	1962-75	1975-92	1992-00	2000-08	2008-11	1962-11	1962	1975	1992	2000	2008	2011	1962	1975	1992	2000	2008	2011
Ama Dablam	10.6	10.5	10.4	10.3	9.8	9.6	39	-44	-56	-86	-39	-186	5183	5199	5247	5264	5337	5387	23	23	25	24	25	26
Bhote Koshi	43.7	43.6	43.2	43.1	42.9	42.7	-140	-215	-80	-146	-42	-623	5224	5382	5492	5544	5606	5632	27	30	37	40	41	41
Chhule	10.2	9.8	9.1	8.8	8.0	7.7	-65	-40	-152	-169	-7	-433	5139	5231	5288	5342	5368	5364	18	24	20	21	26	28
Chhutingpo	8.5	9.3	7.6	7.2	6.5	7.0	-78	-136	-168	-45	0	-427	5324	5257	5321	5299	5360	5372	-	-	5	4	5	5
Cholo	2.3	2.9	1.9	1.5	1.4	1.4	234	212	-74	-15	0	357	4987	4946	5062	5098	5124	5152	40	35	45	59	62	63
Cholotse	2.5	1.7	1.5	1.5	1.5	1.5	0	96	0	-98	-28	-30	5078	5141	5183	5195	5262	5244	44	63	66	76	82	75
Duwo	2.2	2.2	2.1	2.2	2.1	2.1	182	172	-99	0	0	255	-	4984	4969	4985	5039	-		33	39	40	48	-
Imja	28.1	28.0	27.0	27.2	26.4	25.5	-862	-458	-336	-255	-207	-2119	5340	5480	5655	5673	5691	5742	25	23	23	23	25	27
Kdu_gr125	1.9	1.7	1.5	1.4	1.0	0.9	-182	-153	-88	-123	-56	-601	5444	5462	5448	5423	5444	5442	17	-	0	-	-	12
Kdu_gr181	1.3	1.1	1.4	0.7	0.6	0.6	0	0	0	0	0	0	5219	-	-	-	5350	-	-	-	-	-	4	-
Kdu_gr38	2.8	2.1	1.6	0.9	0.8	0.7	-142	-420	-192	-345	-45	-1143	5208	5305	5246	5298	5368	5490	-	-	2	-	-	18
Khangri	18.6	19.1	18.6	17.9	18.5	17.2	0	0	0	0	0	0	5352	5383	5432	5451	5533	5584	25	27	30	32	33	37
Khumbu	40.1	38.9	38.0	38.4	38.4	37.5	0	54	-14	0	0	41	5403	5545	5519	5508	5681	5730	15	19	19	20	23	24
Kyajo	1.6	1.7	1.2	1.0	1.0	1.0	65	-110	0	0	-9	-54	5433	-	5385	5325	5388	5366	-	-	-	-	9	35
Langdak	3.0	2.6	2.0	2.3	2.1	2.2	-117	-426	-103	-115	-103	-863	5193	5094	5249	5206	5214	5220	39	27	38	35	40	41
Langmuche	5.5	4.9	3.7	3.3	2.9	2.8	-598	-350	-27	-203	-112	-1290	5184	5150	5168	5147	5202	5191	12	16	3	6	8	10
Lhotse	15.6	16.8	15.9	15.3	15.4	14.6	0	231	-63	-188	-42	-62	5463	5429	5425	5544	5664	5713	36	31	40	42	45	42
Lobuje	2.0	1.7	1.7	1.8	1.7	1.7	0	-20	-37	0	0	-57	5347	5350	5418	5522	5578	5628	34	35	39	41	43	46
Lumsamba	20.4	21.6	22.9	20.8	19.3	18.4	0	0	0	0	0	0	5445	5518	5454	5480	5582	5608	23	24	19	22	29	31
Machhermo	2.1	2.5	1.9	1.1	1.2	1.2	-166	-302	25	105	0	-339	5361	-	5443	5330	5303	5552	9	-	-	-	-	26
Melung	12.0	11.6	11.4	11.3	10.9	10.8	-234	-425	-45	-170	-46	-919	5263	5339	5386	5440	5493	5480	29	29	32	32	34	30
Nare	9.3	7.6	6.9	6.6	6.0	5.8	-359	-48	-329	-165	-66	-966	5332	5308	5295	5266	5356	5436	15	20	25	24	25	27
Nareyargaip	6.9	6.1	6.4	5.9	5.5	5.5	-186	-74	-40	0	0	-301	5361	5452	5442	5460	5509	5528	27	37	35	41	47	40
Ngojumba	98.7	98.7	98.3	98.0	97.7	97.3	-82	-176	-48	-125	-24	-455	5381	5532	5496	5507	5568	5570	27	27	26	27	28	30
Nuptse	9.2	9.2	8.8	8.0	8.1	7.9	-79	92	0	0	0	14	5515	5505	5615	5569	5574	5588	28	31	35	36	38	37
Phunki	2.0	1.7	1.7	1.8	1.7	1.6	-156	-296	-189	-174	0	-815	-	-	-	-	5028	-	-	-	-	-	-	-
Thyangbo	15.3	14.7	13.6	12.1	8.8	8.6	-210	-36	-72	0	-143	-460	5079	5049	5139	5247	5271	5289	12	10	9	12	20	26
Tingbo	1.5	1.4	1.3	1.2	1.1	1.2	-169	68	-64	0	0	-165	5402	5262	5271	5328	5370	5431		21	40	38	39	40
W-Lhotse	5.6	5.0	4.7	5.0	4.5	4.4	-52	114	16	-46	-70	-39	5299	5252	5280	5384	5398	5492	31	33	37	36	39	40
Other glaciers ($< 1\ km^2$)	21.0	19.4	19.0	16.7	12.4	12.1	-	-	-	-	-		-	-	-	-	-	-	-	-	-	-	-	-

Table S2. Morphological parameters (slope, aspect, elevation and length) of the glaciers for 1962-2011.

Glacier	Slope (deg)						Aspect (deg)						Elevation (m)																		Length of ablation area (km)
													1962			1975			1992			2000			2008			2011			
	1962	1975	1992	2000	2008	2011	1962	1975	1992	2000	2008	2011	Avg.	Min	Max.	Avg.	Min	Max.	Avg.	Min	Max.	Avg.	Min	Max.	Avg.	Min	Max.	Avg.	Min	Max.	
Ama Dablam	29.6	28.1	26.9	29.8	28.7	29.5	236	227	234	236	244	239	5422	4768	6640	5355	4715	6665	5374	4758	6417	5412	4736	6672	5412	4775	6359	5425	4787	6359	4.32
Bhote Koshi	24.3	25.9	24.8	23.6	25.0	24.2	174	170	174	136	168	172	5552	4725	6979	5574	4739	7097	5578	4739	7080	5525	4758	6893	5555	4772	6893	5559	4766	6899	10.46
Chhule	25.3	26.6	24.8	23.5	24.0	21.2	133	120	119	113	111	112	5318	4818	6545	5151	4818	6286	5112	4766	6264	5119	4766	6268	5080	4787	5836	5240	4809	6220	6.02
Chhutingpo	27.3	27.6	26.7	26.0	28.0	26.4	149	133	140	126	155	144	5519	4915	6182	5539	4856	6288	5554	4905	6206	5552	4947	6182	5636	5081	6182	5598	5008	6188	0.95
Cholo	35.7	35.5	31.8	33.1	30.0	30.7	105	105	104	101	103	103	5258	4519	6442	5239	4420	6423	5193	4358	6442	5006	4422	6248	4907	4422	6146	4940	4407	6215	2.21
Cholotse	33.5	27.5	24.2	23.6	24.4	24.6	248	244	226	225	209	235	5338	4865	6281	5319	4883	6301	5270	4846	6301	5111	4857	5588	5098	4851	5660	5108	4879	5662	1.65
Duwo	30.3	32.9	31.9	34.2	30.0	30.1	210	237	227	215	217	218	5198	4746	6654	5169	4719	6452	5191	4719	6452	5236	4749	6332	5101	4744	5973	5103	4740	5973	1.70
Imja	30.2	33.1	32.1	33.5	32.8	33.1	210	204	210	168	215	218	5768	4980	7971	5807	4981	8226	5833	4986	8226	5844	4989	7803	5877	4981	7803	5877	5007	7803	6.89
Kdu_gr125	26.1	27.9	25.7	24.9	18.2	17.6	168	170	172	170	164	162	5540	5118	6005	5592	5255	6097	5605	5258	6097	5601	5329	6102	5522	5332	5759	5515	5361	5695	0.85
Kdu_gr181	46.9	41.7	41.0	41.4	41.8	43.1	215	231	239	231	243	233	5526	4834	6547	5677	4844	6572	5541	4724	6572	5544	4936	6572	5480	4899	6527	5548	4991	6527	-
Kdu_gr38	38.4	40.7	38.0	39.8	38.8	39.7	87	85	77	75	90	74	5463	4800	6603	5487	4878	6527	5478	4939	6527	5594	4917	6504	5708	4917	6529	5626	4947	6511	0.57
Khangri	25.2	25.4	24.7	23.3	23.2	23.3	168	160	167	153	160	160	5597	5081	7105	5581	5027	7111	5605	5027	7111	5558	5100	6844	5568	5100	6844	5557	5091	6844	3.73
Khumbu	29.7	30.6	30.4	30.2	29.7	29.5	212	211	212	192	205	207	6058	4844	8289	6116	4876	8159	6163	4876	8260	6175	4900	8250	6152	4909	8250	6150	4880	8260	8.99
Kyajo	19.4	20.7	15.9	15.8	16.0	13.9	120	123	113	113	115	117	5419	5224	5939	5428	5224	5922	5385	5224	5575	5387	5224	5583	5393	5224	5595	5369	5224	5540	-
Langdak	23.7	25.6	21.4	24.3	22.3	25.9	143	148	130	141	127	166	5287	4803	6164	5399	4795	6179	5285	4737	6179	5315	4824	6126	5307	4820	5880	5297	4842	6155	2.65
Langmuche	35.8	40.6	39.0	40.4	40.7	40.4	114	99	105	97	116	91	5484	4348	6819	5613	4355	6804	5546	4370	6659	5673	4369	6804	5774	4418	6819	5681	4361	6804	2.61
Lhotse	31.3	33.3	31.7	29.6	29.8	30.7	206	203	207	203	202	207	5818	4800	8400	5907	4758	8467	5890	4758	8467	5818	4794	8472	5829	4816	8238	5907	4816	8472	5.53
Lobuje	23.7	22.3	21.9	22.8	21.8	21.2	134	137	145	130	139	140	5361	4960	5940	5379	4959	5997	5356	4923	5997	5382	4960	5885	5357	4960	5852	5352	4960	5843	1.98
Lumsamba	26.4	27.6	26.7	26.5	27.8	26.4	187	192	191	165	186	186	5784	4799	7274	5830	4908	7262	5796	4908	7262	5825	4931	7270	5866	4896	7274	5865	4931	7262	8.18
Machhermo	25.5	27.0	24.9	24.4	25.5	22.6	168	145	145	150	143	149	5505	5165	5991	5321	4819	5808	5447	5166	5808	5499	5208	5808	5499	5176	5814	5468	5166	5808	-
Melung	21.0	22.4	22.1	23.1	24.2	20.9	150	145	144	130	144	146	5349	4834	6600	5211	4950	5632	5164	4950	5578	5144	4950	5588	5157	4949	5530	5407	4950	6600	5.67
Nare	29.0	31.2	29.9	31.9	29.5	30.6	234	228	233	184	239	241	5382	4563	6388	5476	4721	6427	5482	4752	6476	5441	4803	6482	5392	4825	6305	5423	4827	6317	2.72
Nareyargaip	28.2	28.1	26.8	26.4	25.3	25.7	207	214	212	194	213	213	5596	5142	6672	5581	5129	6538	5535	5129	6665	5522	5105	6467	5503	5110	6294	5508	5110	6281	2.22
Ngojumba	23.8	24.5	24.0	24.1	24.5	23.9	185	179	184	133	182	181	5798	4680	8151	5814	4684	8115	5824	4674	8067	5848	4673	8109	5873	4684	8164	5844	4684	8115	15.79
Nuptse	30.8	30.9	31.0	28.9	29.2	29.2	214	212	218	147	211	210	5750	4932	7716	5804	4885	7754	5823	4885	7754	5744	4904	7716	5776	4932	7737	5769	4933	7716	5.15
Phunki	45.7	50.5	50.1	47.8	46.8	48.0	218	207	210	216	215	221	5367	4664	6548	5466	4720	6553	5465	4720	6553	5347	4811	6554	5304	4811	6548	5333	4823	6548	-
Thyangbo	37.0	37.6	36.7	37.2	33.1	33.0	139	131	129	131	130	123	5456	4324	6828	5417	4397	6638	5469	4335	6793	5490	4335	6783	5328	4385	6420	5323	4363	6480	2.91
Tingbo	33.3	36.3	34.8	30.4	29.3	30.9	250	241	241	235	241	237	5460	4899	6631	5576	4937	6677	5440	4886	6090	5342	4899	5955	5289	4899	5888	5347	4894	5955	1.33
W-Lhotse	32.6	35.0	35.7	33.2	34.4	33.4	210	201	203	196	204	197	5625	4942	7465	5727	4954	7649	5742	4954	7649	5633	4935	7072	5746	4924	7496	5654	4955	7072	2.94
Other glaciers (<1 km^2)	35.8	35.0	33.6	37.3	36.4	36.2	198	160	193	186	188	182	5397	4235	6441	5248	4359	6433	5365	4235	6442	5437	4498	6442	5397	4469	6442	5402	4533	6442	-

Table S3. Additional snow-line altitudes (SLAs) derived from 20 Landsat ETM+ imagery of 2000-2011 period for three selected glaciers: Lobuje, Khangri, and Imja. All these images, acquired in the October-December period, present no or minimum cloud cover.

Date	Scene ID	SLA position on glacier (m a.s.l.)		
		Lobuje	Khangri	Imja
10/14/2000	LE71400412000288SGS00	5521	5476	5669
10/17/2001	LE71400412001290SGS00	5514	5471	5644
10/20/2002	LE71400412002293SGS00	5494	5458	5657
11/8/2003	LE71400412003312ASN01	5575	5471	5657
10/25/2004	LE71400412004299PFS00	5555	5471	5663
11/10/2004	LE71400412004315PFS00	5568	5493	5682
10/28/2005	LE71400412005301PFS00	5548	5489	5672
11/13/2005	LE71400412005317EDC00	5591	5498	5685
11/16/2006	LE71400412006320PFS00	5581	5492	5695
12/2/2006	LE71400412006336SGS00	5571	5502	5660
10/18/2007	LE71400412007291PFS00	5564	5492	5673
11/19/2007	LE71400412007323PFS00	5579	5478	5695
10/20/2008	LE71400412008294PFS03	5524	5505	5660
12/7/2008	LE71400412008342SGS00	5576	5544	5664
10/23/2009	LE71400412009296SGS00	5545	5500	5695
11/8/2009	LE71400412009312SGS00	5549	5537	5720
10/26/2010	LE71400412010299SGS00	5558	5509	5697
11/11/2010	LE71400412010315PFS00	5549	5543	5672
10/29/2011	LE71400412011302EDC00	5593	5526	5742
12/16/2011	LE71400412011350PFS01	5612	5566	5733

Table S4. Reference studies on the surface area and terminus glacier changes in the Himalaya and Tibetan Plateau.

Geographic region[a]	Period	Rate	Area (km^2 approx.)[b]	Location	Source
(a) Surface area loss (% a^{-1})					
CH-S	1962-2011	0.27	400	Sagarmatha (Mt. Everest) National Park (SNP) Nepal	This study
CH-S	1976-2000	0.15	1100	Koshi basin Nepal	Yao et al. (2012)
CH-S	1950s-1992	0.14	400	SNP Nepal	Salerno et al. (2008)
CH-S	1962-2005	0.12	90	North-East of SNP Nepal	Bolch et al. (2008)
CH-N	1976-2006	0.50	2700	Mt.Qomolangma National Nature Preserve, TP	Nie et al. (2010)
CH-N	1974-2008	0.30	150	Mt. Qomolangma region, TP	Ye et al. (2009)
CH-N	1970-2001	0.29	650	Pumqu river basin, Tibetan Plataeu	Jin et al. (2005)
WH-S	1960-2004	0.40	6300	Western Himalaya	Kulkarni et al. (2011)
WH-S	1962-2004	0.50	2077	Chenab, Parbati and Baspa	Kulkarni et al. (2007)
WH-N	1969-2010	0.34	90	Kang Tatze Massif, Ladakh	Schmidt and Nusser (2012)
WH-N	1976-2003	0.30	80	Naimona'nyi region	Ye et al. (2006b)
EH-S	1990-2010	0.17	200	Sikkim Himalaya	Basnett et al. (2013)
EH-S	1997-2004	0.38	400	Tista basin	Kulkarni et al. (2011)
EH-S	1963-1993	0.30	130	Bhutan	Karma et al. (2003)
EH-N	1970-2009	0.32	150	Boshula, mountain, Southeastern TP	Wang et al. (2011)
TP	1970-2001	0.20	900	Nam Co Basin, Southeast of West Nyainqentanglha	Yao et al. (2012)
TP	1976-2009	0.30	800	Nam Co basin	Bolch et al. (2010)
(b) Terminus retreat (m a^{-1})					
CH-S	1962-2011	8.2	400 (29)	SNP Nepal	This study
CH-S	1970-1979	2.4	33 (11)	Khumbu region	Yamada et al. (1992)
CH-S	1974-1999	6.9	7 (3)	Nepal Himalaya	Yao et al. (2012)
CH-N	1960-2001	7.1	130 (3)	Mt. Qomolangma region, TP	Ren et al. (2006)
CH-N	1980-2001	6.4	30 (2)	Mt. Xixiabangma, TP	Ren et al. (2006)
WH-S	1962-2008	14.4	15 (2)	Garhwal Himalaya	Mehta et al. (2011)
WH	1960s-2000	16.6	-- (20)	Garhwal, Kumaun, Himachal and sourrounding	Yao et al. (2012)
EH-S	1963-1993	27.0	130 (66)	Bhutan Himalaya	Karma et al. (2003)
EH-S	1976-2005	13.0	-- (26)	Sikkim Himalaya	Raina (2009)
TP	1970-2007	16.3	55 (5)	Nyainqentanglha mountain region	Yao et al. (2012)

[a] CH, WH, EH, and TP represent Central Himalaya, Western Himalaya, Eastern Himalaya and Tibetan Plateau, respectively (suffixes -N and -S indicate the north and south, respectively);

[b] Numbers in bracket represent the number of glaciers

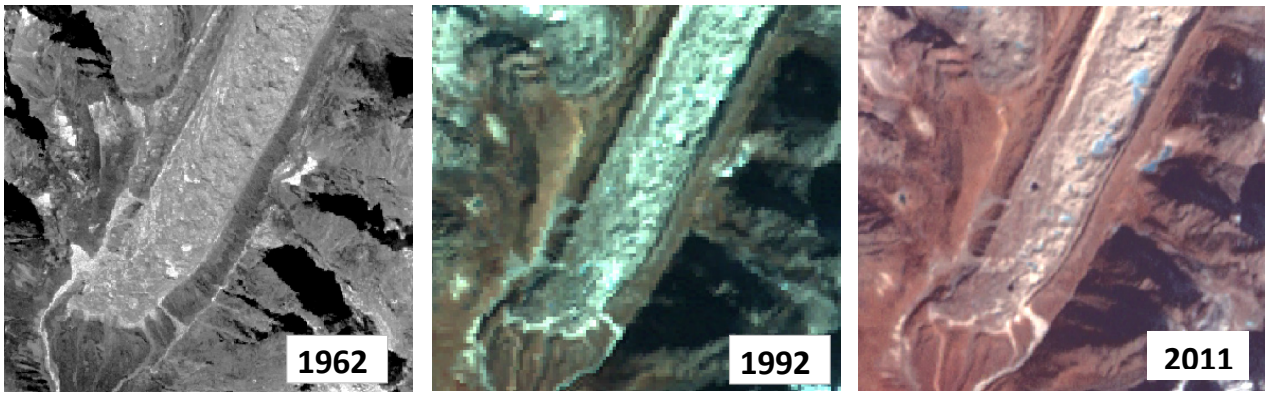

Fig. S1. The terminus of Khumbu glacier based on the 1962 Corona, 1992 Landsat TM, and 2011 Landsat ETM+ imagery. We can observe that since 1962 there is no retreat of the distal part of the terminus.

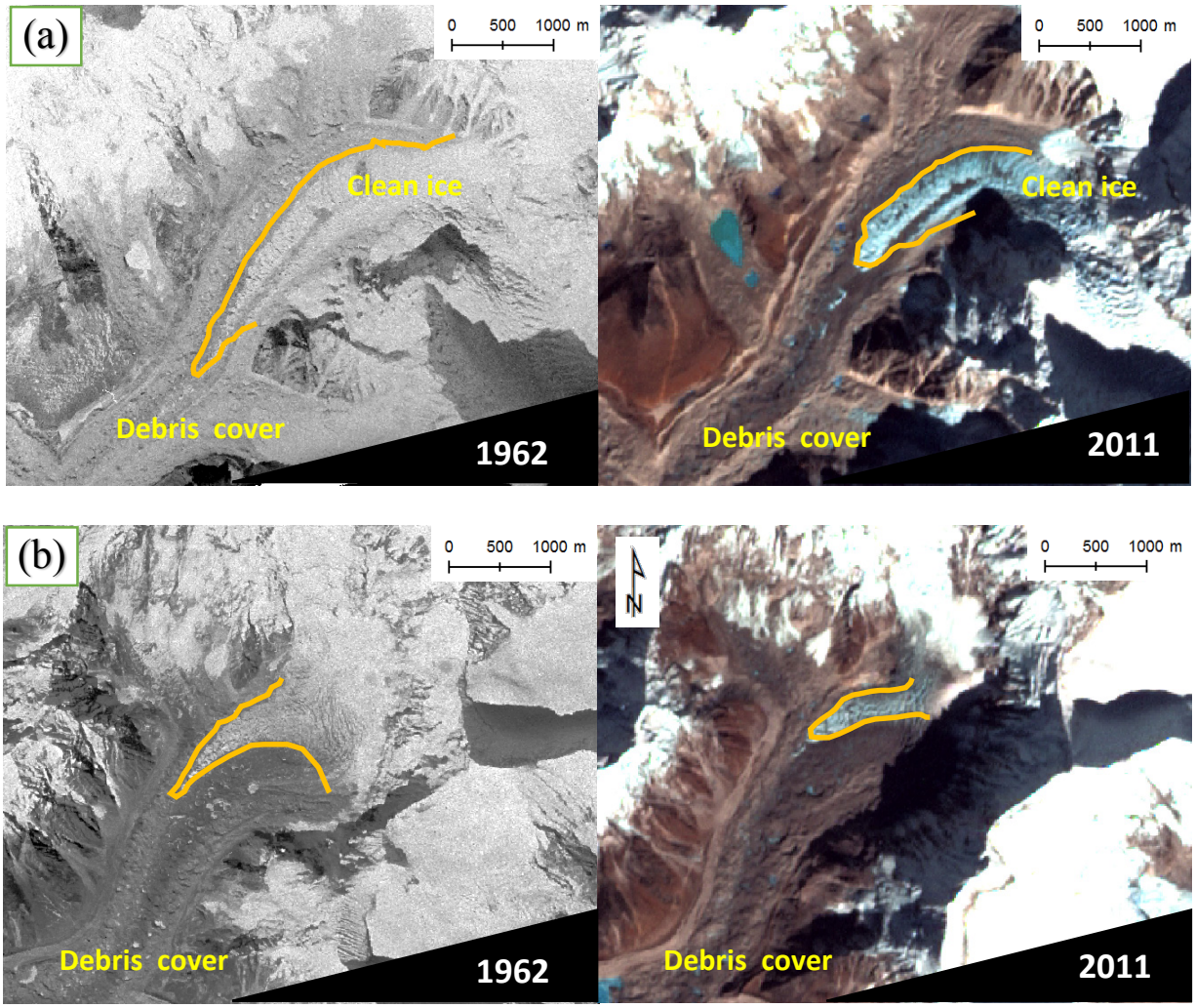

Fig. S2. Transition zone between debris cover and debris-free ice area of, **(a)** Khumbu glacier and **(b)** Imja glacier. The images clearly show an increase in the debris cover area between 1962 and 2011.

References

Basnett, S. Kulkarni, A., and Bolch, T.: The influence of debris cover and glacial lakes on the recession of glaciers in Sikkim Himalaya, India, J. Glaciol., 59, 1035-1046, 2013.

Bolch, T., Yao, T., Kang, S., Buchroithner, M. F., Scherer, D., Maussion, F., Huintjes, E., and Schneider, C.: A glacier inventory for the western Nyainqentanglha Range and the Nam Co Basin, Tibet, and glacier changes 1976–2009, The Cryosphere, 4, 419-433, doi:10.5194/tc-4-419-2010, 2010.

Jin, R., Li, X., Che, T., Wu, L., and Mool, P.: Glacier area changes in the Pumqu river basin, Tibetan Plateau, between the 1970s and 2001, J. Glaciol., 51, 607-610, 2005.

Karma, Ageta, Y., Naito, N., Iwata, S., and Yabuki, H.: Glacier distribution in the Himalayas and glacier shrinkage from 1963 to 1993 in the Bhutan Himalayas, Bull. Glaciol. Res., 20, 29-40, 2003.

Kulkarni, A.V., Bahuguna, I.M., Rathore, B.P., Singh, S.K., Randhawa, S.S., and Sood, R.K. Dhar, S.: Glacial retreat in Himalaya using Indian Remote Sensing satellite data. Curr. Sci., 92, 69-74, 2007.

Kulkarni, A. V., Rathore, B. P., Singh, S. K., and Bahuguna, I. M.: Understanding changes in the Himalayan cryosphere using remote sensing techniques, Int. J. Remote Sens., 32, 601-615, 2011.

Mehta, M., Dobhal, D. P., and Bisht, M. P. S.: Change of Tipra Glacier in the Garhwal Himalaya, India, between 1962 and 2008, Prog. Phys. Geogr., 35, 721-738, 2011.

Nie, Y., Zhang, Y., Liu, L., and Zhang, J.: Glacial change in the vicinity of Mt. Qomolangma (Everest), central high Himalayas since 1976, J. Geogr. Sci., 20, 667-686, 2010.

Raina, V. K.: Himalayan Glaciers: A State-of-Art Review of Glacial Studies, Glacier Retreat and Climate Change, MoEF Discussion Paper, Government of India- Ministry of Environment and Forests, 56 pp., 2009.

Ren, J., Jing, Z., Pu, J., and Qin, X.: Glacier variations and climate change in the central Himalaya over the past few decades, Ann. Glaciol., 43, 218-222, 2006.

Schmidt, S. and Nüsser, M.: Changes of High Altitude Glaciers from 1969 to 2010 in the Trans-Himalayan Kang Yatze Massif, Ladakh, Northwest India, Arct. Antarct. Alp. Res., 44, 107-121, 2012.

Wang, W., Yao, T., and Yang, X.: Variations of glacial lakes and glaciers in the Boshula mountain range, southeast Tibet, from the 1970s to 2009, Ann. Glaciol., 52, 9-17, 2011.

Yamada, T., Shiraiwa, T., Ilda, H., Kadota, T., Watanabe, T., Rana, B., Ageta, Y., and Fushimi, H.: Fluctuations of the glaciers from the 1970s to 1989 in the Khumbu, Shorong and Langtang regions, Nepal Himalayas, Bull. Glacier Res. 10, 11-19, 1992.

Yao, T., Thompson, L., Yang, W., Yu, W., Gao, Y., Guo, X., Yang, X., Duan, K., Zhao, H., Xu, B., Pu, J., Lu, A., Xiang, Y., Kattel, D. B., and Joswiak, D.: Different glacier status with

atmospheric circulations in Tibetan Plateau and surroundings, Nat. Clim. Change, 2, 663-667, 2012.

Ye, Q., Yao, T., Kang, S., Chen, F. and Wang, J.: Glacier variations in the Naimona'nyi region, western Himalaya, in the last three decades. Ann. Glaciol., 43, 385-389, 2006b.

Ye, Q., Zhong, Z., Kang, S., Stein, A., Wei, Q., and Liu, J.: Monitoring glacier and supra-glacier lakes from space in Mt. Qomolangma region of the Himalayas on the Tibetan Plateau in China, J. Mt. Sci. [China], 6, 211–220, 2009.

Article III

8.3 Article III

Thakuri, S., F. Salerno, T. Bolch, N. Guyennon, and G. Tartari (2015) Increased Imja Lake expansion as response to reduced Imja Glacier flow velocity (Mt. Everest region, Nepal). ***Submitted*****.**

Increased Imja Lake expansion as response to reduced Imja Glacier flow velocity (Mt. Everest region, Nepal)

THAKURI Sudeep,[1,2] SALERNO Franco,[1,3] BOLCH Tobias,[4,5]
GUYENNON Nicolas,[1] TARTARI Gianni[1,3]

[1]*National Research Council, Water Research Institute (IRSA-CNR), Via del Mulino 19, 20861 Brugherio, Italy*
E-mail: thakuri@irsa.cnr.it

[2]*Department of Earth Sciences "Ardito Desio", University of Milan, Via Mangiagalli 34, 20133 Milan, Italy*

[3]*Ev-K2-CNR Association, Via San Bernardino 145, Bergamo 24126, Italy*

[4]*Department of Geography, University of Zurich, Winterthurerstr. 190, CH-8057 Zurich, Switzerland*

[5]*Institute for Cartography, Technische Universität Dresden, Helmholtzstr. 10, 01069 Dresden, Germany*

ABSTRACT. In this paper, we link increased Imja Tsho (Lake) with changes in Imja Glacier (area: ~25 km^2) under the effect of climate change using multi-temporal satellite imagery and local climate data. Between 1962 and 2013, Imja Lake has expanded from 0.029 ± 0.010 km^2 to 1.352 ± 0.054 km^2 (0.026 ± 0.001 km^2 a^{-1}). The average glacier flow velocity was 37 ± 30 m a^{-1} in 1992-93; 31 ± 15 m a^{-1} in 2000-01, and 21 ± 15 m a^{-1} in 2013-14, indicating a reduction in the glacier velocity. An average glacier elevation change of -1.59 ± 0.71 m a^{-1} observed for 2001-14 period with a rate of -1.78 ± 0.80 m a^{-1} in 2008-14 and -1.40 ± 0.63 m a^{-1} in 2001-08. We underline that the decrease in velocity is mainly associated with reduced accumulation due to significantly decreasing precipitation in the last decades and increased ablation due to increasing of maximum temperature that effectively impact the glacier during the post-monsoon months. The decreasing glacier flow velocities and the increasing mass losses induce the formation and subsequent expansion of glacial lakes under a favourable topography as boundary condition.

KEYWORDS: glacier flow velocity, elevation change, glacial lake, Everest

1. INTRODUCTION

The Everest region is most characterized by large debris-covered glaciers (Scherler and others, 2011) and many glacial lakes (Gardelle and others, 2011; Salerno and others, 2012). Previous studies revealed that areas of proglacial lakes increased on the south slopes of Mt. Everest since the early 1960s (Bolch and others, 2008a; Tartari and others, 2008; Gardelle and others, 2011). Many studies have indicated that the current moraine-dammed or ice-dammed lakes are the consequences of coalescence and the growth of supraglacial lakes (e.g., Fujita and others, 2009; Watanabe and others, 2009; Thompson and others, 2012). Such lakes pose a potential threat of the glacial lake outburst floods (GLOFs; e.g., Richardson and Reynolds, 2000; Bajracharya and others, 2007; Benn and others, 2012) with the potential consequent loss of human lives and properties in the downstream valley. One of such proglacial lakes in the Everest region, Imja Tsho (Lake), that evolved and in the continuing growth since the early 1960s, has been of great research interest due to its potential GLOF risk (e.g., Yamada, 1998; Bajracharya and others, 2007; Fujita and others, 2009).

Glacier flow velocity (V_f) and elevation change (ΔE) are key variables that reflect the glacier status and provide information about the influence of ongoing climate change (Cuffey and Paterson, 2010; Paul and others, 2013). In the Everest region, using the geodetic approach, Bolch and others (2011) studied the mass change for 10 glaciers and found that the glaciers have exhibited a significant mass loss of 0.32 ± 0.08 m a^{-1} w.e. in 1970-2007 and 0.79 ± 0.52 m a^{-1} w.e. in 2002-2007. However, Gardelle and others (2013) reported lower mass loss (0.41 ± 0.21 m a^{-1} w.e.) in 1999-2011. Some other studies (Scherler and others, 2008; Bolch and others, 2008a; Quincey

and others, 2009; Peters and others, 2010) have addressed V_f for selected glaciers for a short span of time (from days to a few years) and highlighted that the present condition of ice stagnation in the lower ablation region of glaciers is attributable to low V_f generated by a general negative mass balance, but it is not yet clear how the velocities are evolving due to lack of contiguous measurements. Quincey and others (2009), measuring the glacier velocities between 1992 and 2002 in this region, indicated a general flow recession of the glaciers and demonstrated that the stagnant snouts are characterized by very low (<2°) surface slope, suggesting a strong topographic control on the glacier flow in the region.

With regard to glacial lakes, previous studies in the Everest region addressed the evolution of lakes (Tartari and others, 2008; Gardelle and others, 2011; Somos-Valenzuela and others, 2014), their potential GLOF hazard or risk (Yamada, 1998; Bolch and others, 2008a; Watanabe and others, 2009; Benn and others, 2012), and the condition of formation (Benn and others, 2001; Fujita and others, 2009; Sakai and Fujita, 2010; Salerno and others, 2012) using field and remote sensing methods. Bolch and others (2008), Quincey and others (2009), and Salerno and others (2012) pointed out that changes in the V_f are a possible trigger for the formation of glacial lakes. However, still there are no studies addressing the nexus between contemporary variation of glacier properties and lakes surface evolution.

Considering Imja Lake as one of the most potentially dangerous proglacial lakes, in this paper, we present temporal variation of Imja Glacier and Imja Lake between 1960s and 2014, with particular emphasize in last two decades with the aim of linking the glacier properties to the evolution of lake surface area (*Surf*). Further, we present local temperature and precipitation behaviours and discuss on, how could they potentially drive the changes?

2. STUDY AREA

Imja Glacier (27.86 to 27.96 N; 86.90 to 86.98 E), covering an area of 24.7 km^2 in 2013 (this study), lies in the *Sagarmatha* (Mt. Everest) National Park (SNP), the upper catchment area of the Dudh Koshi river in Nepal Himalaya (Fig. 1). In this study, we consider three branches/glaciers that extend towards South (Amphu Lapcha), East (Imja), and Northeast (Lhotse Shar), collectively as Imja Glacier by following the name for this complex as in Salerno and others (2008) and Thakuri and others (2014), that is, in line with the GLIMS database (GLIMS and NSIDC, 2005, updated 2014). Even though three of such glaciers have a separate ice divide in the accumulation area, they were connected to each other through their tongues, but from the last few years, tongue of Amphu Lapcha branch is no more connected to Imja-Lhotse Shar.

The Everest region is one of the most heavily glacierized parts of the Himalaya. Most of the large glaciers are D-type i.e. the ablation zone is partially covered with supraglacial debris (Fujii and Higuchi, 1977). Recently, Thakuri and others (2014) presented 29 glaciers (> 1 km^2) and other small glaciers (< 1 km^2), covering an area of nearly 350 km^2 (in 2011) out of 1148 km^2 of the SNP. They found a glacier surface loss of 13%, an average terminus retreat of ~ 400 m, a snow-line altitude (SLA) upward shifting of 180 m, and an increasing of debris-coverage by 17% from the 1960s to 2011 at the south slope of Mt. Everest. Salerno and others (2012) reported a total of 624 lakes in the SNP: 17 proglacial, 437 supraglacial, and 170 unconnected lakes. Further, they presented that 0.3 to 2.0% of the glacier ablation surface is covered by supraglacial lakes.

Imja Glacier is one of the largest debris-covered glaciers in the region, extending from an elevation of ~ 5000 to 7800 m asl. with an area-weighted mean elevation of 5877 m. Nearly 80% of the glacier *Surf* lies between an elevation range of 5000 - 6500 m (Fig. 1c). In 2011, the glacier had an average slope of 33°, an average SLA position at 5742 m, and 27 % of the glacier *Surf* was covered by debris (Thakuri and others, 2014). Imja Lake evolved close to the glacier terminus (~ 5000 m asl.) during the 1960s. The frontal ice of Imja Glacier is calving into Imja Lake and the lake is continuously increasing in size (e.g., Fujita and others, 2009). Based on a recent study of Somos-Valenzuela and others (2014), the lake had *Surf* of 1.257 km^2 (2012). In the same study, the sonar bathymetric survey in 2012 has indicated a maximum depth of the lake 116.3 ± 5.2 m with an estimated volume of 61.7 ± 3.7 million m^3.

The climate of this region is characterized by the south Asian monsoon and the westerlies. Imja Glacier is a summer accumulation type, the glacier mainly fed by the monsoon, as the winter precipitation caused by westerly wind is minimal (Salerno and others, 2014). The prevailing direction of the monsoons is South–North and Southwest–Northeast (e.g., Ichiyanagi and others, 2007). The observation records from the automatic weather stations (AWSs;) at the Pyramid Observatory Laboratory (27.96 N, 86.81 E;

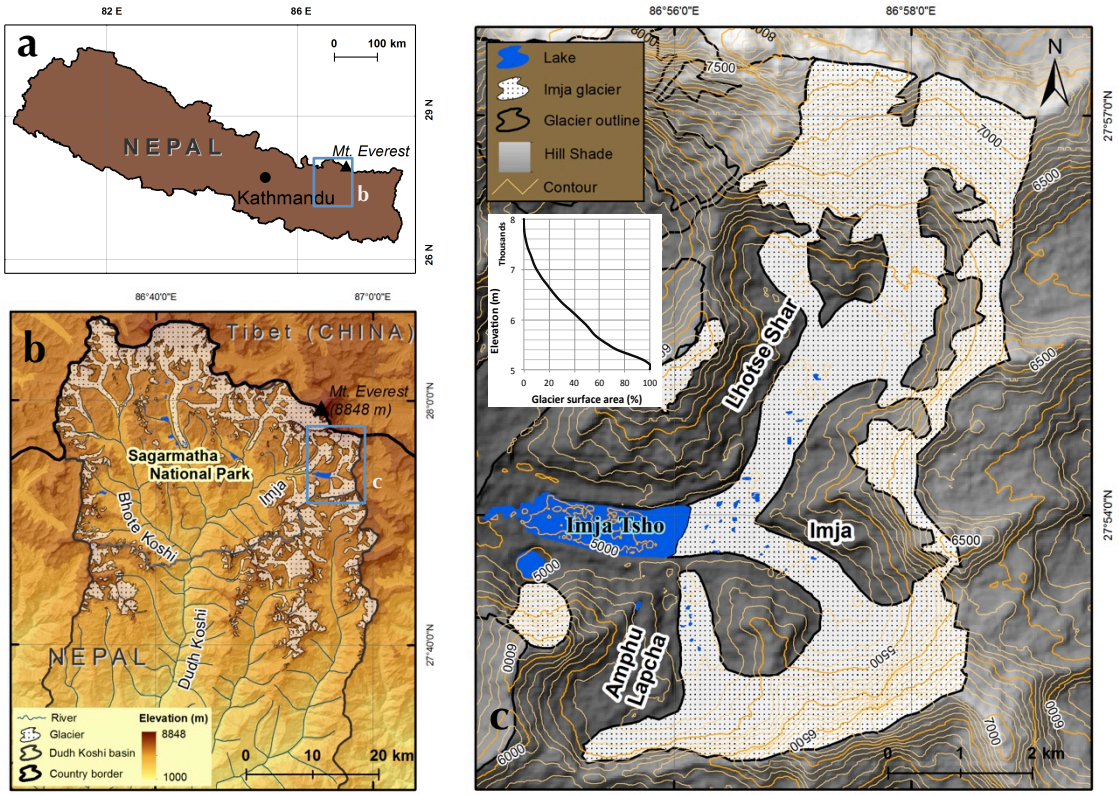

Fig. 1. Location of the reference study site in the map of Nepal (a) and the Dudh Koshi river basin (b), is marked by a rectangular box. The focused map of the site (c) shows Imja Glacier and Lake (s) in 2013. Further, the surface area - elevation curve for Imja Glacier is inset to (c).

elevation 5050 m asl.) from 1994 to 2013 show an annual mean temperature (MeanT) of –2.4 ± 0.5°C and a total annual precipitation of 449 ± 75 mm a^{-1}, with about 90 % of the annual precipitation amount recorded during the summer months (Jun–Sep). The temperature decreases with altitude (0.6 °C per 100 m) and the precipitation increases (116 mm per 100 m) until ~ 2600 m and decreases afterwards, along the Dudh Koshi river valley (Salerno and others, 2014).

3. DATA AND METHODS

3.1 Data sources

Multi-temporal satellite imagery from different sensors and topographic maps were used for assessing glacier properties and lake *Surf* variations (Table 1).

Additionally, 1) topographic map of 1963 (*cf.* Thakuri and others, 2014); 2) all Landsat ETM+ scenes of 2001 and one scene every year from 2002 to 2012 (20 scenes) after the ablation season (Oct to Dec), and 3) Landsat 8 OLI scenes of 2014 (8 scenes), with no or minimum cloud cover, were used for the lake study. For glacier study, same datasets as in Thakuri and others (2014) were used until 2011 and the analysis was updated to 2013 by using Landsat 8 OLI data of 10 Oct, 2013 (Table 1) for homogeneous comparison between the glacier, lakes, and climate. Furthermore, the Advanced Spaceborne Thermal Emission and Reflection Radiometer Global Digital Elevation Model (ASTER GDEM) version 2, a product of METI and NASA, was used. For climate interpretation, the same datasets as in Salerno and others (2014) were used.

Landsat data were used (retrieved from, https://earthexplorer.usgs.gov) for the velocity measurements in three periods: 1992-93, 2000-01, and 2013-14, as they were freely available. The analysis could be extended until the beginning of 1990s with 30 m resolution data and 15 m from 1999, however we reinforced the results by comparison with previous study that used ASTER data. Due to the partial coverage of Imja Glacier by 2014 ASTER scene, we were able to compare the ΔE for only lower ablation part of the glacier.

Table 1. Datasets used in the study

Acquisition date	Mission/Sensor	Resolution (m)	Scene ID	Application*
15 Dec, 1962	Corona KH-4	~8	DS009050054DA175_175	Lake
20 Nov, 1970	Corona KH-4B	~5	DS1112-1023DF157_157	Lake
2 Nov, 1975	Landsat 4 MSS	60	LM21510411975306AAA05	Lake
17 Nov, 1992	Landsat 5 TM	30	LT51400411992322ISP00	V_f, Lake
04 Nov, 1993	Landsat 5 TM	30	LT51400411993308ISP00	V_f
30 Oct, 2000	Landsat 7 ETM+	15**	LE71400412000304SGS00	V_f , Lake
17 Oct, 2001	Landsat 7 ETM+	15**	LE71400412001290SGS00	V_f
10 Oct, 2013	Landsat 8 OLI	15**	LC81400412013283LGN00	V_f, Lake
22 May, 2014	Landsat 8 OLI	15**	LC81400412014142LGN00	V_f, Lake
24 Oct, 2008	ALOS AVNIR 2	10	ALAV2A14647304	Lake
20 Dec, 2001	Terra ASTER	15	AST_L1A_00312202001050229_2009 0617073207_20295	ΔE
06 Jan, 2008	Terra ASTER	15	AST_L1A_00301062008045936_2009 0617065646_14098	ΔE
22 Nov, 2014	Terra ASTER	15	AST_L1A_00311222014045939_2014 1210051220_17098	ΔE

* V_f Glacier flow velocity; ΔE Elevation change
** Panchromatic band and pan-sharpened image.

3.2 Methods

3.2.1 Lake surface area (Surf)

To extract the lake outlines from the Landsat imagery, the normalized difference water index (NDWI, [NIR-BLUE]/[NIR+BLUE]), originally proposed by McFeeters (1996) and successfully applied by Bolch and others (2008a) for our region, was applied with a manual post-correction for shadowed areas and ice parts. When the NDWI method was not appropriate (like, in topographic map and panchromatic Corona imagery) the lake boundaries were manually digitized.

The uncertainties of mapping a single glacial lake from an image were estimated as a product of the linear resolution error (*LRE*) and the perimeter (*l*) (Fujita and others, 2009; Salerno and others, 2012). As of these studies, we used 0.5 pixel resolution for the *LRE* assuming that the lake margin passes through centre of the pixel along its perimeter. Then, the uncertainties in the changes of surface area (Δ*Surf*) were derived according to standard error propagation rule, the root of sum of square (*RSS,* $uncertainty = \sqrt{e_1^2 + e_2^2}$ where e_1 and e_2 are uncertainties from first and second scenes) of the mapping uncertainty for the single scene. We did not consider the coregistration error, as the comparison was not by pixel to pixel.

3.2.2 Glacier variables

In this study, different glacier variables are analysed: Δ*E*, V_f, *Surf*, terminus, SLA, and debris coverage. Detail methods are provided for Δ*E* and V_f here, while for other variables, we applied the same methods and uncertainties as in Thakuri and others (2014).

a. Glacier flow velocity (*Vf*)

The velocities were derived from the image pairs using feature-tracking method on the glacier surface using the normalized cross-correlation (NCC) algorithm in the Correlation Image Analysis Software (CIAS; Kääb and Vollmer, 2000). The NCC algorithm was used among several other options of image correlation because none of the single method outperforms among them. It is a simple and widely used algorithm for correlation of images that performs better in narrow glaciers (Heid and Kääb, 2012; Paul and others, 2013). The image pairs were coregistered before image correlation. The root mean square error (RMSExy) after the coregistration was 21.2, 12.8, and 4.9 m for 1992-93, 2000-01, and 2013-14, respectively. The potential outlier values higher than 100 m offset, and the maximum correlation coefficient lower than 0.6 were discarded. The gaps remaining after the removals of outlier values were filled linearly using kriging interpolation.

The potential uses of Landsat data for velocity measurements are well-demonstrated in previous studies (e.g., Kääb and others, 2006; Paul and others, 2013). Deriving velocities from Landsat imagery with 30 m (TM) and 15 m (ETM+ pan) spatial resolution entails certain limitations that need to be considered while interpreting the results. Paul and others (2013) asserted that the accuracy of velocity measured using high to very-high resolution SAR data with a time interval of one orbital cycle is about 10 m a^{-1}, similar to the accuracy for medium-resolution optical satellite imagery (e.g. Landsat ETM+ pan) that is on the

order of 15 m a^{-1} for images acquired one year apart. Landsat data covers a wide spatial and temporal range and produce good results for fast flowing glaciers, however the capacity to capture the V_f of very slowly flowing glaciers can be limited by their resolution. Previous studies indicated that displacement values below a pixel have high uncertainty. In this study, the images coregistration errors – RMSExy - that was calculated after the coregistration of image pairs for measuring the velocity did not exceed one pixel of the image. Thus, we consider an average uncertainty of one pixel size.

b. Glacier elevation change (ΔE)

The digital elevation model (DEM) differencing method was used for computing the glacier Δ*E* from the multi-spectral Terra ASTER images (Paul and Haeberli, 2008; Bolch and others, 2011). The ASTER has four VNIR (15 m) bands including a backward looking band (3B) that has stereoscopic viewing capabilities for generating DEMs (Toutin, 2008; Kamp and others, 2005). We generated 30 m DEMs for 2001, 2008, and 2014 from the cloud free ASTER stereo bands, Nadir (3N) and backward looking (3B). For coregistration of the ASTER stereo bands, around 25-ground control points (GCPs) were obtained for the identifiable objects (e.g., mountain peaks, river crossings, rocks) in the Landsat OLI of 2013. The elevation information was obtained from the ASTER GDEM. The coregistration model was accepted when the RMSEs of GCPs were less than a pixel (15 m) and applied enhanced Automated Terrain Extractor (eATE) function in Leica Photogrammetric Suite (LPS) of ERDAS Imagine software.

The elevation differences between the generated DEMs of 2001- 2008, and 2001 - 2014 were calculated considering 2001 as the reference DEM. The generated DEMs were coregistered, using method by Nuth and Kääb (2011), to ensure the comparability and quality of the DEMs. We applied the computed horizontal and vertical (i.e. RMSEx,y,z) shift to the 2008 and 2014 DEMs. We filtered the elevation difference values > 7.5 m a^{-1} (higher than 3σ) as possible outliers in the measurement considering the length of analysis period (Nuth and Kääb, 2011; Nuimura and others, 2012). The remaining gaps were filled linearly using the kriging interpolation.

The measurement uncertainties of the Δ*E* were estimated using the Normalized Median Absolute Deviation (NMAD; Höhle and Höhle, 2009) derived from a sample of terrain outside the glacier. The NMAD is a robust method for uncertainties estimation and is considered to be less sensitive to outliers than the standard deviation or RMSE method. It is calculated as,

$$NMAD = 1.4826 * median_i(|\Delta h_i - m_{\Delta h}|),$$

where Δh_i represents the individual errors i = 1, 2, …., n and $m_{\Delta h}$ is the median of the errors.
The estimated NMAD were 4.4 m for the Δ*E* between 2001 and 2008, and 9.2 m for the 2001 and 2014.

4. RESULTS

4.1 Glacier variations

4.1.1 Glacier surface area (Surf), terminus, and snow-line altitude (SLA) variation

The *Surf* of Imja Glacier reduced from 28.1 ± 0.5 km^2 (1962) to 24.7 ± 0.6 km^2 (2013) with a rate of -0.067 ± 0.014 km a^{-1} (-0.24 % a^{-1}) (Fig. 2; Table 2). Previous studies (Bolch and others, 2008b; Thakuri and others, 2014) indicated an accelerated glacier shrinkage after 1990s in the Everest region. We found that Imja Glacier has experienced a loss of 0.11 ± 0.05 km^2 a^{-1} in 1992 to 2013 compared to 0.04 ± 0.03 km a^{-1} from 1962 to 1992, nearly three times more and in agreement with those studies.

The terminus of Imja Glacier has retreated by 2256 ± 9 m (~ 44 m a^{-1}) from 1962 to 2013 (Table 2). This rate of change is the highest one within the SNP (*cf.*, Thakuri and others, 2014). This could be attributed to the presence of the proglacial Imja Lake, which enhance glacier melt and favours mass loss due to calving. A higher retreat of debris-covered glaciers with proglacial lakes than without proglacial lakes was also found in Sikkim Himalaya (Basnett and others, 2013). Further, the SLA position in Imja Glacier has shifted upward by 456 ± 30 m (average ~ 9 m a^{-1}), from 5340 ± 20 m to 5796 ± 21 m between 1962 and 2013 (Fig. 2b) The upwards shift of the SLA indicates a clear negative trend for mass balance. Figure 2c and Table 2 shows an increasing DebrisCov area from 5.59 ± 0.09 km^2 to 6.93 ± 0.16 km^2 (average 0.026 ± 0.004 km^2 a^{-1}) between 1962 and 2013. It was estimated without considering the common glacier *Surf* (2013) impacted by the evolution of the lake in all year.

Figure 2d presents the glacier Δ*Surf* by elevation for two periods: 1962-1992 and 1992-2013. The comparison between them stresses an opposite trend: for 1962-1992, the main *Surf* reductions are below 5750 m, while there is an increasing at

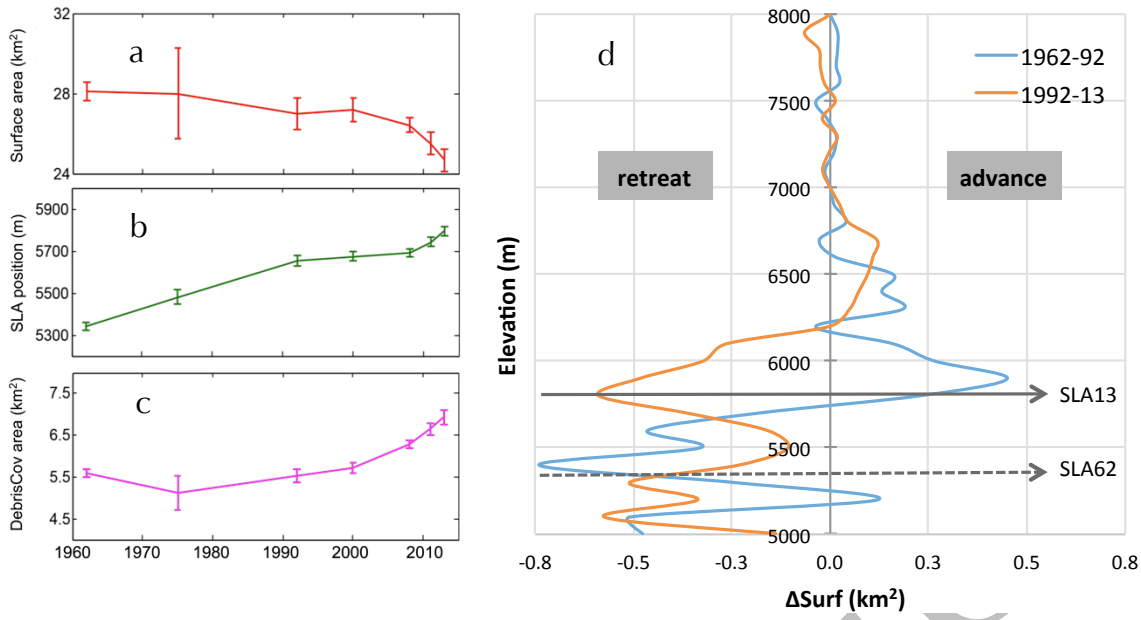

Fig. 2. Changes in Imja Glacier variables. (a) Surface area (*Surf*), (b) Snow-line altitude (SLA), and (c) Debris-covered (DebrisCov) area between 1962 and 2013; (d) The glacier *Surf* change (ΔSurf) by elevation in 1962-1992 and 1992-2013 periods. In the same plot, the SLA positions are marked for 1962 and 2013.

Table 2. Data on surface area (*Surf*), terminus, snow-line altitude (*SLA*), debris-covered (*DebrisCov*) area, and morphological parameters for Imja Glacier and lakes in 1962-2013 period

Variable/parameter	1962	1975	1992	2000	2008	2011	2013
Imja Glacier							
Surf (km²)	28.1 ± 0.5	28.0 ± 2.2	27.0 ± 0.8	27.2 ± 0.6	26.4 ± 0.4	25.5 ± 0.6	24.7 ± 0.6
Terminus change (m)	0	-862 ±30	-1320±11	-1656±9	-1911±6	-2118±9	-2256±9
SLA (m)	5340±20	5480±35	5655±25	5673±21	5691±21	5742±21	5796±21
DebrisCov area (km²)*	5.59±0.09	5.11±0.41	5.53±0.16	5.71±0.12	6.28±0.09	6.65±0.15	6.93±0.16
Slope (°)	30	33	32	33	33	33	33
Aspect (°)	210	204	210	212	215	218	218
Min elevation (m)	4980	4981	4986	4989	4981	5007	5023
Max elevation (m)	7971	8226	8226	7803	7803	7803	7808
Mean elevation (m)	5768	5807	5833	5844	5877	5877	5898
Imja Lake							
Surf (km²)	0.029±0.010	0.139±0.019	0.704±0.029	0.841±0.036	1.013±0.046	1.243±0.054	1.352±0.054
Perimeter (km)	2.605	2.533	3.888	4.793	4.829	5.939	6.866
Supraglacial lakes							
Surf (km²)	0.037 ±0.014	-	0.077±0.038	0.065±0.029	0.066±0.024	0.082±0.045	0.102±0.045
Number	8	-	16	23	24	25	25

** DebrisCov area was calculated by excluding common (2013 Imja Lake) glacier Surf impacted by Imja Lake growth in all years*

Table 3. Glacier elevation change (Δ*E*)

	Period	Imja Glacier	For 10 common glaciers*	Source
ΔE m a^{-1}	2008-2014	–1.78 ± 0.80	-	This study
	2001-2014	–1.59 ± 0.71	-	
	2001-2008	–1.40 ± 0.63	–0.73 ± 0.63	
Δm m a^{-1} w.e.	2002-2007	–1.45± 0.52	–0.79 ± 0.52	Bolch and others (2011)
	2000-2008	–0.93± 0.60	–0.45 ± 0.60	Nuimura and others (2012)
	1999-2011	–0.70 ± 0.52	–0.41 ± 0.21	Gardelle and others (2013)

** in the south of Mt. Everest as in Bolch and others (2011); ΔE elevation change; Δm mass change*

higher elevation. For 1992-2013, a clearly decreasing of glacier *Surf* was observed even in further higher elevations (until 6200 m). Such different behaviours are a response to climate as discussed in Section 5.2.

4.1.2 Glacier elevation change (ΔE)

Imja Glacier has experienced an average Δ*E* of –1.59 ± 0.71 m a^{-1} for 2001-14 compared to –1.40 ± 0.63 m a^{-1} in 2001-08 indicating an increased negative rate (–1.78 ± 0.80 m a^{-1} in 2008-14) in the last few years. However, the difference is not significant given the high uncertainty (Fig. 3, Table 3). The glacier area close to Imja Lake in 2001 has experienced a Δ*E* of -2.30 ± 0.71 m a^{-1} in 2001-14 period, relatively higher than the rest of the glacier, due to the expansion of the lake from 2001 to 2014.

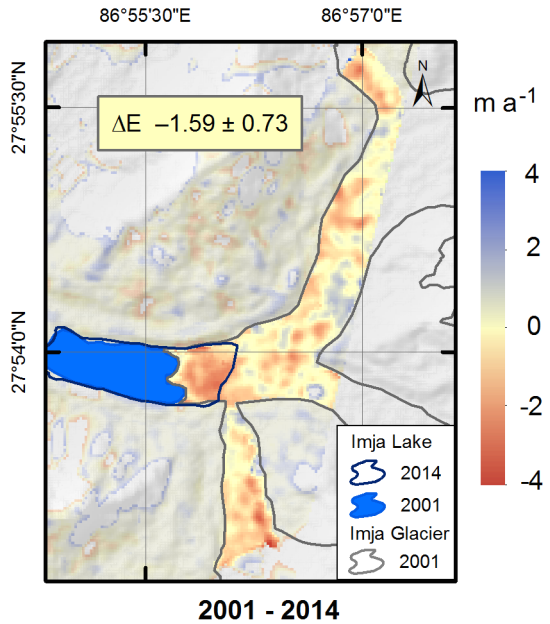

Fig. 3. Glacier elevation change (Δ*E*) of Imja Glacier for 2001-2014 period

The observed rate of Δ*E* for Imja Glacier was the highest one among the analysed glaciers of this region. During calculation of Δ*E* for Imja Glacier in 2001-2008, we simultaneously considered other glaciers in SNP and found that glaciers in this region (102.5 km^2) have experienced an overall Δ*E* of –0.66 ± 0.63 m a^{-1}. The estimated Δ*E* for 2001-08 is comparable with previous findings. Bolch and others (2011), Nuimura and others (2012), and Gardelle and others (2013) studied the mass loss for 10 glaciers in the Everest region (Table 3). We found a mass loss of -0.62 ± 0.68 m a^{-1} w.e. (0.73 ± 0.63 m a^{-1}) for 2001-2008 considering the same glaciers set (using ice density 850 ± 60 kg m^{-3} by Huss, 2013). Furthermore, all three studies reported the highest negative mass loss for Imja Glacier (Imja–Lhotse Shar; Table 5 of Gardelle and others, 2015 and Table 3 in this study). Bolch and others (2011) and Nuimura and others (2012) further affirmed an accelerated rate of mass loss in 2000-2008 compared to the previous period and suggested that the glacier surfaces connecting to a glacial lake in their terminus have experienced higher surface lowering.

4.1.3 Glacier flow velocity (Vf)

The computed velocities of Imja Glacier suggest an overall decreasing pattern of flow velocities (Fig. 4; Table 4). The glacier-wide average V_f was 37 ± 30 m a^{-1} in 1992-93, 31 ± 15 m a^{-1} in 2000-01, and 21 ± 15 m a^{-1} in 2013-14. On comparing the velocity profiles along the central flow line in each glacier's branch *(α, β, or γ)* for each period (Fig. 4b), we observe that lower V_f towards the terminus and higher velocities towards the glacier upward. Further, it indicates a clear decreasing of the V_f overtime.

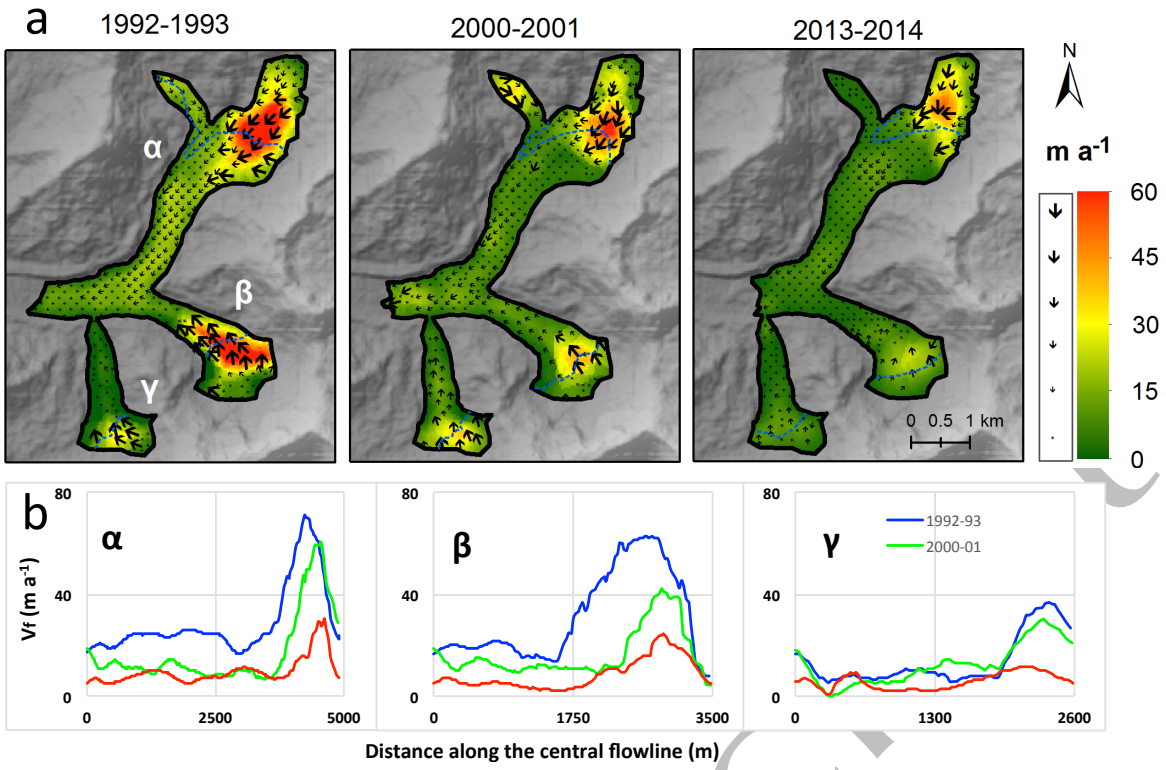

Fig. 4. Changes in the glacier flow velocity (*V*). (a) The *V* of glacier in three measurement times between 1990s and 2014; The estimated positions of the transition zone between debris-covered and debris-free glacier parts are marked by dotted blue lines; (b) The *V* profiles along the glacier central flow lines (α – Lhotse Shar, β – Imja, and γ – Amphu Lapcha) as shown in Figure 5c.

Table 4. Flow velocity (V_f) of Imja glacier

Measurement Time	Computed *Vf* (m yr^{-1}) for			Uncertainty (m yr^{-1})
	Debris-covered area	*Debris-free area*	*Glacier-wide average*	
1992-01	34	57	43	±30
2000-01	22	45	31	±15
2013-14	14	33	21	±15

The transition zone between debris-covered and debris-free glacier parts exhibits higher flow velocities (Fig. 4a), while glacier areas near Imja Lake have relatively lower velocities. In 1992-93, the glacier V_f was 34 ± 30 m a^{-1} and 57 ± 15 m a^{-1} for DebrisCov and upper debris-free area, respectively, while in 2013-14, it was 14 ± 15 m a^{-1} and 33 ± 15 m a^{-1} for DebrisCov and debris-free area respectively (Table 4). Considering the uncertainty of the measurement, we assert that V_f were very low or stagnant in the lower part of the glaciers, but the more striking differences were on the clean part of the glacier, where the decreasing V_f was apparently observed. Indeed, V_f has decreased by 43 % in 2013-14 compared to 1992-93. This confirms that a general decreasing of V_f in recent years. Further, the glacier

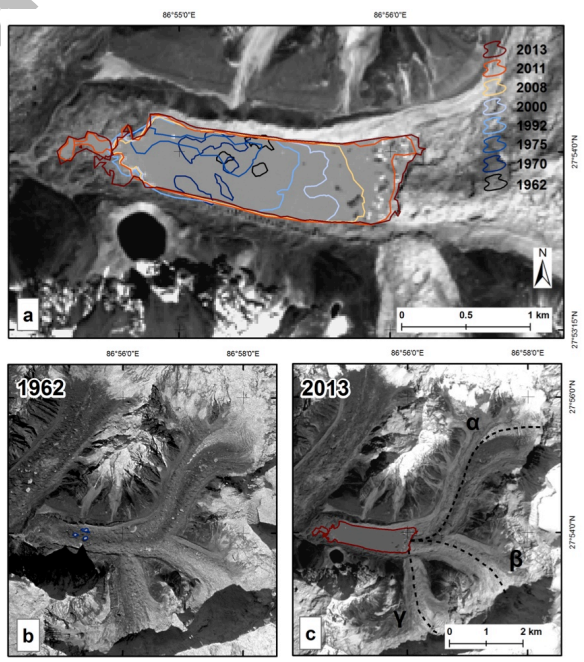

Fig. 5. Evolution of Imja Lake. (a) Temporal variation of surface area from 1962 to 2013. In the background, the Landsat 8 OLI image acquired on 10 October 2013; (b) Corona KH-4 scene of 2 Dec, 1962 and (c) again a Landsat scene of 2013 showing Imja Glacier and lake. Further, in (c), the central flow paths of the glacier's three branches are annotated as α, β, and γ.

experienced a higher velocity loss where higher negative ΔE was observed in 2001-2014 period, indicating that the decreasing of V_f could be induced by a more negative glacier mass balance (Fig. 3 and 4).

Few studies investigated the V_f in the region and most of them, only focused on the Khumbu glacier (Müller, 1968; Seko and others, 1998; Kodama and Mae, 1976; Nakawo and others, 1999; Luckman and others, 2007). Quincey and others (2007) estimated for a Lhotse Shar (α) branch, based on the Interferometry Synthetic Aperture Radar (InSAR) data of 29-30 March 1996, a glacier V_f of ~18 m a^{-1}, which is lower than our observed values of 1990s and 2000s. As discussed by Willis (1995), the intra-annual variations of the V_f are determined by various factors and thus, the V_f changes over the year. Our results are in line with Bolch and others (2008a) who showed, using ASTER data, that velocities of more than 40 m a^{-1} can be observed on the upper part of the Lhotse-Shar branch of Imja Glacier and found significantly lower velocities downwards the glacier (toward its terminus) for the period 2000 to 2003.

4.2 Lake evolution

4.2.1 Inter-annual variation of Imja Lake

Table 2, Figure 5, and Figure 6 present the variation of Imja Lake from 1962 to 2013. Imja Lake appeared in the 1960s as small ponds (Fig. 5b). The size of the lake (s) was 0.029 ± 0.010 km^2 in 1962 and has continuously increased to 1.352 ± 0.054 km^2 in 2013 (Fig. 6a) with the rate of 0.026 ± 0.001 km^2 a^{-1}. Imja Lake rapidly increased after 2008 (Fig. 6a).

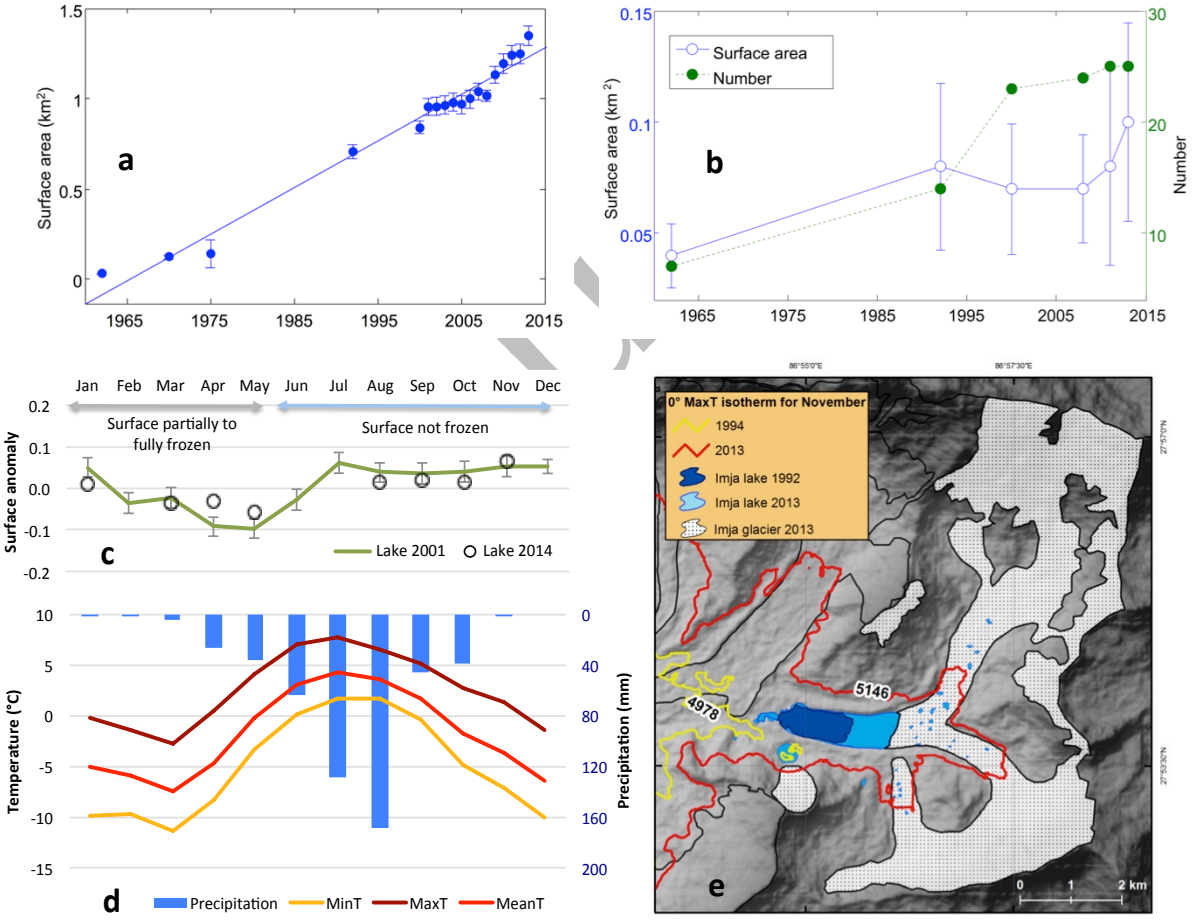

Fig. 6. Lake surface area change ($\Delta Surf$) and the climatic driver. **(a) The** $\Delta Surf$ of Imja Lake (~ 5000 m asl.) from 1962 to 2013; **(b)** Numbers and surface area variation of the supraglacial lakes present in Imja Glacier; **(c)** Intra-annual *Surf* variation for Imja Lake. The green line represents the surface anomaly (difference from mean, km) for 2001 and black circles for the 2014; **(d)** Variations of monthly minimum temperature (MinT), maximum temperature (MaxT), mean temperature (MeanT), and precipitation in 2001 from Pyramid station (5050 m asl.); The vertical bars in (a-c) represents uncertainty of measurement as described in the methods; **(e)** The 0°C isotherms of Nov. MaxT for the 1994 and 2013 are plotted. Further, the lakes distributions are indicated.

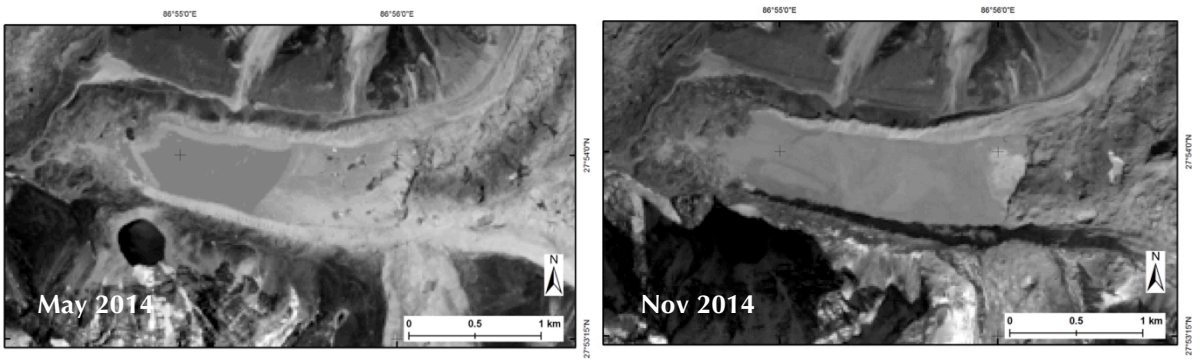

Fig. 7. Imja Lake, as seen from the Landsat 8 OLI image, acquired (a) on 22 May, 2014 indicating partially frozen and reduced lake surface area (*Surf*) and (b) on November 2014.

Based on the sonar bathymetric survey, Somos-Valenzuela and others (2014) reported that the depth of Imja Lake has increased from 90.5 to 116.3 ± 5.2 m and the volume raised from 35.8 ± 0.7 million m^3 to 61.7 ± 3.7 million m^3 in 2002 to 2012 period. They further indicated the *Surf* expansion rate for Imja Lake was 0.039 km^2 a^{-2} in 2002-2012, while in the same period we observed 0.029 ± 0.007 km^2 a^{-1}.

4.2.2 Intra-annual variation of Imja Lake

Figure 6c and 7 presents the intra-annual variation for Imja Lake *Surf*. We considered 2001 (Fig. 6c, green-line) as the main data for this analysis due to availability of good quality images covering all seasons for this year, however we enforced the analysis with available data of 2014 (circles). The figure indicates Minimum Lake surface in May (starting decreasing from Jan), just before the beginning of monsoon. In just two months, corresponding to the beginning of the monsoon and the possible glacier melting (as highlighted observing the lake surface in this period is not frozen), the lake surface reached a sort of plateau in terms of size. The size of the lake can be considered constant from Jul - Jan. So, the variability among lake surface in Jul - Jan is very low. Therefore, their inter-annual trend as detected in Fig. 6a, is not influenced significantly by the intra-annual variability inevitably introduced in the analysis as the satellite images are referred to post-monsoon period when the lake surface, as we observed, is constant.

4.2.3 Supraglacial lakes variation

Imja Glacier includes several supraglacial lakes (ponds) on its surface. We found 25 supraglacial lakes (all below 5210 m), with a total area of 0.102 ± 0.045 km^2 in 2013, and 8 lakes in 1962/63, with a total area of 0.037 ± 0.014 km^2. The differences was about three times more for both lake number and size in 2013 compared to 1960s. However, due to their very small sizes, the associated uncertainties in *Surf* are large (Fig. 6b). Such supraglacial lakes are ephemeral and very unstable in space and time as they can suddenly drain when they reach the sub-glacial drainage system (Benn and others, 2001).

5. DISCUSSION

5.1 Boundary conditions for evolution of lakes

Topographic settings are important parameters as they provide a boundary condition for the evolution of lakes (Quincey and others, 2009; Sakai and Fujita, 2010; Salerno and others, 2012). Some previous studies (Reynolds, 2000; Quincey and others, 2007; Röhl, 2008; Sakai and Fujita, 2010) demonstrated that in different parts of the world large glacial lakes can form on glaciers whose slope before lake formation is always < 2°, as surface gradient influences in ice dynamics. Further, Reynolds (2000) from the Bhutan Himalaya reported that isolated small ponds might form where the glacier slope is 6-10°. A glacial lake can develop due to low flow at high elevations and due to the occurrence of stagnant areas around the glacier terminus (Quincey and others, 2009). Lower slopes correspond to lower gravitational driving stresses that, by decreasing the glacier flow, allow the development of stagnant ice (Scherler and others, 2011), which is a favourable condition for the formation of lakes.

Salerno and others (2012) demonstrated that where lakes formed, both glacier slope and the interaction between the two glacier parts occur: upglacier (with steep slopes) and downglacier (with gentle slopes) influence the velocity of glaciers and, consequently, creates a favourable condition for lake formation. Thus, they reported that Imja Glacier is representative of this case. We observed a gentle slope (13°) in the DebrisCov part of Imja Glacier (downglacier) and a steep slope

(37°) in the upglacier part . The supraglacial lakes are mainly located in the first 2 km, where the slope, is ~10°. This is the upper limit of slope range by Reynolds (2000), so this fact and the interactions between the upglacier and downglacier slopes could be providing a favourable boundary condition for the evolution of supraglacial lakes on Imja Glacier. The growth of those lakes could still be prevented by slope limit or by local variations in the glacier velocity and surface morphology (Quincey and others, 2007). Conversely, continuously increasing Imja Lake is situated in location just next to the glacier tongue that has experienced continuously decreasing flow velocity and has more or less stagnant ice, favouring the continuous expansion of the lake.

Suzuki and others (2007), based on the inference from the calculated thermal resistance of debris-covered glaciers, demonstrated that the development of glacial lakes at the terminus due to enhanced ablation is typical in glaciers with relatively thin debris layers. By analysing the difference in height between the glacier surface and the lateral moraine ridges, Sakai and Fujita (2010) observed that glaciers that record a relatively large decrease in their surface are likely to develop glacial lakes, thus providing evidence that glaciers with high ablation rates tend to develop glacial lakes.

A decreasing glacier flow velocity can be attributed to a decreasing glacier surface slope, caused by an imbalance between the amounts of accumulation and ablation (mass balance). Both slope and thickness of the ice, as well as temperature, are the key influencing factors for glacier flow velocity (Cuffey and Paterson, 2010). Benn and others (2001) stated that a negative mass balance favours the growth of the lake.

Here, we underline that the changes in the glacier V_f favour the formation and expansion of lakes. The observed decreasing V_f induced by changes in the slope, caused in turn by negative ΔE in the ablation part, is likely a cause for the continuous growth of Imja Lake. Furthermore, the decreasing V_f due to more negative ΔE in the upper ablation part (Fig. 3 and Fig. 4a) might be a reason for the disintegration of Amphu Lapcha branch from the rest Imja-Lhotse Shar glaciers. These processes further enhance the debris-fall and the ice avalanche from the upper glacier zone. In this respect, low-velocity and high-ablation rates of the glacier seem to be the two key glacier factors linked with lake evolution.

5.2 Climate as a driver of glacier and lake variation

The observed responsible glacial factors of the lake evolution - the decreased V_f and the increased glacier thinning (i.e. negative ΔE) - could be attributed to changes in the precipitation that influence accumulation and the temperature that controls the ablation process of glacier.

Climatic data from ground stations rarely exist for higher elevations (above 3000 m asl.). Salerno and others (2014) based on the available ground stations data presented spatio-temporal variations of the temperature and precipitation for the 1994-2013 period in this region. The study found, at an elevation of ~ 5000 m, the annual minimum temperature (MinT) has increased more than MaxT (0.072 ± 0.011 °C a^{-1} MinT and 0.009 ± 0.012 °C a^{-1} MaxT) in the last two decades. In the same period, the MeanT has increased by 0.044 ± 0.008 °C a^{-1}. About the precipitation, they demonstrated at an elevation of ~ 5000 m, a significant decreasing (-9.3 ± 1.8 mm a^{-1}) for all months, corresponding to a loss of 47% during the monsoon. Several previous studies have indicated the weakening of monsoon (e.g., Palazzi and others, 2013). For the period before 1990s, Sharma and others (2000) showed an increasing tendency of precipitation from 1948–1993 in the Dudh Koshi basin and further, as inferred in Salerno and others (2008) and Thakuri and others (2014) that the increasing of the precipitation has favoured the south-facing glaciers and thus, low shrinkage of the glaciers before 1990s. In this respect, the weakening of the monsoon precipitation has most likely led to the decreasing of the *Vf*, observed for Imja Glacier in 1990s to 2014, due to lower accumulation on the glacier.

In Figure 2d, the decreasing glacier $\Delta Surf$ only in the lower elevation before 1990s and along the much higher elevation after 1990s, could be explained by the observed temperature and precipitation behaviours during those periods. In the first period (1962-92), the glacier area loss in the lower elevation could be a result of an increasing temperature, while an increasing precipitation favoured glaciers above 5750 m. In the second period (1992-2013), although the loss of *Surf* in lower elevation was continued due to increasing temperature, a significant decreasing precipitation could have resulted the decreasing *Surf* in the higher elevations (above 5750 m). In conclusion, before 1990s, the glacier *Surf* has decreased mainly due to temperature, but after 1990s, the precipitation has augmented *Surf* loss impacting the accumulation area.

Figure 6e presents the 0°C isotherms of Nov MaxT, in the surrounding area of Imja Lake, for 1994 and 2013 that was calculated using the temperature lapse rates derived from the station data (Salerno and others, 2014). The figure implies a significant shift (+168 m) of the isotherm extending from below the terminus position of Imja Glacier in 1994 to above the location of Imja Lake in 2013. Significant shifts of the 0° MaxT isotherms from lower to higher elevation observed for Apr (+268 m) and Nov (+168 m) that crossed the lake, and for Dec (+201 m) that arrived to the lake, from 1994 to 2013, making the glacier more susceptible to melting by these shifts.

The significant increase of Apr MaxT likely has not affected the evolution of lake surface, because during that month, the temperature of lake on the surface is below 0 °C and the lake is reviving from the coldest period, as can be observed from climate data (e.g. Fig. 6d). On the contrary, the increasing 0 °C MaxT isotherms in post-monsoon months can have longer melting process of the glacier by introducing an increased inflow to the lake that brought to constant lake surface as observed in Figure 6c, in recent year not justifiable by low precipitation. We observed only significant change of MaxT in Nov, Dec, and Apr months. No significant change was observed for MinT and MeanT that could influence for increasing glacier melting. In this regard, in addition to decreasing precipitation that induced the lower velocities of the glacier, an increasing of MaxT has augmented the glacier melting and likely driving the evolution of the lakes.

5. CONCLUSION

This study implies that the evolution of Imja lake are driven by the climatic impacts on the glacier mass balance and thus, the glacier flow velocities in the Everest region. Using multi-temporal optical satellite imagery, we detected the changes in both Imja Glacier variables and Imja Lake surface and provided the possible nexus between their contemporary evolutions. From 1960s to 2013, Imja Glacier has experienced a loss of *Surf* (0.067 ± 0.014 km a^{-1}) with an accelerated rate in the last two decades, a significant upward shift of the snow-line (~ 9 m a^{-1}), a retreat of the terminus (~44 m a^{-1}), and an increase in the debris-cover (0.026 ± 0.004 km^2 a^{-1}). Further, it has recently experienced a thinning of glacier ice and has shown an overall decreasing trend of flow velocities. The surface of Imja Lake and the number of supraglacial lakes on Imja Glacier increased coincidently with the glacier from 1960s to 2013.

We conclude that the weakening of the monsoon precipitation in the last decades, is most likely leading the decreasing of *Vf* due to lower accumulation and thus negative mass balance, and ultimately triggering to the evolution of the lake. Furthermore, in particular, increasing of maximum temperatures during the post-monsoon months is likely driving a rapid growth of the lake due to increased ablation of the glacier surface close to lake location. Such phenomenon could be prevalence for all glacial lakes in this region. The examination of glacier velocities together with lake variations from the region could therefore, provide a regional perspective on the evolution of lakes.

ACKNOWLEDGEMENTS

This work was supported by the Ministry of Education, Universities and Research (MIUR) through Ev-K2-CNR/SHARE and CNR-DTA/NEXTDATA projects within the framework of the Ev-K2-CNR and Nepal Academy of Science and Technology (NAST) collaboration in Nepal. S. Thakuri is recipient of a doctoral research grant from the Intergovernmental Panel on Climate Change (IPCC) and the Prince Albert II of Monaco Foundation under the IPCC Scholarship Programme. T. Bolch acknowledges funding through Deutsche Forschungsgemeinschaft (DFG) and the ESA Glaciers_cci project.

REFERENCES

Bajracharya B, Shrestha AB, and Rajbhandari L (2007) Glacial lake outburst floods in the Sagarmatha region- hazard assessment using GIS and hydrodynamic modeling. *Mt. Res. Dev.,* **27** (4), 336–344

Basnett S, Kulkarni AV, and Bolch T (2013) The influence of debris cover and glacial lakes on the recession of glaciers in Sikkim Himalaya, India. *J Glaciol.,* **59**(218), 1035-1046

Benn D, Wiseman S, and Hands K (2001) Growth and drainage of supraglacial lakes on debris-mantled Ngozumpa Glacier, Khumbu Himal, Nepal. *J. Glaciol.,* **47** (159), 626–638

Benn DI, Benn T, Hands K, Gulley J, Luckman A, Nicholson LI, Quincey D, Thompson S, Toumi R, and Wiseman S (2012) Response of debris-covered glaciers in the Mount Everest region to recent warming, and implications for outburst flood hazards. *Earth-Sci. Rev.,* **114**, 156–174

Bolch T, Buchroithner MF, Peters J, Baessler M, and Bajracharya S (2008a) Identification of glacier motion and potentially dangerous glacial lakes in the Mt. Everest region/Nepal using spaceborne imagery. *Nat. Hazards Earth Syst. Sci.,* **8**, 1329–1340 (doi:10.5194/nhess-8- 1329-2008)

Bolch T, Buchroithner M, Pieczonka T, and Kunert A (2008b) Planimetric and volumetric glacier changes

in the Khumbu Himalaya since 1962 using Corona, Landsat TM and ASTER data. *J. Glaciol.,* **54**, 592–600

Bolch T, Pieczonka T, and Benn DI (2011) Multi-decadal mass loss of glaciers in the Everest area (Nepal Himalaya) derived from stereo imagery. *The Cryosphere,* **5**, 349-358, (doi:10.5194/tc-5- 349-2011)

Cuffey KM and Paterson WSB (2010) The Physics of Glaciers. **4**th edition, Elsevier, Inc. pp. 704

Fujii Y and Higuchi K (1977) Statistical analysis of the forms of the glaciers in the Khumbu Himal. *J. Jap. Soc. Snow Ice,* (39), 7–14

Fujita K, Sakai A, Nuimura T, Yamaguchi S, and Sharma RR (2009) Recent changes in Imja Glacial Lake and its damming moraine in the Nepal Himalaya revealed by in situ surveys and multi-temporal ASTER imagery. *Environ. Res. Lett.,* **4,** 045205 (doi:10.1088/1748-9326/4/4/045205)

Gardelle J, Arnaud Y, and Berthier E (2011) Contrasted evolution of glacial lakes along the Hindu Kush Himalayan mountain range between 1990 and 2009. *Global Planet. Change*, **75**, 47-55

Gardelle J, Berthier E, Arnaud Y, and Kääb A (2013) Region-wide glacier mass balances over the Pamir-Karakoram-Himalaya dur- ing 1999-2011. *The Cryosphere*, **7**, 1263–1286 (doi:10.5194/tc- 7-1263-2013, 2013)

GLIMS and NSIDC (2005, updated 2014) Global Land Ice Measurements from Space glacier database. Compiled and made available by the international GLIMS community and the National Snow and Ice Data Center, Boulder CO, U.S.A. (doi:10.7265/N5V98602)

Heid T and Kääb A (2012) Evaluation of existing image matching methods for deriving glacier surface displacements globally from optical satellite imagery. *Remote Sens. Environ.,* **118**, 339-355

Höhle J and Höhle M (2009) Accuracy assessment of digital elevation models by means of robust statistical methods. *ISPRS J. Photogramm. Remote Sens.,* **64**, 398–406, (doi:10.1016/j.isprsjprs.2009.02.003)

Huss M (2013) Density assumptions for converting geodetic glacier volume change to mass change. *The Cryosphere*, **7**, 877-887 (doi: 10.5194/tc-7-877-2013)

Ichiyanagi K, Yamanaka MD, Muraji Y, and Vaidya BK (2007) Precipitation in Nepal between 1987 and 1996. *Int. J. Climatol.*, **27**, 1753–1762 (doi:10.1002/joc.1492)

Kääb A and Vollmer M (2000) Surface geometry, thickness changes and flow fields on creeping mountain permafrost: Automatic extraction by digital image analysis. *Permafrost Periglac. Process.,* **11**, 315-326

Kääb A, Lefauconnier B, and Melvold K (2006) Flow field of Kronebreen, Svalbard, using repeated Landsat 7 and ASTER data. *Ann. Glaciol.,* **42**(1), 7-13

Kamp U, Bolch T, and Olsenholler JA (2005) Geomorphometry of Cerro Sillajhuay, Chile/Bolivia: comparisons of DEMs derived from ASTER remote sensing data and contour maps. *Geocarter Int.,* **20**(1), 23–34

Kodama H and Mae S (1976) Flow of glaciers in the Khumbu region. *J. Jap. Soc.* (Snow and Ice Special Issue), 38, Part I, 31–36

Luckman A, Quincey D, and Bevan S (2007) The potential of satellite radar interferometry and feature tracking for monitoring flow rates of Himalayan glaciers. *Rem. Sens. Environ.,* **111**(2–3), 172–181

McFeeters SK (1996) The use of the Normalized Difference Water Index (NDWI) in the delineation of open water features. *Int. J. Remote Sens.,* **17**(7), 1425-1432

Müller F (1968) Mittelfristige Schwankungen der Oberflaechengeschwindigkeiten des Khumbugletschers am Mount Everest, Schweizerische Bauzeitung, **86**(31), 569–573

Nakawo M, Yabuki H, and Sakai A (1999) Characteristics of Khumbu Glacier, Nepal Himalaya: recent changes in the debris-covered area. *Ann. Glaciol.,* **28,** 118–122

Nie Y, Zhang Y, Liu L, and Zhang J (2010) Glacial change in the vicinity of Mt. Qomolangma (Everest), central high Himalayas since 1976. *J. Geogr. Sci.*, **20**(5), 667–686.

Nuimura T, Fujita K, Yamaguchi S, and Sharma RR (2012) Elevation changes of glaciers revealed by multitemporal digital elevation models calibrated by GPS survey in the Khumbu region, Nepal Himalaya, 1992–2008. *J. Glaciol.,* **58**, 648–656

Nuth C and Kääb A (2011) Co-registration and bias corrections of satellite elevation data sets for quantifying glacier thickness change. *The Cryosphere*, **5**(1), 271–290 (doi:10.5194/tc-5-271-2011)

Quincey DJ, Richardson SD, Luckman A, Lucas RM, Reynolds JM, Hambrey MJ, and Glasser NF (2007) Early recognition of glacial lake hazards in the Himalaya using remote sensing datasets. *Global Planet. Change,* **56**(1-2), 137-152.

Quincey DJ, Luckman A, and Benn D (2009) Quantification of Everest region glacier velocities between 1992 and 2002, using satellite radar interferometry and feature tracking. *J. Glaciol.,* **55**(192), 596–606

Palazzi E, von Hardenberg J, and Provenzale A (2013) Precipitation in the Hindu-Kush Karakoram Himalaya: observations and future scenarios. *J. Geophys. Res.-Atmos.* **118**, 85–100

Paul F and Haeberli W (2008) Spatial variability of glacier elevation changes in the Swiss Alps obtained from two digital elevation models. *Geophys. Res. Lett.,* **35**, L21502 (doi:10.1029/2008GL034718)

Paul F and Others (2013) The glaciers climate change initiatives: Methods for creating glacier area, elevation change and velocity products. *Rem. Sens. Environ.,* In Press (doi: http://dx.doi.org/10.1016/j.rse.2013.07.043)

Peters J, Bolch T, Buchroithner MF, and Bäßler M (2010) Glacier Surface Velocities in the Mount Everest Area/Nepal using ASTER and Ikonos

imagery. Proceeding of 10th International Symposium on High Mountain Remote Sensing Cartography, Kathmandu, Nepal, 313-320

Reynolds JM (2000) On the formation of supraglacial lakes on debris-covered glaciers. *IAHS Publ.,* **264** (Symposium at Seattle 2000 – Debris-Covered Glaciers), 153–161

Richardson SD and Reynolds JM (2000) An overview of glacial hazards in the Himalayas, *Quatern. Int.,* **65/66**(1), 31–47

Röhl K (2008) Characteristics and evolution of supraglacial ponds on debris-covered Tasman Glacier, New Zealand. *J. Glaciol.*, **54**(188), 867–880.

Sakai A and Fujita K (2010) Formation conditions of supraglacial lakes on debris-covered glaciers in the Himalaya. *J. Glaciol.,* **56** (195), 177-181

Salerno F, Buraschi E, Bruccoleri G, Tartari G, and Smiraglia C (2008) Glacier surface-area changes in Sagarmatha National Park, Nepal, in the second half of the 20th century, by comparison of historical maps. *J. Glaciol.,* **54**, 738–752

Salerno F, Guyennon N, Thakuri S, Viviano G, Romano E, Vuillermoz E, Cristofanelli P, Stocchi P, Agrillo G, Ma Y, and Tartari G (2014) Weak precipitation, warm winters and springs impact glaciers of south slopes of Mt. Everest (central Himalaya) in the last two decades (1994-2013). *The Cryosphere Discuss.,* **8**, 5911-5959 (doi:10.5194/tcd-8-5911-2014)

Salerno F, Thakuri S, D'Agata C, Smiraglia C, Manfredi EC, Viviano G, and Tartari G (2012) Glacial lake distribution in the Mount Everest region: Uncertainty of measurement and conditions of formation. *Global Planet. Change,* **92–93**, 30–39.

Scherler D, Bookhagen B, and Strecker MR (2011) Spatially variable response of Himalayan glaciers to climate change affected by debris cover. *Nat. Geosci.,* **4**, 156–159

Scherler D, Leprince S, and Strecker MR (2008) Glacier-surface velocities in alpine terrain from optical satellite imagery - Accuracy improvement and quality assessment, *Rem. Sens. Environ.,* **112**(10), 3806–3819

Seko K, Yabuki H, Nakawo M, Sakai A, Kadota T, and Yamada Y (1998) Changing surface features of Khumbu Glacier, Nepal Himalayas, revealed by SPOT images. *Bull. Glac. Res.,* **16**, 33–41

Sharma KP, Moore B, and Vorosmarty CJ (2000) Anthropogenic, climatic, and hydrologic trends in the Kosi basin, Himalaya. *Clim. Change*, **47**, 141–165

Somos-Valenzuela MA, McKinney DC, Rounce DR, and Byers AC (2014) Changes in Imja Tsho in the Mount Everest region of Nepal. *The Cryosphere,* **8**, 1661–1671 (doi:10.5194/tc-8-1661-2014)

Suzuki R, Fujita K, and Ageta Y (2007) Spatial distribution of thermal properties on debris-covered glaciers in the Himalayas derived from ASTER data. *Bull. Glaciol. Res.,* **24**, 13–22

Tartari G, Salerno F, Buraschi E, Bruccoleri G, and Smiraglia C (2008) Lake surface area variations in the North-Eastern sector of Sagarmatha National Park (Nepal) at the end of the 20th Century by comparison of historical maps. *J. Limnol.,* **67**, 139–154

Thakuri S, Salerno F, Smiraglia C, Bolch T, D'Agata C, Viviano G, and Tartari G (2014) Tracing glacier changes since the 1960s on the south slope of Mt. Everest (central Southern Himalaya) using optical satellite imagery. *The Cryosphere*, **8**, 1297-1315 (doi:10.5194/tc-8-1297-2014)

Thompson SS, Benn DI, Dennis K, and Lukman A (2012) A rapidly growing moraine-dammned glacial lake on Ngozumpa Glacier, Nepal. *Geomorphology,* **145-146**, 1-11.

Toutin T (2008) ASTER DEMs for geomatic and geoscientific applications: a review. Int. J. Remote Sens., **29,** 1855-1875.

Watanabe T, Lamsal D, and Ives JD (2009) Evaluating the growth characteristics of a glacial lake and its degree of danger of outburst flooding: Imja-Lhotse Shar glacier, Khumbu Himal, Nepal. *Norsk Geogr. Tidssk.,* **63**, 255–267

Willis IC (1995) Intra-annual variations in glacier motion: a review. *Prog. Phys. Geog.,* **19**(1), 61-106 (doi: 10.1177/030913339501900104)

Yamada T (1998) Glacier lake and its outburst flood in the Nepal Himalaya. Monograph No. 1, Data Center for Glacier Research. Japanese Society of Snow and Ice, Pp. 96

Article IV

8.4 Article IV

Salerno, F., S. Thakuri, C. D'Agata, C. Smiraglia, E. C. Manfredi, G. Viviano, and G. Tartari (2012) Glacial lake distribution in the Mount Everest region: Uncertainty of measurement and conditions of formation. ***Global Planet. Change,*** **92–93, 30–39, doi: 10.1016/j.gloplacha.2012.04.001.**

Global and Planetary Change 92–93 (2012) 30–39

Contents lists available at SciVerse ScienceDirect

Global and Planetary Change

journal homepage: www.elsevier.com/locate/gloplacha

Glacial lake distribution in the Mount Everest region: Uncertainty of measurement and conditions of formation

Franco Salerno [a,b,*], Sudeep Thakuri [a,b], Carlo D'Agata [b,c], Claudio Smiraglia [b,c], Emanuela Chiara Manfredi [a,b], Gaetano Viviano [a,b], Gianni Tartari [a,b]

[a] Water Research Institute, National Research Council (IRSA-CNR), Via del Mulino 19, Brugherio (MB) 20861, Italy
[b] Ev-K2-CNR Committee, Via San Bernardino, 145, Bergamo 24126, Italy
[c] Department of Earth Sciences "Ardito Desio", University of Milan, Italy

ARTICLE INFO

Article history:
Received 22 April 2011
Accepted 4 April 2012
Available online 13 April 2012

Keywords:
ALOS
Supraglacial lakes
Proglacial lakes
Mount Everest
Accuracy
Glacier distribution

ABSTRACT

This study provides a complete mapping (October 2008) of glacial lakes and debris-covered glaciers in the Mount Everest region. These types of analyses are essential in studies of the impact of recent climate change, and therefore the uncertainty of measurements is discussed with the aim of creating a reference study for use when glaciers and lakes are delineated using remote sensing imagery. Moreover, attention is focused on conditions related to the formation of lakes, which is the greatest evidence of the impact of climate change at high altitudes characterized by debris-covered glaciers. Regarding the formation process of *supraglacial lakes*, our findings confirm that the slope of the glacier where lakes are located is primarily responsible for the low flow velocity of this zone. Otherwise, this study is novel in its identification of a further boundary condition. The slope of the glacier upstream is able to influence both the low flow velocity and the high ablation rates at the glacier terminus. In fact, the imbalance between the two glacier zones generates the downslope passage of debris, snow and ice. We found the slope of the glacier upstream to be inversely correlated with the relevant total surface of the lakes downstream. The multiple regression model developed in this study, considering the slopes of the two glacier areas distinctly, has been able to predict 90% of the *supraglacial lake* surfaces. Concerning the surfaces of lakes not directly connected with glaciers (*unconnected glacial lakes*), we found they are correlated with the dimensions of their drainage basin, whereas no correlation was found with the glacier cover in the basin. Considering that the evaporation/precipitation ratio at these altitudes is approximately 0.34, the evolution of these lakes appears to be a helpful sign for detecting the precipitation trend of these high-altitude regions.

1. Introduction

Scherler et al. (2011) provide a comprehensive study along the entire Hindu Kush-Himalaya range underlining the non-uniform response of glaciers to climate change. In particular, the study highlights the importance of debris cover for understanding glacier evolution, an effect that has so far been neglected in predictions of future water availability. The southern central Himalayas are the region with glaciers that presents the highest debris coverage. Supraglacial debris cover influences the terminus dynamics and can thereby modify a glacier's response to climate change. Supplementary material 1 describes previous studies on glacier and lake distribution in the Mount Everest region. Recent studies in this region have found several debris-covered glaciers with stagnant ice in the glacier termini (Scherler et al., 2008; Quincey et al., 2009). Although surface lowering indicates that such glaciers are currently shrinking, their fronts remain remarkably stable. The retreat rate of a debris-covered glacier is thus unsuitable as an indicator of recent climate change (Scherler et al., 2011). Moreover, Jacobs et al. (2012) note that the high mountains of Asia are subject to a mass loss for the years 2003 through 2010 at a level that is significantly lower (4 ± 20 Gt yr^{-1}) than previous estimates (47 to 55 ± 20 Gt yr^{-1}). Nevertheless, these glaciers have the potential to develop widespread melting ponds and build up moraine-dammed lakes (Ageta et al., 2000; Sakai et al., 2000; Quincey et al., 2009).

Three types of glacial lakes can be distinguished according to Ageta et al. (2000): (*i*) lakes that are not directly connected with glaciers but that may have a glacier located in their basin, referred to in this paper as *unconnected glacial lakes*; (*ii*) *supraglacial lakes* (melting ponds), which develop on the surface of the glacier downstream; or (*iii*) *proglacial lakes*, which are moraine-dammed lakes that are in contact with the glacier front. Some of these lakes store large quantities of water and are susceptible to GLOFs (glacial lake outburst floods).

Little is known about the conditions of formation, distribution and evolution of all of these three types of glacial lakes in the southern

* Corresponding author at: IRSA-CNR Via Del Mulino 19, Località Occhiate 20861 Brugherio (MB), Italy. Tel.: +39 39 21694203; fax: +39 39 2004692.
E-mail address: salerno@irsa.cnr.it (F. Salerno).

0921-8181/$ – see front matter © 2012 Elsevier B.V. All rights reserved.
doi:10.1016/j.gloplacha.2012.04.001

central Himalayas, even though these lakes are a suitable indicator for evaluating the impact of climate change at high elevations (Richardson and Reynolds, 2000; Benn et al., 2001). Gardelle et al. (2010), considering *supraglacial* and *proglacial lakes*, note that the southern side of Mt Everest is the region that is most characterized by glacial lakes in the Hindu Kush-Himalaya. Moreover, these lakes have indicated the largest surface area increase of the lakes in the mountain range, estimated at +33% (1990–2009), and thus indicates that the region is appropriate for this survey.

In this context, the glacier and lake mapping indicates the need to pay attention to the uncertainty of the topographical measurements obtained from remote sensing imagery so that data can be analyzed according to the correct relevance to their accuracy. In addition, multi-temporal analysis usually employs data sources (map and satellite) with different degrees of uncertainty that should be taken into account during temporal comparisons.

The overall aim of this work is to provide an updated and complete outline of the three types of glacial lakes and glaciers in the southern region of Mt Everest (October 2008). Considering that these types of measurements are essential in recent studies of the impact of climate change, the analysis on uncertainty of measurements is discussed with the aim of proving this to be a reference study that can be used when glaciers and lakes are measured using remote sensing imagery. Moreover, the attention is focused on the conditions of the formation of glacial lakes, specifically, *unconnected* and *supraglacial lakes*.

2. Study area

The current study is focused on the Everest-region and in particular in the Sagarmatha (Mt Everest) National Park (SNP), the highest protected mountainous area in the world, situated in Solu-Khumbu District in the north-eastern region of Nepal (Fig. 1). This area includes the upper catchment of the Dudh Koshi River Basin which is the part of the Koshi River Basin (or Sapta Koshi River Basin), one of the three large river basins of Nepal. The northern part of the park bounds with the Autonomous Region of Tibet (China). The SNP covers an area of 1148 km^2 encompassing altitudes from 2845 m (at Jorsale) to 8848 m at the summit of Mount Everest (Sagarmatha in Nepali). The park falls between latitude 27°45'00″ to 28°06′36″ N and longitude 85°58'48'' to 86°30'36'' E (Salerno et al., 2010; Lami et al., 2010). Land cover classification shows that almost one-third of the territory is characterized by snow and glaciers, while less than 10% of the park area is forested (Bajracharya et al., 2010).

The glaciers in Everest-region show morphological features common to glaciers throughout the Himalayas. Nearly all (28 out of a total of 29) are debris-covered glaciers; these are glaciers in which the ablation zone is almost entirely covered by surface debris that significantly alters the energy exchanges between the ice and the atmosphere (Mattson et al., 1993.). Because the minimum threshold for considering glacier areas in this study was set at 1 km^2 (Supplementary material 1) the only debris-free glacier we consider is Langmuche glacier (Salerno et al., 2008).

Glacier lakes in this region are very vulnerable to climate change and some of them, like Nare Drangka lake and Dig Tsho lake, have already experienced GLOFs in 1977 and 1985 respectively (Fushimi et al., 1985; Yamada and Sharma, 1993). All glacial lakes plotted in Tartari et al., 2008 on a 1992 map for the north-eastern sector of Everest-region were at between 4460 m and 5560 m in altitude, with the maximum frequency of altitude distribution falling between 5100 m and 5300 m. The lakes were fed prevalently by perennial snow and glaciers, than direct runoff from precipitation. However some lakes were detected without glacial masses in their hydrographic basin. These often prove to be temporary ponds, although in

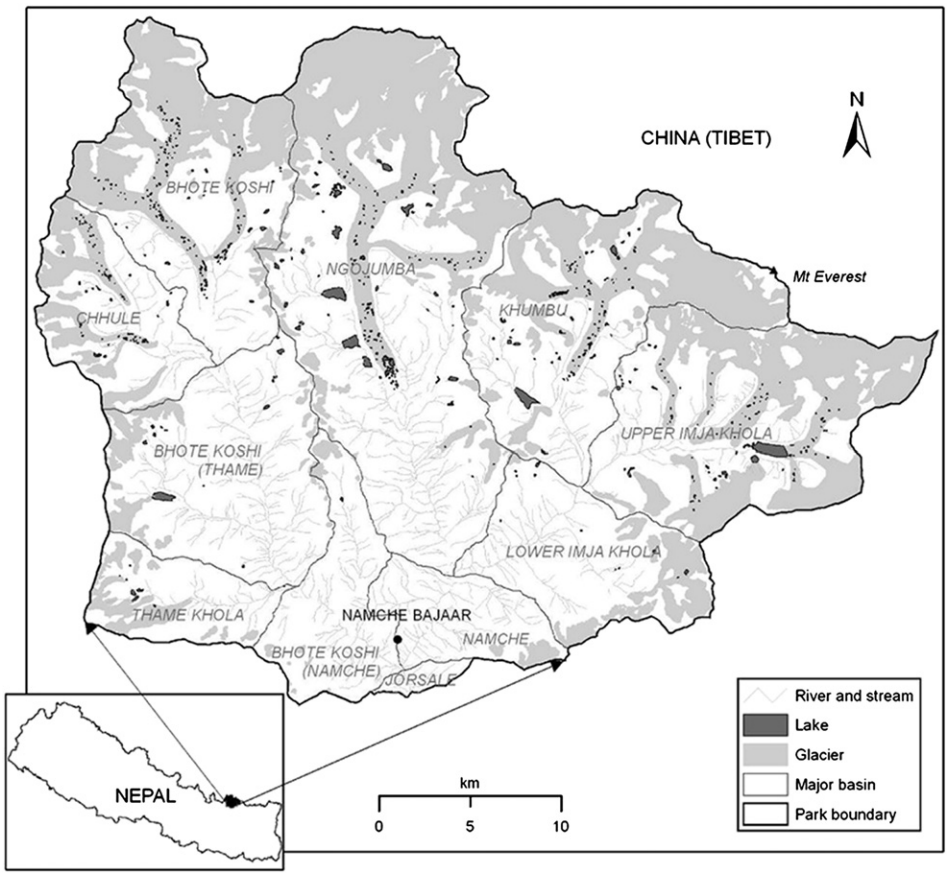

Fig. 1. Location of the study area: Sagarmatha National Park, Nepal.

the case of lakes fed by glaciers and/or snowfields it is not infrequent to observe strong variations in level during the inter-monsoon period (October-March).

3. Data and methods

3.1. Satellite data

Glaciers and lakes were manually identified and digitized using the Advanced Visible and Near Infrared Radiometer type 2 (AVNIR-2) on-board ALOS image, received from a Japanese Earth Observation satellite launched in January 2006. AVNIR-2 is a multispectral radiometer for observing land and coastal zones with a 10 m spatial resolution, a 70 km swath width (at nadir), and a revisiting time of 46 days. AVNIR-2 data investigated in this study were acquired on 24th October 2008 (Scene ID ALAV2A146473040) in a cloudless sky. The image was acquired at the end of the monsoon season before the first heavy snowfall. Image data were orthorectified and corrected for the atmospheric effects using the 6 S code (Vermote et al., 1997; Giardino et al., 2010).

3.2. Uncertainty of measurements

3.2.1. Glacier and lake surfaces

In general the measurement accuracy of the position of a single point or an edge in the space ($n=1$, $i=1$), within the use of the *GIS* (Geographical Information System), is limited by the resolution of the source data used (i.e., cartography, satellite image), which we define LRE_i (Linear Resolution Error) and by the error of referencing with regard to a reference system (RE_i, co-REgistration error or co-georeferencing error).

In this study the *RE* calculated as to the *Official Nepali map* was ±18 m (Salerno et al., 2008). In the case one would compute the error of two measurements of similar quantities ($n=2$) as regards to a unique reference system common to the two source data (for instance a temporal comparison of the point shifting or of the edge by using two satellite images both co-registered as per a topographical map), the overall Linear Error ($LE_{1\text{-}2}$) should be calculated as the root mean square (rms) of the errors related to the two measurements (1), (Ye et al., 2006). The overall *LE* would be lower in the case the source data were co-registered between them, thus reducing the uncertainty to a single co-registration.

$$LE_{1-2} = \sqrt{\sum_{i=1}^{n=2} LRE^2} + \sqrt{\sum_{i=1}^{n=2} RE^2} \quad (1)$$

This approach is the one usually adopted in studies on the evolution (retreat and advance) of the glacial front (Ye et al., 2006; Shangguan et al., 2010).

In the case that the source data is a topographical map, Inghilleri (1974) points out that at the graphical resolution limit an arbitrary value of 0.2 mm can be assigned, based on the threshold visible to the human eye. The level of approximation of a map (*LRE*) is conventionally given by this limit of 0.2 mm multiplied by the scale factor (Inghilleri, 1974; Salerno et al., 2008).

For satellite imagery, the *LRE* is limited by the sensor resolution, i.e. by the pixel resolution (Williams et al., 1997). It is obvious that a higher sampling resolution yields the ability to measure the location of an object more accurately; however it is not obvious just how high a resolution is required for a specified spatial accuracy. Gorman (1996) tackles this problem starting from the assumption that the boundary of an object region is straight within the length it crosses a pixel region, and that the object width is greater than one pixel unit. With these definitions, the precision error with respect to a point on the boundary of a region is defined as the minimum distance between the point and the object edge. Gorman (1996) asserts the precision error is 0.5 pixels that can be added to or subtracted from the measurement of the outside edge of an object. If this is done, the error will range between −0.5 and 0.5, and in the worst case, the error will be 0.5. Within the wide field of application of the GIS, Zhang et al. (2001) state the accuracy of any data derived from the imagery is around 0.5 pixels or better. But in the specific field of the study of temporal variations that Himalayan lakes undergo, Fujita et al. (2009) also assumed an error of ±0.5 pixel. Consequently in this study we also consider half pixel, thus adopting the worst *LRE* (±5 m).

The uncertainty in the measurement of the dimension of a shape (Aerial Error, AE_i) is dependent both upon the linear error $LE_{1\text{-}2}$ and its perimeter, l_i (McMillan et al., 2007; Salerno et al., 2008) (2). As a consequence, the error for large shapes is proportionally smaller than that for small shapes.

$$AE_i = LE_{1-2} \times l_i \quad (2)$$

This approach has been used to define the uncertainty in lake measurement by McMillan et al. (2007), Fujita et al. (2009), and Gardelle et al. (2010). In the calculation of LE_i, these authors exclusively consider the LRE_i, probably considering that the co-registration error RE_i does not play a key role, since they are small-sized shapes and the comparison is not made pixel by pixel, but entity by entity.

By sharing the approach to exclude the co-registration error, in this study the AE_i for the lakes has been calculated following the Eq. (3). It can be noticed that in the equation the *LRE* relative to a hypothetic comparison with a second measurement with the same error is also calculated (Williams et al., 1997).

$$AE_i = \left(\sqrt{\sum_{i=1}^{n=2} LRE^2}\right) \times l_i = \left(LRE_i\sqrt{2}\right) \times l_i \quad (3)$$

In regard to the error made in the estimation of the glaciers' extension, in this study we thought it correct to use the canonical equation of the AE_i computation (3), considering the larger dimensions as regards the lakes (Silverio and Jaquet, 2005).

3.2.2. The digital elevation model

The digital elevation model (DEM) was created by digitizing the contours of the 1992 map. The interpolation was performed using the kriging method, setting a pixel dimension of 20 m × 20 m. To judge the uncertainty of the interpolation method, 100 map control points were used for validation, obtaining an average absolute difference of 6.3 m. In the application to surface gradient calculations, the measurements are based on the relative values between DEM pixels, and therefore the accuracy of the absolute values is less important (Quincey et al., 2007) and can be disregarded. Consequently, the uncertainty related to the slope calculated using this DEM is also neglected.

To explain *supraglacial lake* distribution as a function of explanatory predictors, we divided the glacier into upstream and downstream zones relative to their slope. To this end, we applied the *CuSum* (cumulative sum) control chart statistical technique to detect the changing point of the glacier slope along the glacier's longitudinal profile. The *CuSum* control chart is a sequential analysis technique used in various disciplines for monitoring change detection. It provides comparative information that can be useful in series analysis (in our case, the hypsographic curve) to identify potential changes in trend means (in our case, a change in glacier slope). The test is relatively powerful in comparison with other tests (Buishand, 1982) for a change-point that occurs toward the center of the time series (Kundzewicz and Robson, 2004). We used the techniques described by Taylor (2000) that combine the use of *CuSum* charts and a bootstrapping technique to compute 1000 iterations of the *CuSum* chart.

4. Results

4.1. Glacier distribution

A total of 29 glaciers accounting for nearly the entire glacier area in the Mount Everest region (97%) was plotted. Supplementary material 1 describes criteria for glacier identification and cataloging. Table 1 shows the morphometric characteristics of each glacier in 2008, and Table 2 provides a general summary of the main features of the glaciers. We observe that the total glacier area is 356.2 (±2%) km^2. The largest glacier is Ngojumba Glacier, with an area of 98.8 (±1%) km^2.

The average aspect of the glaciers is 172.7°; in other words the glaciers are, on average, oriented toward the south. Specifically, Nare and Ama Dablam glaciers are exposed to the west, Cholo, Kdu_gr 38 and Langmuche Glacier to the east, and the remaining majority of the glacier surfaces are exposed mainly to the south. The average glacier slope is 25.8%. The two extremes are Melung, with the lowest average slope (8.5%), and Phunki Glacier, with the highest average slope (44.0%).

Fig. 2 shows the frequency distribution of glaciers relative to their elevation. The glaciers present a mean elevation of the glacial fronts (minimum glacier elevation) of 4900 m (standard deviation 5%), a maximum elevation of 6519 m (standard deviation 13%) and in general a mean elevation of 5487 m (standard deviation 5%). Chhule Glacier has the lowest elevation (4832 m), and Khumbu Glacier has the highest average elevation (6154 m).

4.2. Lake distribution

The first step in creating the lakes cadastre involved analyzing the surface hydrographic network plotted on the 1992 map. This analysis led to the identification of 9 sub-basins of the Dudh Koshi River, which were by convention given the name of their largest associated glacier or the main tributary: Thame Khola and Bhote Koshi River (at Thame) basins, Chhule Glacier and Bhote Koshi Glacier basins, Ngojumba Glacier basin, Khumbu Glacier and Upper Imja Khola basins, and Lower Imja Khola and Bhote Koshi River (at Namche) basins (Supplementary material 2). Supplementary material 1 describes in detail the criteria for lake identification and cataloging.

The total number of lakes plotted in 2008 is 624, corresponding to an overall surface of 7.43 (±18%) km^2. Of these lakes, the *unconnected glacial lakes* are the most frequently represented typology (170 lakes with a total surface of 4.28 (±14%) km^2 equivalent to 58% of the overall lake surface). The second typology in terms of area is represented by the *proglacial lakes* (17 lakes with a total surface of 1.76 (±7%) km^2 equivalent to 24%), while the *supraglacial lakes* typology shows the highest number of water bodies (437 lakes with a total surface of 1.39 (±45%) km^2 equivalent to 18%). This last typology consequently presents the lowest median size for each lake (0.001 km^2), but with a high standard deviation (0.007 km^2). The *unconnected glacial lakes* show a median surface 6 times higher (0.006 km^2), with a proportionally similar standard deviation (0.076 km^2). Finally, the *proglacial lakes* are clearly larger in size compared with the other two typologies (0.025 km^2), and in this case as well, the standard deviation is more than twice the mean (0.245 km^2). Fig. 3 shows the frequency distribution of lakes relative to their area. It can be noted that this distribution for each typology is far from normality (lognormal), with an abundance of small lakes and few large lakes. In addition, although the *supraglacial lakes* show a *kurtosis* of 79, the *proglacial* and *unconnected glacial lakes* have a lower *kurtosis* value (11) and, thus, a frequency distribution highlighting a wider dimensional range compared to the *supraglacial lakes* (Joanes and Gill, 1998).

Fig. 2 shows the frequency distribution of glaciers and lakes relative to their altitude. Starting with the *supraglacial lakes*, we notice

Table 1
Morphometric characteristics of the glaciers and supraglacial lakes of Sagarmatha National Park in 2008 (Up = glacier upstream; Down = glacier downstream; Tot = all glaciers).

Glacier name	Glacier features								Supraglacial lakes features					
	Glacier surface	Aspect	Slope			Elevation a.s.l.			Number of lakes	Elevation a.s.l.		Lakes perimeter	Lakes surface	
	Total	Mean	Up	Down	Mean	Mean	Min	Max	Total	Mean	Stand. Dev.	Total	Total	Density
	(km^2)	(°)	(°)	(°)	(°)	(m)	(m)	(m)	N	(m)	(m)	(km)	(km^2)	(%)
Ama Dablam	9.8	255	37	11	26	5416	4786	6328	8	4976	60	1.76	0.023	0.57
Bhote Koshi	41.6	164	38	10	22	5526	4797	6825	100	5111	136	17.57	0.227	0.92
Chhuitingpo	6.5	148	31	17	27	5618	5105	6199	0					
Chhule	3.1	101	34	7	22	5091	4802	5812	21	4916	77	4.81	0.077	1.81
Cholo	1.4	87	44	13	21	4832	4451	5536	0					
Cholotse	1.5	247	40	13	20	5102	4868	5519	2	4991	90	0.40	0.005	0.46
Duwo	2.1	239	45	9	28	5115	4747	6039	1	4776		0.39	0.008	0.84
Imja	35.1	198	39	12	31	5787	4997	7719	24	5136	62	5.18	0.066	0.65
Kdu_gr 125	1.0	150	32	13	20	5529	5374	5713	0					
Kdu_gr 181	0.6	254	45	26	41	5551	4943	6348	0					
Kdu_gr 38	0.8	82	42	21	40	5700	4944	6532	0					
Khangri	18.5	153	41	9	21	5570	5143	6812	30	5205	20	6.84	0.098	0.82
Khumbu	38.4	206	37	8	29	6154	4907	8199	32	5054	116	7.13	0.108	1.01
Kyajo	1.0	103	33	12	15	5397	5262	5582	0					
Langdak	2.1	103	27	11	18	5259	4785	5810	0					
Langmuche	2.9	83	46	25	43	5639	4456	6788	0					
Lhotse	15.4	210	48	12	28	5807	4854	8254	21	5100	57	3.76	0.046	0.55
Lobuje	1.7	143	26	8	20	5366	4978	5911	2	4992	1	0.68	0.012	2.07
Lumsamba	19.3	179	37	10	25	5860	4937	7272	28	5105	146	6.84	0.087	0.99
Machhermo	1.2	148	29	11	23	5520	5190	5795	0					
Melung	3.7	144	40	10	22	5168	4999	5586	39	5193	114	5.78	0.062	0.86
Nare	6.0	257	32	15	28	5423	4866	6246	0					
Nareyargaip	5.5	217	36	10	23	5512	5149	6157	3	5327	51	1.40	0.048	1.34
Ngojumba	99.8	179	29	9	22	5848	4701	8163	108	4959	199	25.02	0.502	1.32
Nuptse	8.1	205	45	10	28	5758	4963	7764	10	5118	102	1.79	0.023	0.57
Phunki	1.7	206	50	20	45	5390	4853	6329	0					
Thyangbo	8.8	95	36	12	31	5264	4404	6344	1	4621		0.31	0.006	0.32
Tingbo	1.1	254	33	16	29	5148	4922	5867	0					
W. Lhotse	4.5	199	50	9	32	5774	4918	7599	7	5045	60	0.85	0.005	0.29
Other glaciers	12.4								1	5073		0.12	0.001	

Table 2
General summary of the morphometric features of glaciers and lakes divided by typology in the LCN 2008 cadastre.

Glaciers in SNP			Lakes in SNP					
					Proglacial	Supraglacial	Unconnected	All lakes in SNP
Number of glaciers (N)		29	Number of lakes (N)		17	437	170	624
Elevation a.s.l. (m)	Mean	5487	Elevation a.s.l. (m)	Mean	4996	5057	5073	5060
	Max	6154		Max	5660	5394	5484	5660
	Min	4832		Min	4377	4621	3800	3800
	Stand. Dev.	151		Stand. Dev.	307	172	259	199
	Median	5520		Median	4920	5079	5120	5086
Perimeter (km)	Mean	37.9	Perimeter (km)	Mean	1.05	0.20	0.51	0.31
	Max	224.6		Max	4.83	1.77	4.14	4.83
	Min	4.9		Min	0.09	0.04	0.07	0.04
Glacier surface (km^2)	Mean	11.9	Lake surface (km^2)	Mean	0.104	0.003	0.025	0.012
	Max	99.8		Max	0.979	0.086	0.613	0.979
	Min	0.6		Min	0.0006	0.0001	0.0003	0.0001
	Stand. Dev.	20.1		Stand. Dev.	0.245	0.007	0.076	0.032
	Median	3.7		Median	0.025	0.001	0.006	0.003
	Total	356.2		Total	1.762	1.389	4.279	7.430
Slope (°)	Mean	25.8	Sub-basins surface (km^2)	Mean	–	–	1.32	–
	Max	44.0		Max	–	–	16.22	–
	Min	8.5		Min	–	–	0.01	–
	Stand. Dev.	8.3		Stand. Dev.	–	–	2.47	–
	Median	25.9		Median	–	–	0.57	–
Basin surface (km^2)	Mean	25.0	Basin surface (km^2)	Mean	–	–	2.12	–
	Max	192.7		Max	–	–	20.81	–
	Min	2.3		Min	–	–	0.01	–
	Stand. Dev.	37.8		Stand. Dev.	–	–	3.61	–
	Median	13.2		Median	–	–	0.86	–
Aspect (°)	Mean	173	Glacier surface in basin (km^2)	Mean	–	–	0.38	–
	Max	257		Max	–	–	3.04	–
	Min	82		Min	–	–	0.00	–
	Stand. Dev.	58		Stand. Dev.	–	–	0.64	–
	Median	179		Median	–	–	0.08	–

that these lakes are located at a mean altitude of 5055 m a.s.l., i.e., 155 m higher than the glacial fronts (25° and 75° percentiles, corresponding to 4950–5190 m, standard deviation 3%). The generic *unconnected glacial lakes* are approximately 80 m higher, within an elevation zone ranging from 4800 to 5300 m (mean 5073 m, standard deviation 5%). In the Mount Everest region, the elevations of all lakes generally range between 4850 and 5250 m (the weighted average elevation of the area is 5080 m).

Concerning the *supraglacial lakes,* Fig. 4 shows a few examples of longitudinal profiles of selected glaciers traced on the DEM following an equidistant line between the lateral glacier margins from the highest peak to the glacier front. To begin we observe the changing points of the surface slope detected by applying the *CuSum* control chart statistical technique. This technique clearly distinguishes the steeper glacier upstream from the flatter glacier downstream. For all of the glaciers, we observed that *supraglacial lakes*, when present, are located below this changing point of slope and also close to it. This type of glacier subdivision appears to be strictly related and most likely functional to the lake distribution. The slopes of glaciers downstream show that the lakes range from 7° to 13° (Table 1). Reynolds (2000) reported that in the Bhutan Himalayas, small isolated ponds could be found up to 10°. For the Mt Everest region, we observed evidence of *supraglacial* ponds for slightly higher slopes. For the same glaciers, the slopes of the glacier upstream range from 26° to 50° (Table 1). These slopes are typical of the southern central Himalayan range, as reported by Scherler et al. (2011).

5. Discussion

5.1. Consideration for uncertainty of measurements

Until the early 1970s, aerial photography was the primary remote sensing technique available for extracting glacier and lake parameters. Medium-resolution satellite data (10–90 m) have been available for cryospheric studies since that time. Among them, we can mention here sensors such as TERRA ASTER and LANDSAT MSS, TM, ETM+ with a mean resolution of 30 m (15–90 m), the SPOT HRVIR, the IRS LISS III and, more recently, the ALOS AVNIR-2 launched in 2006 and used in this study with a resolution of 10 m (2.5-10 m). In addition to these sensors, there are sensors with high resolution (meter and

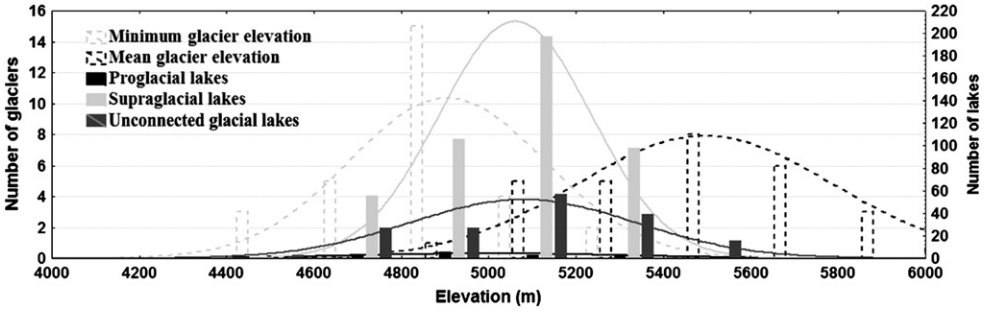

Fig. 2. Frequency distribution of glaciers and lakes relative to their elevation.

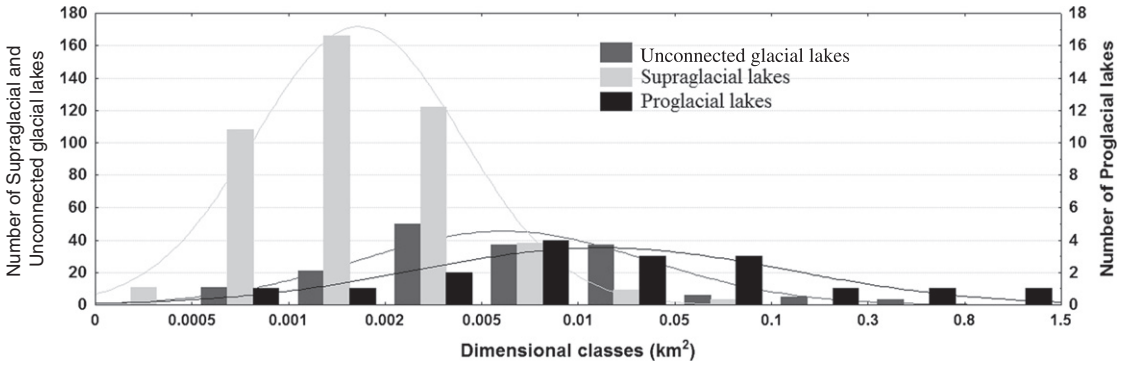

Fig. 3. Frequency distribution of lakes relative to their area and typology.

sub-meter spatial resolution) such as IKONOS, Quickbird and GeoEye-1 (Racoviteanu et al., 2008).

We have noted in this study that the uncertainty in measurement of lake surfaces has been estimated as a function of the sensor resolution and its perimeter according to Eq. (3). As a consequence, the error for large shapes is proportionally smaller than that for small shapes and when sensors with higher resolution are used. In the graph in Fig. 5, we illustrate the relationship between the hypothetic surface of circular lakes and the respective uncertainty of measurement from sensors that differentiate by the degree of resolution. By setting a generic error threshold of 15%, corresponding to the differences observed by Tartari et al. (2008) over a decade, we notice that a high-resolution sensor (1 m) would be able to determine the lake surface with sizes up to and over 0.001 km^2, whereas the dimensional threshold would decrease to 0.01 km^2 for a sensor with a resolution of 5 m, 0.05 km^2 for a sensor with a resolution of 10 m, 0.5 km^2 for a sensor with a resolution of 30 m and 5 km^2 for a sensor with a resolution of 80 m. To simplify, among the resolutions reported in Fig. 5 corresponding to the most common sensors currently available, we notice a capacity of accurately detecting diverging lake sizes by approximately one order of magnitude.

In the following sections, we discuss the conditions of formation of glacial lakes through inference analysis and by weighing the uncertainty as the inverse of the AE_i. The possible significance of the correlations guarantees the uncertainty of measurements considered is sufficiently low for properly describing the relationship.

Concerning the uncertainty in the measurement of glacier surfaces, we noted that, for lakes, the errors are estimated in this study as depending on the sensor resolution and its perimeter according to Eq. (3). For lakes, we compute an overall average *AE* of 18% with a sensor with 10-m resolution; in contrast, using the same sensor, the error associated with glaciers presents a lower order of magnitude (2%). This uncertainty appears to be suitable, considering that Salerno et al. (2008) report that the reduction of the glaciers in terms of surface observed by comparing topographical maps of this region between the 1960s and the 1990s is approximately 5%. If a sensor with 30-m resolution (e.g., LANDSAT TM) was used, the error would become 5%, whereas using a sensor with 80-m resolution (e.g., LANDSAT MSS) would increase the error to 13%, exceeding the magnitude of glacier variations in the region.

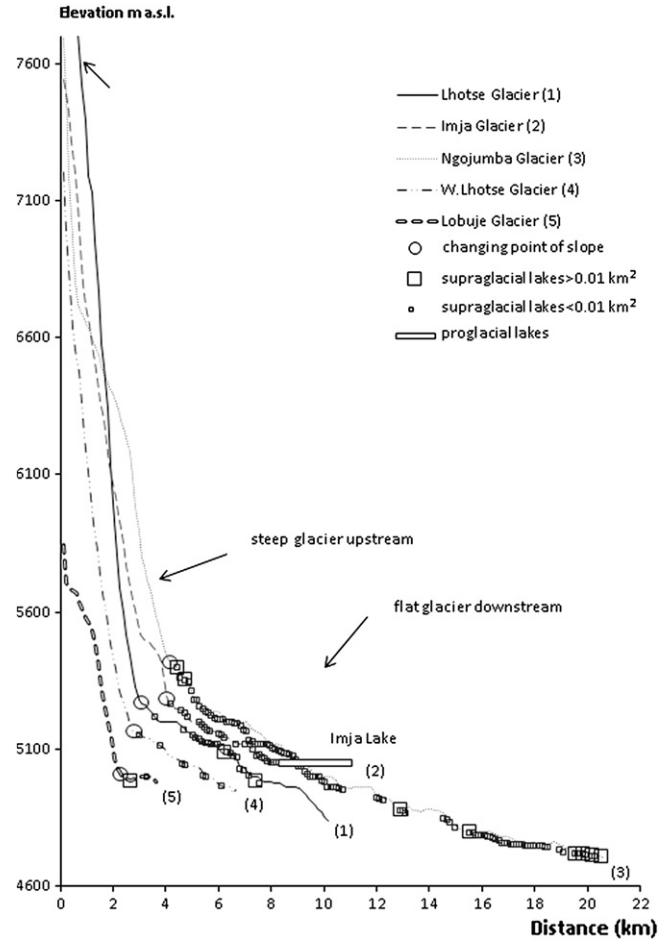

Fig. 4. Elevation profiles of five glaciers in Mt Everest Region. The location of changing point of glacier slopes and *supraglacial lakes* is shown.

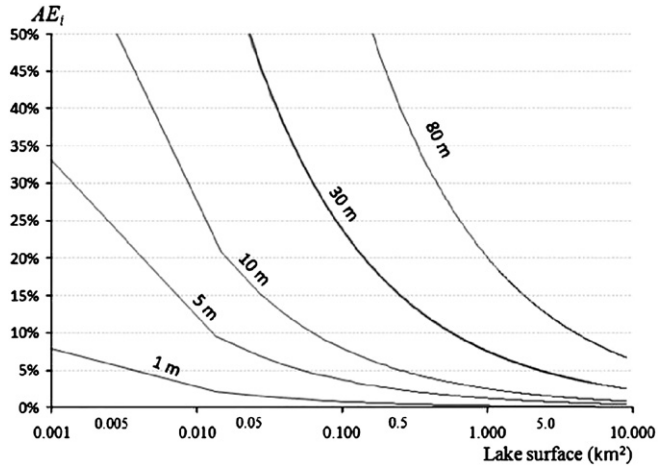

Fig. 5. Relationship between the hypothetical surface of circular lakes and the respective uncertainty of measurement according to sensors that differ by degree of resolution.

5.2. Unconnected glacial lakes

Lakes without direct connections with glaciers (referred to as *unconnected glacial lakes*) are reported without a specific suffix in Supplementary material 3. The median area of the direct drainage sub-basins is found to be 0.57 km^2, whereas if the surfaces of basins belonging to lakes of lower order are included, the area is 0.86 km^2. The size of the basin ranged from 0.01 km^2 for LCN (Lake Cadaster Number) 126 to 20.81 km^2 for LCN 24 (Supplementary material 2 d).

The majority of *unconnected glacial lakes* are located in the Ngojumba Glacier basin: 55 lakes for a total surface of $2.41 \pm 11\%$ km^2 (Supplementary material 2 c), corresponding to 56% of *unconnected glacial lakes* of the entire park in terms of area and 32% in terms of number. Moreover, in this basin, the larger lakes, such as LCN 76 with a surface of $0.61 \pm 4\%$ km^2, represent the lakes of this typology. Even the Khumbu Glacier basin presents a high number of lakes (30) for a total surface of $0.86 \pm 13\%$ km^2 (20% of *unconnected glacial lakes* of the entire park in terms of area and 18% in terms of number). LCN 24 located within the basin of the Khumbu Glacier is the second biggest lake of this typology and has, precisely, a surface of $0.57 \pm 5\%$ km^2.

The basins of the *unconnected glacial lakes* have an average glacial surface of 20% in what is considered to be a wide range of contingent situations; indeed, 45% of the lakes do not present glacial surfaces within the basin that directly drains the lake. In this regard, Fig. 6 compares the sub-basin surface and the glacial surface of each basin with the respective lake size. We observe that the lake surface is significantly correlated ($R^2 = 0.62$, $p < 0.001$) with the size of its drainage basin, whereas no correlation is found with the glacial surface ($R^2 = 0.10$, $p > 0.05$). This analysis legitimates the hypothesis that the supply of *unconnected glacial lakes* is determined mainly by the runoff rather than by the glacial melting waters. In fact, the direct proportionality between lake surfaces and their contributing watershed area is evidence that is consistent with the notion that precipitation is the main factor influencing the lake water balance if the evaporation/precipitation ratio is small. In effect, the drainage basin/lake area ratio is related directly to climatic variables of precipitation and evaporation (Sack, 2001; Sack, 2009). Based on the meteorological observations at Pyramid Laboratory-Observatory (2001–2005) located at an elevation of 5050 m and considering that the elevation mean of these lakes is 5073 m, we calculated the evaporation/precipitation ratio. At this high elevation, the annual mean temperature is below

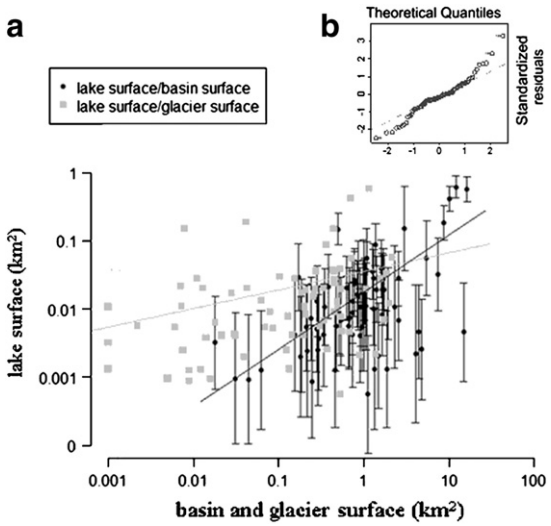

Fig. 6. a) Relationship among the lake sizes, the basin surface and its glacial coverage in the basin. The error bar represents the *AEi*. The linear model is computed considering the inverse of the *AEi* for each lake. b) Normal quantile–quantile plot of residuals of the regression model basin surface/lake sizes.

0 °C (-2.5 ± 0.5 °C), and the mean evaporation, applying the Jensen-Haise model for a rough estimation at these altitudes (Gardelle et al., 2010), is 160 ± 6 mm. In our case, the evaporation/precipitation ratio is approximately 0.34 ± 0.07 (mean annual precipitation 490 ± 74 mm). Therefore, a possible variation in precipitation regime affects the lake water balance three times more than the same variation for the evaporation rate. This further evidence allows us to assert that the evolution of these lakes is mainly influenced by the precipitation regime. This remark is critical, considering the current climate change scenario. The monitoring of these lakes thus provides useful indications of the precipitation trend. Similar to this research, we can observe that Fassett and Head (2008), investigating the possible hydrological system of Mars, found that open-basin lakes have volumes that are proportional to their watershed area. These authors considered this evidence to be consistent with what would be expected if the lakes were sourced predominantly by precipitation to their catchments.

5.3. Supraglacial lakes

Supraglacial lakes are highly variable in space and time, and their lifetime is unpredictable (Benn et al., 2001). Therefore, as suggested by Gardelle et al. (2010), it is more meaningful and relevant to investigate the conditions of formation considering the total area of these lakes located on a given glacier. Table 1 shows the morphometric characteristics of *supraglacial lakes* grouped by the glacier that each lake belongs to, and Table 2 provides a general statistical summary.

We observe that the majority of lakes are located on the surface of the Ngojumba Glacier (Supplementary material 2 c). Overall, the glacier is associated with more than 100 lakes for a total surface of $0.50 \pm 37\%$ km^2. The other glaciers that present a surface clearly interspersed with *supraglacial lakes* are the Bhote Koshi and Khumbu glaciers. In general, 55% of *supraglacial lakes* (60% in terms of surface) of the entire park are situated over these three glaciers. If we consider the total lake surface in respect to the glacier downstream surface of the relevant glacier (Lake Density in Table 1), in general, we can observe that lakes occupy from approximately $0.3 \pm 0.1\%$ to $2 \pm 0.6\%$ of glacier surfaces. Lobuje and Chhule present the glacier downstream surfaces with the highest relative development of *supraglacial lakes*.

To investigate the controlling parameters of supraglacial lake development further we derived a simple multiple regression model (Fig. 7a). We observed that the mean slope of glacier upstream, the mean slope of glacier downstream and the mean slope of the overall glacier present significant inverse correlations with the *supraglacial lake* surface density, whereas among these predictors, the mutual relationships are less consistent. Even the mean elevation of the glacier downstream is inversely correlated with the *lake* surface density, although at a limited significance level.

All variables were tested for their ability to predict the *lake* surface density. Quadratic terms and interactions were also considered. First, we developed a regression model considering as predictors the mean slope of the overall glacier and the mean elevation of glacier downstream, but this model was able to predict only 47% of *supraglacial lake* surfaces ($R^2 = 0.47$), slightly incrementing the ability of the mean slope of the overall glacier, taken individually, to predict the response variable ($R^2 = 0.40$). The second model tested was between the mean slope of glacier upstream, the mean slope of glacier downstream and the mean elevation of glacier downstream. In this case, the results were definitely better ($R^2 = 0.93$, AIC $= -197$). The process of model development is conducted with a stepwise simplification through the evaluation of the AIC index. In the final step, we identify the additive model between the mean slope of glacier upstream, the mean slope of glacier downstream and their relevant interaction as the model showing at the same time the highest quality of fit (Fig. 7b) and the lowest number of parameters and equation terms ($R^2 = 0.90$, AIC $= -199$). The mean elevation of glacier downstream was excluded from this setting because its contribution did

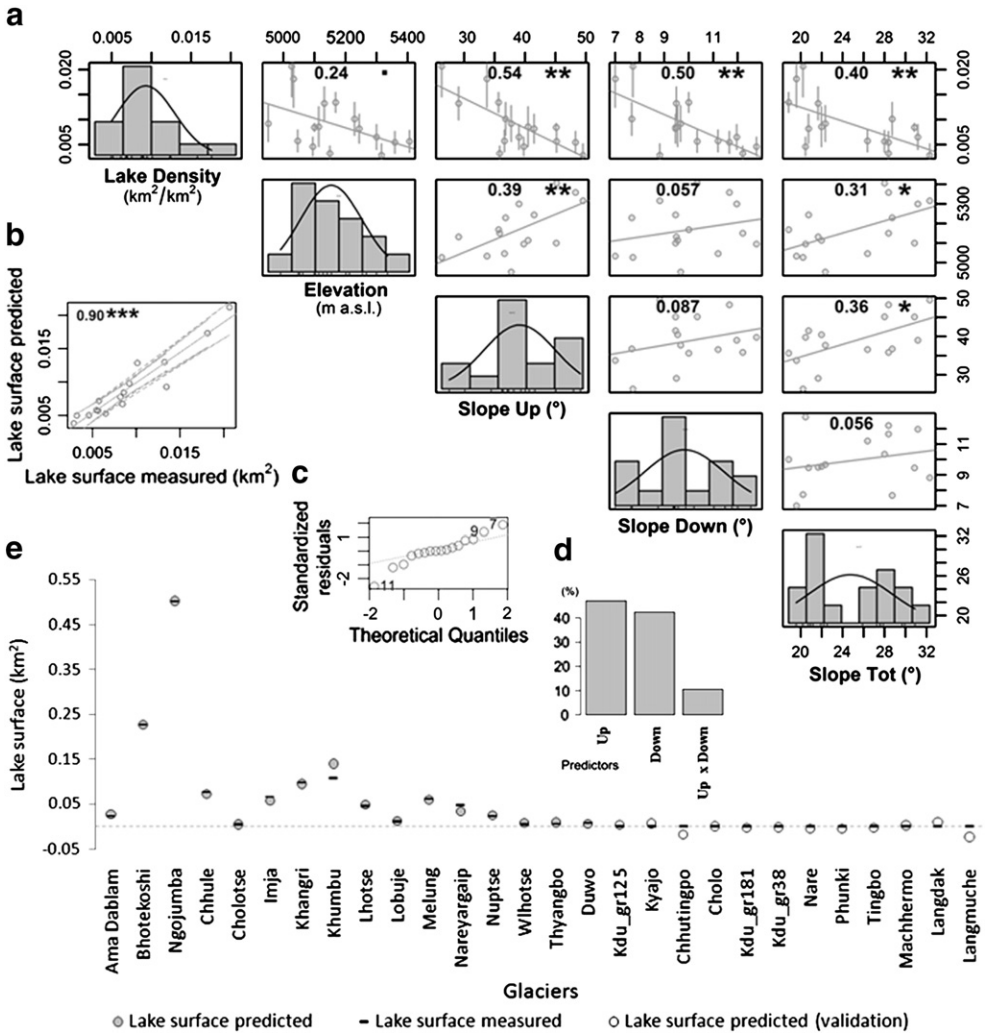

Fig. 7. Multiple regression analysis to explain the supraglacial lake distribution. a) Correlation matrix among predictors and supraglacial lake surface density (Lake Density) (Up = glacier upstream; Down = glacier downstream; Tot = all glacier; Elevation represents the mean elevation of the glacier downstream). For each correlation, the coefficient of determination (R^2) is plotted with a relevant level of significance ($p<0.001$ '***'; $p<0.01$ '**'; $p<0.05$ '*'; $p<0.1$ '.') b) Scatterplot of final regression model relevant confidence levels at 95%. c) Normal quantile-quantile plot of residuals of final regression model. d) Relative importance of the contribution of each predictor for the final regression model (metrics are normalized to sum to 100% of the R^2 of Fig. 7b). e) Comparison between predicted and measured supraglacial lake surfaces for each glacier.

not appear to be significant in improving the predictive ability of the model. Eq. (4) represents the final selected model able to predict the *lake* surface density and consequently the *supraglacial lake* surface of each glacier:

$$LakeSur_i = \left[0.11-(0.0022 * SlopeUp_i)-(0.0088 * SlopeDown_i) + (0.00019 * SlopeUp_i * SlopeDown_i)\right] * SurDown_i \quad (4)$$

where $LakeSur_i$ represents the total *supraglacial lake* surface for each glacier (ith), $SurDown_i$ is the surface downstream of each glacier, and $SlopeUp_i$ and $SlopeDown_i$ refer to the mean slopes of glacier upstream and downstream, respectively. Fig. 7c, presenting the normal quantile–quantile plot of model residuals, shows that the model approaches a normal distribution. Our analysis is completed with a type of further validation applying the model at those glaciers that do not currently present *supraglacial lakes*. Fig. 7e shows a visual evaluation of the estimation of the total *supraglacial lake* surfaces realized by applying the Eq. (4) both at the glaciers used in the calibration phase of the model (full circles) and at the glaciers not presenting lake surfaces (empty circles). We can observe that the model developed can even correctly predict the absence of lakes. In such cases, we obtain negative values that provide an indication of how far the glacier is from developing lakes on its surface. We complete the description of the developed model by discussing the relative contribution of each predictor. Fig. 7d shows that to explain the *supraglacial lake* surfaces, the slope downstream (42%) on which the ponds are located is crucial as well as the slopes upstream (47%) and the interaction of the slopes of these two glacier portions (11%).

Our findings confirm that slope in the glacier area where lakes are located provides the boundary conditions favorable for *supraglacial lake* formation. Reynolds (2000) reports that in the Bhutan Himalaya, small isolated ponds could be found up to 10°. This work demonstrated that where large glacial lakes currently exist, the surface gradient of the glacier prior to lake formation is always less than 2°. These lakes could already be or could evolve to become moraine-dammed lakes (*proglacial* lakes). In our case, having used inferential statistics, the conditions of formation among lakes have to be homogeneous. Therefore, we excluded *proglacial lakes* from this analysis, considering that other variables, as discussed below, can influence their possible development.

Scherler et al. (2011) suggest that lower slopes correspond to lower gravitational driving stresses that, by decreasing the glacier flow, allow the development of stagnant ice, which is a favorable

condition for the formation of lakes. Suzuki et al. (2007), calculating the thermal resistance of debris-covered glaciers, found that those with relatively thin layers of debris tend to develop glacial lakes at their terminus. Sakai and Fujita (2010), analyzing the difference in height between the glacier surface and lateral moraine ridges, observed that the glaciers that record a relatively large decrease in their surface are likely to develop glacial lakes, and therefore, in general, glaciers with high ablation rates tend to develop glacial lakes.

Therefore, the two key factors that appear to be responsible for lake formation are low velocity and high ablation rates at the glacier terminus. Although the mean slope of glacier downstream primarily influences the first requirement, the mean slope of glacier upstream, in our opinion, is able to condition both of these factors. To begin we consider that Scherler et al. (2011) demonstrate that high and deeply incised mountain ranges, in particular in the southern central Himalayas, are responsible for the debris accumulation because the hillslope-erosion rates usually increase with the hillslope angle. The abundance of debris coverage reduces the melt rate of these glaciers, preserving their surfaces from further recession. Therefore, the inverse relationship we found between the mean slope of glacier upstream and lake surfaces favors the formation of lakes because thin debris layers correspond to high ablation rates. Furthermore, we have to consider that many studies highlight the present condition of ice stagnation of glaciers in the Mt Everest region, specifically in the southern central Himalayas, is attributable to low flow velocity generated by a general negative mass balance (Bolch et al., 2008; Quincey et al., 2009; Scherler et al.;, 2011). It is well established that an increase in the glacier flow can be attributed to an increase in the glacier surface slope brought on by an imbalance between the amounts of accumulation versus ablation. This imbalance favors the shear stress on a glacier until it begins to flow. Key factors (boundary conditions) that influence the flow velocity are the slope of the ice as well as the ice thickness and temperature (Cuffey and Paterson, 2010). The greater the top glacier slope, the greater the possibility that an addition of new snow and ice will be transferred to the bottom zone, and therefore higher flow velocity of the glacier termini is expected. Therefore, of two glaciers, the one with a flatter glacier upstream presents more favorable conditions for the development of *supraglacial lakes* caused by a minor transport of debris, which increases the ablation rate, and a minor transport of new snow and ice, which decreases the flow velocity of the glacier termini.

We conclude this analysis by emphasizing that the model that generally considers the overall slope of the entire glacier has a lower capability of predicting the lake distribution because a key factor in determining favorable conditions for lake formation is likely to be the interaction between two glacier zones. The differences between the two glacier zones determine the imbalance, which contributes to the down-slope passage of debris, snow and ice, determining the flow velocity and ablation rate of the glacier termini and consequently the formation conditions for *supraglacial lakes*.

5.4. Proglacial lakes

Supplementary material 3 presents the hydro-morphological features of *proglacial* (suffixed here as *Pro*), while Table 2 provides a general statistical summary. Of the 12 lakes ascribed to this typology, the largest lake is LCN 161, namely, Imja Lake, one of the most studied GLOF-risk lakes in the world (Yamada, 1998; Mool et al., 2001; Bajracharya et al., 2007b; Fujita et al., 2009). In this study, this lake has a surface of $0.98 \pm 3\%$ km^2 (Supplementary material 2 d). The same lake was assessed by Fujita et al. (2009), who found it had a surface of $0.92 \pm 3\%$ km^2 in the same year as our census, although the measurements were performed before the monsoon season and with a sensor of lower resolution (ASTER, 15 m). Another large lake that caused a GLOF event in 1985 is LCN 136, namely, Dig Tsho, which has formed at the foot of the Langmoche Glacier with a surface of $0.40 \pm 5\%$ km^2. At the end of the 1990s, the same lake, studied by Bajracharya et al. (2007a), presented a surface of 0.35 km^2 (0.36 km^2 in 2000 and 0.33 in 2005, according to Bajracharya et al., 2007b) (Supplementary material 2 a).

The formation of *proglacial lakes* is closely connected with the formation of *supraglacial* lakes. Many authors (e.g., Röhl, 2008; Sakai et al., 2009) consider *supraglacial lakes* to be precursors of terminus disintegration by growing and coalescing, to culminate in large *proglacial lakes*. However, these lakes can also disappear from the glacier surface, leaving only a depression behind. Ponds enlarge predominantly by melting, but coalescence of ponds may eventually lead to a calving terminus. Quincey et al. (2007) affirms that while the mean slope of glacier downstream provides the boundary conditions favorable for *supraglacial lake* formation, their growth and therefore the potential to become a large *proglacial lake* depends on local conditions. These researchers suggest that local variations in glacier velocity and surface morphology between flow units control lake growth. Integrating the surface gradient and velocity information into a single analysis, these authors highlight those glaciers that are particularly vulnerable to development as *proglacial lakes*.

In this study, we contribute to defining the conditions of formation of *supraglacial lakes* and therefore of *proglacial* ones, although we agree with the authors mentioned that the enlargement phenomena of these lakes need to be explained at a lower scale, allowing the peculiarity of single lakes to emerge (Hambrey et al., 2008; Röhl, 2008).

6. Conclusions

In this study, we use ALOS imagery (October 2008) with a medium-high resolution (10 m) for a concomitant hand mapping of glaciers and lakes of the entire southern side of the Mt Everest region. We examined 29 glaciers and 624 lakes (17 *proglacial*, 437 *supraglacial* and 170 *unconnected glacial lakes*). Our attention was focused on the conditions of the formation of lakes, examining the relationship between local basin topography, glacier features and lake dimensions.

The results confirm that the slope of the glacier where lakes are located influences the *supraglacial lake* formation. Moreover, this study is novel in highlighting a further boundary condition. The slope of glacier upstream favors the formation of *supraglacial* lakes because of the minor transport of debris, which increases the ablation rate, and the minor transport of new snow and ice, which decreases the flow velocity of the glacier termini. The regression model developed here has been tested in the most representative comparison of processes that determine the formation of *supraglacial* lakes (Scherler et al., 2011; Gardelle et al., 2010). Nevertheless, the model does not aim to predict the behavior of future lakes but rather encourages further testing in similar environments (debris-covered glaciers) for evaluating possible different behaviors.

The formation of *proglacial lakes* is closely connected with the formation of *supraglacial* ones. These lakes are indeed considered to be precursors of terminus disintegration by growing and coalescing, to culminate in large *proglacial lakes*. However, the enlargement phenomena of these lakes could be explained only on a local scale, thus allowing the peculiarity of the single lake to emerge.

Moreover, these high altitudes are characterized by a significant presence of *unconnected glacial lakes*. Although these bodies of water have been neglected to date, we found they can provide useful indications on the precipitation trend in these remote areas. Our analysis has been completed by an accurate assessment of the uncertainties of topographical measurements made by remote sensing imagery. The results highlight that medium-resolution sensors (10 m) are able to describe lake and glacier surfaces correctly and possibly their variations in the case of multi-temporal analysis, although a direct comparison between lakes needs to be confined to the largest ones. The use of lower resolution sensors could highlight greater uncertainty than the observed evolutions. Regarding glaciers,

the error associated with the estimation of their surfaces presents a lower order of magnitude than that associated with the lakes, thus correctly characterizing the entire resource.

Supplementary data to this article can be found online at http://dx.doi.org/10.1016/j.gloplacha.2012.04.001.

Acknowledgments

The study was conducted by IRSA-CNR and University of Milan within the framework of the Ev-K2-CNR and Nepal Academy of Science and Technology joint research project in Nepal under the terms of the Memorandum of Understanding between Nepal and Italy, with the support of the Italian National Research Council and the Italian Ministry of Foreign Affairs. ALOS AVNIR-2 data were acquired within the ESA AO553 MELINOS Project.

References

Ageta, Y., Iwata, S., Yabuki, H., Naito, N., Sakai, A., Narama, C., Karma, T., 2000. Expansion of glacier lakes in recent decades in the Bhutan Himalayas. IAHS Publication, 264, pp. 165–175.

Bajracharya, B., Shrestha, A.B., Rajbhandari, L., 2007a. Glacial lake outburst floods in the Sagarmatha region- hazard assessment using GIS and hydrodynamic modeling. Mountain Research and Development 27 (4), 336–344.

Bajracharya, S.R., Mool, P.K., Shrestha, B.R., 2007b. Impact of climate change on Himalayan glaciers and glacial lakes. ICIMOD/UNEP Publication. 119 pp.

Bajracharya, B., Uddin, K., Chettri, N., Shrestha, B., Siddiqui, S.A., 2010. Understanding land cover change using a harmonized classification system in the Himalayas: A case study from Sagarmatha National Park, Nepal. Mountain Research and Development 30 (2), 143–156.

Benn, D.I., Wiseman, S., Hands, K.A., 2001. Growth and drainage of supraglacial lakes on debris-mantled Ngozumpa Glacier, Khumbu Himal, Nepal. Journal of Glaciology 47 (159), 177–185.

Bolch, T., Buchroithner, M., Pieczonka, T., Kunert, A., 2008. Planimetric and volumetric glacier changes in the Khumbu Himal, Nepal, since 1962 using Corona, Landsat TM and ASTER data. Journal of Glaciology 54, 592–600.

Buishand, T.A., 1982. Some methods for testing the homogeneity of rainfall records. Journal of Hydrology 58, 11–27.

Cuffey, K.M., Paterson, W.S.B., 2010. The Physics of Glaciers, 4th edition. Elsevier, Inc.. 704 pp.

Fassett, C.I., Head III, J.W., 2008. Valley network-fed, open-basin lakes on Mars: Distribution and implications for Noachian surface and subsurface hydrology. Icarus 198, 37–56.

Fujita, K., Sakai, A., Nuimura, T., Yamaguchi, S., Sharma, R., 2009. Recent changes in Imja Glacial lake and its damming moraine in the Nepal Himalaya revealed by in situ surveys and multi-temporal ASTER imagery. Environmental Research Letters 4, 1–7.

Fushimi, H., Ikegami, K., Higuchi, K., Shankar, K., 1985. Nepal case study: Catastrophic floods. AHS Publication, 149, pp. 125–130.

Gardelle, J., Arnaud, Y., Berthier, E., 2010. Contrasted evolution of glacial lakes along the Hindu Kush Himalaya mountain range between 1990 and 2009. Global and Planetary Change 75 (1–2), 47–55.

Giardino, C., Oggioni, A., Bresciani, M., Huimin, Y., 2010. Remote sensing of suspended particulate matter in Himalayan lakes: A case study of Alpine lakes in the Mount Everest region. Mountain Research and Development 30 (2), 157–168.

Gorman, L.O., 1996. Subpixel precision of straight-edged shapes for registration and measurement. IEEE Transactions on Pattern Analysis and Machine Intelligence 18 (7), 746–751.

Hambrey, M.J., Quincey, D.J., Glasser, N.F., Reynolds, J.M., Richardson, S.J., Clemmens, S., 2008. Sedimentological, geomorphological and dynamic context of debris mantled glaciers, Mount Everest (Sagarmatha) region, Nepal. Quaternary Science Reviews 27, 2361–2389.

Inghilleri, G., 1974. Topografia generale. UTET Publication, Torino. 445 pp.

Jacob, T., Wahr, J., Pfeffer, W.T., Swenson, S., 2012. Recent contributions of glaciers and ice caps to sea level rise. Nature 482, 514–518.

Joanes, D.N., Gill, C.A., 1998. Comparing measures of sample skewness and kurtosis. Journal of the Royal Statistical Society Series D: The Statistician 47 (1), 183–189.

Kundzewicz, Z.W., Robson, A.J., 2004. Change detection in hydrological records—a review of the methodology. Hydrological Sciences Journal 49 (1), 7–19.

Lami, A., Marchetto, A., Musazzi, S., Salerno, F., Tartari, G., Guilizzoni, P., Rogora, M., Tartari, G.A., 2010. Chemical and biological response of two small lakes in the Khumbu Valley, Himalayas (Nepal) to short-term variability and climatic change as detected by long-term monitoring and paleolimnological methods. Hydrobiologia 648, 189–205.

Mattson, L.E., Gardner, J.S., Young, G.J., 1993. Ablation on debris covered glaciers: an example from the Rakhiot Glacier, Panjab, Himalaya. IAHS Publication, 218, pp. 289–296.

McMillan, M., Nienow, P., Shepherd, A., Benham, T., Sole, A., 2007. Seasonal evolution of supra-glacial lakes on the Greenland Ice Sheet. Earth and Planetary Science Letters 262, 484–492.

Mool, P.K., Bajracharya, S.R., Joshi, S.P., 2001. Inventory of glaciers, glacial lakes and glacial lake outburst floods: monitoring and early warning systems in the Hindu Kush–Himalayan region, Nepal. ICIMOD/UNEP Publication. 197 pp.

Quincey, D.J., Richardson, S.D., Luckman, A., Lucas, R.M., Reynolds, J.M., Hambrey, M.J., Glasser, N.J., 2007. Early recognition of glacial lake hazards in the Himalaya using remote sensing datasets. Global and Planetary Change 56 (1–2), 137–152.

Quincey, D.J., Luckman, A., Benn, D., 2009. Quantification of Everest region glacier velocities between 1992 and 2002, using satellite radar interferometry and feature tracking. Journal of Glaciology 55 (192), 596–606.

Racoviteanu, A.E., Williams, M.W., Barry, R.G., 2008. Optical remote sensing of glacier characteristics: A review with focus on the Himalaya. Sensors 8, 3355–3383.

Reynolds, J.M., 2000. On the formation of supraglacial lakes on debris-covered glaciers. IAHS publications, 264, pp. 153–161.

Richardson, S., Reynolds, J., 2000. An overview of glacial hazards in the Himalayas. Quaternary International 65–66, 31–47.

Röhl, K., 2008. Characteristics and evolution of supraglacial ponds on debris-covered Tasman Glacier, New Zealand. Journal of Glaciology 54 (188), 867–880.

Sack, D., 2001. Shoreline and basin configuration techniques in paleolimnology. In: Last, W.M., Smol, J.P. (Eds.), Tracking Environmental Change Using Lake Sediments. Basin Analysis, Coring, and Chronological Techniques, 1. Kluwer Academic Publishers, pp. 49–72.

Sack, D., 2009. Evidence for climate change from desert basin palaeolakes. In: Parsons, A.J., Abrahams, A.D. (Eds.), Geomorphology of desert environments. Springer, Dordrecht, The Netherlands, pp. 743–756.

Sakai, A., Fujita, K., 2010. Formation conditions of supraglacial lakes on debris-covered glaciers in the Himalaya. Journal of Glaciology 56 (195), 177–181.

Sakai, A., Takeuchi, N., Fujita, K., Nakawo, M., 2000. Role of supraglacial ponds in the ablation process of a debriscovered glacier in the Nepal Himalayas. IAHS Publication, 264, pp. 119–130.

Sakai, A., Nishimura, K., Kadota, T., Takeuchi, N., 2009. Onset of calving at supraglacial lakes on debris covered glaciers of the Nepal Himalayas. Journal of Glaciology 55 (193), 909–917.

Salerno, F., Buraschi, E., Bruccoleri, G., Tartari, G., Smiraglia, C., 2008. Glacier surface-area changes in Sagarmatha National Park, Nepal, in the second half of the 20th century, by comparison of historical maps. Journal of Glaciology 54 (187), 738–752.

Salerno, F., Viviano, G., Thakuri, S., Flury, B., Maskey, R.K., Khanal, S.N., Bhuju, D., Carrer, M., Bhochhibhoya, S., Melis, M.T., Giannino, F., Staiano, A., Carteni, F., Mazzoleni, S., Cogo, A., Sapkota, A., Shrestha, S., Pandey, R.K., Manfredi, E.C., 2010. Energy, forest, and indoor air pollution models for Sagarmatha National Park and Buffer zone, Nepal: Implementation of a participatory modeling framework. Mountain Research and Development 30 (2), 113–126.

Scherler, D., Leprince, S., Strecker, M.R., 2008. Glacier-surface velocities in alpine terrain from optical satellite imagery-Accuracy improvement and quality assessment. Remote Sensing of Environment 112, 3806–3819.

Scherler, D., Bookhagen, B., Strecker, M.R., 2011. Spatially variable response of Himalayan glaciers to climate change affected by debris cover. Nature Geoscience 4, 156–159.

Shangguan, D., Liu, S., Ding, Y., Zhang, Y., Li, J., Li, X., Wu, Z., 2010. Changes in the elevation and extent of two glaciers along the Yanglonghe river, Qilian Shan, China. Journal of Glaciology 56 (196), 309–317.

Silverio, W., Jaquet, J.M., 2005. Glacial cover mapping (1987–1996) of the Cordillera Blanca (Peru) using satellite imagery. Remote Sensing of Environment 95 (3), 342–350.

Suzuki, R., Fujita, K., Ageta, Y., 2007. Spatial distribution of thermal properties on debris-covered glaciers in the Himalayas derived from ASTER data. Bulletin of Glaciological Research 24, 13–22.

Tartari, G., Salerno, F., Buraschi, E., Bruccoleri, G., Smiraglia, C., 2008. Lake surface area variations in the north-eastern sector of Sagarmatha National Park (Nepal) at the end of the 20th century by comparison of historical maps. Journal of Limnology 67, 139–154.

Taylor, W.A., 2000. Change-Point Analysis: A Powerful New Tool For Detecting Changes. http://www.variation.com/cpa/tech/changepoint.html 2000.

Vermote, E.F., Tanrè, D., Deizè, J.L., Herman, M., Morcrette, J.J., 1997. Second simulation of the satellite signal in the solar spectrum, 6S: An overview. IEEE Transactions on Geoscience and Remote Sensing 35, 675–686.

Williams, R.S., Hall Jr., D.K., Chien, J.Y.L., 1997. Comparison of satellite-derived with ground-based measurements of the fluctuations of the margins of Vatnajokull, Iceland, 1973–92. Annals of Glaciology 24, 72–80.

Yamada, T., 1998. Glacier lake and its outburst flood in the Nepal Himalaya. Monograph No. 1, Data Center for Glacier Research. Japanese Society of Snow and Ice. 96 pp.

Yamada, T., Sharma, C.K., 1993. Glacier lakes and outburst floods in Nepal Himalaya. Snow and Glacier Hydrology: IAHS Publication, 218, pp. 319–330.

Ye, Q., Kang, S., Chen, F., Wang, J., 2006. Monitoring glacier variations on Geladandong mountain, Central Tibetan Plateau, from 1969 to 2002 using remote-sensing and GIS technologies. Journal of Glaciology 52 (179), 537–545.

Zhang, B., Walker, S., Miller, S., 2001. 3D feature extraction from imagery using ArcSDE. Proceedings of ESRI International Users Conference, 2001, San Diego, CA.

Supplementary material 1

PREVIOUS STUDIES ON GLACIER AND LAKE DISTRIBUTION IN MT EVEREST REGION

Müller (1970) reports an inventory of glaciers in Mt Everest region which can be considered as a pioneering work in this field. The work was undertaken using map of late 1950s on 1:50,000 scale (Schneider, 1967). In 2001, the International Center for Integrated Mountain Development (ICIMOD; Mool *et al.,* 2001) constructed a glacier inventory for whole Nepal, and thus also for SNP. Working at the national level, a variety of data sources were used including satellite images, aerial photographs and maps. However, the inventory too, proved unsuitable as a basis of area comparison for the present work, because the multiplicity of its sources cannot be attributed to a precise historical period. Salerno *et al.,* 2008 decided to adopt the glacier codes proposed by ICIMOD for tracing the glaciers extension at the end of the 1950s and early 1990s based on the *Khumbu–Himal* map (scale 1:50,000, Schneider, 1967), published in 1978 and the current *Official Nepali map* (scale 1:50,000, Survey Department of His Majesty's Government of Nepal, 1997), respectively.

A complete review of the limnological studies carried out in Mt Everest region is provided by Tartari *et al.,* 2008. We just remember here that after the first pioneering work of 1960s (Löffler 1969), the interest for these environments has carried on in 1980s within the framework of research activities coordinated by Ev-K2-CNR Committee by the Water Research Institute (IRSA-CNR) and the Institute of Ecosystem Studies (ISE-CNR). The research activities were initially focused on the hydro-geochemical characterization of the lakes over a wide spatial radius (Tartari *et al.,* 1998a; Bortolami, 1998; Smiraglia, 1998). In seven expeditions conducted between 1989 and 1997, 48 lakes were visited (Tartari *et al.,* 1998b), leading to the identification of many temporary water bodies.

A first cartographic study was carried out to compile a lake cadastre using the *Mount Everest map* (scale 1:50,000, National Geographic Society, Washington D.C., 1988) which represented the lakes morphology of the north-eastern sector of SNP in December 1984 (Tartari *et al.,* 1998c). Each water body was assigned a univocal sequential code (Lake Cadastre Number, LCN), suffixed LCN '80s as pertaining to the map "of the eighties". This initial cadastre was after 10 years integrated for the same territory with the *Official Nepali map* (scale 1:50,000, Survey Department of His Majesty's Government of Nepal, 1997) dated December 1992 (Tartari *et al.,* 2008). These lakes were suffixed as "of the nineties" (LCN '90s).

We highlight that in these cadastres, *supraglacial lakes* had been excluded because they were not deemed ecological relevant, in light of their rapid evolution and recent formation. In fact such water bodies can be better defined as ice-melt ponds rather than fully fledged lakes. Contrary to previous studies, considering the accelerated process of deglaciation in the last decades, in the present cadastre (LCN 2008) we regarded it right to take a census also of *supraglacial lakes*. For these lakes, considering their elevated number and rapid evolution, we deemed it appropriate not to assign them an identification code, but rather simply group them together according to the glacier they belong to.

GLACIER AND LAKE IDENTIFICATION

The glaciers identification is based on the ICIMOD inventory (Mool *et al.,* 2001) as a reference, giving it preference in assigning unambiguous place names. For those glaciers that were not assigned a name in the ICIMOD inventory, we used, if reported, the name given in the *Khumbu–Himal* and the *Official Nepali maps* or the ICIMOD glacier code. For classification criteria used to define the extent of each glacier (Tab. 1), we referred to the glacier classification guidance for the GLIMS glacier inventory (Rau *et al.,* 2005), while we choose to consider only those glaciers whose area exceeded a threshold of 1 km^2. For further details on glaciers

identification, refer to Salerno *et al.,* 2008. Table 2 presents a summary of the morphometric characteristics of lakes and glaciers, while more specifically Table 3(a-d), provided as supplementary material, details the features of each lakes and the relevant basins in the 2008 cadastre.

To maintain consistency with the 1980s and 1990s cadastre of the north-eastern sector of SNP, the same nomenclature for identifying the lakes was retained, consisting of the acronym LCN (Lake Cadastre Number) followed by a number (Tab. 3 a-d). The attribution of the Lake Code to newly formed lakes was done proceeding from east to west. Some code does not appear in the lists of the present cadastre for the following different reasons. The LCN '80s included 7 lakes situated outside the boundaries of SNP (LCN: 57, 58, 59, 60, 61, 64 and 65). Lakes 3 and 4 have become *supraglacial lake*. Furthermore some lakes in the previous maps appeared as independent water bodies, while appear instead united in the current cadastre (12, 13; 26, 27; 108, 109). Therefore, they have been designated in the new cadastre as LCN 1213, LCN 2627 and LCN 108109. In the previous cadastres some codes were not erroneously assigned (46, 69, 79, 88, 90, 147, 148, 159 and 1001). A large number of lakes have disappeared for natural drivers since the LCN'90 (7, 22, 23, 25, 39, 45, 47, 48, 49, 50, 51, 52, 56, 1002, 1003, 1004, 1005, 1006, 1008, 1009, 1010, 1011, 1012, 1013, 1015, 1016, 1017, 1018, 1019, 1020, 1021, 1022, 1023, 1024, 1025, 1026, 1027, 1029, 1031 and 1033). Finally some water bodies have disappeared since the LCN'90 (100, 107, 108, 109, 116, 117, 146, 149, 153 and 160).

The *Link* field in Table 3 shows the codes of their constituent lower-order basins, the *Sub-basin surface* field shows the area of the sub-basin draining directly into the lake, while the total basin area of the lake in question, obtained by summing the areas of all its constituent sub-basins, is shown in the field *Basin surface*. Table 3 also shows the extent of glacial cover present in each lake's direct drainage sub-basin (*Glacier surface in the sub-basin*) and the extent of glacial cover on the entire basin pertaining to the lake (*Glacier surface in the basin*). Moreover the table shows the list of the morphometric measurements of lakes: the area, its perimeter, the cartographic elevation (obtained on the *Official Nepali maps)*, the plane coordinates of the lake centroid, and the presence of any influents and/or effluents (identified on the *Official Nepali maps)*.

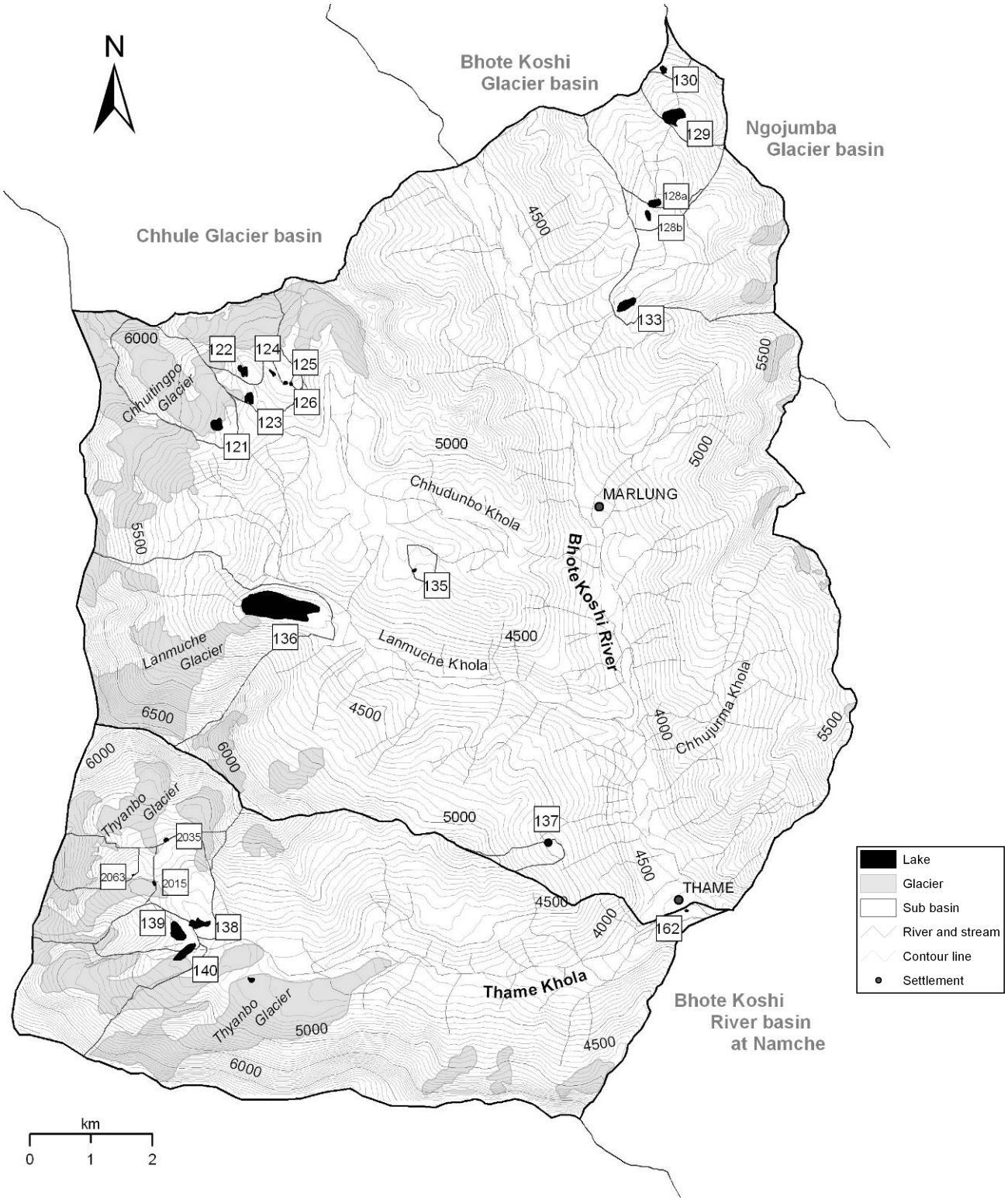

Supplementary material 2 a. Map of the surface water bodies of Thame Khola and Bhote Koshi River (at Thame) basins.

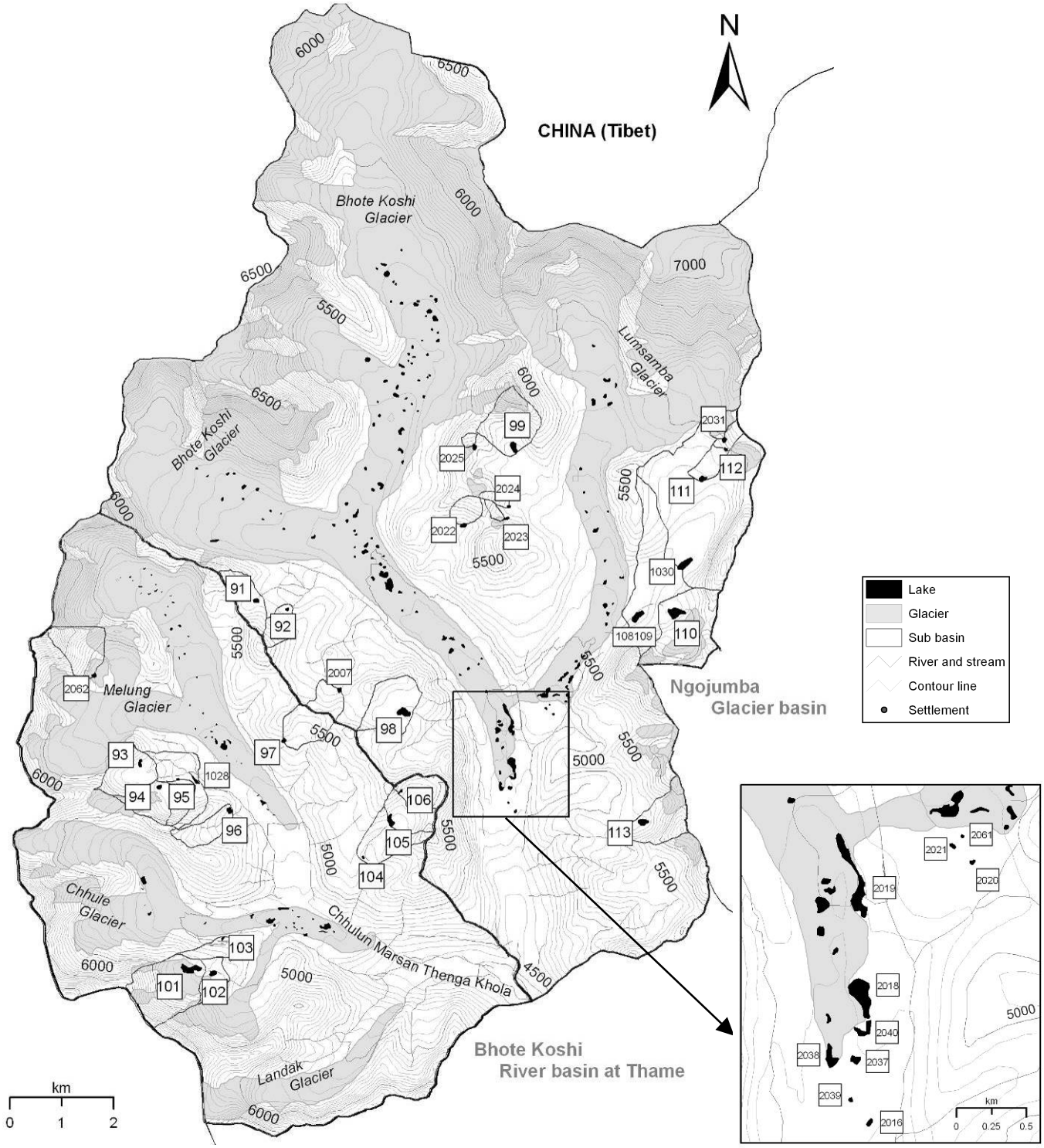

Supplementary material 2 b. Map of the surface water bodies of Chhule Glacier and Bhote Koshi Glacier basins

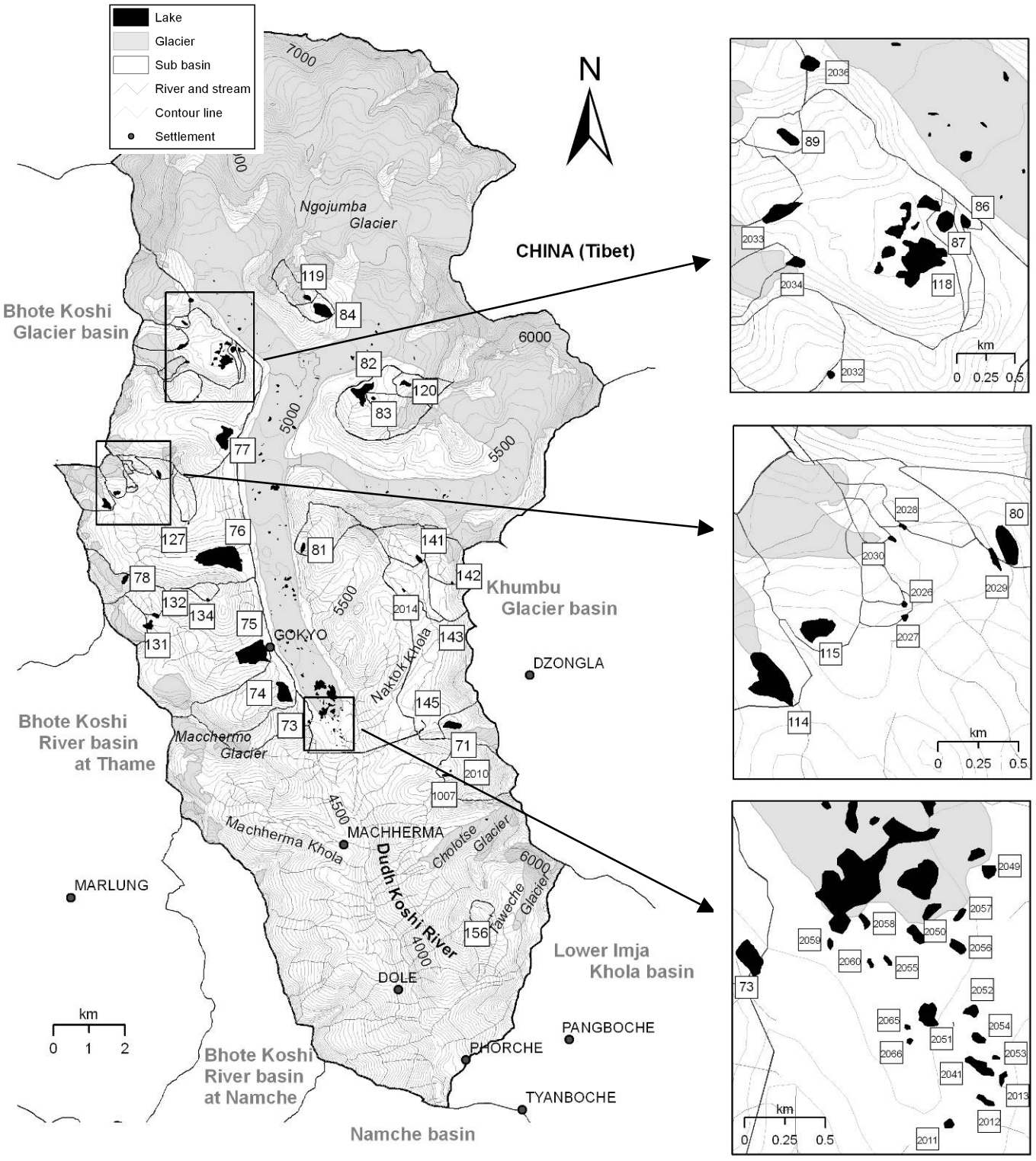

Supplementary material 2 c. Map of the surface water bodies of Ngojumba Glacier basin.

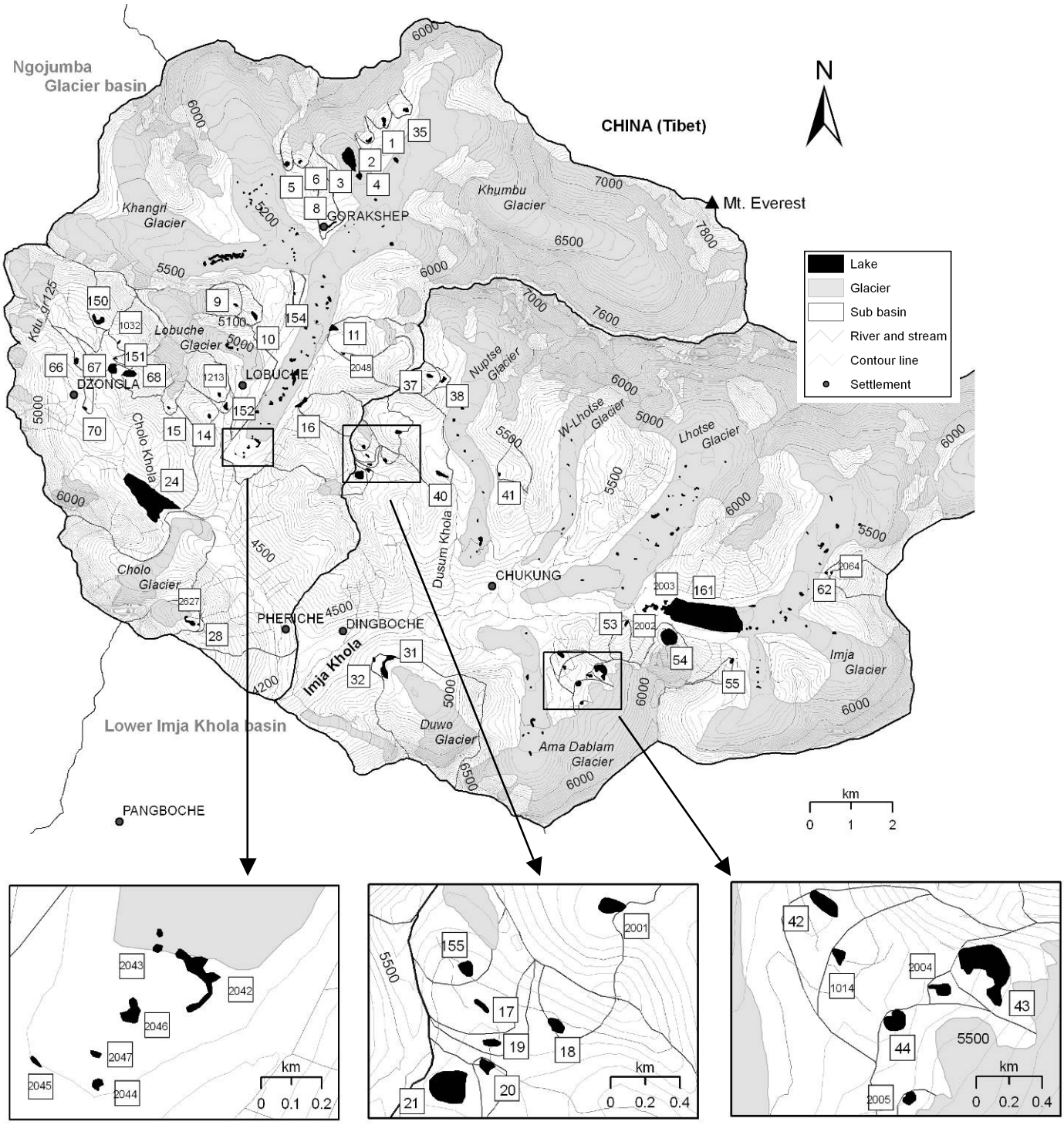

Supplementary material 2 d. Map of the surface water bodies of Khumbu Glacier and Upper Imja Khola basins.

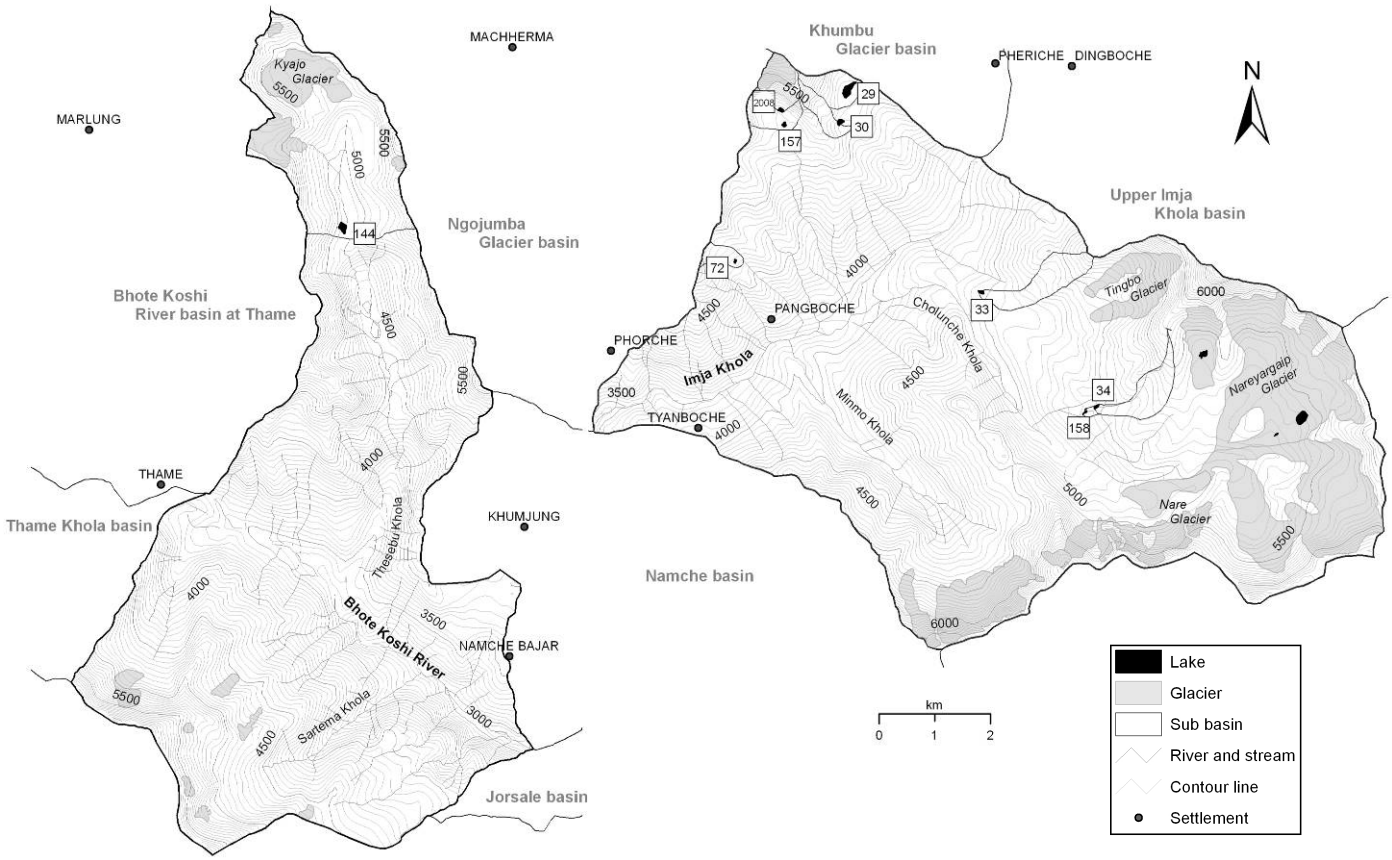

Supplementary material 2 e. Map of the surface water bodies of Lower Imja Khola and Bhote Koshi River (at Namche) basins.